A genome scale census of virulence factors in the major mould pathogen of human lungs, *Aspergillus fumigatus*

A thesis submitted to the University of Manchester for the degree of Doctor of Philosophy in the Faculty of Biology, Medicine and Health

2019

Norman van Rhijn

School of Biological Sciences

Division of Infection, Immunity and Respiratory Medicine

Table of contents

Word count: 48,676

List of Figures

List of Tables

List of Supplementary Figures

List of Supplementary Tables

Abbreviations

ABPA	Allergic bronchopulmonary aspergillosis
ACM	Aspergillus complete medium
AMM	Aspergillus minimal medium
bHLH	Basic helix-loop-helix
BMDC	Bone-marrow derived cells
BPS	Bathophenanthrolinedisulfonic acid
bZIP	Basic region leucine zipper
CaM	Calmodulin
CAS	CRISPR associated nucleases
CBC	CCAAT binding complex
CCR	Carbon catabolite repression
ChIP	Chromatin immunoprecipitation
COPD	Chronic obstructive pulmonary disease
CPA	Chronic pulmonary aspergillosis
CRISPR	Clustered regularly interspaced short palindromic repeats
CTAB	Cetyl trimethyl ammonium bromide
CWI	Cell wall integrity
DMEM	Dulbecco's Modified Eagle's Medium
FBS	Fetal bovine serum
fRPMI	Fungal RPMI
GCPR	G-coupled protein receptor
GFP	Green fluorescent protein
GMS	Grocott's methanamine silver
GO	Gene Ontology
gRNA	guide RNA
HDR	Homologous directed repair
HE	Haematoxylin eosin
HOG	High osmolarity glycerol
Hsp70	Heat shock protein 70
Hsp90	Heat shock protein 90
IA	Invasive aspergillosis
LDH	Lactodehydrogenase
LHA	Long homology arms
MEME	Multiple em for motif elicitation

MIC	Minimum inhibitory concentration
NC2	Negative complex 2
NHEJ	Non-homologous end joining
OD	Optical density
PAMPs	Pathogen associated molecular patterns
PBS	Phosphate buffered saline
PCR	Polymerase chain reaction
qPCR	quantitative polymerase chain reaction
RNP	Ribonucleoprotein
SREBP	Sterol responsive element binding protein
TBP	TATA-box binding protein
TF	Transcription factor
TFKO	Transcription factor knockout
TOR	Target of rapamycin
UPR	Untranslated protein response
WMM	Watch minimal medium

Abstract

The University of Manchester
Norman van Rhijn
Doctor of Philosophy
A genome scale census of virulence factors in the major mould pathogen of human lungs, *Aspergillus fumigatus*
2019

It is estimated that over 150 million individuals suffer from serious fungal infections, resulting in 1.5 million deaths a year. *Aspergillus fumigatus* is a filamentous saprophytic fungus. However, in hosts with an altered immune system it can cause a variety of diseases. The most serious is invasive aspergillosis, which is estimated to cause over 200,000 life-threatening infections annually with high mortality rates. Fungal diseases are increasing due to the expansion of the immunocompromised cohorts of patients. The current antifungal arsenal is limited and paired with severe sides effects. Additionally, antifungal resistance is on the rise. To develop new antifungals, a mechanistic understanding of *A. fumigatus* pathogenicity is required. This thesis will address current methodologies available to phenotype large collections of mutants for fitness, infection-related stresses and invasion and will identify transcription factors required for these processes by utilising the genome-wide transcription factor knockout library.

Gene expression is tightly regulated at the transcriptional level. This project outlines the importance of transcription factors in azole resistance as a pilot phenotype screening and explores the regulatory mechanism of the multi-drug resistant negative cofactor transcription factors, NctA and NctB. These key regulators control many processes, including ergosterol biosynthesis, a direct target of the azoles.

Additionally, the transcription factor knockout library is screened under infection-related stresses, for detachment and cytotoxicity of epithelial cells. This first in field screening identifies previous uncharacterised transcription factors and explores new phenotypes for previous characterised transcription factors. Furthermore, regulators required for environmental adaptation are a distinct set from ones required for epithelial invasion. This provides the first evidence for the accidental pathogen hypothesis.

Lastly, the genome editing technique CRISPR-Cas9 is explored to allow marker-free transformation in *A. fumigatus.* This technique can be used for gene replacement and epitope tagging without the need of labour- and time-intensive construct generation. Furthermore, marker-free transformation will reduce the chance of off-target effects.

Declaration

No portion of the work referred to in the thesis has been submitted in support of an application for another degree or qualification of this or any other university or other institute of learning

Copyright Statement

i. The author of this thesis (including any appendices and/or schedules to this thesis) owns certain copyright or related rights in it (the "Copyright") and s/he has given The University of Manchester certain rights to use such Copyright, including for administrative purposes.

ii. Copies of this thesis, either in full or in extracts and whether in hard or electronic copy, may be made only in accordance with the Copyright, Designs and Patents Act 1988 (as amended) and regulations issued under it or, where appropriate, in accordance with licensing agreements which the University has from time to time. This page must form part of any such copies made.

iii. The ownership of certain Copyright, patents, designs, trademarks and other intellectual property (the "Intellectual Property") and any reproductions of copyright works in the thesis, for example graphs and tables ("Reproductions"), which may be described in this thesis, may not be owned by the author and may be owned by third parties. Such Intellectual Property and Reproductions cannot and must not be made available for use without the prior written permission of the owner(s) of the relevant Intellectual Property and/or Reproductions.

iv. Further information on the conditions under which disclosure, publication and commercialisation of this thesis, the Copyright and any Intellectual Property and/or Reproductions described in it may take place is available in the University IP Policy (see http://documents.manchester.ac.uk/DocuInfo.aspx?DocID=2442 0), in any relevant Thesis restriction declarations deposited in the University Library, The University Library's regulations (see http://www.library.manchester.ac.uk/about/regulations/) and in The University's policy on Presentation of Theses

Acknowledgements

Firstly, I would like to thank my family and friends for all of their support and care, especially my girlfriend Francesca who have encouraged me from the day we met. Francesca: Rwy'n dy garu di, for all the times I made fun of your language. All the sleepless night, thanks to my feline companion Bubba, not only provided many a night-time lightbulb moments, but probably also fuelled my caffeine addiction. I would also like to thank my mother; voor al het aanhoren van mijn gezeur en langdurige telefoongesprekken wanneer ik het nodig had. Ik hoop dat ik je trots blijf maken!

I would like to extend my gratitude to my supervisors Prof Elaine Bignell and Dr Mike Bromley for their expertise, knowledge and guidance throughout my PhD. Over the last 5 years during my Masters and PhD they have been a source of inspiration and pushed me when I needed it. I'm confident the skills I have developed in this lab will be instrumental in my future career. I would like to thank Takanori for a productive lab bromance, that our output may never go unnoticed.

Also, I'd like to share my thanks with the rest of the Manchester Fungal Infection Group members who have helped me with numerous experiments and supported me with cake and coffee throughout my PhD.

Lastly, I would like to thank everyone who doubted me. Proving you wrong has driven me and been a source of constant motivation.

Chapter

1

Introduction and Aims

1.1 Overview of thesis

This thesis is written in an alternative format. Chapter 1 will provide the context of the thesis, Chapters 2-4 are written as manuscript, which are either submitted, or in the process of being submitted soon. Chapter 5 presents general conclusions and future work. The format has been modified with figures and tables near the citation to provide consistency throughout the thesis. The contributions of each author is listed below:

Chapter 2: The Negative Cofactor 2 complex is a master regulator of drug resistance in Aspergillus fumigatus.

Authors: Takanori Furukawa†, Norman van Rhijn†, Marcin Fraczek, Fabio Gsaller, Emma Davies, Paul Carr, Sara Gago, Rachael Fortune-Grant, Sayema Rahman, Jane Mabey Glisenan, Emma Houlder, Caitlin Kowalski, Shriya Raj, Sanjoy Paul, Josie Parker, Steve Kelly, Robert A. Cramer, Jean-Paul Latge, Peter Cook, Scott Moye-Rowley, Elaine Bignell, Paul Bowyer, Michael J Bromley

†The authors wish it to be known that, in their opinion, the first two authors should be regarded as joint First Authors.

Target Journal: Nature communications

Abstract:

The frequency of antifungal resistance, particularly to the azole class of ergosterol biosynthetic inhibitors is a growing global health problem. Survival rates for those infected with resistant isolates are exceptionally low. Although our understanding of the molecular basis of clinically significant azole resistance is limited, data from the fungal pathogen *Aspergillus fumigatus* indicates that resistance is associated with transcriptional modifications that potentiate ergosterol biosynthesis without significantly compromising pathogenicity. Based on this evidence, we reasoned that clinically relevant antifungal resistance could derive from transcriptional rewiring, promoting drug resistance without concomitant reductions in pathogenicity. In order to identify transcriptional regulators, which have the potential to drive clinically relevant resistance phenotypes, we constructed a genome-wide library of 484 null mutants. Here we describe that loss of the negative cofactor 2 complex leads to resistance, not only to the azoles but also the salvage therapeutics amphotericin B and terbinafine without significantly affecting pathogenicity.

Authors' Contributions:

Takanori Furukawa: Itraconazole phenotype screening, RNA-seq and ChIP-seq experiments and analysis, *In vivo* cytokine analysis

Norman van Rhijn: Itraconazole phenotype screening, Phenotypic analysis, Sterol content analysis, Bioinformatic analysis, *In vivo* survival experiments, *In vitro* cytotoxicity and macrophage damage, SEM and TEM analysis, MIC analysis

Marcin Fraczek: Transcription factor knockout generation

Fabio Gsaller: Transcription factor knockout generation

Emma Davies: Co-immunoprecipitation of NctA

Paul Carr: Transcription factor knockout generation

Sara Gago: *In vitro* cytotoxicity and macrophage damage

Rachael Fortune-Grant: Technical support with *in vivo* experiments

Sayema Rahman: Microscopic analysis

Jane Mabey Gilsenan: Bioinformatic primer design for knockout generation

Emma Houlder: *In vitro* cytokine analysis

Caitlin H. Kowalski: Support with *in vivo* experiments

Shriya Raj: Validation of transcription factor library (Southern Blot)

Sanjoy Paul: Western blot

Josie Parker: Sterol content analysis

Steve Kelly: Sterol content analysis

Robert A. Cramer: Support with *in vivo* experiments

Jean-Paul Latge: Support with library validation

Peter Cook: Support with *in vitro* and *in vivo* cytokine analysis.

Scott Moye-Rowley: Western blot

Elaine Bignell: Support with *in vivo* experiments, project supervisor

Paul Bowyer: Advisor on transcription factor knockout generation

Michael J Bromley: Project supervisor

Chapter 3: Genetically distinct transcriptional circuits drive stress-adaptation and host cytotoxicity in a mould pathogen of the human lung

Authors: Norman van Rhijn†, Takanori Furukawa†, Sayema Rahman, Panos Papastamoulis, Frans Rodenburg, Rachael Fortune-Grant, Magnus Rattray, Elaine Bignell, Michael J Bromley

†The authors wish it to be known that, in their opinion, the first two authors should be regarded as joint First Authors.

Target Journal: Nature Microbiology

Abstract:

Aspergillus fumigatus is a saphrophytic environmental mould, which can cause life threatening lung diseases in humans. Inhaled spores are able to reach deep into the alveoli due to their small size and airborne buoyancy. Here, the fungus is able to resist to exogenous stress imposed by the lung environment and grow, when not sufficiently cleared by the immune system. Regulation of adaptation within the lung is tightly regulated by transcription factors. Here, we explore transcription factors that are required for fitness, adaptation to environmental stress and epithelial invasion by high-throughput phenotyping of a genome wide transcription factor null library. This resulted in identification of two distinct regulatory networks required for adaptation and invasion, pointing towards the environmental nature of this fungus and lays the basis for exploring the coincidental evolution of pathogenicity theory.

Authors' Contributions:

Norman van Rhijn: Fungal RPMI development and optimisation, growth curve experiments and analysis, high-throughput phenotyping experiments and analysis, multifactorial stress phenotyping and analysis, analysis of slow growing mutant phenotyping, murine studies and analysis, RNA-seq experiment and analysis, Aspergillus species stress experiments, analysis of detachment and cytotoxicity

Takanori Furukawa: Fungal RPMI development and optimisation, Growth curve experiments, high-throughput phenotyping experiments

Sayema Rahman: Detachment and Cytotoxicity screening, Cytotoxicity and microscopic analysis slow growing mutants

Panos Papastamoulis: Bioinformatic support for single stress screenings and growth curves

Frans Rodenburg: Bioinformatic support for multifactorial stress

Rachael Fortune-Grant: Technical support murine studies

Magnus Rattray: Support with bioinformatics

Elaine Bignell: Project supervisor

Michael J Bromley: Project supervisor

Chapter 4: Development of marker-free gene tagging and gene mutation system using a CRISPR-Cas9 mediated transformation in the pathogenic mold Aspergillus fumigatus

Authors: Norman van Rhijn, Takanori Furukawa, Can Zhao, Beth McCann, Elaine Bignell, Michael J Bromley

Target Journal: Fungal Biology & Genetics

Abstract:

Aspergillus fumigatus is a saphrophytic fungal pathogen, which is the cause of more than 200,000 life-threatening infections annually. Our understanding of pathogenesis and factors contributing to disease progression are limited. Development of rapid and versatile gene editing methodologies is essential. CRISPR-Cas9 mediated transformation has been widely used as a novel genome editing tool. In *A. fumigatus*, this technique has been recently developed and used for a variety of editing techniques, such as protein tagging and gene deletions. However, successful transformation relies on extensive cloning paired with the use of selection markers. We have used an *in vitro* CRISPR-Cas9 assembly methodology to perform selection free transformations. The repair template used during this transformation can be obtained with a single PCR reaction, decreasing time required for difficult genome editing techniques such as protein tagging and gene deletion.

Authors' Contributions:

Norman van Rhijn: Development of CRISPR-Cas9 transformation system, screening of CRISPR mutants and analysis, Development of gene tagging and design of gRNA.

Takanori Furukawa: Development of CRISPR-Cas9 transformation system, development of gene tagging and design of gRNA, Western Blotting

Can Zhao: SrbA-GFP microscopy

Beth McCann: PacC-GFP microscopy

Elaine Bignell: Project supervisor

Michael J Bromley: Project supervisor

1.2 Fungi

The kingdom Fungi contains approximately 150,000 characterised species. Using molecular methods it has been estimated that there are 1.5 to 5.1 million species of fungi on Earth [1]. Most fungi grow as multinuclear cylindrical cells called hyphae. These structures can grow indefinitely and are used to penetrate substrates and extract nutrients from their environment. Due to nutritional versatility and the ability to degrade complex substrates such as polymers and hydrophobic molecules, fungi can be found in nearly every environmental niche [2]. Additionally, fungi have highly unique secretomes, ranging from cellulases to toxins to gain advantages over other microbes [3].

Fungi have evolved to thrive in various niches. They can be found as saprophytes, in symbioses with plants and algae, as predators, pathogens or parasites afflicting insects, birds, amphibians and mammals. Moreover, fungi have been used in biotechnology to produce many compounds ranging from antibiotics to natural flavourings. While the vast majority of fungi do not generally cause mycoses, around 400 species are able to cause infections in a range of hosts. This has been an increasing concern for various reasons. Firstly, a rapid rise in fungal infections has been observed in humans [4]. This has been associated with an increase of immunocompromised individuals and procedures that involve immunosuppression, such as chemotherapy and organ transplants [5]. Secondly, resistance to available antifungals is rising. Mortality for infections caused by antifungal resistant fungi is much higher and can be as close as 100% [6]. Lastly, fungi are evolutionarily more closely related to animals than to most other pathogens, increasing the difficulty in developing antifungals that are specific to these fungal pathogens [7].

1.3 Aspergillus and aspergillosis

Aspergillus species are saprophytic moulds, which are ubiquitous in the environment. They grow in organic material and have been associated with composting heaps. When the compost heaps are disrupted high concentrations of uninucleate spores are released into the air [8]. Airborne conidia (1-5 μm in diameter) are inhaled and are small enough to reach the lung alveoli. If conidia germinate, they produce hyphae that can invade lung tissue. Aspergillosis is a term that includes several diseases causes by *Aspergillus* species. From the more than 200

Aspergillus species reported, around 10% have been reported as human pathogens [9]. *Aspergillus fumigatus* is the main cause of morbidity and mortality among *Aspergillus* species (up to 90% of all *Aspergillus* related infections). There are three different forms of aspergillosis. These are allergic bronchopulmonary aspergillosis (ABPA), chronic pulmonary aspergillosis (CPA) and invasive aspergillosis (IA).

Allergic bronchopulmonary aspergillosis (ABPA) is a fungal allergic disease occurring as a common complication of other respiratory diseases such as asthma, COPD or cystic fibrosis. ABPA burden of disease has been estimated as 3.5 million cases annually, while Severe Asthma with Fungal Sensitization has been estimated at 4 million cases annually [10]. Affected patients exhibit a hypersensitive response of the immune system to *Aspergillus*, which is characterized as a T-cell shift towards a Th2 response [11]. Patients generally present with symptoms such as fever, wheezing, infiltrates combined with an increase in the number of asthma exacerbations. Diagnosis of ABPA is based upon 3 criteria: 1) predisposing asthma or CF, 2) an increase in IgE levels and increased eosinophils, IgG or 3) radiographic abnormalities [12]. The majority of ABPA patients (~60%) respond to treatment with an azole antifungal, which can be supplemented with corticosteroids to suppress the hyper-immune response [13].

CPA is a long-term illness. CPA has an estimated incidence of 3 million cases worldwide, with a mortality rate of 15% in the first 6 months and of 80% over 5 years, which equates to 450,000 deaths annually [14, 15]. While the majority of CPA patients have an underlying disease, such as COPD, ABPA, asthma or lung cancer, CPA is not restricted to patients diagnosed with these underlying diseases. Several forms of CPA are clinically recognised. The most common form is chronic cavitary pulmonary aspergillosis, which can develop into chronic fibrosing pulmonary aspergillosis. These forms are generally found in patients that are not immunocompromised, such as asthma and COPD patients. Subacute invasive pulmonary aspergillosis is found in slight immunocompromised patients, such as lung cancer patients, and can develop into invasive aspergillosis if not diagnosed in a timely manner and treated appropriately. Diagnosis of this spectrum of diseases is based upon three main characteristics; radiological evidence such as *Aspergillus* nodules or a fungal ball, microbiological evidence including molecular detection and

an immunological response. It has been recommended if possible to remove affected tissue by surgery combined with long-term antifungal treatment [16]. However, long-term antifungal treatment can cause resistance or severe adverse effects. Therefore, continuous monitoring is recommended [17].

The most severe form of aspergillosis is the invasive form of the disease. Invasive aspergillosis (IA) is a life-threatening infection occurring worldwide with mortality rates ranging from 30-95% [18]. It was estimated that worldwide more than 3,000,000 fungal infection cases per year occur, corresponding to around 200,000 deaths by invasive aspergillosis per annum [10]. This aggressive fungal disease is mainly found in immunocompromised hosts. Populations at high risk are CGD, neutropenic and solid organ or allogeneic bone marrow transplant patients. In allogeneic hematopoietic stem cell transplant recipients the one-year incidence was 7.5% in a retrospective cohort study [19].

These cohorts of patients are at high risk of developing secondary infectious complications. Extensive monitoring paired with prophylaxis is essential for patient survival. Early diagnosis improves the outcome of disease drastically [20]. Therefore, effective laboratory diagnostics are key for treatment. Presentation of fever despite antibiotic treatment in neutropenic patients, paired with chests pain and coughs are indicative of IA. In these patients, the gold standard for diagnosis relies on laboratory culture and radiological imaging [21]. However, these methods have low sensitivity and are dependent on subjective interpretation from the clinician. In recent years, serological techniques based on the detection of galactomannan and beta-glucan has been used to monitor patients [22]. These assays are based upon fungal specific molecules. Beta-glucan is a cell wall component that can be found in all fungi, while galactomannan is found in *Aspergillus, Fusarium* and *Penicillium* species. While these assays have a high specificity, they lack sensitivity and are not available on a global scale [23].

In recent years, *Aspergillus* DNA detection based on polymerase chain reaction (PCR) is upcoming as a diagnostic tool. The strength of this method is: the signal is amplified, which can work on a range of clinical samples, resulting in high sensitivity [24]. Quantifying this signal can distinguish between colonization and infection, making this a strong diagnostic tool [25]. Furthermore, PCR methods can

be modified to either detect fungi, *Aspergillus* species or specific *Aspergilli*. However, to date no standard protocol for DNA extraction and amplification has been produced, preventing study comparisons [26]. Being able to extract DNA of clinical samples also allows monitoring of resistance. Through either sequencing or qPCR, point mutations commonly seen in resistant isolates can be amplified. Commercial kits are available, but require specialist equipment that is expensive and requires intensive maintenance [27].

Aspergillus fumigatus is able to invade lung tissue, when spore clearance does not occur, and causes damage to the host tissue. In the mammalian lung growth conditions are not optimal and the fungus must adapt to a range of stresses. Adaptation to maintain growth and overcome killing by the immune system is tightly regulated at the transcriptional level [28]. Several transcription factors have previously been linked to regulate an important aspect of *Aspergillus* infection (see Table 1.1). These can be classified into adaptation to development, nutrient acquisition, environmental stress, host-pathogen interaction and secondary metabolism. This discussion will focus on nutrient acquisition and environmental stress adaptation.

Table 1.1: Previously characterized transcription factors in *A. fumigatus*

	TF	AF293 Locus ID	Function	Reference(s)	Required for pathogenicity
Conidiation and development	Ace2	Afu3g11250	Conidial formation, cell wall architecture	Ejzykowicz et al. (2009)	+ (CA), -
	BrlA	Afu1g16590	Condiation, hyphael maturation	Twumasi-Boaten et al (2009)	NP
	MtfA	Afu6g02690	Conidiation, protease and gliotoxin production	Smith and Calvo (2014)	✓
	AbaA	Afu1g04830	Coniditation	Tao and Yu (2011)	NP
	StuA	Afu2g07900	Asexual reproduction, secondary metabolite pathways	Sheppard et al. (2005) Twumasi-Boateng et al. (2009)	-
	MybA	Afu3g07070	Conidiation, maturation	Valsecchi et al. (2017)	✓
	FlbB	Afu1g03210	Morphological development, gliotoxin production	Xiao et al. (2010)	NP
	FlbC	Afu2g13770	Asexual development	Xiao et al. (2010)	NP
	FlbD	Afu1g0210	Asexual development	Xiao et al. (2010)	NP
	NsdC	Afu3g13870	Asexual development/sexual development	Gross et al. (2008)	NP
	Ads4	Afu1g16460	Antifungal azole stress	Szewczyk et al. (2010)	NP
	NosA	Afu4g09710	Sexual development	Soukup et al. (2012)	+ (hyper)
Adhesion	MedA	Afu2g13260	Biofilm formation, adherence	Gravelat et al. (2010) Al Abdallah et al. (2012)	✓
	SomA	Afu7g02260	Conidiation, adhesion	Lin et al. (2015)	✓ (Tet mutant)
Nutrient acquisition	SrbA	Afu2g01260	Hypoxia response, ergosterol biosynthesis, siderophore biosynthesis	Blatzer et al. (2011) Chung et al. (2014) Willger et al. (2008)	✓
	SrbB	Afu4g03460	Hypoxia response, carbohydrate metabolism, heme biosynthesis	Chung et al. (2014)	✓
	AtrR	Afu2g02690	Hypoxia response, ergosterol biosynthesis	Hagiwara et al. (2017), Paul et al. (2019)	✓
	Afmac1	Afu1g13190	Copper starvation	Kusuya et al. (2017), Wiemann et al. (2017)	Conflicted reports
	AceA	Afu6g07780	Copper toxicity	Wiemann et al. (2017)	✓/-
	CufA	Afu2g01190	Copper binding TF	Wiemann et al. (2017)	-
	HapX	Afu5g03920	Iron homeostasis (deplete conditions)	Brandon et al. (2015) Schrettl et al. (2010)	✓
	SreA	Afu5g11260	Iron homeostasis (replete conditions)	Brandon et al. (2015) Schrettl et al. (2008)	-
	AcuK	Afu2g05830	Gluconeogenesis, iron acquisition	Pongpom et al. (2015)	✓/-
	AcuM	Afu2g12330	Gluconeogenesis, iron acquisition	Liu et al. (2010) Pongpom et al. (2015)	✓
	CrzA	Afu1g06900	Calcium homeostasis	De Castro et al. (2014) Soriani et al. (2008) Cramer et al. (2008)	✓
	MetR	Afu4g06530	Acquisition of inorganic sulfur	Amich et al. (2013)	✓
	LeuB	Afu2g03460	Leucine biosynthesis/ iron acquisition	Long et al. (2018)	✓
	ZafA	Afu1g10080	Zinc homeostasis	Amich et al. (2010) Amich et al. (2014) Moreno et al. (2007) Amich and Calera (2014) Vicentefranqueira et al. (2015)	✓
	AreA	Afu6g01970	Nitrogen utilization	Hensel et al. (1998) Krappmann et al. (2005)	✓
Environmental stress adaptation	PacC	Afu3g11970	Alkaline pH response	Bertuzzi et al. (2014) Amich et al. (2010) Tilburn et al. (1995)	✓
	SebA	Afu4g09080	Heat shock, nutrient and oxidative stress	Dinamarco et al. (2012)	✓
	HacA	Afu3g04070	Unfolded protein response	Richie et al. (2009) Richie et al. (2011)	✓
	CpcA	Afu4g12470	Cross-pathway control system	Krappmann et al. (2004)	✓
	Yap1	Afu6g09930	Oxidative stress response	Lessing et al. (2007) Qiao et al. (2008)	-
	AtfA	Afu3g11330	Conidia stress response	Hagiwara et al. (2014), Takahashi et al. (2017)	✓
	ZipD	Afu2g03280	Calcium/calcineurin-dependent response	Ries et al. (2017)	NP
	CreA	Afu2g11780	Hypoxic adaptation, carbon catabolite repression	Beattie et al. (2017)	✓/-
Host-pathogen interaction	DvrA	Afu3g09820	Host cell damage	Ejzykowicz et al. (2010)	+ (Gall), +(CA), - (CA,CP)
	RlmA	Afu3g08520	Cell wall integrity	Rocha et al. (2016) Valiante et al. (2016)	✓
Secondary metabolism	GliZ	Afu6g09630	Gliotoxin production	Bok et al. (2006)	-
	RsmA	Afu2g02540	Gliotoxin production	Sekonyela et al. (2013)	- (OE)
	HasA	Afu3g12890	hexadehydro-astechrome production	Yin et al. (2013)	+ (OE)
	FumR	Afu8g00420	Fumagillin production	Dhingra et al. (2013)	NP
	GipA	Afu6g01910	Gliotoxin production	Shorberle et al. (2014)	NP
	PrtT	Afu4g10120	Extracellular proteolytic activities	Bergmann et al. (2009)	-
	XprG	Afu8g04050	Protease prodution	Shemesh et al. (2018)	-
	LaeA	Afu1g14660	Secondary metabolite production	Bok and Keller (2004), Sugui et al (2007)	✓

1.4 Nutrient acquisition

Fungal growth is dependent on nutrient availability. Fungi have extreme metabolic plasticity and can utilise a wide range of molecules as nutrients. Carbon is one of the basic building blocks of life and is required for fungal growth. In the mammalian lung carbon availability varies per microenvironment. While in the airway surface liquid glucose levels are less than 0.5 mM, in serum levels are much higher typically being 3.5-5.5 mM [29]. Additionally, lactate is present within the airway surface liquid, which increases upon infection [30, 31]. An additional source of carbon and nitrogen that *A. fumigatus* could exploit would be mucin, the glycoprotein most available in the lung mucous layer [32]. The availability of carbon sources changes with corticosteroid treatment, showing that nutrients within the lung environment are flexible [33].

Glucose is sensed through two mechanisms: through G-protein Coupled Receptors (GPCRs) and through hexose transporters. In *A. fumigatus* there are 15 predicted GPCRs [34]. Nine classes of receptors are encoded by *A. fumigatus* with each class having a distinctive role in sensing [reviewed in [35]]. However, to date only three receptors, GprC, GprD and GprK, have been studied. Deletion of either one of these receptors changed colony morphology on media with several carbon sources. However, different behaviours were observed during infection. A GprK deletion strain was not significantly different from wild type in a wax moth larvae model [36]. A murine model of infection with the GprC deletion strain resulted in delayed mortality, while for the GprD deletion strain virulence was fully attenuated [37].

The *A. fumigatus* genome encodes 15 predicted hexose transporters. This is contrast to *A. nidulans,* which encodes 17 and *C. albicans,* which encodes 20 transporters [38]. In *C. albicans* expression of these transporters vary according to the microenvironments encountered within the host [39, 40]. To date only the *HGT4* transporter has been assessed for virulence in an immunocompetent systemic murine model. Deletion of this transporter resulted in increased survival of mice [41].

While *A. fumigatus* preferably uses glucose as a carbon source, it can use a variety of substrates. To regulate metabolism and maximise nutrient usage, many microbes use carbon catabolite repression (CCR). In *A. fumigatus* this process is

regulated by the CreA transcription factor [33]. This transcription factor normally binds to the promoter of genes required under carbon repressing conditions, downregulating these. On non-preferable carbon sources, such as ethanol, urea and lactate, this transcription factor activates carbon-repressing genes by releasing itself from their promoters [42]. Interestingly, this transcription factor is required under poor nitrogen conditions, which was not observed in other organisms [33]. In several *A. fumigatus* isolates a different response was found in the CCR in response to several carbon sources. No correlation between the ability to utilise non-favourable carbon sources and virulence could be found. However, difference in CCR and nitrogen metabolism related protease secretion play an important role during murine infection [43].

Nitrogen is an essential building block for protein synthesis. In general, the preferred source of nitrogen is in the form of ammonium and glutamine. These two molecules are linked by glutamine synthetase, which can convert ammonium and glutamate into glutamine [44]. Fungi have developed nitrogen sensing and uptake systems that are highly complex. Uptake of ammonium in *C. albicans* is regulated by two ammonium permeases, *MEP1* and *MEP2* [45]. *A. fumigatus* contains homologues of these permeases, but these have not been characterised to date.

In fungi, the main sensory pathway for nitrogen is the target of rapamycin (TOR) pathway. *C. albicans* and *A. fumigatus* encode one TOR kinase, while several other fungi encode two TOR kinases. Deletion of this single TOR kinase results in inviability [46]. In *A. fumigatus* this kinase, called TorA, regulates amino acid transport and metabolism. The phosphatase involved in this pathway, SitA, is involved in cell wall integrity as well as adhesion. Moreover, deletion of this phosphatase results in an avirulent strain in a neutropenic murine model of infection [47]. On non-preferable nitrogen sources the nitrogen catabolite repression pathway is activated. In *A. nidulans,* NmrA mediates regulation of this pathway, by repressing genes under favourable conditions and de-repressing upon non-favourable conditions [48]. However, this regulator has not been characterised in *A. fumigatus*.

Upon detection of non-favourable nitrogen sources, the fungus switches to nitrogen catabolism and the expression of genes required for utilisation of these alternative nitrogen sources. In *A. fumigatus* this process is regulated by the AreA

transcription factor. Deletion of this transcription factor results in growth defects upon alternative nitrogen sources. The deletion strain showed significant delay of murine mortality in a neutropenic model of infection [49]. Moreover, growth *in vivo* was significantly reduced. In *A. nidulans* NmrA interacts with AreA to prevent it from activating catabolic genes [50] and involves another transcription factor called MeaB, which mirrors NmrA in expression patterns.

To scavenge nitrogen fungi can secrete proteases to degrade proteins. Released peptides and amino acids can be used as a nutrient source. Expression of proteases is upregulated upon nitrogen starvation linking these processes [51]. *A. fumigatus* has an arsenal of at least 99 secreted proteases [52]. Secretion of these proteases is regulated by the transcription factor PrtT. While this transcription factor is essential for secretion of these proteases, deletion of this regulator is not essential for virulence in murine models of infection [53]. However, further study of functionality of these proteases is required and their role during infection.

1.4.1 Amino Acids

While humans are not able to produce their own amino acids, fungi are autonomous in their production through multiple biosynthesis pathways. Absence of these pathways in humans makes amino acid biosynthesis a focal point for antifungal drug development [54]. Amino acids are derived from several carbon intermediates via enzymatic reactions. Most of these pathways are essential for pathogenicity of *A. fumigatus* as biosynthesis is essential for growth under amino acid limiting conditions [55]. However, relatively high concentrations of amino acids can be found within the blood and intracellularly in most tissues [56, 57]. From 22 amino acids that exist, essentiality has been assessed for lysine, valine, leucine, histidine, alanine, trypthophane, tyrosine, methionine and cysteine [58].

Lysine biosynthesis has been studied in detail as a drug target. Via the alpha-aminoadipate pathway, acetyl-CoA and alpha-ketoglutarate are converted into homocitrate, which is further processed into lysine via several enzymes including *HscA*. Deletion of the gene encoding this enzyme resulted in growth defects if not supplemented with lysine. While this null mutant was attenuated in a murine model of infection, supplementation with lysine in the drinking water restored pathogenicity [59].

Additionally, as part of the valine biosynthetic pathway, 2-ketoisovalerate can be converted into alpha-isopropylmalate, which will activate the *leu3/leuB* transcription factor. Interestingly, this will not only induce the leucine biosynthetic pathway, but also nitrogen and iron metabolism. Characterisation of the LeuB transcription factor showed binding of the transcription factor to promoter regions of genes involved amino acid biosynthesis, but not limited to leucine, iron, nitrogen and sulphur metabolism. Functionality of these pathways seems to be essential for virulence as a LeuB null mutant showed attenuated pathogenicity in a *Galleria* infection model [60].

Production of histidine is governed by condensation of PRPP and ATP via several enzymatic reactions. Histidine binds free metals easily and is therefore tightly linked to iron metabolism. This crosstalk between pathways made the *hisB* gene, encoding imidazoleglycerol-phosphate dehydratase, an interesting target for antifungal drug development. A *hisB* null mutant in *A. fumigatus* did not only show a histidine auxotrophy but was required for heavy metal resistance except to cadmium [61]. Furthermore, a hypoxic environment reduced the histidine requirement, likely due to upregulation of amino acid transporters [62]. Taken together, this lead to an attenuation of pathogenicity in both a murine intranasal and intravenous infection model [61].

The highly complex biosynthetic pathway generating methionine and cysteine was assessed for pathogenicity in *A. fumigatus*. Whilst the upstream part of the pathway, importing sulphate, was shown to be dispensable for pathogenicity, the downstream part is essential. Through generating a *cysB;mecA* double null mutant, the entire pathway could be inactivated. Single mutants were fully virulent, while the double mutant was attenuated showing the essentiality of this pathway for growth *in vivo* and pathogenicity [63]. Furthermore, the transcription factor involved in regulating methionine and cysteine biosynthesis, *metR,* was shown to be indispensible in a leukopenic murine model of infection [64].

1.4.2 Vitamins

Vitamins are essential micronutrients for fungal growth, which makes vitamin biosynthetic pathways interesting as antifungal targets. Several vitamin pathways (Vitamin A, C, D, E and K) were immediately excluded for antifungal drug

development, as these are either only present in plants or were not found to alter the fungus phenotypically or affect virulence. However, B vitamin biosynthetic pathways were found to be potential antifungal targets due to its importance as a cellular co-factor providing specificity to fungal species [65].

Thiamine (Vitamin B1) is not synthesized by animals. It is generally a cofactor for reactions involved in glycolysis, carbohydrate or amino acid biosynthesis. In *A. fumigatus* thiamine is either generated through a *thi6/thiB*-mediated reaction or through Thi7 uptake from the environment. While a *thiB* mutant was slightly attenuated, no difference in fungal load was found. Therefore, the mammalian lung environment must supply enough thiamine to support fungal growth [61]. Riboflavin (Vitamin B2) plays an important role in metabolism as it is used by over 200 flavoproteins. Furthermore, it was found that a mutant deficient in riboflavin biosynthesis was unable to grow on iron limiting media and produced less siderophores [61]. This mutant was attenuated in three murine models of infection with severely reduced fungal load. Through a small-molecule screening for antifungal activity two components were found that are able to inhibit riboflavin biosynthesis [66]. A similar connection between siderophore production and vitamin biosynthesis has been found for pantothenic acid (Vitamin B5). A deletion mutant, *panA/pan6*, was attenuated in a murine infection model [61]. However, no antifungals inhibiting this pathway have been developed.

1.4.3 Trace elements

Iron at micromolar levels is an essential nutrient for fungal growth. Iron can be found in many forms and is mainly used as heme or iron-sulfur clusters for multiple processes within the cell. This includes respiration and acquisition of nitrogen, TCA cycle and biosynthesis of many compounds such as amino acids, sterols and lipids [reviewed in [67]]. Due to the capability of iron to lose or gain electrons, it is used during many enzymatic reactions. However, at pH 7 iron exists predominantly as $Fe(OH)_2$, which has a solubility below the capacity of iron uptake systems [68]. Therefore microorganisms have evolved to overcome this problem.

In the mammalian lung iron can be found in high abundance. Not only through circulating iron, but also through iron particles from the atmosphere. To protect cells from iron excess, several approaches have been adopted. First, the mucoid layers on

epithelial cells contain high levels of antioxidants and mucins to reduce iron availability [69]. Secondly, airway secretions contain high levels of lactoferrin and transferrin, which can bind iron to make it unavailable for further reactions since excess can cause oxidative damage [70]. When high concentrations of iron are reached, this functions as a catalyst for the production of reactive oxygen species, which can damage lipids, protein and can cause cell lysis. Epithelial cells take up these molecules and the iron is transferred to ferritin, a large molecule that can store up to 4000 iron atoms [71].

Iron acquisition in *A. fumigatus* is regulated by two systems, siderophore-mediated iron uptake and reductive iron assimilation. Reductive iron assimilation is *A. fumigatus* specific and not found in other *Aspergilli*. Metalloreductases reduce ferrous iron to a more soluble form for uptake. Siderophore-mediated iron uptake is performed by excretion of siderophores, iron-binding compounds. These compounds sequester iron from the host cells and chelate iron and are taken up by the fungal cell in their ironbound form. Iron acquisition is a key driver of infection as a deficiency in intracellular and extracellular siderophores leads to avirulence in mouse models of aspergillosis [72].

The main transcription factors regulating iron acquisition are HapX and SreA. SreA represses HapX when intracellular iron levels are high and HapX represses SreA when intracellular iron levels are low, acting as a negative feedback loop [73]. SreA belongs to the GATA transcription factor family and is expressed during high iron levels. It functions as a repressor of iron uptake to avoid reaching toxic levels of intracellular iron. HapX is a Janus transcription factor that regulates genes through protein-protein interaction with the CCAAT-binding complex (CBC) [74]. Expression of the HapX transcription factor is regulated by several other transcription factors, which are not involved in the iron regulatory pathway.

A systems biology approach to map the regulatory network for iron acquisition in *A. fumigatus* was used to predict interactions between transcription factors and genes via the NetGenerator tool [75]. The advantage of this software is that prior knowledge can be used to refine the network. The model calculates the influence of genes on one other, either as activator or repressor, from previous data obtained from transcriptomics. However, the model does not require a physical interaction.

Validation of this network by physical binding experiments, such as ChIP-Seq, is therefore required. However, this model revealed new regulatory interactions between HapX, SrbA and the PacC transcription factor [76].

Another trace element that has been studied in more detail is zinc. Zinc is an essential element for homeostasis and growth of microorganisms. It has been estimated that about 5% of fungal proteomes are zinc binding proteins [77]. However, in the mammalian lung the levels of zinc are considered low as it is instead bound to proteins, such as calprotectin. Calprotectin is secreted in high levels by neutrophils, chelating not only zinc but also manganese [78]. This has been shown to limit *A. fumigatus* hyphal growth [79]. However, manganese limitation by the host during *A. fumigatus* infection has not been studied. To utilize zinc, *A. fumigatus* regulates zinc uptake through the transcription factor ZafA by inducing zinc transporters. The ZafA transcription factor and one of the zinc transporters was shown to be essential for pathogenicity [80].

Not only zinc and iron are linked, but also copper acquisition is tightly associated to iron acquisition. The transcription factor Afmac1/MacA has been shown to be indispensible for copper acquisition and virulence [81, 82]. Furthermore, this transcription factor regulates the iron regulon and transcription factors HapX, SrbA and SreA through the copper-binding motif [83]. Interestingly, a deficiency in copper acquisition resulted in significantly lower sporulation. Copper homeostasis is involved in many biochemical processes such as the generation of superoxide dismutases (SODs) and laccases. A reduction of laccases results in less biosynthesis of DHN-melanin and lower sporulation [84]. While copper acquisition is essential for the fungal cell, high copper levels result in elevated levels of reactive oxygen intermediates (ROI). Therefore, copper efflux is regulated by the AceA transcription factor [85]. Inability to detoxify the cell from copper is tightly linked to reactive oxygen species stress and defense to the host immune system. Inhibition of the NOX complex in mice, mimicking CGD, could remediate *ΔaceA* pathogenicity [85].

1.5 Environmental stress tolerance

1.5.1 pH tolerance

pH stress is one of the major stresses that the fungus can encounter within microenvironments. A change in pH causes a number of types of stresses. First and foremost, changes in pH alter the availability of nutrients. Solubility of, for example, iron is drastically lower under alkaline pH, while zinc bioavailability is lowered under acid conditions. Furthermore, secondary metabolite production is affected by pH [86]. A change in environmental pH alters the membrane potential of the plasma membrane as a differential proton gradient is being maintained intracellularly and extracellularly [87]. Alkalinasation of the environment, such as the mammalian lung, has shown to impair phospholipid flipping and cause depolarization of the plasma membrane. Induction of depolarization or impairing membrane flipping in *Saccharomyces cerevisae* has a similar effect on the cell as alkalinisation by activating the same pathways [88]. Adapting to an alkaline environment has been shown to involve cell wall remodeling and activation of proton and ion pumps [89]. This has been shown to be crucial for *A. fumigatus* survival in the mammalian lung, which has a slightly alkaline environment [90].

The PacC/Rim pathway is one of the best studied pH response signaling pathways in fungi, especially in *A. nidulans* [91]. In *A. nidulans* there are two membrane-bound pH-sensing proteins, PalI and PalH. In an alkaline environment the arrestin-like protein PalF is phosphorylated and ubiquitinated in a PalH-dependent manner. The ubiquitination event gives rise to recruitment of PalC and various components of the ESCRT complex of the endosome [92]. PalA and PalC colocalise with the Vps24 interactor PalB at alkaline pH-induced cortical structures [93]. PalB is a cysteine protease which effects the pH-dependent processing of PacC from a 72-kDa precursor into a 53-kDa, and finally to a 27-kDa form [94]. The active 27-kDa form is translocated to the nucleus where it acts as a transcription factor that activates genes involved in the alkaline response and represses genes involved in the acidic response [95].

In *A. fumigatus* PacC is required for pathogenicity and for epithelial invasion [89]. However, differences in alkaline responsive genes between *A. nidulans* and *A. fumigatus* have been found. In *A. nidulans* the calcium-signaling pathway, mediated by the CrzA transcription factor, can activate alkaline responsive genes. This

interconnectivity has not been found in *A. fumigatus* where the two pathways are completely independent of each other [96]. However, a link between *pacC* and zinc regulation was found through the *zrfA* and *zrfB* zinc transporters [97]. These genes are repressed in a PacC-dependent manner under alkaline conditions, suggesting an additional regulatory role for PacC under acidic conditions [98].

1.5.2 Cell wall stress

Fungi are characterised by having a cell wall, an outer layer of mostly polymers of sugar that is highly adaptable. By changing the composition of the cell wall the fungus can adapt to stresses from the external environment or stress from internal pressure and turgor [99]. Generally, the core of the cell wall consists of branched beta-1,3-glucan-chitin. However, the *A. fumigatus* cell wall consists of additional alpha-1,3-glucan, galactofuran and mannan [100]. Several proteins are part of the cell wall, such as hydrophobins. These hydrophobins differ per morphological stage of growth [101]. Dormant conidia consist of an envelope of RodA proteins, which shield the spores from detection by the immune system [102]. Furthermore, the cell surface of *A. fumigatus* is coated with melanin, which has been shown to shield from environmental stressors and have effect on the immune response [as reviewed in [103]].

To overcome cell wall stresses, the cell activates several pathways such as the cell wall integrity (CWI), the TOR, Calcineurin and cAMP pathways [46, 104, 105]. The CWI pathway consists of several components. Several sensors can lead to activation of these pathways. *A. fumigatus* contains four putative CWI and stress response components (WSC) receptors, Wsc1, Wsc2, Wsc3 and Mid2. These receptors likely operate in a redundant manner, as phenotypes could only be found upon deletion of multiple receptors [106]. From studies on the receptors in *S. cerevisiae* it was suggested that these receptors operate as nanosprings, detecting mechanical stress directly [107]. Other receptors such as the GprC and GprD receptors also play a role in CWI as deletion resulted in reduced growth under stress conditions [37]. Interestingly, other proteins have been identified that activate the CWI pathway. For example, the mucin MsbA is involved in activation of this pathway [108]. However, to date the mode of activation and its interaction has not been studied in detail.

Signal from the receptors are transduced via a MAPK module, consisting of MAP kinases that are activated upon phosphorylation. The two components upstream of this module are Rho1 and PkcA. Both of these proteins are essential in *A. fumigatus* suggesting additional roles besides the CWI pathway [106, 109]. The last component called MpkA moves into the nucleus upon activation where it interacts with transcription factors [110]. MpkA activates the RlmA transcription factor, which upregulates expression of chitin synthases and glucanases to modify the cell wall [111]. This pathway is upregulated upon caspofungin exposure and involved in the paradoxical effect [112]. Furthermore, deletion of any of the components results in an attenuated strain in a murine model of infection, making this pathway of interest for antifungal development. Besides the RlmA transcription factor, it has been suggested that the DvrA and Ace2 transcription factors have a role in CWI. Deletion strains exhibit hypersensitivity to cell wall perturbing agents. Interestingly, both of these strains are more virulent than the wild type in a murine model of infection [113, 114].

Another pathway involved in regulating the cell wall and membrane is the high osmolarity glycerol (HOG) pathway. Salts, like NaCl or KCl cause osmotic and cation stress. These stresses change the flow of water and influence the transport of substrates, resulting in deflating of the cell [115]. To combat these stresses the HOG pathway is activated resulting in activation of glycerol biosynthetic genes and carbohydrate metabolism [116]. Adding additional glycerol to the media stabilised the cell wall and membrane to allow turgor to restabilise [117]. The HOG pathway consists of the MAPK module including the SskB, SakA and MpkC kinases. SakA and MpkC are homologues of the *S. cerevisiae* Hog1, the main regulator of the HOG pathway. However, these kinases differ in their reponse to environmental stress. The MpkC deletion mutant is unable to grow on complex carbon sources, while the SakA deletion mutant is hypersensitive to high osmolarity [118]. Both of these strains are attenuated in a murine model of infection. Both these kinases are activated and translocate to the nucleus upon osmotic stress [119]. Furthermore, these kinases physically interact during osmotic stress [120]. In *A. nidulans* it was shown that these kinases have distinct and sometimes opposing effects during general growth but common roles during environmental stress [121]. However, this is yet not assessed in *A. fumigatus*.

Downstream of this MAPK module is the AtfA transcription factor. The AtfA transcription factor is expressed at high levels during asexual development, which seems to be in an MpkC independent manner, suggesting posttranslational activation. This transcription factor regulates genes important for stress resistance during germination of conidia [122]. *A. fumigatus* encodes multiple ATF1 transcription factors, AtfA-D. Mainly AtfA and AtfB seem to be involved in adaptation to osmotic stress and cell wall damage. AtfA and AtfB are attenuated in a *Galleria mellonella* model while AtfC and AtfD are as virulent as wild type [123]. Interestingly, cross talk between the HOG pathway and the Calcineurin pathway has been observed. The transcription factor CrzA directly regulates SskB and the PhkB kinase of the HOG pathway [124].

Calcineurin is composed of two subunits, CnaA and CnaB. These subunits have their own functions, the CnaA is the catalytic protein and the CnaB is the regulatory [125]. This complex is activated through binding of Ca^{2+}-calmodulin (CaM) [126]. Calcineurin is highly conserved throughout eukaryotes, but exhibits different functions per organism. In *S. cerevisiae* calcineurin is required for cell wall integrity, cation homeostasis, mating and adaptation to several environmental stresses [127]. In *C. albicans* it regulates adaptation to alkaline pH, high temperature and dimorphism [128]. In *A. fumigatus* calcineurin is required for stress adaptation, cell wall integrity and hyphal growth [129]. Upon increased calcium in the cytosol, calcineurin activates the CrzA transcription factor [130].

The CrzA transcription factor accumulates in the cytosol to be dephosphorylated by calcineurin [131]. This will localise it towards the nucleus where it activates genes with the calcineurin-dependent response element at their promoters [132]. These genes are involved in calcium homeostasis, cell wall integrity and stress adaptation. Regulation of calcium homeostasis is achieved through activation of several calcium pumps, the PmrA, PmcA and PmcB calcium ATPases [124, 133, 134]. Deletion of *crzA* caused a downregulation of several transcription factors, which might explain its phenotype when exposed to other environmental stresses [135]. One of these is the ZipD transcription factor. This transcription factor regulates chitin synthases and is involved in resistance to caspofungin and high

calcium concentrations [136]. However, other transcription factors directly or indirectly regulated by CrzA have not been characterised to date.

1.5.3 Hypoxia

Most microorganisms are obligatory aerobic using oxygen for essential biochemical reactions within the cell. Oxygen functions as an electron acceptor during respiration. Energy is stored in the form of ATP by oxidising glucose into carbon dioxide and water. This is where pyruvate, generated from complex carbon sources, is reduced through the citric acid cycle.

It is generally accepted that during infection hypoxic conditions (reduction of available oxygen) occur. Within the alveoli, the oxygen levels drop from 21% in the atmosphere to 14%. Levels are lower in inflamed tissue, where less than 1% oxygen is available [137]. During infection with *A. fumigatus* hypoxia can be detected in microenvironments around inflamed areas [138]. The ability of *Aspergillus* to adapt to these conditions is essential for growth and causing infection. In the environment *Aspergillus* species are found in soil and decaying material, where oxygen levels can be low. Oxygen levels vary from 21% to hypoxic conditions (>1.5%) [139]. Hypoxia causes the fungal cell to shrink while the cell wall is thickened. These cell wall changes activate macrophages and neutrophils through the beta-glucan receptor dectin-1 [140].

During hypoxic conditions *Aspergillus* is able to ferment glucose or other carbon sources into ethanol [138]. Fermentation differs between fungi, animals and bacteria. Animals and many bacteria use homolactic fermentation where glucose is reduced to lactic acid to produce energy. However, fungi use heterolatic fermentation, which results in ethanol and carbon dioxide production. *A. fumigatus* utilizes this latter type of fermentation. While *A. fumigatus* Af293 and CEA10 could grow under hypoxic conditions when glucose was used as a carbon source, growth was reduced when ethanol was used as carbon source [141]. Moreover, enzymatic assays showed an increase of acetate and ethanol during fermentation *in vitro* [142]. This phenomenon also occurs *in vivo* as ethanol could be detected from BAL samples from infected mice [138].

In *A. fumigatus* utilization of complex carbon sources, is regulated through the carbon catabolite repressor CreA. Using ethanol as a carbon source, CreA derepresses genes involved in gluconeogenesis and glyoxylate cycle. Furthermore, additional roles for CreA as an activator have been proposed due to a reduction in mRNA for several genes. A *creA* deletion mutant showed changes in bioenergetics and cell wall homeostasis resulting in reduced growth under hypoxic conditions and attenuation of virulence in a murine model of infection [33].

During hypoxia, *A. fumigatus* upregulates genes involved in glycolysis and fermentation and downregulates genes in the TCA cycle and respiration associated genes. Surprisingly, when a core set of genes required for fermentation was deleted this did not result in attenuation in a murine model of infection [138]. Several fungi are able to use nitrate as an alternative electron acceptor [143]. However, null mutants of nitrate reductases (NiaD and NiiA) did not show a growth reduction under hypoxic conditions or attenuation of fungal virulence in an infection model of embryonated eggs [62]. Besides nitrate, several fungi are able to use fumarate as electron acceptor [144]. However, deletion of fumarate reductases did not result in reduced growth in hypoxia or attenuation of virulence [62]. Upon hypoxia, sterol content of the fungal cell decreases [145]. To overcome low sterol levels, biosynthesis genes are upregulated to restore sterol content [142]. Ergosterol biosynthesis is dependent on iron acquisition as iron is an essential cofactor for many biochemical reactions. Increased iron acquisition is mediated through HapX and repression of SreA, which was confirmed during hypoxia [146]. Sensing sterol content and therefore regulating genes in response to hypoxia is regulated through SrbA [147].

SrbA (Sre1) is a transcription factor of the sterol regulatory element-binding protein class (SREBPs). The first SREBP was first found in *Schizosaccharomyces pombe* where Sre1 regulates cholesterol and lipid metabolism [148]. SREBPs are characterized by being membrane bound transcription factors that become actived by cleavage of the N-terminus by a Golgi E3 ligase complex [149]. A homologue of SrbA is also present in *A. fumigatus* and is required for cell polarity and growth under hypoxic conditions [141].

SrbA regulates genes involved in iron homeostasis; cell wall biosynthesis and the GABA shunt. Furthermore, SrbA binds to the promoter regions of several genes, including *cyp51a*, required for ergosterol biosynthesis [150]. A null mutant of SrbA exhibits an increased sensitivity towards azoles, which target ergosterol biosynthesis [151]. Through ChIP-seq analysis, another SREBP was discovered, called SrbB. Deletion of *srbB* resulted in a growth defect in hypoxic conditions. Furthermore, this mutant was attenuated in a murine model of infection Differences between the SrbA and SrbB regulon have been observed as SrbB plays a limiting role in ergosterol biosynthesis, but regulates carbohydrate metabolism. Both transcription factors co-regulate alcohol fermentation and heme biosynthesis [150]. However, a complete mechanistic understanding of hypoxia during *A. fumigatus* infection has yet to be fully revealed.

1.5.4 Thermotolerance

Fungi can be generally divided into thermophilic and thermotolerant based on their preferred growth temperature. While thermophilic fungi generally grow at 20 °C or below; thermotolerant fungi can grow up till 55 °C. One of the important differences between *A. fumigatus* and other *Aspergilli* is its ability to grow at elevated temperatures. *A. fumigatus* is able to tolerate temperatures over 50 °C and grow rapidly at 37 °C, the temperature within the mammalian lung [152]. In general high temperatures cause synthesis of heat shock proteins, synthesis of trehalose, detoxification of reactive oxygen and activation of ATPases to maintain pH [153]. Heat shock proteins have been well characterized in *S. cerevisiae* and *C. albicans* but not in depth in *A. fumigatus* [154].

Mechanisms of thermotolerance involve stress genes that are induced upon elevated temperature. Gene expression profiling comparing growth at 37 °C to 48 °C resulted in 323 upregulated genes under increased temperature [52]. Many of the genes found include heat-shock responsive genes. Another transcriptome study showed that heat shock at 48 °C caused a severe change in metabolism, including amino acid, fatty acid metabolism and glycolysis [155]. Similar trends were observed in the proteome during exposure to increased temperature, together with increased protein levels of heat shock proteins [156].

Heat shock proteins are involved in the refolding and degradation of damaged proteins, a key feature of damage by temperature [157]. These proteins are generally divided by their molecular mass and have distinct functions. One of the best-studied heat shock proteins is heat shock protein 90 (Hsp90). In *S. cerevisiae* Hsp90 is at the center of a network of proteins and transcription factors consisting of over 10% of the proteome [158]. Through deletion studies the essential nature of Hsp90 was shown in *S. cerevisiae, C. albicans* or *A. fumigatus* [154, 159, 160]. However, through genetic manipulation with inducible promoters it was shown that Hsp90 is involved in cell wall integrity and heat stress response [160]. Furthermore, it was shown that Hsp90 is linked to the mitochondrial respiratory chain and ATP generation [161]. Protein folding through Hsp90 involves several other proteins such as heat shock protein 70 (Hsp70) and the Hop protein/StiA [162]. The StiA protein facilitates complex formation of Hsp70 and Hsp90. However, StiA does not seem to be required for the physical interaction between Hsp70 and Hsp90. StiA likely facilitates Hsp90 localisation to the nucleus, but this remains to be proven [163].

Heat shock proteins are important for ribosome assembly, as mutations in these genes cause ribosome defects [164]. Ribosome assembly is localized in the nucleolus, where large amounts of proteins gather during this process. This includes many nucleolar chaperones, such as heat shock proteins, to maintain protein denaturation and aggregation [165]. During germination ribosome biogenesis is essential for growth and requires the nucleolar protein CgrA. Nucleolar protein CgrA, an orthologue of *S. cerevisiae* nucleolar protein is responsible for synthesis of the 60S ribosomal unit and rRNA processing [166]. *CgrA* was found to be upregulated during elevated temperatures [167]. The *cgrA* null mutant is attenuated in a murine model of invasive aspergillosis linking thermotolerance and ribosome biogenesis [167].

The unfolded protein response (UPR) is essential for growth under high temperature. The ER-bound sensor IreA senses the accumulation of unfolded protein. This sensor cleaves an intron of the transcription factor HacA, which regulates the UPR [168]. Deletion of HacA results in a phenotype under ER-stressed conditions and under elevated temperature. Furthermore, HacA is essential for

adaptation to cell wall stress, integrity and for virulence in neutropenic and corticosteroid murine models of infection [169].

1.6 High throughput phenotyping in fungi

The mammalian lung is a multifactorial dynamic environment. As the precise conditions within the lung are as of yet unknown, adaptation to stress is mostly measured *in vitro* inducing one single stress. However, in several *Candida* species it is shown that combinations of stress can have a synergistic effect [170, 171]. However, a regulatory network describing adaptation to these stresses has not been produced for *A. fumigatus*. Genetic tools in other fungi are more developed and have allowed researchers to construct regulatory networks and phenotype screenings involved in a range of behavior, which are important during infection. To assess regulatory networks, knockout collections prove to be key tools for genome wide phenotype screenings.

The model organism *S. cerevisiae* was the first fungus to be sequenced. This raised the idea that a full genome gene deletion project should be undertaken [172]. This project would require a multi-laboratory network to accomplish it. The project started in 1986, resulting in the first description in 1999 [173]. About a third of the deletion strains were constructed at this time and phenotyped to describe potential essential genes. Completion of the library was achieved in 2002, resulting in description of roughly 19% essential genes and 15% where deletion resulted in slow growth. Interestingly, little correlation was found between transcript level and fitness [174]. However, the library was generated with the criteria that ORFs had to generate proteins longer than 100 amino acids. Smaller gene products have been observed [175]. Therefore, the library is incomplete and is still missing around 140 deletion strains. To date, 205 articles have screened the library for several phenotypes, which resulted in annotation of almost 3500 genes [172]. The development of CRISPR-Cas9 methodologies made precise genome engineering faster and more efficient. Applying the CHAnGE technique, a genome wide gene disruption collection with single-nucleotide resolution was constructed, which is available for future studies [176].

In *C. albicans* the idea for a full genome deletion collection and associated protocols were assessed in 2005. *C. albicans* is diploid which complicated constructing deletion strains. Heterozygous deletions are single copy deletions and less time consuming to construct. This strategy was followed to construct 2868 mutants to screen for susceptibility to 35 compounds [177]. Other strategies involve insertional mutagenesis with a transposon. Using the split marker approach with the Tn7-*UAU1* transposon results in homozygous mutants [178]. This approach has been used to characterize regulatory networks for the cell surface and biofilm formation [179, 180]. Historically, the *URA3* gene was used as selectable marker for homozygous deletion mutants. However, changes in virulence have been observed. Therefore, the *HIS1*, *LEU2* and *ARG4* selectable markers were used for the full genome project [181]. A subset of 143 transcription factor null mutants (n=2) were generated and assessed for growth under 55 different conditions [182]. In 2010, 674 unique gene null mutants were generated and screened for morphology and proliferation. The ability to cause infection was assessed in a pooled infection murine model resulting in identification of 115 mutants [183].

In *C. albicans*, biofilm synthesis was assessed by generating 165 transcription factor mutants representing the full genomic cohort [184]. These mutants were screened for biofilm production and six mutants that were compromised in their biofilm production were found. Besides *in vitro* analysis, the lack of biofilm production was assessed *in vivo*. By RNA-seq 1,061 target genes were found including 23 genes that were differentially expressed and directly regulated by all transcription factor null mutants. Integrating this data in an inferred network resulted in the identification of six master regulators and a cluster of genes that are regulated by all the master regulators [184].

Following a similar approach to construct gene deletions a gene deletion library was constructed for *C. glabrata*, which identified 1047 non-essential genes and constructing 619 unique gene deletion strains. This library was screened for fitness, defects in morphology and several environmental stresses including susceptibility to antifungals [185]. This library has subsequently been used to screen for genes essential for biofilm formation under normoxia and hypoxia. This resulted in identification of eight genes essential for biofilm formation that can potentially be

antifungal targets [186]. Furthermore, these strains have been used to elucidate a mechanistic basis of iron homeostasis [187]. In another pathogenic yeast, *C. neoformans*, a library consisting of 1200 mutants was generated and screened for growth, capsule formation, melanin content and proliferation *in vivo*. This resulted in 40 previously uncharacterized genes that are essential for infection of the mammalian host [188].

The first gene deletion collection in filamentous fungi was generated in the model organism *Neurospora crassa*. 103 transcription factors were replaced with a hygromycin resistance cassette by homologous recombination. This library was screened for defects in asexual and sexual development resulting identification of over 40 genes essential for one of these processes [189]. This was followed by generation of knockout cassettes for the full genome knockout collection of *N. crassa* [190, 191]. This collection is currently managed by the Fungal Genetics Stock Center and contains 4729 deletion strains [192]. There have been many studies using the genome wide deletion collection to screen for specific phenotypes. Being able to filter for specific subsets of genes has been proven powerful and in depth analyses have been performed for kinases and G-coupled protein receptors [193, 194]. Furthermore, various conditions have been used to screen the genome knockout library, such as induction of alternative oxidases, cellulose production and induction of cell fusion [195-197]. Recently, the full genomic cohort of 312 transcription factors was reanalyzed for growth and sexual/asexual development. This resulted in the identification of many more phenotypes due to almost doubling the amount of mutants available [198].

In several other filamentous fungi only smaller collections of knockout strains have been generated. In *Magnaporthe oryzae* a collection of 78 secreted protein knockout strains was established. This library was screened for the ability to cause disease in barley and rice [199]. In 2014 a high throughput deletion method was developed for *M. oryzae* and was subsequently used to generate 104 transcription factor null mutants, representing about 20% of predicted transcription factors [200]. In *Fusarium graminearum* the full genomic cohort of transcription factor null mutants was generated and screened for 17 conditions, which resulted in over 11,000 phenotypes [201]. In *Aspergillus* species large collections of deletion strains have

not yet been published. The largest collections to date were constructed in *A. nidulans* being the polyketide synthase and kinase knockout library, consisting of 32 and 128 strains respectively [202, 203].

1.7 Aims and hypothesis

Aims of this thesis:

1. Optimise parallel fitness assays for phenotyping of the *A. fumigatus* transcription factor knockout collection. A high-throughput phenotyping pipeline will be developed to screen the library for itraconazole susceptibility as a prototype phenotyping study.

2. Identify transcription factors associated with fitness, environmental adaptation and epithelial invasion. These transcription factors will be further characterise and integrated into a regulatory network to highlight mechanistic drivers of pathogenicity.

3. Design and optimise a CRISPR-Cas9 transformation methodology without the need of the integration of a selection marker. This method will speed up epitope tagging of proteins for future analysis of transcription factors identified in aim 2.

1.8 References

1. Blackwell, M., *The fungi: 1, 2, 3 ... 5.1 million species?* Am J Bot, 2011. **98**(3): p. 426-38.
2. Chavez, R., et al., *Filamentous fungi from extreme environments as a promising source of novel bioactive secondary metabolites.* Front Microbiol, 2015. **6**: p. 903.
3. Boer, W., et al., *Living in a fungal world: impact of fungi on soil bacterial niche development.* FEMS Microbiol Rev, 2005. **29**(4): p. 795-811.
4. Enoch, D.A., et al., *The Changing Epidemiology of Invasive Fungal Infections.* Methods Mol Biol, 2017. **1508**: p. 17-65.
5. Low, C.Y. and C. Rotstein, *Emerging fungal infections in immunocompromised patients.* F1000 Med Rep, 2011. **3**: p. 14.
6. Wiederhold, N.P., *Antifungal resistance: current trends and future strategies to combat.* Infect Drug Resist, 2017. **10**: p. 249-259.
7. Denning, D.W. and M.J. Bromley, *Infectious Disease. How to bolster the antifungal pipeline.* Science, 2015. **347**(6229): p. 1414-6.
8. Swan, A.K.a.B.C., *Occupational and environmental exposure to bioaerosols from composts and potential health effects - A critical review of published data* Health and Safety Executive 2003 2003. **Research Report 130**.
9. Brakhage, A.A., *Systemic fungal infections caused by Aspergillus species: epidemiology, infection process and virulence determinants.* Curr Drug Targets, 2005. **6**(8): p. 875-86.
10. Bongomin, F., et al., *Global and Multi-National Prevalence of Fungal Diseases-Estimate Precision.* J Fungi (Basel), 2017. **3**(4).
11. Bhushan, B., et al., *Suppression of epithelial signal transducer and activator of transcription 1 activation by extracts of Aspergillus fumigatus.* Am J Respir Cell Mol Biol, 2015. **53**(1): p. 87-95.
12. Agarwal, R., et al., *Allergic bronchopulmonary aspergillosis: review of literature and proposal of new diagnostic and classification criteria.* Clin Exp Allergy, 2013. **43**(8): p. 850-73.
13. Hogan, C. and D.W. Denning, *Allergic bronchopulmonary aspergillosis and related allergic syndromes.* Semin Respir Crit Care Med, 2011. **32**(6): p. 682-92.

14. Denning, D.W., A. Pleuvry, and D.C. Cole, *Global burden of chronic pulmonary aspergillosis as a sequel to pulmonary tuberculosis.* Bull World Health Organ, 2011. **89**(12): p. 864-72.
15. Denning, D.W., A. Pleuvry, and D.C. Cole, *Global burden of chronic pulmonary aspergillosis complicating sarcoidosis.* Eur Respir J, 2013. **41**(3): p. 621-6.
16. Maghrabi, F. and D.W. Denning, *The Management of Chronic Pulmonary Aspergillosis: The UK National Aspergillosis Centre Approach.* Curr Fungal Infect Rep, 2017. **11**(4): p. 242-251.
17. Ullmann, A.J., et al., *Diagnosis and management of Aspergillus diseases: executive summary of the 2017 ESCMID-ECMM-ERS guideline.* Clin Microbiol Infect, 2018. **24 Suppl 1**: p. e1-e38.
18. Brown, G.D., et al., *Hidden killers: human fungal infections.* Sci Transl Med, 2012. **4**(165): p. 165rv13.
19. Harrison, N., et al., *Incidence and characteristics of invasive fungal diseases in allogeneic hematopoietic stem cell transplant recipients: a retrospective cohort study.* BMC Infect Dis, 2015. **15**(1): p. 584.
20. Nucci, M., et al., *Invasive fungal diseases in haematopoietic cell transplant recipients and in patients with acute myeloid leukaemia or myelodysplasia in Brazil.* Clin Microbiol Infect, 2013. **19**(8): p. 745-51.
21. Reichenberger, F., et al., *Diagnosis and treatment of invasive pulmonary aspergillosis in neutropenic patients.* Eur Respir J, 2002. **19**(4): p. 743-55.
22. Hope, W.W., T.J. Walsh, and D.W. Denning, *Laboratory diagnosis of invasive aspergillosis.* Lancet Infect Dis, 2005. **5**(10): p. 609-22.
23. Hoenigl, M., K. Seeber, and R. Krause, *Antifungal prophylaxis following allogeneic haematopoietic stem cell transplantation: what is the role of voriconazole?* Infection, 2014. **42**(1): p. 233-4.
24. Springer, J., et al., *A novel extraction method combining plasma with a whole-blood fraction shows excellent sensitivity and reproducibility for patients at high risk for invasive aspergillosis.* J Clin Microbiol, 2012. **50**(8): p. 2585-91.
25. Imbert, S., et al., *Aspergillus PCR in Bronchoalveolar Lavage Fluid for the Diagnosis and Prognosis of Aspergillosis in Patients With Hematological and Non-hematological Conditions.* Front Microbiol, 2018. **9**: p. 1877.

26. Barton, R.C., *Laboratory diagnosis of invasive aspergillosis: from diagnosis to prediction of outcome.* Scientifica (Cairo), 2013. **2013**: p. 459405.
27. Pelzer, B.W., et al., *Performance of the AsperGenius(R) PCR assay for detecting azole resistant Aspergillus fumigatus in BAL fluids from allogeneic HSCT recipients: A prospective cohort study from Essen, West Germany.* Med Mycol, 2019.
28. McDonagh, A., et al., *Sub-telomere directed gene expression during initiation of invasive aspergillosis.* PLoS Pathog, 2008. **4**(9): p. e1000154.
29. Baker, E.H., et al., *Hyperglycaemia and pulmonary infection.* Proc Nutr Soc, 2006. **65**(3): p. 227-35.
30. Ostroukhova, M., et al., *The role of low-level lactate production in airway inflammation in asthma.* Am J Physiol Lung Cell Mol Physiol, 2012. **302**(3): p. L300-7.
31. Worlitzsch, D., K.C. Meyer, and G. Doring, *Lactate levels in airways of patients with cystic fibrosis and idiopathic pulmonary fibrosis.* Am J Respir Crit Care Med, 2013. **188**(1): p. 111.
32. Cowley, A.C., et al., *Aspergillosis and the role of mucins in cystic fibrosis.* Pediatr Pulmonol, 2017. **52**(4): p. 548-555.
33. Beattie, S.R., et al., *Filamentous fungal carbon catabolite repression supports metabolic plasticity and stress responses essential for disease progression.* PLoS Pathog, 2017. **13**(4): p. e1006340.
34. Lafon, A., et al., *G-protein and cAMP-mediated signaling in aspergilli: a genomic perspective.* Fungal Genet Biol, 2006. **43**(7): p. 490-502.
35. Grice, C.M., M. Bertuzzi, and E.M. Bignell, *Receptor-mediated signaling in Aspergillus fumigatus.* Front Microbiol, 2013. **4**: p. 26.
36. Jung, M.G., et al., *Characterization of gprK Encoding a Putative Hybrid G-Protein-Coupled Receptor in Aspergillus fumigatus.* PLoS One, 2016. **11**(9): p. e0161312.
37. Gehrke, A., et al., *Heptahelical receptors GprC and GprD of Aspergillus fumigatus Are essential regulators of colony growth, hyphal morphogenesis, and virulence.* Appl Environ Microbiol, 2010. **76**(12): p. 3989-98.
38. Wei, H., et al., *A putative high affinity hexose transporter, hxtA, of Aspergillus nidulans is induced in vegetative hyphae upon starvation and in*

ascogenous hyphae during cleistothecium formation. Fungal Genet Biol, 2004. **41**(2): p. 148-56.

39. Cheng, S., et al., *Profiling of Candida albicans gene expression during intra-abdominal candidiasis identifies biologic processes involved in pathogenesis.* J Infect Dis, 2013. **208**(9): p. 1529-37.
40. Fanning, S., et al., *Functional control of the Candida albicans cell wall by catalytic protein kinase A subunit Tpk1.* Mol Microbiol, 2012. **86**(2): p. 284-302.
41. Brown, V., J.A. Sexton, and M. Johnston, *A glucose sensor in Candida albicans.* Eukaryot Cell, 2006. **5**(10): p. 1726-37.
42. Ries, L.N.A., et al., *Overview of carbon and nitrogen catabolite metabolism in the virulence of human pathogenic fungi.* Mol Microbiol, 2018. **107**(3): p. 277-297.
43. Ries, L.N.A., et al., *Nutritional Heterogeneity Among Aspergillus fumigatus Strains Has Consequences for Virulence in a Strain- and Host-Dependent Manner.* Front Microbiol, 2019. **10**: p. 854.
44. Margelis, S., et al., *Role of glutamine synthetase in nitrogen metabolite repression in Aspergillus nidulans.* J Bacteriol, 2001. **183**(20): p. 5826-33.
45. Biswas, K. and J. Morschhauser, *The Mep2p ammonium permease controls nitrogen starvation-induced filamentous growth in Candida albicans.* Mol Microbiol, 2005. **56**(3): p. 649-69.
46. Baldin, C., et al., *Comparative proteomics of a tor inducible Aspergillus fumigatus mutant reveals involvement of the Tor kinase in iron regulation.* Proteomics, 2015. **15**(13): p. 2230-43.
47. Bom, V.L., et al., *The Aspergillus fumigatus sitA Phosphatase Homologue Is Important for Adhesion, Cell Wall Integrity, Biofilm Formation, and Virulence.* Eukaryot Cell, 2015. **14**(8): p. 728-44.
48. Andrianopoulos, A., et al., *Characterization of the Aspergillus nidulans nmrA gene involved in nitrogen metabolite repression.* J Bacteriol, 1998. **180**(7): p. 1973-7.
49. Hensel, M., et al., *The role of the Aspergillus fumigatus areA gene in invasive pulmonary aspergillosis.* Mol Gen Genet, 1998. **258**(5): p. 553-7.

50. Wong, K.H., et al., *Transcriptional control of nmrA by the bZIP transcription factor MeaB reveals a new level of nitrogen regulation in Aspergillus nidulans.* Mol Microbiol, 2007. **66**(2): p. 534-51.
51. Monod, M., et al., *Secreted proteases from pathogenic fungi.* Int J Med Microbiol, 2002. **292**(5-6): p. 405-19.
52. Nierman, W.C., et al., *Genomic sequence of the pathogenic and allergenic filamentous fungus Aspergillus fumigatus.* Nature, 2005. **438**(7071): p. 1151-6.
53. Sharon, H., S. Hagag, and N. Osherov, *Transcription factor PrtT controls expression of multiple secreted proteases in the human pathogenic mold Aspergillus fumigatus.* Infect Immun, 2009. **77**(9): p. 4051-60.
54. Amich, J. and E. Bignell, *Amino acid biosynthetic routes as drug targets for pulmonary fungal pathogens: what is known and why do we need to know more?* Curr Opin Microbiol, 2016. **32**: p. 151-158.
55. Stein, W.H. and S. Moore, *The free amino acids of human blood plasma.* J Biol Chem, 1954. **211**(2): p. 915-26.
56. Brosnan, J.T., *Interorgan amino acid transport and its regulation.* J Nutr, 2003. **133**(6 Suppl 1): p. 2068s-2072s.
57. Stumvoll, M., et al., *Role of glutamine in human carbohydrate metabolism in kidney and other tissues.* Kidney Int, 1999. **55**(3): p. 778-92.
58. Sasse, A., et al., *Mutant characterization and in vivo conditional repression identify aromatic amino acid biosynthesis to be essential for Aspergillus fumigatus virulence.* Virulence, 2016. **7**(1): p. 56-62.
59. Schobel, F., I.D. Jacobsen, and M. Brock, *Evaluation of lysine biosynthesis as an antifungal drug target: biochemical characterization of Aspergillus fumigatus homocitrate synthase and virulence studies.* Eukaryot Cell, 2010. **9**(6): p. 878-93.
60. Long, N., et al., *The Zn2Cys6-type transcription factor LeuB cross-links regulation of leucine biosynthesis and iron acquisition in Aspergillus fumigatus.* PLoS Genet, 2018. **14**(10): p. e1007762.
61. Dietl, A.M., et al., *Histidine biosynthesis plays a crucial role in metal homeostasis and virulence of Aspergillus fumigatus.* Virulence, 2016. **7**(4): p. 465-76.

62. Kroll, K., et al., *Identification of hypoxia-inducible target genes of Aspergillus fumigatus by transcriptome analysis reveals cellular respiration as an important contributor to hypoxic survival.* Eukaryot Cell, 2014. **13**(9): p. 1241-53.
63. Amich, J., et al., *Exploration of Sulfur Assimilation of Aspergillus fumigatus Reveals Biosynthesis of Sulfur-Containing Amino Acids as a Virulence Determinant.* Infect Immun, 2016. **84**(4): p. 917-929.
64. Amich, J., et al., *Regulation of sulphur assimilation is essential for virulence and affects iron homeostasis of the human-pathogenic mould Aspergillus fumigatus.* PLoS Pathog, 2013. **9**(8): p. e1003573.
65. Meir, Z. and N. Osherov, *Vitamin Biosynthesis as an Antifungal Target.* J Fungi (Basel), 2018. **4**(2).
66. Ben Yaakov, D., et al., *The quinoline bromoquinol exhibits broad-spectrum antifungal activity and induces oxidative stress and apoptosis in Aspergillus fumigatus.* J Antimicrob Chemother, 2017. **72**(8): p. 2263-2272.
67. Gerwien, F., et al., *Metals in fungal virulence.* FEMS Microbiol Rev, 2018. **42**(1).
68. Chipperfield, J.R. and C. Ratledge, *Salicylic acid is not a bacterial siderophore: a theoretical study.* Biometals, 2000. **13**(2): p. 165-8.
69. Fahy, J.V. and B.F. Dickey, *Airway mucus function and dysfunction.* N Engl J Med, 2010. **363**(23): p. 2233-47.
70. Ghio, A.J., et al., *Respiratory epithelial cells demonstrate lactoferrin receptors that increase after metal exposure.* Am J Physiol, 1999. **276**(6): p. L933-40.
71. Arosio, P. and S. Levi, *Cytosolic and mitochondrial ferritins in the regulation of cellular iron homeostasis and oxidative damage.* Biochim Biophys Acta, 2010. **1800**(8): p. 783-92.
72. Schrettl, M., et al., *Siderophore biosynthesis but not reductive iron assimilation is essential for Aspergillus fumigatus virulence.* J Exp Med, 2004. **200**(9): p. 1213-9.
73. Schrettl, M., et al., *HapX-mediated adaption to iron starvation is crucial for virulence of Aspergillus fumigatus.* PLoS Pathog, 2010. **6**(9): p. e1001124.

74. Gsaller, F., et al., *The Janus transcription factor HapX controls fungal adaptation to both iron starvation and iron excess.* Embo j, 2014. **33**(19): p. 2261-76.
75. Weber, M., et al., *Inference of dynamical gene-regulatory networks based on time-resolved multi-stimuli multi-experiment data applying NetGenerator V2.0.* BMC Syst Biol, 2013. **7**: p. 1.
76. Linde, J., et al., *Regulatory interactions for iron homeostasis in Aspergillus fumigatus inferred by a Systems Biology approach.* BMC Syst Biol, 2012. **6**: p. 6.
77. Staats, C.C., et al., *Fungal zinc metabolism and its connections to virulence.* Front Cell Infect Microbiol, 2013. **3**: p. 65.
78. McCormick, A., et al., *NETs formed by human neutrophils inhibit growth of the pathogenic mold Aspergillus fumigatus.* Microbes Infect, 2010. **12**(12-13): p. 928-36.
79. Clark, H.L., et al., *Zinc and Manganese Chelation by Neutrophil S100A8/A9 (Calprotectin) Limits Extracellular Aspergillus fumigatus Hyphal Growth and Corneal Infection.* J Immunol, 2016. **196**(1): p. 336-44.
80. Moreno, M.A., et al., *The regulation of zinc homeostasis by the ZafA transcriptional activator is essential for Aspergillus fumigatus virulence.* Mol Microbiol, 2007. **64**(5): p. 1182-97.
81. Kusuya, Y., et al., *Transcription factor Afmac1 controls copper import machinery in Aspergillus fumigatus.* Curr Genet, 2017. **63**(4): p. 777-789.
82. Park, Y.S., T.H. Kim, and C.W. Yun, *Functional characterization of the copper transcription factor AfMac1 from Aspergillus fumigatus.* Biochem J, 2017. **474**(14): p. 2365-2378.
83. Park, Y.S., et al., *A copper transcription factor, AfMac1, regulates both iron and copper homeostasis in the opportunistic fungal pathogen Aspergillus fumigatus.* Biochem J, 2018. **475**(17): p. 2831-2845.
84. Upadhyay, S., G. Torres, and X. Lin, *Laccases involved in 1,8-dihydroxynaphthalene melanin biosynthesis in Aspergillus fumigatus are regulated by developmental factors and copper homeostasis.* Eukaryot Cell, 2013. **12**(12): p. 1641-52.

85. Wiemann, P., et al., *Aspergillus fumigatus Copper Export Machinery and Reactive Oxygen Intermediate Defense Counter Host Copper-Mediated Oxidative Antimicrobial Offense.* Cell Rep, 2017. **19**(5): p. 1008-1021.
86. Bignell, E., et al., *Secondary metabolite arsenal of an opportunistic pathogenic fungus.* Philos Trans R Soc Lond B Biol Sci, 2016. **371**(1709).
87. Monk, B.C. and D.S. Perlin, *Fungal plasma membrane proton pumps as promising new antifungal targets.* Crit Rev Microbiol, 1994. **20**(3): p. 209-23.
88. Obara, K., H. Yamamoto, and A. Kihara, *Membrane protein Rim21 plays a central role in sensing ambient pH in Saccharomyces cerevisiae.* J Biol Chem, 2012. **287**(46): p. 38473-81.
89. Bertuzzi, M., et al., *The pH-responsive PacC transcription factor of Aspergillus fumigatus governs epithelial entry and tissue invasion during pulmonary aspergillosis.* PLoS Pathog, 2014. **10**(10): p. e1004413.
90. DeCoursey, T.E. and V.V. Cherny, *Voltage-activated hydrogen ion currents.* J Membr Biol, 1994. **141**(3): p. 203-23.
91. Cornet, M. and C. Gaillardin, *pH signaling in human fungal pathogens: a new target for antifungal strategies.* Eukaryot Cell, 2014. **13**(3): p. 342-52.
92. Calcagno-Pizarelli, A.M., et al., *Establishment of the ambient pH signaling complex in Aspergillus nidulans: PalI assists plasma membrane localization of PalH.* Eukaryot Cell, 2007. **6**(12): p. 2365-75.
93. Calcagno-Pizarelli, A.M., et al., *Rescue of Aspergillus nidulans severely debilitating null mutations in ESCRT-0, I, II and III genes by inactivation of a salt-tolerance pathway allows examination of ESCRT gene roles in pH signalling.* J Cell Sci, 2011. **124**(Pt 23): p. 4064-76.
94. Diez, E., et al., *Activation of the Aspergillus PacC zinc finger transcription factor requires two proteolytic steps.* Embo j, 2002. **21**(6): p. 1350-9.
95. Tilburn, J., et al., *The Aspergillus PacC zinc finger transcription factor mediates regulation of both acid- and alkaline-expressed genes by ambient pH.* Embo j, 1995. **14**(4): p. 779-90.
96. Loss, O., et al., *Mutual independence of alkaline- and calcium-mediated signalling in Aspergillus fumigatus refutes the existence of a conserved druggable signalling nexus.* Mol Microbiol, 2017. **106**(6): p. 861-875.

97. Amich, J., F. Leal, and J.A. Calera, *Repression of the acid ZrfA/ZrfB zinc-uptake system of Aspergillus fumigatus mediated by PacC under neutral, zinc-limiting conditions.* Int Microbiol, 2009. **12**(1): p. 39-47.
98. Amich, J., et al., *Aspergillus fumigatus survival in alkaline and extreme zinc-limiting environments relies on the induction of a zinc homeostasis system encoded by the zrfC and aspf2 genes.* Eukaryot Cell, 2010. **9**(3): p. 424-37.
99. Lew, R.R., *How does a hypha grow? The biophysics of pressurized growth in fungi.* Nat Rev Microbiol, 2011. **9**(7): p. 509-18.
100. Latge, J.P. and A. Beauvais, *Functional duality of the cell wall.* Curr Opin Microbiol, 2014. **20**: p. 111-7.
101. Gautam, P., et al., *Proteomic and transcriptomic analysis of Aspergillus fumigatus on exposure to amphotericin B.* Antimicrob Agents Chemother, 2008. **52**(12): p. 4220-7.
102. Aimanianda, V., et al., *Surface hydrophobin prevents immune recognition of airborne fungal spores.* Nature, 2009. **460**(7259): p. 1117-21.
103. Smith, D.F.Q. and A. Casadevall, *The Role of Melanin in Fungal Pathogenesis for Animal Hosts.* Curr Top Microbiol Immunol, 2019.
104. Grosse, C., et al., *Protein kinase A regulates growth, sporulation, and pigment formation in Aspergillus fumigatus.* Appl Environ Microbiol, 2008. **74**(15): p. 4923-33.
105. Rispail, N. and A. Di Pietro, *Fusarium oxysporum Ste12 controls invasive growth and virulence downstream of the Fmk1 MAPK cascade.* Mol Plant Microbe Interact, 2009. **22**(7): p. 830-9.
106. Dichtl, K., et al., *Deciphering cell wall integrity signalling in Aspergillus fumigatus: identification and functional characterization of cell wall stress sensors and relevant Rho GTPases.* Mol Microbiol, 2012. **83**(3): p. 506-19.
107. Dupres, V., et al., *The yeast Wsc1 cell surface sensor behaves like a nanospring in vivo.* Nat Chem Biol, 2009. **5**(11): p. 857-62.
108. Gurgel, I., et al., *The Aspergillus fumigatus Mucin MsbA Regulates the Cell Wall Integrity Pathway and Controls Recognition of the Fungus by the Immune System.* mSphere, 2019. **4**(3).
109. Zhang, X., et al., *Role of the small GTPase Rho1 in cell wall integrity, stress response, and pathogenesis of Aspergillus fumigatus.* Fungal Genet Biol, 2018. **120**: p. 30-41.

110. Valiante, V., et al., *The MpkA MAP kinase module regulates cell wall integrity signaling and pyomelanin formation in Aspergillus fumigatus.* Fungal Genet Biol, 2009. **46**(12): p. 909-18.
111. Rocha, M.C., et al., *Aspergillus fumigatus MADS-Box Transcription Factor rlmA Is Required for Regulation of the Cell Wall Integrity and Virulence.* G3 (Bethesda), 2016. **6**(9): p. 2983-3002.
112. Altwasser, R., et al., *Network Modeling Reveals Cross Talk of MAP Kinases during Adaptation to Caspofungin Stress in Aspergillus fumigatus.* PLoS One, 2015. **10**(9): p. e0136932.
113. Ejzykowicz, D.E., et al., *The Aspergillus fumigatus transcription factor Ace2 governs pigment production, conidiation and virulence.* Mol Microbiol, 2009. **72**(1): p. 155-69.
114. Ejzykowicz, D.E., et al., *Role of Aspergillus fumigatus DvrA in host cell interactions and virulence.* Eukaryot Cell, 2010. **9**(10): p. 1432-40.
115. Kuhn, C. and E. Klipp, *Zooming in on yeast osmoadaptation.* Adv Exp Med Biol, 2012. **736**: p. 293-310.
116. de Assis, L.J., et al., *Protein Kinase A and High-Osmolarity Glycerol Response Pathways Cooperatively Control Cell Wall Carbohydrate Mobilization in Aspergillus fumigatus.* MBio, 2018. **9**(6).
117. Saxena, A. and R. Sitaraman, *Osmoregulation in Saccharomyces cerevisiae via mechanisms other than the high-osmolarity glycerol pathway.* Microbiology, 2016. **162**(9): p. 1511-1526.
118. Reyes, G., et al., *Novel mitogen-activated protein kinase MpkC of Aspergillus fumigatus is required for utilization of polyalcohol sugars.* Eukaryot Cell, 2006. **5**(11): p. 1934-40.
119. Bruder Nascimento, A.C., et al., *Mitogen activated protein kinases SakA(HOG1) and MpkC collaborate for Aspergillus fumigatus virulence.* Mol Microbiol, 2016. **100**(5): p. 841-59.
120. Manfiolli, A.O., et al., *Aspergillus fumigatus High Osmolarity Glycerol Mitogen Activated Protein Kinases SakA and MpkC Physically Interact During Osmotic and Cell Wall Stresses.* Front Microbiol, 2019. **10**: p. 918.
121. Garrido-Bazan, V., et al., *SakA and MpkC Stress MAPKs Show Opposite and Common Functions During Stress Responses and Development in Aspergillus nidulans.* Front Microbiol, 2018. **9**: p. 2518.

122. Hagiwara, D., et al., *The role of AtfA and HOG MAPK pathway in stress tolerance in conidia of Aspergillus fumigatus.* Fungal Genet Biol, 2014. **73**: p. 138-49.
123. Pereira Silva, L., et al., *Genome-wide transcriptome analysis of Aspergillus fumigatus exposed to osmotic stress reveals regulators of osmotic and cell wall stresses that are SakA(HOG1) and MpkC dependent.* Cell Microbiol, 2017. **19**(4).
124. de Castro, P.A., et al., *ChIP-seq reveals a role for CrzA in the Aspergillus fumigatus high-osmolarity glycerol response (HOG) signalling pathway.* Mol Microbiol, 2014. **94**(3): p. 655-74.
125. Juvvadi, P.R., et al., *Localization and activity of the calcineurin catalytic and regulatory subunit complex at the septum is essential for hyphal elongation and proper septation in Aspergillus fumigatus.* Mol Microbiol, 2011. **82**(5): p. 1235-59.
126. da Silva Ferreira, M.E., et al., *Functional characterization of the Aspergillus fumigatus calcineurin.* Fungal Genet Biol, 2007. **44**(3): p. 219-30.
127. Mendoza, I., et al., *Activated calcineurin confers high tolerance to ion stress and alters the budding pattern and cell morphology of yeast cells.* J Biol Chem, 1996. **271**(38): p. 23061-7.
128. Lee, S.C., et al., *Calcineurin plays key roles in the dimorphic transition and virulence of the human pathogenic zygomycete Mucor circinelloides.* PLoS Pathog, 2013. **9**(9): p. e1003625.
129. Juvvadi, P.R. and W.J. Steinbach, *Calcineurin Orchestrates Hyphal Growth, Septation, Drug Resistance and Pathogenesis of Aspergillus fumigatus: Where Do We Go from Here?* Pathogens, 2015. **4**(4): p. 883-93.
130. Soriani, F.M., et al., *Functional characterization of the Aspergillus fumigatus CRZ1 homologue, CrzA.* Mol Microbiol, 2008. **67**(6): p. 1274-91.
131. Karababa, M., et al., *CRZ1, a target of the calcineurin pathway in Candida albicans.* Mol Microbiol, 2006. **59**(5): p. 1429-51.
132. Stathopoulos, A.M. and M.S. Cyert, *Calcineurin acts through the CRZ1/TCN1-encoded transcription factor to regulate gene expression in yeast.* Genes Dev, 1997. **11**(24): p. 3432-44.

133. Dinamarco, T.M., et al., *Functional characterization of an Aspergillus fumigatus calcium transporter (PmcA) that is essential for fungal infection.* PLoS One, 2012. **7**(5): p. e37591.
134. Pinchai, N., et al., *The Aspergillus fumigatus P-type Golgi apparatus Ca2+/Mn2+ ATPase PmrA is involved in cation homeostasis and cell wall integrity but is not essential for pathogenesis.* Eukaryot Cell, 2010. **9**(3): p. 472-6.
135. Soriani, F.M., et al., *Identification of possible targets of the Aspergillus fumigatus CRZ1 homologue, CrzA.* BMC Microbiol, 2010. **10**: p. 12.
136. Ries, L.N.A., et al., *The Aspergillus fumigatus CrzA Transcription Factor Activates Chitin Synthase Gene Expression during the Caspofungin Paradoxical Effect.* MBio, 2017. **8**(3).
137. Jain, M. and J.I. Sznajder, *Effects of hypoxia on the alveolar epithelium.* Proc Am Thorac Soc, 2005. **2**(3): p. 202-5.
138. Grahl, N., et al., *In vivo hypoxia and a fungal alcohol dehydrogenase influence the pathogenesis of invasive pulmonary aspergillosis.* PLoS Pathog, 2011. **7**(7): p. e1002145.
139. Wang, W., et al., *Effect of Oxygen Concentration on the Composting Process and Maturity.* Compost Science & Utilization 2007. **15**(3).
140. Shepardson, K.M., et al., *Hypoxia enhances innate immune activation to Aspergillus fumigatus through cell wall modulation.* Microbes Infect, 2013. **15**(4): p. 259-69.
141. Willger, S.D., et al., *A sterol-regulatory element binding protein is required for cell polarity, hypoxia adaptation, azole drug resistance, and virulence in Aspergillus fumigatus.* PLoS Pathog, 2008. **4**(11): p. e1000200.
142. Barker, B.M., et al., *Transcriptomic and proteomic analyses of the Aspergillus fumigatus hypoxia response using an oxygen-controlled fermenter.* BMC Genomics, 2012. **13**: p. 62.
143. Takasaki, K., et al., *Fungal ammonia fermentation, a novel metabolic mechanism that couples the dissimilatory and assimilatory pathways of both nitrate and ethanol. Role of acetyl CoA synthetase in anaerobic ATP synthesis.* J Biol Chem, 2004. **279**(13): p. 12414-20.

144. Camarasa, C., V. Faucet, and S. Dequin, *Role in anaerobiosis of the isoenzymes for Saccharomyces cerevisiae fumarate reductase encoded by OSM1 and FRDS1.* Yeast, 2007. **24**(5): p. 391-401.
145. Porter, J.R., et al., *Ergosterol regulates sterol regulatory element binding protein (SREBP) cleavage in fission yeast.* J Biol Chem, 2010. **285**(52): p. 41051-61.
146. Losada, L., et al., *Large-scale transcriptional response to hypoxia in Aspergillus fumigatus observed using RNAseq identifies a novel hypoxia regulated ncRNA.* Mycopathologia, 2014. **178**(5-6): p. 331-9.
147. Blatzer, M., et al., *SREBP coordinates iron and ergosterol homeostasis to mediate triazole drug and hypoxia responses in the human fungal pathogen Aspergillus fumigatus.* PLoS Genet, 2011. **7**(12): p. e1002374.
148. Hughes, A.L., B.L. Todd, and P.J. Espenshade, *SREBP pathway responds to sterols and functions as an oxygen sensor in fission yeast.* Cell, 2005. **120**(6): p. 831-42.
149. Willger, S.D., et al., *Dsc orthologs are required for hypoxia adaptation, triazole drug responses, and fungal virulence in Aspergillus fumigatus.* Eukaryot Cell, 2012. **11**(12): p. 1557-67.
150. Chung, D., et al., *ChIP-seq and in vivo transcriptome analyses of the Aspergillus fumigatus SREBP SrbA reveals a new regulator of the fungal hypoxia response and virulence.* PLoS Pathog, 2014. **10**(11): p. e1004487.
151. Blosser, S.J. and R.A. Cramer, *SREBP-dependent triazole susceptibility in Aspergillus fumigatus is mediated through direct transcriptional regulation of erg11A (cyp51A).* Antimicrob Agents Chemother, 2012. **56**(1): p. 248-57.
152. Beffa, T., et al., *Mycological control and surveillance of biological waste and compost.* Med Mycol, 1998. **36 Suppl 1**: p. 137-45.
153. Tereshina, V.M., *[Thermal resistance in fungi: the role of heat shock proteins and trehalose].* Mikrobiologiia, 2005. **74**(3): p. 293-304.
154. Cowen, L.E. and S. Lindquist, *Hsp90 potentiates the rapid evolution of new traits: drug resistance in diverse fungi.* Science, 2005. **309**(5744): p. 2185-9.
155. Do, J.H., R. Yamaguchi, and S. Miyano, *Exploring temporal transcription regulation structure of Aspergillus fumigatus in heat shock by state space model.* BMC Genomics, 2009. **10**: p. 306.

156. Albrecht, D., et al., *Integrative analysis of the heat shock response in Aspergillus fumigatus.* BMC Genomics, 2010. **11**: p. 32.
157. Feder, M.E. and G.E. Hofmann, *Heat-shock proteins, molecular chaperones, and the stress response: evolutionary and ecological physiology.* Annu Rev Physiol, 1999. **61**: p. 243-82.
158. Zhao, R. and W.A. Houry, *Hsp90: a chaperone for protein folding and gene regulation.* Biochem Cell Biol, 2005. **83**(6): p. 703-10.
159. Borkovich, K.A., et al., *hsp82 is an essential protein that is required in higher concentrations for growth of cells at higher temperatures.* Mol Cell Biol, 1989. **9**(9): p. 3919-30.
160. Lamoth, F., et al., *Heat shock protein 90 is required for conidiation and cell wall integrity in Aspergillus fumigatus.* Eukaryot Cell, 2012. **11**(11): p. 1324-32.
161. Aruanno, M., et al., *Link between Heat Shock Protein 90 and the Mitochondrial Respiratory Chain in the Caspofungin Stress Response of Aspergillus fumigatus.* Antimicrob Agents Chemother, 2019. **63**(7).
162. Jackson, S.E., *Hsp90: structure and function.* Top Curr Chem, 2013. **328**: p. 155-240.
163. Lamoth, F., et al., *Hsp70 and the Cochaperone StiA (Hop) Orchestrate Hsp90-Mediated Caspofungin Tolerance in Aspergillus fumigatus.* Antimicrob Agents Chemother, 2015. **59**(8): p. 4727-33.
164. Bugl, H., et al., *RNA methylation under heat shock control.* Mol Cell, 2000. **6**(2): p. 349-60.
165. Szebeni, A., et al., *Role of protein kinase CK2 phosphorylation in the molecular chaperone activity of nucleolar protein b23.* J Biol Chem, 2003. **278**(11): p. 9107-15.
166. Moy, T.I., et al., *Identification of a role for Saccharomyces cerevisiae Cgr1p in pre-rRNA processing and 60S ribosome subunit synthesis.* Microbiology, 2002. **148**(Pt 4): p. 1081-90.
167. Bhabhra, R., et al., *Disruption of the Aspergillus fumigatus gene encoding nucleolar protein CgrA impairs thermotolerant growth and reduces virulence.* Infect Immun, 2004. **72**(8): p. 4731-40.

168. Feng, X., et al., *HacA-independent functions of the ER stress sensor IreA synergize with the canonical UPR to influence virulence traits in Aspergillus fumigatus.* PLoS Pathog, 2011. **7**(10): p. e1002330.
169. Richie, D.L., et al., *A role for the unfolded protein response (UPR) in virulence and antifungal susceptibility in Aspergillus fumigatus.* PLoS Pathog, 2009. **5**(1): p. e1000258.
170. Kaloriti, D., et al., *Mechanisms underlying the exquisite sensitivity of Candida albicans to combinatorial cationic and oxidative stress that enhances the potent fungicidal activity of phagocytes.* MBio, 2014. **5**(4): p. e01334-14.
171. Kaloriti, D., et al., *Combinatorial stresses kill pathogenic Candida species.* Med Mycol, 2012. **50**(7): p. 699-709.
172. Giaever, G. and C. Nislow, *The yeast deletion collection: a decade of functional genomics.* Genetics, 2014. **197**(2): p. 451-65.
173. Winzeler, E.A., et al., *Functional characterization of the S. cerevisiae genome by gene deletion and parallel analysis.* Science, 1999. **285**(5429): p. 901-6.
174. Giaever, G., et al., *Functional profiling of the Saccharomyces cerevisiae genome.* Nature, 2002. **418**(6896): p. 387-91.
175. Cherry, J.M., et al., *Saccharomyces Genome Database: the genomics resource of budding yeast.* Nucleic Acids Res, 2012. **40**(Database issue): p. D700-5.
176. Bao, Z., et al., *Genome-scale engineering of Saccharomyces cerevisiae with single-nucleotide precision.* Nat Biotechnol, 2018. **36**(6): p. 505-508.
177. Xu, D., et al., *Genome-wide fitness test and mechanism-of-action studies of inhibitory compounds in Candida albicans.* PLoS Pathog, 2007. **3**(6): p. e92.
178. Davis, D.A., et al., *Candida albicans Mds3p, a conserved regulator of pH responses and virulence identified through insertional mutagenesis.* Genetics, 2002. **162**(4): p. 1573-81.
179. Finkel, J.S., et al., *Portrait of Candida albicans adherence regulators.* PLoS Pathog, 2012. **8**(2): p. e1002525.
180. Nobile, C.J. and A.P. Mitchell, *Regulation of cell-surface genes and biofilm formation by the C. albicans transcription factor Bcr1p.* Curr Biol, 2005. **15**(12): p. 1150-5.

181. Noble, S.M. and A.D. Johnson, *Strains and strategies for large-scale gene deletion studies of the diploid human fungal pathogen Candida albicans.* Eukaryot Cell, 2005. **4**(2): p. 298-309.
182. Homann, O.R., et al., *A phenotypic profile of the Candida albicans regulatory network.* PLoS Genet, 2009. **5**(12): p. e1000783.
183. Noble, S.M., et al., *Systematic screens of a Candida albicans homozygous deletion library decouple morphogenetic switching and pathogenicity.* Nat Genet, 2010. **42**(7): p. 590-8.
184. Nobile, C.J., et al., *A recently evolved transcriptional network controls biofilm development in Candida albicans.* Cell, 2012. **148**(1-2): p. 126-38.
185. Schwarzmuller, T., et al., *Systematic phenotyping of a large-scale Candida glabrata deletion collection reveals novel antifungal tolerance genes.* PLoS Pathog, 2014. **10**(6): p. e1004211.
186. Gupta, P., R.C. Meena, and N. Kumar, *Functional analysis of selected deletion mutants in Candida glabrata under hypoxia.* 3 Biotech, 2017. **7**(3): p. 193.
187. Thiebaut, A., et al., *The CCAAT-Binding Complex Controls Respiratory Gene Expression and Iron Homeostasis in Candida Glabrata.* Sci Rep, 2017. **7**(1): p. 3531.
188. Liu, O.W., et al., *Systematic genetic analysis of virulence in the human fungal pathogen Cryptococcus neoformans.* Cell, 2008. **135**(1): p. 174-88.
189. Colot, H.V., et al., *A high-throughput gene knockout procedure for Neurospora reveals functions for multiple transcription factors.* Proc Natl Acad Sci U S A, 2006. **103**(27): p. 10352-10357.
190. Collopy, P.D., et al., *High-throughput construction of gene deletion cassettes for generation of Neurospora crassa knockout strains.* Methods Mol Biol, 2010. **638**: p. 33-40.
191. Park, G., et al., *High-throughput production of gene replacement mutants in Neurospora crassa.* Methods Mol Biol, 2011. **722**: p. 179-89.
192. McCluskey, K., *The Fungal Genetics Stock Center: from molds to molecules.* Adv Appl Microbiol, 2003. **52**: p. 245-62.
193. Cabrera, I.E., et al., *Global Analysis of Predicted G Protein-Coupled Receptor Genes in the Filamentous Fungus, Neurospora crassa.* G3 (Bethesda), 2015. **5**(12): p. 2729-43.

194. Park, G., et al., *Global analysis of serine-threonine protein kinase genes in Neurospora crassa.* Eukaryot Cell, 2011. **10**(11): p. 1553-64.
195. Fu, C., et al., *Identification and characterization of genes required for cell-to-cell fusion in Neurospora crassa.* Eukaryot Cell, 2011. **10**(8): p. 1100-9.
196. Nargang, F.E., et al., *Identification of genes required for alternative oxidase production in the Neurospora crassa gene knockout library.* G3 (Bethesda), 2012. **2**(11): p. 1345-56.
197. Reilly, M.C., et al., *Deletion of homologs of the SREBP pathway results in hyper-production of cellulases in Neurospora crassa and Trichoderma reesei.* Biotechnol Biofuels, 2015. **8**: p. 121.
198. Carrillo, A.J., et al., *Functional Profiling of Transcription Factor Genes in Neurospora crassa.* G3 (Bethesda), 2017. **7**(9): p. 2945-2956.
199. Saitoh, H., et al., *Large-scale gene disruption in Magnaporthe oryzae identifies MC69, a secreted protein required for infection by monocot and dicot fungal pathogens.* PLoS Pathog, 2012. **8**(5): p. e1002711.
200. Lu, J., et al., *Systematic analysis of Zn2Cys6 transcription factors required for development and pathogenicity by high-throughput gene knockout in the rice blast fungus.* PLoS Pathog, 2014. **10**(10): p. e1004432.
201. Son, H., et al., *A phenome-based functional analysis of transcription factors in the cereal head blight fungus, Fusarium graminearum.* PLoS Pathog, 2011. **7**(10): p. e1002310.
202. De Souza, C.P., et al., *Functional analysis of the Aspergillus nidulans kinome.* PLoS One, 2013. **8**(3): p. e58008.
203. Nielsen, M.L., et al., *A genome-wide polyketide synthase deletion library uncovers novel genetic links to polyketides and meroterpenoids in Aspergillus nidulans.* FEMS Microbiol Lett, 2011. **321**(2): p. 157-66.

Chapter

2

The Negative Cofactor 2 complex is a key regulator of drug resistance in *Aspergillus fumigatus*.

Takanori Furukawa, Norman van Rhijn, Marcin Fraczek, Fabio Gsaller, Emma Davies, Paul Carr, Sara Gago, Rachael Fortune-Grant, Sayema Rahman, Jane Mabey Gilsenan, Emma Houlder, Caitlin Kowalski, Shriya Raj, Sanjoy Paul, Josie Parker, Steve Kelly, Robert Cramer, Jean-Paul Latge, Peter Cook, Scott Moye-Rowley, Elaine Bignell, Paul Bowyer, Michael Bromley

2. The Negative Cofactor 2 complex is a master regulator of drug resistance in Aspergillus fumigatus.

Authors: Takanori Furukawa†[1,2], Norman van Rhijn†[1,2], Marcin Fraczek[1], Fabio Gsaller[1], Emma Davies[1], Paul Carr[1, 2], Sara Gago[1,2], Rachael Fortune-Grant[1,2], Sayema Rahman[1,2], Jane Mabey Glisenan[1], Emma Houlder[2], Caitlin H. Kowalski[6], Shriya Raj[3], Sanjoy Paul[4], Josie E. Parker[5], Steve Kelly[5], Robert A. Cramer[6], Jean-Paul Latge[3], Peter Cook[2], Scott Moye-Rowley[4], Elaine Bignell[1,2], Paul Bowyer[1,2], Michael J Bromley[1,2]

[1] Manchester Fungal Infection Group, Division of Infection, Immunity and Respiratory Medicine, Faculty of Biology, Medicine and Health, University of Manchester, CTF Building, 46 Grafton Street, Manchester, M13 9NT, UK.

[2] Lydia Becker Institute of Immunology and Inflammation, Manchester Collaborative Centre for Inflammation Research, Division of Infection, Immunity and Respiratory Medicine, Faculty of Biology, Medicine and Health, University of Manchester, Manchester Academic Health Science Centre, Manchester, UK.

[3] Unité des Aspergillus , Institut Pasteur , 25 rue du Docteur Roux , 75724 Paris Cedex 15 , France.

[4] Department of Molecular Physiology and Biophysics, Carver College of Medicine, University of Iowa, Iowa City, IA, 52242, USA.

[5] Institute of Life Science, Swansea University Medical School, Swansea University, Swansea, Wales, SA2 8PP, UK.

[6] Department of Microbiology and Immunology, Geisel School of Medicine at Dartmouth, Hanover, NH, 03766, USA.

†The authors wish it to be known that, in their opinion, the first two authors should be regarded as joint First Authors.

Submitted to: Nature communications

Abstract:

The frequency of antifungal resistance, particularly to the azole class of ergosterol biosynthetic inhibitors is a growing global health problem. Survival rates for those infected with resistant isolates are exceptionally low. Although our understanding of the molecular basis of clinically significant azole resistance in *A. fumigatus* is limited, data from the fungal pathogen *A. fumigatus* indicates that resistance is associated with genetic modifications that potentiate ergosterol biosynthesis without significantly compromising pathogenicity. Based on this evidence, we reasoned that clinically relevant antifungal resistance could derive from transcriptional rewiring, promoting drug resistance without concomitant reductions in pathogenicity. In order to identify transcriptional regulators, which have the potential to drive clinically relevant resistance phenotypes, we constructed a genome-wide library of 484 null mutants. Here we describe that loss of the negative cofactor 2 complex leads to resistance, not only to the azoles but also the salvage therapeutics amphotericin B and terbinafine, without significantly affecting pathogenicity.

2.1 Introduction

Aspergillus fumigatus is an important airborne mould pathogen and allergen worldwide. Estimates suggest that over 3 million people have invasive or chronic infections that lead to in excess of 600,000 deaths every year [1]. Only three classes of drugs are currently recommended for the treatment of aspergillosis with the azole class being recommended for primary therapeutic purposes and amphotericin B and the echinocandins (caspofungin and micafungin) for salvage therapy. With an optimal treatment regime, mortality rates for invasive disease remain around 50% [2]. It is of great concern, however that drug resistance to the azoles is rapidly emerging. For individuals that are infected with a resistant isolate the mortality rate exceeds 80% [3, 4]. As disease progression is so rapid in invasive aspergillosis (IA) [5], therapy failure is attributable to delays in administering alternative agents. Methods to rapidly detect resistance are critical to ensure effective transition to alternative appropriate therapies.

Our understanding of the factors governing azole resistance in *A. fumigatus* is not fully defined. The azoles act by inhibiting the hemoprotein lanosterol demethylase (Cyp51A) resulting in a reduction of the key sterol, ergosterol, in the fungal membrane and an accumulation of toxic sterol intermediates [6]. Azole resistance is frequently associated with an allelic variant of *cyp51A* that incorporates a tandem repeat in the promoter, typically TR_{34} or TR_{46} with a secondary mutation L98H within its coding commonly associated with TR_{34} [7]. These modifications appear to have no substantial impact on pathogenicity in murine models of invasive aspergillosis [8]. The mechanism of resistance in a significant proportion of other isolates remains unclear [7]. This hinders the development of rapid molecular diagnostics to detect drug resistance in the clinic. Our limited understanding of the mechanisms of azole resistance also prevents the development of combination therapeutic strategies that specifically target drug resistance mechanisms [9].

We and others have recently reported on the role played by various *A. fumigatus* transcriptional regulators in response to azole antifungal drugs [10-12]. The sterol regulatory element binding protein (SREBP), SrbA is a basic helix-loop-helix (bHLH) transcriptional activator, which directly regulates at least seven genes in the ergosterol biosynthetic pathway, including *cyp51A* [10]. Loss of *srbA* through gene

replacement results in a significant increase in susceptibility to azoles [13] in part due to significant reductions in *cyp51A* mRNA levels [14]. The binding site for SrbA in the *cyp51A* promoter falls within the 34 and 46 mers duplicated in TR34/46 pandemic azole resistant isolates [12]. The repeat duplicates the DNA binding site leading to SrbA mediated upregulation of *cyp51A* and a concomitant increase in azole resistance. AtrR, a Zn2-Cys6 transcription factor, also positively regulates sterol biosynthesis and directly binds the *cyp51A* promoter at the TR site, and additionally the promoter of an azole exporter, *cdr1B* [11, 15]. The CCAAT-binding domain complex CBC, a heterotrimer comprising HapB, HapC and HapE, is a negative regulator of sterol biosynthesis directly binding the promoters of 14 ergosterol biosynthetic genes including *cyp51*A [12]. Loss of CBC function leads to pan-azole resistance. Notably, a clinical azole resistant isolate with a defect in HapE that results in perturbed DNA binding at the *cyp51A* promoter has been described [12, 16]. Binding of the CBC at the *cyp51A* promoter is facilitated by another transcriptional regulator, HapX [12]. HapX is an iron responsive basic region leucine zipper (bZIP) transcription factor that regulates the expression of genes linked to iron acquisition, storage and metabolism and facilitates binding of the CBC [17]. It is also notable that loss of SrbA, the CBC, HapX or AtrR is associated with significant reductions in virulence in murine models of invasive pulmonary aspergillosis [11-13, 17].

The transcriptional network governing azole resistance is therefore highly complex and involves multiple regulators, some of which remain to be identified. Our current models of this network are not able to explain all of the existing clinically significant mechanisms of azole resistance in *A. fumigatus*. We therefore postulated that other perturbations of the transcriptional network would lead to alterations in azole resistance without affecting pathogenicity. To accomplish this objective, we have generated and screened a library of 484 *A. fumigatus* transcription factor null mutant strains and identified a cohort of 12 factors that affect azole resistance and sensitivity. Here we describe in detail the role of two CBF/NF-Y family transcription regulators, AFUB_029870 (NctA) and AFUB_045980 (NctB) where loss of function leads to azole resistance. We show that, like their orthologues in *S. cerevisiae* (Bur6 and Ncb2) [18] which act as a heterodimer known as Negative Cofactor 2 (NC2), *A. fumigatus* NctA and NctB (Negative cofactor two A and B) are

part of the same transcriptional regulatory complex. We demonstrate that the NC2 complex is a key regulator of ergosterol biosynthesis and the azole exporter CDR1B. We also report that loss of the NC2 complex leads to a multi-drug resistance phenotype including the azoles (itraconazole, voriconazole and posaconazole) as well as the salvage therapeutic amphotericin B [19] and terbinafine, an agent used in the treatment of chronic and allergic disease[20]. Furthermore loss of this complex results in a notable increase in the immunogenic properties of *A. fumigatus* but does not result in loss of virulence.

2.2 Materials and methods

2.2.1 Generation and validation of transcription factor null mutants

The transcription factor null mutant collection was generated in the *A. fumigatus* strain MFIG001 (previously known as A1160 *Δku80 pyrG+* [21]). Gene replacement cassettes were generated using a fusion PCR approach (Figure S2.2) [22]. Briefly primers P1 and P2 were used to amplify around 1 kb of the 5' flank, while P3 and P4 were used to amplify the 3' flank. Primers hph_F and hph_R were used to amplify a 2.8 kb hygromycin B phosphotransferase cassette from pAN7-1. PCR products were purified by solid phase extraction with the Qiagen QIAquick® PCR purification kit (Qiagen). Fusion of the three products was facilitated by the presence of common linker sequences on primers P2 and hph_F, P3 and hph_R and the use of the nested primers P5 and P6. PCR amplification was carried out using the protocols defined in Szewczyk et al [22]. Transformation was carried out as previously reported [23]. The sequences of all primers used are given in Appendix I.

Validation of homologous recombination and single integration of the deletion cassette was performed by PCR (Figure S2.1). PhusionFlash High-Fidelity Master mix (ThermoFisherScientific) was used for all reactions. Primers P1 with hph-chk 5'-Rv and hph-chk 3'-Fw with P4 were used to amplify a region of about 1kb from within the deletion cassette to the flanking region outside of the deletion cassette. Furthermore, PCR was performed with P1 and P4 as primers to check the purity of the gene knockout strain.

2.2.2 Drug sensitivity screening

Conidia of 484 TFKO strains were inoculated in 25 mL culture flasks containing ACM + 100 μM hygromycin. Conidia were harvested by filtration and counted via optical density measurements. Approximately 2,000 spores were inoculated per well of a CytoOne® 96-well plate (StarLab) containing RPMI-1640 medium 2.0 % glucose and 165 mM MOPS buffer (pH7.0) with 0, 0.06, 0.12 or 1.0 mg/L itraconazole. Plates were incubated at 37 °C for 48 h (0, 0.06, 0.12 mg/L or 96 h (1.0 mg/L) and optical density measurements were taken at 600 nm. Fitness was calculated by normalizing optical density to the wild-type strain. Relative fitness was obtained by normalizing fitness under itraconazole challenge to fitness of this strain

under no itraconazole challenge. MIC determination for all drugs was carried out according to methods outlined by EUCAST [24].

2.2.3 Radial growth germination rate and hyphal extension analysis

Radial growth of the wild type strain (MFIG001), the *nctA* null mutant or the *nctA* reconstituted strains was measured by inoculating 500 spores on *Aspergillus* Minimal Media (AMM), *Aspergillus* Complete Media (ACM), RPMI 1640 medium with 2.0 % glucose and 165 mM MOPS buffer (pH7.0) or Dulbecco's Modified Eagle's Medium (DMEM) on petri dishes. Plates were incubated at 37 °C for 72 h and the radius of colonies was measured every 24 h.

Germination rate and hyphal extension rate were determined as follows. 500 µl of $5x10^5$ spores of the strains were inoculated in RPMI 1640 medium containing 2.0 % glucose and 165 mM MOPS buffer (pH7.0) in a 24 well glass bottom plate. The culture was incubated at 37 °C and either optical density (600 nm) was measured on a Synergy 2 Multidetection Microplate reader (BioTek) or images were taken on a Leica SP8X confocal microspoce (Leica). Sporulation and hyphal length were measured in ImageJ.

2.2.4 S-tag co-immunoprecipitation

C-terminal S-tagged cassettes were generated by fusion PCR using primers SP1-SP8 (Appendix I). Three separate PCR reactions were performed for initial amplification of the cassette components. Primers SP1 and SP2 were used to amplify the 5' flank and TF coding sequence, primers SP3 and SP4 amplified the downstream region of the TF (ca. 1 kb) from MFIG001 genomic DNA. Primers SP5 and SP6 were used to amplify the S-Tag, G5A linker and *pyrG* gene from pHL81 [25]. PCR products were purified by solid phase extraction with the QIAquick® PCR purification kit (Qiagen). Fusion of the three products was facilitated by the presence of linker sequences on primers SP2, SP3, SP5 and SP6 and the use of nested primers SP7 and SP8. The cassette was transformed into *A.fumigatus* A1160p+ and NctA-Stag and NctB-Stag strains were validated by PCR as described above for the gene KO process. Proteins were extracted from 16 h shake flask cultures (SAB medium, incubated at 37˚C). Briefly, biomass was frozen in liquid nitrogen and ground to a fine powder before incubation on ice in 6 ml of ice cold HK

buffer (100 mM NaCl) per 1 g biomass for 30 min. Samples were centrifuged at 7500 x *g* for 30 min and filtered through glass wool to remove cellular debris. To purify the S-tagged proteins, crude protein extract was incubated with S-protein agarose beads (Novagen) with gentle agitation at 4 °C for 2 h. Samples were centrifuged and the agarose bead pellet was washed in ice cold HK Buffer with 100mM NaCl and transferred to a S-Protein spin column (Novagen) where the beads were washed a further six times with 700 µl HK Buffer with 100 mM NaCl. S-tagged proteins were eluted using 50 µl Laemmli sample buffer. Eluted proteins were analysed by the Protein Mass Spectrometry at the Biological Mass Spectrometry Core Facility at the University of Manchester.

2.2.5 Chromatin Immunoprecipitation (ChIP) of S-tagged NctA.

$1x10^6$ spores/ml of the wild-type strain (*A. fumigatus* A1160) or the S-tagged NctA expressing strain were grown in 50 ml of Vogel's minimal medium for 18 h at 37 °C with constant shaking at 180 rpm. The mycelia were harvested by filtration, washed twice with distilled water, and were transferred into 50 ml of RPMI 1640 medium (Sigma-Aldrich) containing 2.0 % glucose and 165 mM MOPS buffer (pH7.0). The cells were incubated for 4 h in the absence and the presence (0.5 mg/mL) of itraconazole at 37 °C under shaking. Cross-linking was carried out by the addition of formaldehyde to a final concentration of 1.0 % followed by incubation at 37 ˚C for 20 min.

Chromatin immunoprecipitation (ChIP) was performed essentially as described previously [26]. ChIP reaction was performed with an Anti-S tag polyclonal antibody (ab18588, abcam) on Dynabeads Protein A magnetic beads (ThermoFischerScientific). Immunoprecipitated DNA was reverse cross-linked, treated with RNase A (Sigma-Aldrich), and then purified using a MinElute PCR purification kit (Qiagen). To prepare input control, 100 µL of the sonicated extract was reverse cross-linked, treated with RNaseA (Sigma-Aldrich), and then purified using a MinElute PCR purification kit (Qiagen).

2.2.6 ChIP-sequencing analysis.

ChIP-seq libraries were constructed following the manufacturers instructions for Illumina ChIP-seq library preparation. Eight samples were indexed and sequenced in a single lane on the Illumina HiSeq2500 as paired-end reads.

Raw sequencing reads were quality controlled with Illumina chastity filter and fastqc v0.11.3, and then Illumina adapters were trimmed from them using Trimmomatic. The resulting reads were aligned to the *A. fumigatus* A1163 CADRE genome from Ensemble fungi, version 26 using Bowtie2. Peak calling was carried out using a Model-based Analysis for ChIP-Sequencing (MACS2[27]) version 2.1.0 with a q-value cutoff of 0.01. Results reported herein are for the combined reads from two biological replicate samples. All ChIP-seq experiments were carried out in two biological replicate samples. All ChIP-seq datasets are deposited in the NCBI Gene Expression Omnibus (GEO; https://www.ncbi.nlm.nih.gov/geo/) under accession number GSE129967.

2.2.7 Conserved motif discovery.

The reproducible 100 bp of the merged ChIP peak regions with more than 2-fold read enrichment compared to the corresponding were analyzed for conserved nucleotide motifs using the MEME suite [28] version 4.12.0. DNA sequence of the ChIP peak regions were retrieved from the genomic locations using the getfasta function from the BED tools suite [29] and analyzed with the default setting.

2.2.8 Transcriptomic analysis.

$1x10^6$ spores/ml of *A. fumigatus* CEA10 was grown in 50 ml of Vogel's minimal medium containing 1.0 % glucose for 18 h at 37 °C on a rotary shaker (180 rpm). Mycelia were collected by filtration, and washed twice with distilled water. About 1.0 g of wet mycelia were transferred into 50 ml of RPMI-1640 medium containing 2.0 % glucose and 165 mM MOPS buffer (pH7.0), and the cells were incubated for 4 h in the absence or the presence of itraconazole (0.5 mg/mL) at 37 °C with shaking. The drug treated mycelia were then collected by filtration, immediately frozen with liquid nitrogen, and kept at -80 ˚C until use.

Total RNA was extracted using TRI Reagent® (Sigma-Aldrich) according to the manufacture's instructions. The extracted RNA samples were treated with RQ1

RNase-Free DNase (Promega) and further purified using the RNeasy Mini Kit (Qiagen).

For paired-end RNA sequencing, libraries were generated using the TruSeq® Stranded mRNA assay (Illumina, Inc.) according to the manufacturer's instructions. Eight samples were indexed and sequenced in a single lane on the Illumina HiSeq2500. Generated Fastq files were analysed with FastQC and any low-quality reads were trimmed with Trimmomatic. All libraries were aligned to the *A. fumigatus* A1163 genome assembly GCA_000150145.1) with the gene annotation from CADRE/Ensembl Fungi v24 using Bowtie and only matches with the best score were reported for each read. All RNA-seq experiments were carried out in three biological replicates. Differential expression analysis was performed using DESeq [30]. All RNAseq datasets are available in the NCBI Gene Expression Omnibus under accession number GSE133464.

2.2.9 Gene Set Enrichment analysis.

Gene ontology, Functional category, and KEGG pathway enrichment analysis were carried out using the FungiFun2 2.2.8 BETA[31] web-based server (https://elbe.hki-jena.de/fungifun/fungifun.php) with the *A. fumigatus* A1163 genome annotation. Differentially expressed genes showing more than 2-fold enrichment with FDR <0.05 were subjected to the enrichment analysis. Significance level of the enrichment was analyzed using the Benjamini-Hochberg adjustment method with a p-value cutoff <0.05.

2.2.10 Sterol analysis

Conidia (1 x 10^6) were grown in 50 mL RPMI-1640, incubated for 24 h at 37 °C with shaking (200 rpm). Mycelia were harvested, freeze dried and dry weights obtained prior to processing. Pellets were sonicated thoroughly (6 x 30 sec with Branson Digital Sonifier 250) in 1 ml ddH_2O and an internal standard of 10 µg of cholesterol was added to each sample.

Sterols were extracted and derivatised as previously described [32]. Briefly, lipids were saponified using alcoholic KOH and non-saponifiable lipids extracted with hexane. Samples were dried in a vacuum centrifuge and were derivatised by the addition of 0.1 ml BSTFA TMCS (99:1, Sigma-Aldrich) and 0.3 ml anhydrous

pyridine (Sigma-Aldrich) and heating at 80 °C for 2 h. TMS-derivatised sterols were analysed and identified using GC/MS (Thermo 1300 GC coupled to a Thermo ISQ mass spectrometer, ThermoFischerScientific) and Xcalibur software (ThermoFischerScientific). The retention times and fragmentation spectra for known standards were used to identify sterols. The quantity of ergosterol (w/w) was calculated using the peak areas of ergosterol and the cholesterol internal standard from triplicate biological samples.

2.2.11 Western Blotting of CDR1B

Western Blotting of CDR1B was performed essentially as previously described [33]. The rabbit anti-CDR1B polyclonal antibody_ENREF_42 [33] was used with a Horseradish peroxidase-conjugated secondary antibody and an ECL kit (Pierce) to visualize imunoreactive protein.

2.2.12 Murine infection models

The murine infection experiments were performed under UK Home office Project Licence PDF8402B7 and approved by the University of Manchester Ethics Committee. *A. fumigatus* was cultured on ACM containing 5 mM ammonium tartrate for 6 days at 37 ˚C and conidia were harvested in sterile saline.

CD1 male mice (Charles River UK, Ltd.) were housed in groups of 3-4 in IVC cages with access to food and water *ab libitum*. All mice were given 2 g/L neomycine sulphate in their drinking water throughout the course of the study. For the leukopenic model of infection, mice were rendered leukopenic by administration of cyclophosphamide (150 mg/kg of body weight; intraperitoneal) on days -3, -1, +2, and every subsequent third day, and a single subcutaneous dose of cortisone acetate (250 mg/kg) was administrated on day -1. For the cortisone acetate model, mice were immunosuppressed with cortisone acetate (250 mg/kg), which were administrated subcutaneously on days -3, -1, +2, and every subsequent third day. Mice were anaesthetized by exposure to 2-3 % inhalational isoflurane and infected by intranasally with a spore suspension of 1.25 x 10^7 conidia/ml (leukopenic model) or 1.75 x 10^8 conidia/ml (cortisone acetate model) in 40 µl of saline solution. Mice were weighed every 24 h from day -3, relative to day of infection, and visual inspections were made twice daily. In the majority of cases, the endpoint for survival

in experimentation was a 20% reduction in body weight measured from day of infection, at which point mice were sacrificed. Kaplan-Meier survival analysis was used to create a population survival curve and to estimate survival over time, and p-values were calculated through a log rank analysis.

2.2.13 Histology analysis

Immunosuppressed male CD1 mice (n = 3) were infected as described above. After 36 h of infection mice were sacrificed and lungs were partitioned into lobes destined for histology analysis or fungal burden and cytokine mRNA expression analysis. Lobes for fungal burden and cytokine analysis were snap-frozen in liquid nitrogen and stored at -80 ˚C until use. Lobes for histological analysis were immediately fixed in 4.0 % (v/v) formaldehyde (Sigma-Aldrich), and subsequently embedded in paraffin. 4 µm sections were stained with haematoxylin-eosin (HE) and Grocott's Methenamine Silver (GMS). Images were taken using a Pannoramic 250 Flash Slide Scanner (3D HISTECH) using brightfield illumination.

2.2.14 Fungal burden analysis

Total genomic DNA was extracted from the infected lung samples using a standard CTAB DNA extraction method. Fungal burden was determined by quantitative Real-time PCR (qPCR) as described previously [34] qPCR was performed in a 7500 Fast Real-Time PCR system (Applied Biosystems) using the SsoAdvanced Universal SYBR Green Supermix (Bio-Rad) with the primers listed in the Appendix I. Amplification reactions were performed in triplicate in a final volume of 20 µL using 0.5 µM forward primer, 0.5 µM reverse primer, and 100 ng of total DNA. qPCR data were analysed as described [34]. The statistical significance of variances between fungal burdens was calculated by using a non-parametric Mann-Whitney *t* test.

2.2.15 Cytokine expression analysis

Total RNA was extracted from the infected lung samples using the RNeasy kit (Qiagen). First-strand cDNA was synthesized using the iScript cDNA synthesis kit (Bio-Rad) with 500 ng of total RNA as a template. Amplification reactions were performed using the iTaq Universal SYBR Green Supermix (Bio-Rad) in a final volume of 20 µL using 0.5 µM forward primer, 0.5 µM reverse primer, and 2µL of

5-fold diluted cDNA. Primers used in this analysis are listed in Appendix I. Relative expression level of gene expression was analyzed using the ΔΔCt method with the murine actin encoding *actB* as the reference. Experiments were performed in biological triplicates. A two-sided Student's t-test was used for statistical analysis where *p*-value of <0.05 were considered as significant.

2.2.16 Cell toxicity assays

A549 human pulmonary carcinoma epithelial cells (American type culture collection, CCL-185) and Raw 264.7 macrophages were used under passage 20. Cells were maintained at 37 °C, 5% CO_2 in Dulbecco's Modified Eagle's Medium (DMEM), 10 % foetal bovine serum (FBS), 1 % Penicillin-Streptomycin (Sigma-Aldrich). For all experiments, $2x10^5$ A549 or RAW 264.7 cells were seeded in 24-well plates and incubated for 16 h when confluence equals 90 %. Cells were then challenged with 10^5 spores of Δ*nctA*, *nctA rec* and the isogenic control and incubated for 24 h. Following co-incubation with *A. fumigatus* spores, cell culture supernatants were collected and the level of inflammatory markers or cell toxicity via lactate dehydrogenase assay were measured (Promega).

The concentration of IL-8 and IL-6 were determined in A549 epithelial cells co-cultured with *A. fumigatus* strains by using the Human IL-8/CXCL8 and IL-6 DuoSet ELISA according to manufacturer's instructions (R&D systems). Experiments were performed in five biological replicates and technical triplicates. For data analysis, a four-parameter logistic (4-PL) curve was created plotting the absorbance versus Log_{10} concentration of the standards and then sample concentrations determined by using a non-linear regression. Differences in IL-8 and IL-6 concentration between A549 cells challenged with Δ*nctA*, *nctA rec* and the isogenic control spores and uninfected controls were determined by One-way multiparametric ANOVA with Dunnet's correction using GraphPad Prism 7.0 (La Jolla, CA, USA)

2.2.17 BMDC culture

GM-CSF induced BMDCs were generated as previously described ([35]). Bone marrow cells from C57BL/6 mice were seeded at $2x10^5$/ml in complete media (RPMI-1640 (Sigma) plus 20 ng/ml GM-CSF (Peprotech), 10 % FCS, 2mM L-

glutamine (Gibco), 100U/ml penicillin 100 µg/ml streptomycin (Sigma)). Cells were cultured for 10 days, with 50 % of the media replaced on days 3, 6, and 8. On day 10 DCs were re-plated at $2x10^5$ cells/well, with $10x10^5$ *A. fumigatus* spores (MOI 5:1), and incubated for 6 hours at 37 °C.

2.2.18 Flow cytometry and ELISA

Post incubation, cells were taken for flow cytometry, and supernatants for ELISA. Cells were plated at $1x10^6$ cells/well, washed twice in PBS, and stained with Zombie UV (Biolegend). FcR block (Biolegend) was then added, in addition to the following antibodies: CD11c-APCef780, CD40-PE CD80-PerCP/Cy5.5 (all Biolegend). Cells were washed twice in flow buffer (PBS 2mM EDTA (Sigma) 2% FCS (Sigma)), and samples were acquired on a BD Fortessa, and analysed using Flowjo v10 (TreeStar). Cytokines for ELISA were measured using purified coating, detection antibodies and standards (Biolegend) or duosets (R&D), as per manufacturers protocol.

2.2.19 TEM imaging

For Transmission Electron Microscopy the samples were fixed with 4% formaldehyde + 2.5% glutaraldehyde in 0.1 M HEPES buffer (pH 7.2). Then samples were incubated in 1 % sodium met-periodate (in H_2O) for 1 h. After that they were postfixed with 1% osmium tetroxide + 1.5% potassium ferrocyanide in 0.1 M cacodylate buffer (pH 7.2) for 1 h and finally in 1 % uranyl acetate in water for 1 h. Specimens were dehydrated in ethanol series infiltrated with TAAB Low Viscosity resin and polymerized for 24 h at 60 ˚C. Sections were cut with Reichert Ultracut ultramicrotome and observed with FEI Tecnai 12 Biotwin microscope at 100 kV accelerating voltage. Images were taken with Gatan Orius SC1000 CCD camera.

2.2.20 Data availability

All RNA-seq and ChIP-seq datasets are available in the NCBI Gene Expression Omnibus (GEO; https://www.ncbi.nlm.nih.gov/geo/) under accession number GSE133464 (RNA-seq) and GSE129967 (ChIP-seq).

2.3 Results

2.3.1 Generation of a library of transcription factor null mutants in Aspergillus fumigatus

A systematic review of the genes previously annotated as transcription factors (TFs) in the databases at ENSEMBL fungi, ASPGD and DBD [36] resulted in the identification of 495 putative TFs (Appendix I). To further characterise this cohort, we classified each TF according to its Pfam domains, identified using Hidden Markov Model profiling (hmmscan). The majority of TFs were shown to have either one (n=239) or two (n=157) functional domains associated with transcriptional regulation (Figure 2.1). The most common domains identified were zinc finger (n=249) and fungal specific transcription domains (n=194; Figure 2.1). This is consistent with previous reports that describe domains of transcription factors in ascomycetes [37]. Although 84 proteins either lacked any Pfam domains (70) or only had domains of unknown function (14), DNA binding domains were identified in these proteins using InterPro.

Unlike in the model yeast, *Saccharomyces cerevisiae*, gene replacement strategies in *A. fumigatus* are complicated by relatively low levels of homologous recombination. This problem can be mitigated by the use of strains lacking components of the non-homologous end joining machinery [38] such as Ku70 [39], Ku80 [40] and Lig4 [41]. However, even in strains lacking these factors, gene replacement cassettes require around 1kb of homologous sequence flanking each side of a target gene [40]. To facilitate the disruption of all of the TFs identified we chose to employ a fusion PCR approach similar to that described by Szewczyk et al [22] (see schematic Figure S2.1) and used custom developed scripts to design the primers for amplification of the gene replacement cassettes. Cassettes were successfully amplified for all 495 of the TFs and were used to transform MFIG001, a *Δku80*, *pyrG*+ strain derived from FGSC strain A1160 [21]. We isolated null homokaryons for 97.7% (484) transcription factor genes as defined by our ability to isolate strains in which we could amplify from the hygromycin resistance cassette to a region beyond the gene replacement cassette in addition to a lack of a PCR product corresponding to the target gene (see schematic Figure S2.1). Precise replacement was further confirmed for a randomly selected subset of 12 mutants by Southern blot

analysis (data not shown). Despite several attempts (minimum n=3) we were unable to isolate null mutants for 11 genes (Appendix I). The majority of these genes encode components of the RNA polymerase I/II/III transcription factor complexes, or are transcription factors, which locate at a higher-level of a regulatory hierarchy [42].

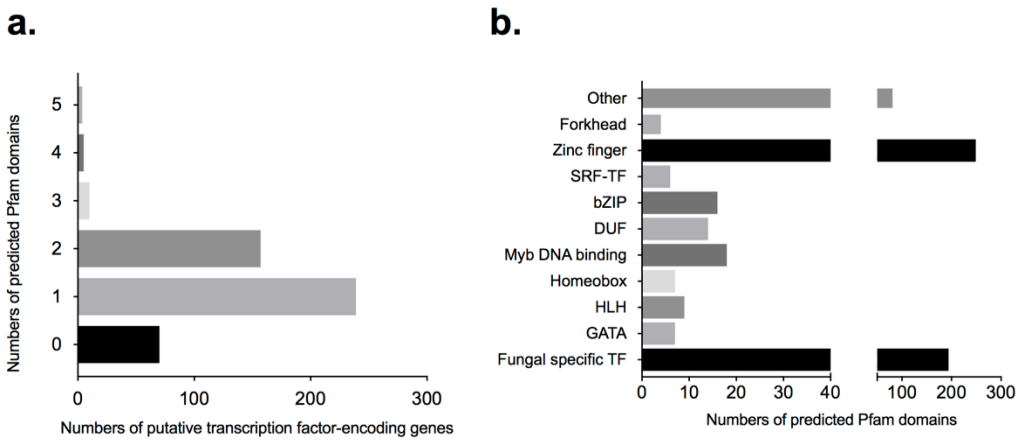

Figure 2.1: Overview of the identified 495 putative transcrption factors in the A. fumigatus A1163 genome. (a) Domain compositions of the putative transcription factors. The number of predicted Pfam domains in a single transcription factor is shown. **(b)** Distribution of A. fumigatus transcription factors among the fungal class of Pfam regulator families.

2.3.2 A genome wide screen of the transcription factor mutant library reveals key regulators associated with azole resistance and sensitivity in A. fumigatus.

To identify novel transcriptional regulators associated with azole resistance and sensitivity, we screened the transcription factor null library at itraconazole concentrations representing sub-minimum inhibitory concentrations (MIC) (0.06 and 0.12 mg/L) for the isogenic isolate MFIG001 (MIC = 0.5 mg/L) and above MIC (0.5 mg/L) levels in RPMI-1640 medium following procedures outline by EUCAST [24].

Six transcription factor null mutants exhibited clear and reproducible fitness defects in sub-MIC levels of itraconazole when compared to the cohort of mutants in the collection (Figure 2.3a). The transcription factors knocked out in two of these mutants have previously been defined as activators of the ergosterol biosynthetic pathway including *cyp51*A, namely SrbA and AtrR. The other null mutants identified in the screen lacked the carbon catabolite repressor CreA [43], the calcium

responsive regulator ZipD [44], the SAGA complex subunit AdaB [45] and the orthologue of the *S. cerevisiae* stress responsive regulator GIS2 herein described as GisB [46]. When the library was screened at itraconazole levels in excess of the MIC we identified six transcription factor mutants, two of which we have previously described (Δ*hapX* and Δ*hapB*) [12] and four of which we associate with azole resistance in *A. fumigatus* for the first time (Δ*nctA*, Δ*nctB*, Δ*areA* and Δ*rscE*).

We extended our phenotypic profiling of these isolates to assess their general growth phenotype (Figure 2.2) and sensitivity profiles to additional antifungal drugs (Figure 2.3b-c). Among the 12 screened regulators, 3 sensitive (Δ*adaB*, Δ*creA*, and Δ*zipD*) and 3 resistant isolates (Δ*hapB*, Δ*nctA*, and Δ*nctB*,) showed reduced growth rate on a solid Aspergillus complete medium (ACM), but the remaining strains retained similar growth rate with the parental strain (Figure 2.2). In comparison to the isogenic wild-type control, Δ*creA* and Δ*zipD* showed increased sensitivity to the ergosterol biosynthetic inhibitor terbinafine. Interestingly, the *nctA* and *nctB* null mutants phenocopied each other and were resistant to the triazoles voriconazole (>32-fold increase in MIC) and posaconazole (>128-fold increase), terbinafine (2-fold increase in MIC), miltefosine (8-fold increase in MIC) and amphotericin B (8-fold increase in MIC). Conversely, the *nctA* and *nctB* null mutants showed hypersensitivity to the cell wall perturbing agents Congo Red, Calcofluor White, caspofungin and micafungin.

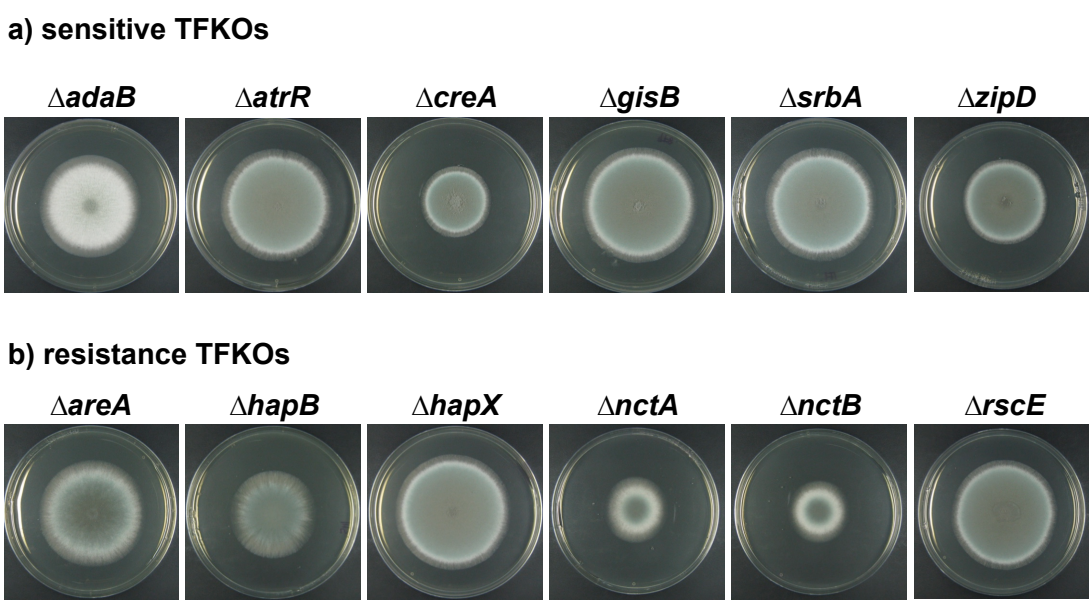

Figure 2.2: **Normal growth of transcription factors associated with azole tolerance in *A. fumigatus*. (a)** Phenotype of itraconazole sensitive transcription factors knockout (TFKO) mutants spotted on Aspergillus complete medium and grown for 72 hours. **(b)** Phenotype of itraconazole resistant transcription factors knockout (TFKO) mutants spotted on Aspergillus complete medium and grown for 72 hours. A1160p+ parental isolate control of this experiment can be found in Figure S2.3.

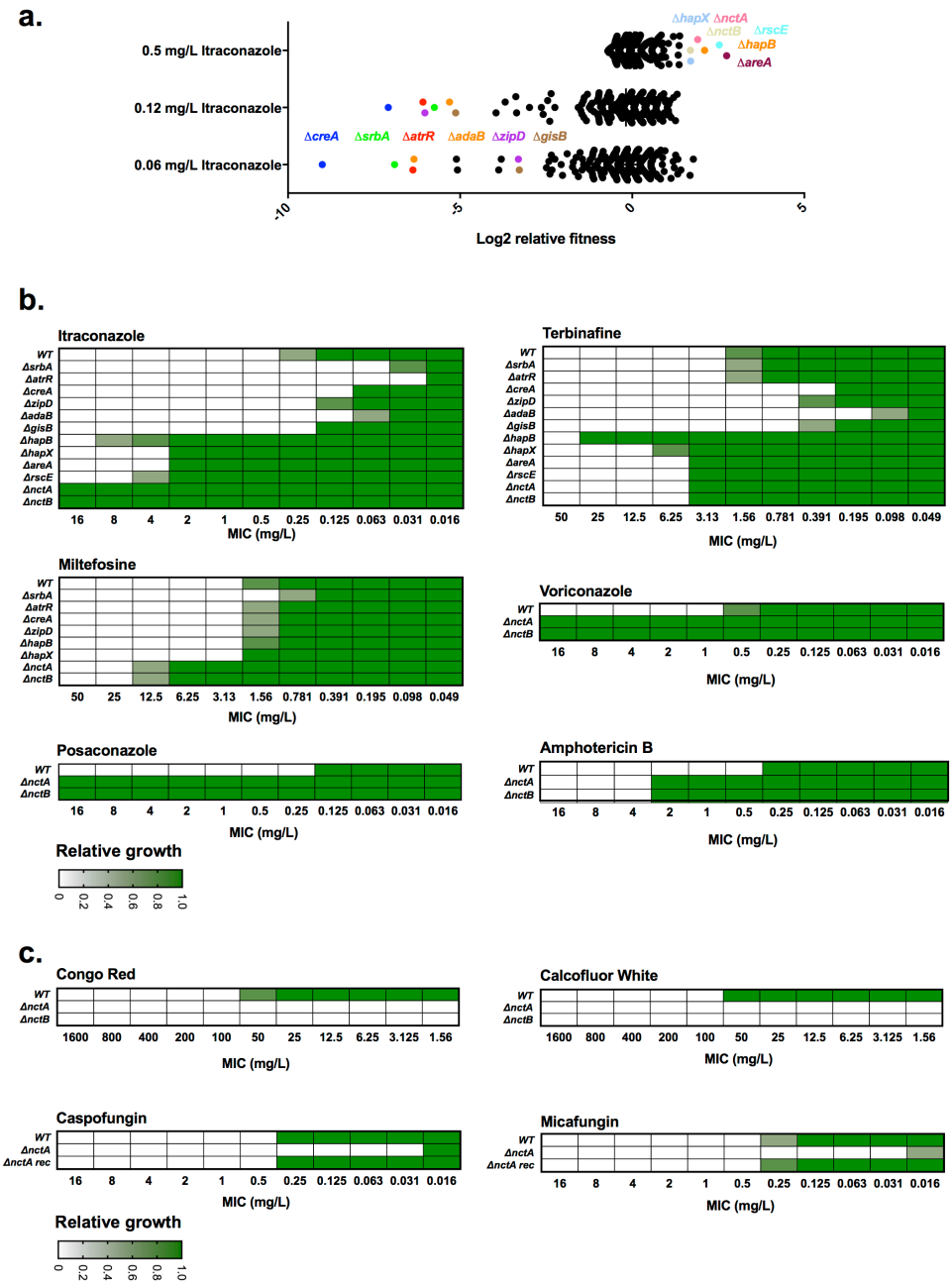

Figure 2.3: Identification of transcription factors associated with azole tolerance in *A. fumigatus*. (a) Relative growth fitness of the 484 constructed TFKO mutants in MIC (0.5mg/L) and sub-MIC (0.06, and 0.12 mg/L) levels of itraconazole. Each dot represents the mean of three replicate experiments. The TFKOs which exhibited significant fitness defects (fitness less than -4 for sub-MIC, and more than 1.5 for MIC condition) are indicated by colored circles. **(b, c)** Heatmaps showing drug susceptibility profiles of the screened TFKO mutants to different antifungal drugs. Susceptibility assays were performed in triplicate, where optical density readings of fungal growth were standardized to no-drug control wells and shown as a relative growth values.

2.3.3 NctA and NctB are members of the CBF/NF-Y family of transcription factors

Pfam domain searches indicate that NctA and NctB are members of the evolutionarily conserved CBF/NF-Y family of transcription factors, which include the CBC transcription regulator complex (Figure 2.4) [47]. NctA (AFUB_029870) encodes a 247 aa protein and is a reciprocal BLAST match of the *S. cerevisiae* negative cofactor 2 (NC2) complex α-subunit Bur6. NctA and Bur6 however, show little sequence similarity with the exception of the CBF/NFYB domain where they share 49% identity over 75 contiguous amino acids. NctA has two paralogues in *A. fumigatus*, HapE and an as yet un-named regulator encoded by AFUB_058240. Consistent with the similar phenotypes of the *nctA* and *nctB* null mutants, *nctB* (AFUB_045980) encodes a 142 aa protein that is the reciprocal BLAST match of the *S. cerevisiae* NC2 complex β-subunit (Ncb2) sharing 49% sequence identity over 86% of the protein. NctB has one readily identifiable paralogue in *A. fumigatus*, HapC.

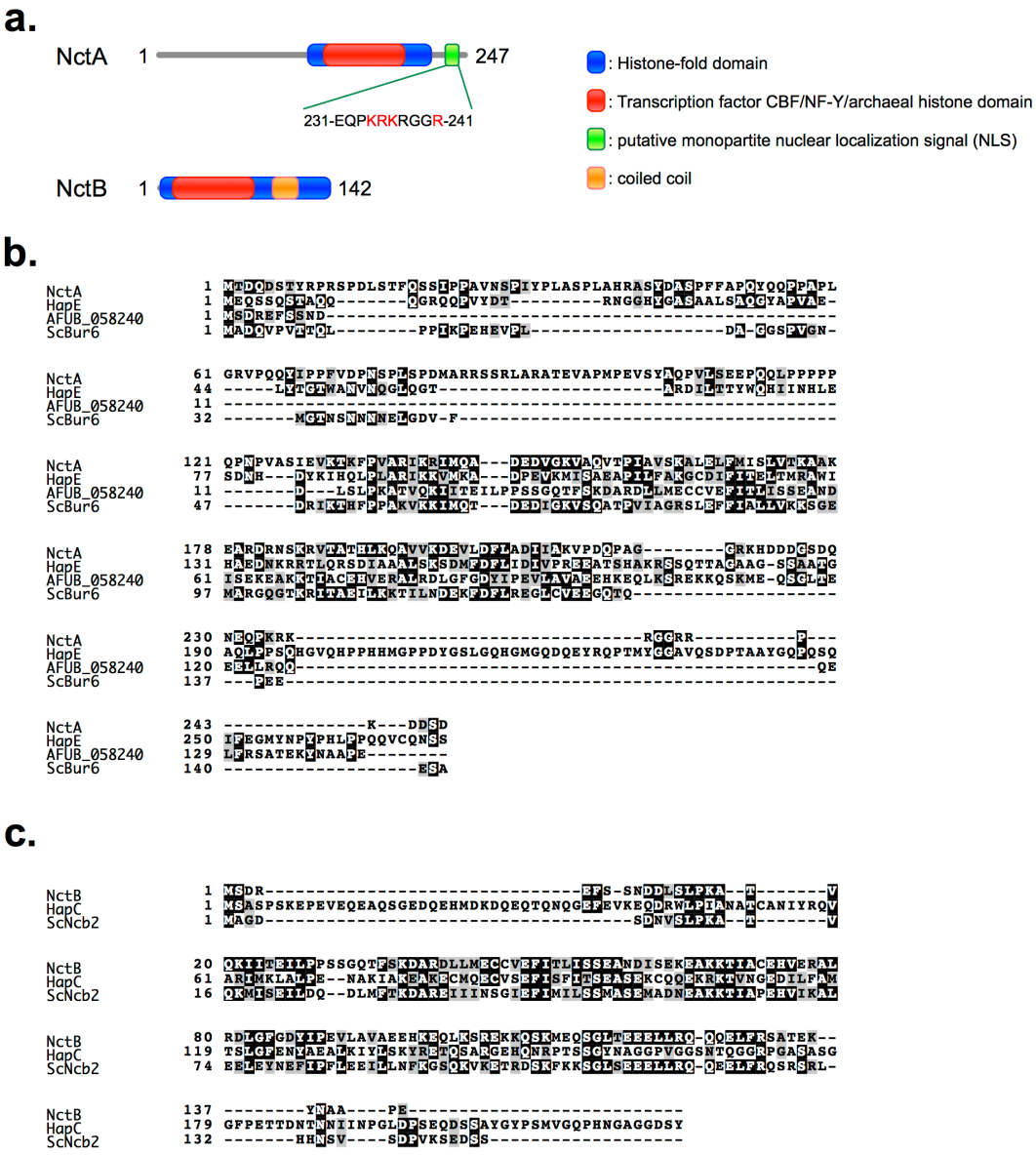

Figure 2.4: Domain structure and sequence alignment of NctA and NctB. (a) Schematic representation of the domain structure of *A. fumigatus* NctA and NctB. The histone-fold domain (IPR009072) predicted by InterPro Scan is shown in blue. The transcription factor CBF/NF-Y/archaeal histone domain (PF00808) predicted by PfamScan is shown in red. The position of the putative monopartite nuclear localization signal (NLS) identified by NLS-mapper within the C-terminal region of NctA is shown in green with amino acid sequence, and the predicted coil region found within the histone-hold domain of NctB is depicted in orange, respectively. **(b)** Multiple protein sequence alignment of *A. fumigatus* NctA, its paralogues (HapE and AFUB_058240), and the orthologue Bur6 in *Saccharomyces cerevisiae*. (c) Multiple protein sequence alignment of *A. fumigatus* NctB, its paralogue (HapC), and the orthologue Ncb2 in *S. cerevisiae*.

2.3.4 Loss of NctA leads to a reduction in growth rate and delayed germination.

To determine if the effects of *nctA* loss were due solely to the gene replacement and not other mutagenic events from transformation, a *nctA* reconstituted strain was generated. The growth rate of the *nctA* null alongside the parent strain MFIG001 (WT) and the *nctA* reconstituted strain (*nctA* rec) was assessed on Aspergillus complete media (ACM), Aspergillus minimal media (AMM), RPMI-1640, and DMEM. In all conditions the *nctA* null mutant had a significantly reduced growth rate (36 to 44 % reduction) compared to MFIG001 (Figure 2.5a and b, Figure S2.3). Importantly, the reconstituted strain was indistinguishable in these assays from MFIG001. This reduction in growth rate is associated with a decrease in the initial rate of germination (5-6 Hrs) and hyphal extension (Figures 2.5c and d).

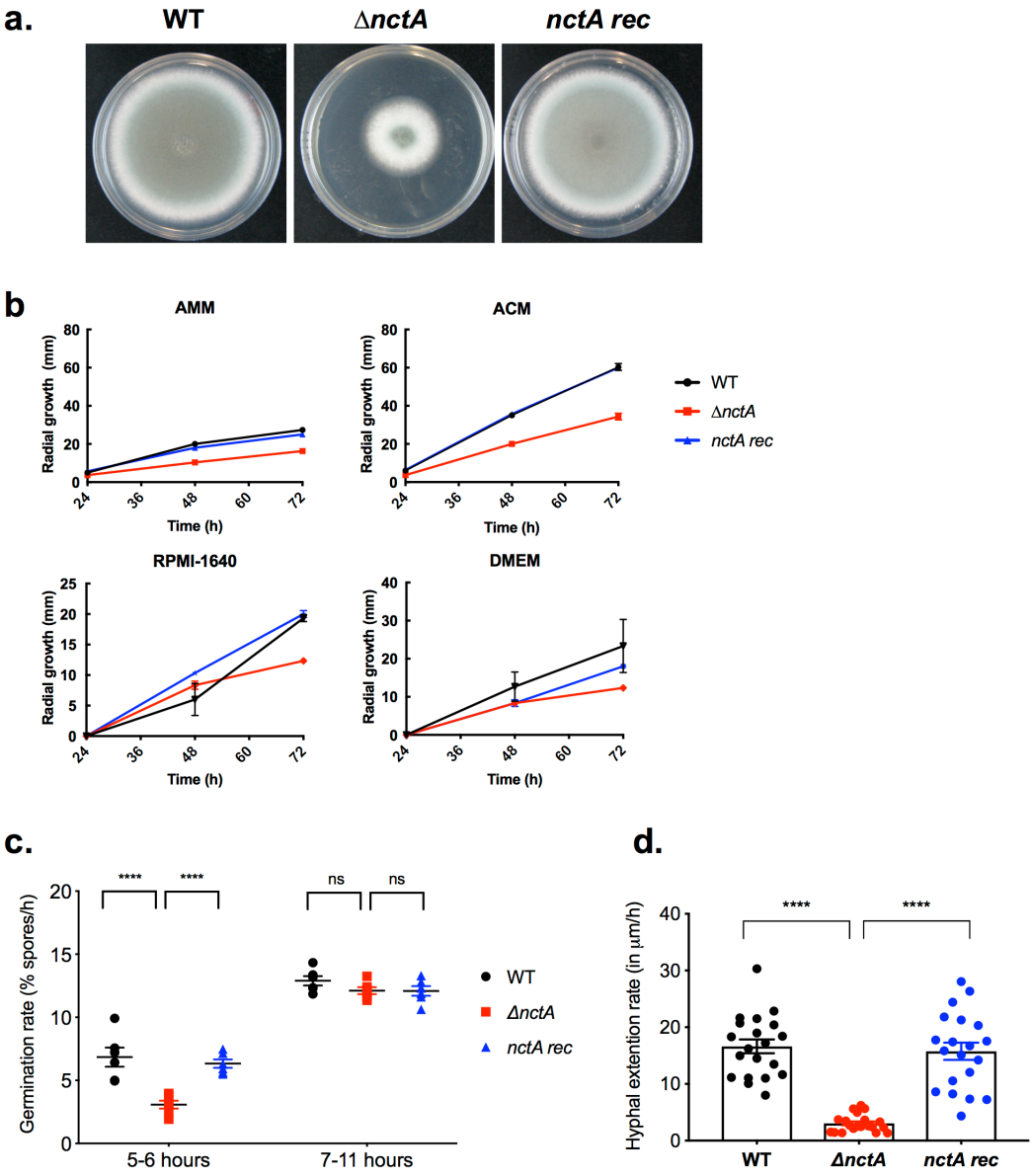

Figure 2.5: Impact of *nctA* deletion upon *A. fumigatus* growth. (a) Colonial growth phenotypes of the wild-type MFIG001 (WT), the *nctA* null *(ΔnctA*), and the *nctA* reconstituted strain (*nctA rec*) grown on a solid Aspergillus complete medium (ACM) for 24 h at 37 ˚C. **(b)** Radial growth phenotypes on solid ACM, Aspergillus minimal medium (AMM), RPMI-1640, and DMEM. The error bars represent standard error of the mean of three independent experiments. **(c)** Germination rates in liquid RPMI-1640 at 37 ˚C. *p*-value was calculated by repeated measures 2way-ANOVA with Sidaks correction: ****, P<0.0001; NS, P>0.05. **(d)** Hyphal extension rates in RPMI-1640 at 37 ˚C. *p*-value was calculated by Kruskal-Wallis test with Dunn's correction: ****, P<0.0001; NS, P>0.05. Percentages of germination rates and hyphal extension rates were measured under the microscope.

2.3.5 NctA and NctB regulate the same network of genes.

To assess the role of NctA and NctB on global regulation of gene expression in *A. fumigatus* we carried out transcriptomic analysis (RNAseq) using RNA extracted from cultures grown in RPMI-1640 media. In the absence of itraconazole, 1,244 genes were upregulated (>2 fold; FDR<0.05) and 1,049 (>2 fold; FDR <0.05) genes were downregulated in the *nctA* null when compared with the isogenic parent strain. Similarly, 1,183 genes were upregulated and 1,104 were downregulated in the *nctB* null mutant. In the presence of itraconazole, 735 genes were upregulated and 736 genes were downregulated in the *nctA* null mutant, and 865 genes were upregulated and 852 genes were downregulated in the *nctB* null mutant. Direct comparison of the two data sets shows that the regulons of both transcription factors have a very high degree of similarity in both conditions (Figure 2.7a and b), suggesting that both transcription factors work co-operatively.

To assess if NctA physically interacts with NctB, and to determine if any other proteins are found complexed with NctA, we generated a strain, which encoded a C-terminally S-tagged derivative of NctA (NctA-S-tag, see Figure S2.2a and S2.3) and performed co-immunoprecipitation followed by LC/MS identification of interacting proteins. Prior to this analysis, functionality of the S-tagged NctA allele was investigated, where the S-tagged NctA expressing strain showed indistinguishable growth rate with the wild-type MFIG001 strain (Figure S2.3). In addition to NctA, 20 unique proteins were identified (Table 2.1; >2 matched peptides), including NctB, the TBP associated transcriptional regulator Mot1, the transcriptional co-repressor Cyc8 and 9 ribosomal or ribosome associated proteins. The interaction between NctA and NctB and Mot1 was supported with reciprocal co-immunoprecipitation using a C-terminally S-tagged version of NctB. Taken together these data suggest that, consistent with the role of Bur6 and Ncb2 in yeast [48, 49], NctA and NctB form a complex with the TBP associated co-regulator Mot1 in *A. fumigatus* and are responsible for regulating the same cohort of genes.

Table 2.1. Identification of the interacting proteins of NctA and NctB using co-immunoprecipitation followed by liquid chromatography-spectrometry. The number of peptides identified by NctA or NctB co-immunoprecipitation respectively compared to the native control. NctA co-immunoprecipitation showed identification of the NctB protein (BOXTT5_ASPFC) and co-immunoprecipitation of NctB identified the NctA protein (BOY0F3_ASPFC)

Protein identified	Accession Number	Molecular Weight	Number of peptides identified			Gene ID
			Control (native NctA/NctB)	NctA-S-tag	NctB-S-tag	
TBP associated factor (Mot1), putative	B0XPE7_ASPFC	210 kDa	0	19	3	AFUB_006220
CBF/NF-Y family transcription factor, putative	B0XTT5_ASPFC	27 kDa	0	11	3	AFUB_029870
40S ribosomal protein S24	B0YC29_ASPFC	15 kDa	0	7	5	AFUB_088700
60S ribosomal protein L27a, putative	B0XZ73_ASPFC	17 kDa	0	6	2	AFUB_043390
60S ribosomal protein L20	B0XNN1_ASPFC	20 kDa	0	5	5	AFUB_004870
Ribosomal protein L26	B0Y8G7_ASPFC	18 kDa	0	4		AFUB_077280
Hsp70 chaperone Hsp88	B0XR33_ASPFC	80 kDa	0	4		AFUB_012080
Glyceraldehyde-3-phosphate dehydrogenase	B0Y207_ASPFC	36 kDa	0	4	4	AFUB_050490
Ribosomal protein	B0XQU0_ASPFC	24 kDa	0	3	4	AFUB_011140
60S ribosomal protein L5	B0XR75_ASPFC	35 kDa	0	3	3	AFUB_012370
Casein kinase I, putative	B0XTZ5_ASPFC	46 kDa	0	3		AFUB_019630
Ctr copper transporter family protein	B0XUP5_ASPFC	28 kDa	0	3		AFUB_020800
Transcriptional corepressor Cyc8, putative	B0XSL1_ASPFC	95 kDa	0	3		AFUB_027580
60S Ribosomal protein L37	B0XYW1_ASPFC	11 kDa	0	3	2	AFUB_042280
60S ribosomal protein L8	B0Y3E2_ASPFC	27 kDa	0	3	3	AFUB_053890
Alanine--tRNA ligase	B0YA78_ASPFC	107 kDa	0	3		AFUB_083700
CBF/NF-Y family transcription factor	B0Y0F3_ASPFC	16 kDa	0	3	4	AFUB_045980
ATP citrate lyase, subunit 1, putative	B0Y8A8_ASPFC	72 kDa	0	2	3	AFUB_076690
UTP-glucose-1-phosphate uridylyltransferase Ugp1, putative	B0YBZ9_ASPFC	58 kDa	0	2	7	AFUB_088400
Ribosome associated DnaJ chaperone Zuotin, putative	B0YEJ2_ASPFC	51 kDa	0	2	3	AFUB_099370
Eukaryotic translation initiation factor 3 subunit J	EIF3J_ASPFC	30 kDa	0	2	4	AFUB_072690
Nitrilase	B0XM85_ASPFC	45 kDa	0		6	AFUB_001300
Mitochondrial aconitate hydratase, putative	B0XM04_ASPFC	85 kDa	0		3	AFUB_001810
14-3-3 family protein ArtA, putative	B0XUD6_ASPFC	29 kDa	0		4	AFUB_020360
Nucleolar protein nop5	B0XWG2_ASPFC	65 kDa	0		3	AFUB_035810
ATP citrate lyase subunit (Acl), putative	B0Y8A9_ASPFC	53 kDa	0		3	AFUB_076700
Putative uncharacterized protein	B0YAT7_ASPFC	105 kDa	0		3	AFUB_085790

2.3.6 The NCT complex is a global regulator of sterol biosynthesis.

The negative cofactor complex has been defined as a general regulator of transcription. However, it is clear from the data presented in Figure 2.7 that the NctA/B complex is responsible for regulating only a subset of genes at any one time. To assess if these subsets of genes are enriched for particular processes or biochemical pathways, GO term and Metabolic Pathway Enrichment analysis was performed on genes dysregulated more than 2-fold. Such analyses are somewhat limited when applied to *A. fumigatus* as GO terms and metabolic maps for

filamentous fungi are poorly defined. However, we were able to identify enriched classes of genes in our upregulated cohort that are associated with secondary metabolism, transcriptional and translational processing, transport, and, notably sterol biosynthesis (Figure 2.6).

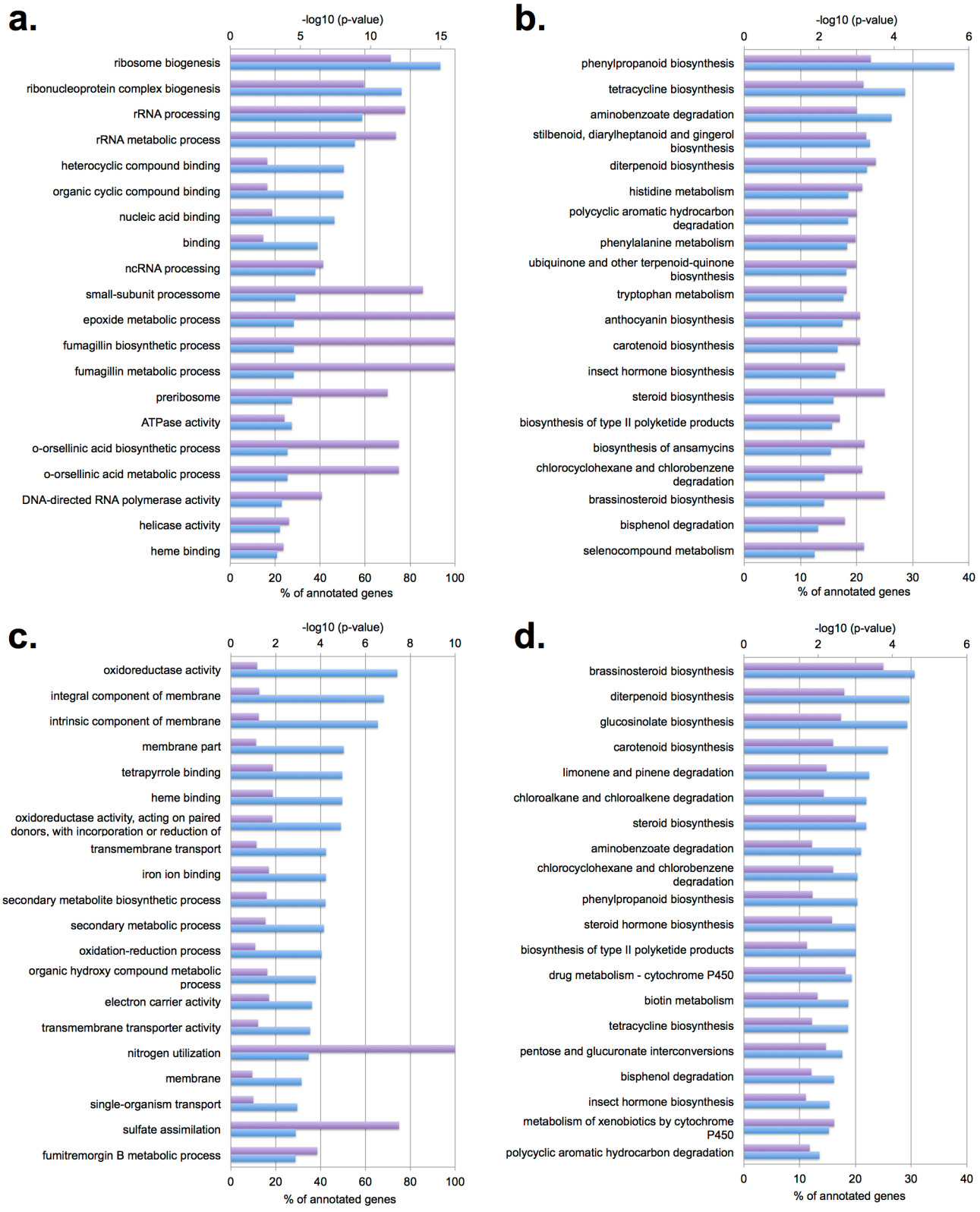

Figure 2.6: NCT complex is a global regulator of diverse biological processes including secondary metabolism and steroid biosynthesis. Gene Ontology (GO) term and KEGG pathway enrichment analysis of *A. fumigatus* genes that are

differentially expressed in the *nctA* null mutant compared to the wild-type. The top 20 significantly over-represented GO terms (**a and c**) and KEGG pathways (**b and d**) in **(a and b)** no-drug and **(c and d)** 0.5 mg/mL itraconazole conditions are shown. The number of differentially expressed genes in each term (in blue) and their statistical significance (–log10 *p*-values in purple) are plotted on the x-axis.

As both *nctA* and *nctB* null mutants are pan-azole resistant and our metabolic enrichment analysis identified steroid biosynthesis as an enriched class in genes upregulated in the null mutants we assessed the mRNA levels of the genes in the ergosterol biosynthetic pathway (Figure 2.7c and d) [50]. Of the 29 genes annotated as being associated with the pathway, 7 *(erg13A, hmg2, erg12, erg11A, erg24A, erg6, and erg2*) have increased mRNA levels more than 1.5 fold in the *nctA* null mutant (Figure 2.6) while 9 have reduced mRNA levels (*erg10A, erg13B, erg7C, erg24B, erg25A, erg26B, erg27, smt1, and erg5*). Intriguingly for 3 of the downregulated genes, their paralogues are upregulated (*erg13B*, *erg24*B, *smt1* [paralog to *erg6*].). Notably, *erg7C* has recently been identified as an oxidosqualene:protostadienol cyclase which diverts 2,3-epoxysqualene from ergosterol biosynthesis into the helvoic acid biosynthetic pathway [51]. Potentially, reduced levels of *erg7C* would result in increased flux through the ergosterol biosynthetic pathway. In relation to this, significant downregulation of several siderophore biosynthesis genes, especially *sidI*, which divert an important ergosterol precursor mevalonate into the siderophore biosynthesis pathway, was observed in the *nctA and nctB* null mutant. This suggested a role of the NCT complex in balancing ergosterol and siderophore biosynthesis pathways.

Our RNA-seq analysis also indicates that the NCT complex is a master regulator of other transcription factors associated with azole resistance. Loss of *nctA* leads to upregulation of activators of the ergosterol biosynthetic pathway (2.2-fold for *srbA* and 1.6-fold for *atrR* in the no-drug conditions) and downregulation of the negative regulator encoding gene *hapC* (approximately 2-fold). Interestingly, we also found upregulation of *mot1*, an interacting partner of the NCT complex that was identified during the co-immunoprecipitation analysis, in the *nctA* null mutants. These results suggest that the NCT complex affects expression levels of ergosterol biosynthesis genes both directly and indirectly by modulating these transcription factors.

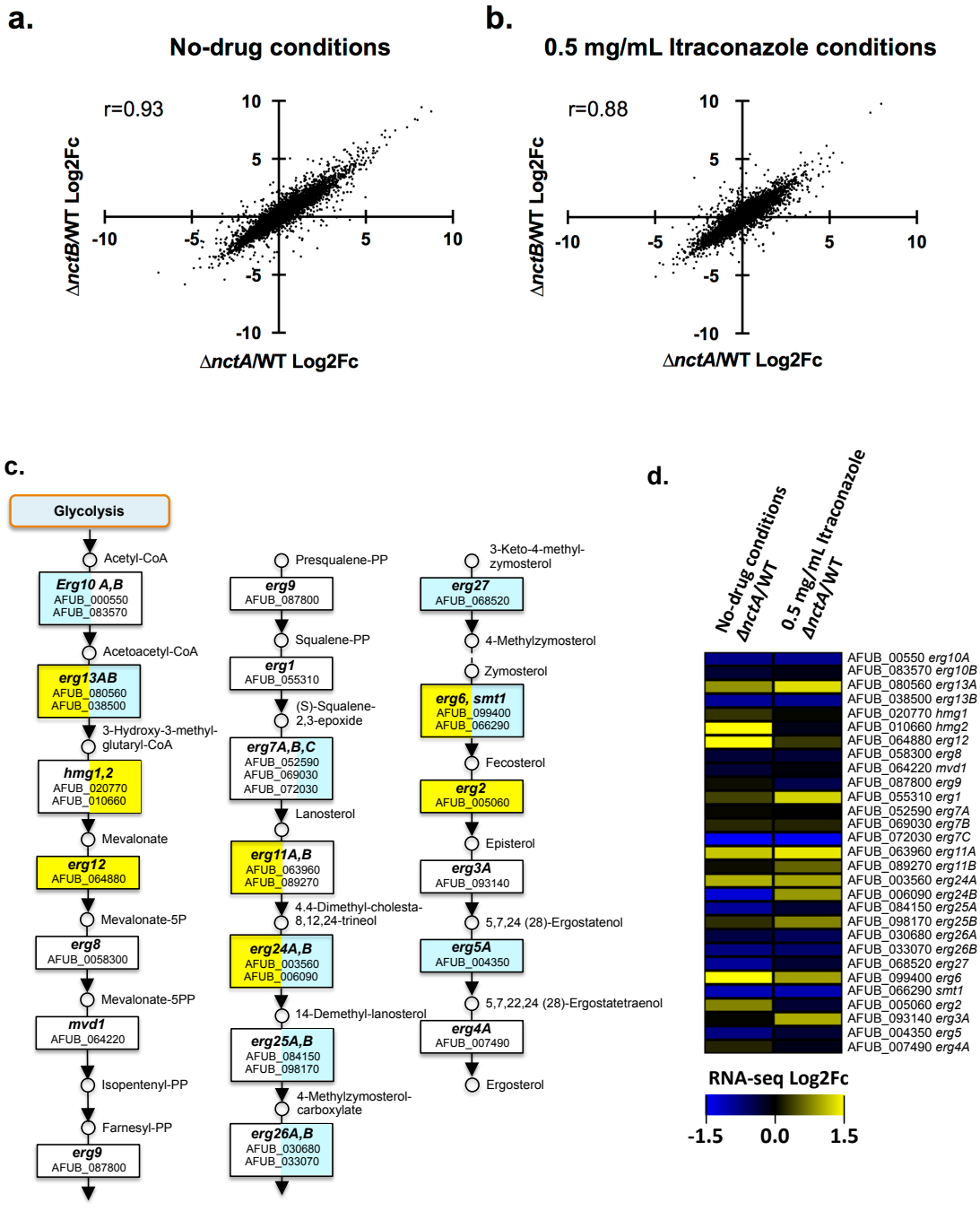

Figure 2.7: Effects of *nctA* and *nctB* deletion on the global and the ergosterol biosynthetic gene expression. (a and b) Comparison of differential gene expression in the *nctA* and the *nctB* null mutants. Scatter plot comparison of the log2 differential expression ratio of gene expression data in **(a)** no-drug, and **(b)** 0.5 mg/mL itraconazole conditions. The log2 expression ratio between the *nctA* null mutant and the wild-type are plotted on the x-axis, and the *nctB* null mutant and the wild-type are plotted on the y-axis. The Pearson's correlation (r) between the two gene expression datasets is shown. **(c and d)** Effects of *nctA* deletion on the expression of the genes involved in ergosterol biosynthesis. **(c)** Putative ergosterol biosynthetic pathway in *A. fumigatus*. The genes highlighted in yellow are those whose expression levels were upregulated more than 1.5 fold in the *nctA* null mutant compared to the wild-type. The genes highlighted in light blue are those whose

expression levels were downregulated more than 1.5 fold in the *nctA* null mutant compared to the wild-type. **(d)** Heatmap showing the RNA-seq expression levels of the genes involved in ergosterol biosynthesis. Log2 differential expression values are scaled between -1.5 and 1.5, and displayed.

2.3.7 ChIP-seq analysis reveals that NCT regulators bind the promoters of several ergosterol biosynthetic genes and their transcriptional regulators.

To identify the promoters of genes that are directly bound by the NCT complex we performed chromatin-immunoprecipitation sequencing (ChIP-seq) using an anti-S-tag polyclonal antibody to isolate DNA bound to the NctA-S-tag fusion protein *in vivo*.

We identified 4,811 and 4,290 NctA binding peak regions in the absence and the presence (0.5 mg/mL,) of itraconazole, respectively (p-value <0.01, fold enrichment >1.5). A comparison of the ChIP-seq datasets showed that more than 70 % of the peak regions are common between the conditions (Figure 2.8a). Analysis of genome-wide occupancy of NctA revealed that the large majority (about 70%) of NctA binding peaks are located within 1.5 kb upstream of the translational start site (TSS) of an annotated gene (Figure 2.8b). 32 % (3,273 genes in no-drug conditions) and 28 % (2,868 genes in 0.5 mg/mL itraconazole conditions), of the total predicted ORFs were assigned to have at least one NctA binding event within their upstream region. Frequency distribution of NctA binding peak summits showed that NctA is predominantly positioned around 300 bp upstream from the TSS (Figure 2.8b). Applying the Multiple Em for Motif Elicitation (MEME) *de novo* motif discovery program [52], we identified several conserved nucleotide motifs within the ChIP peak regions (Figure 2.8c). TATA-box like AT-rich motives were identified as the common nucleotide motifs with the highest e-value. This is consistent with the result from previous studies with NCT orthologues, which have been shown to form a stable complex with the TATA-box binding protein (TBP) [53-56]. The results of the motif discovery suggest that the NCT complex in *A. fumigatus* also interacts with TBP to regulate gene expression as also suggested by the physical interaction studies.

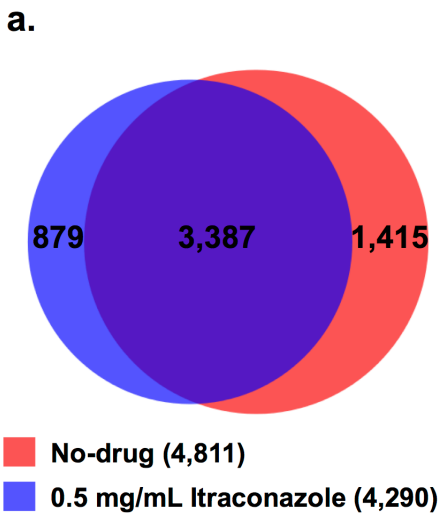

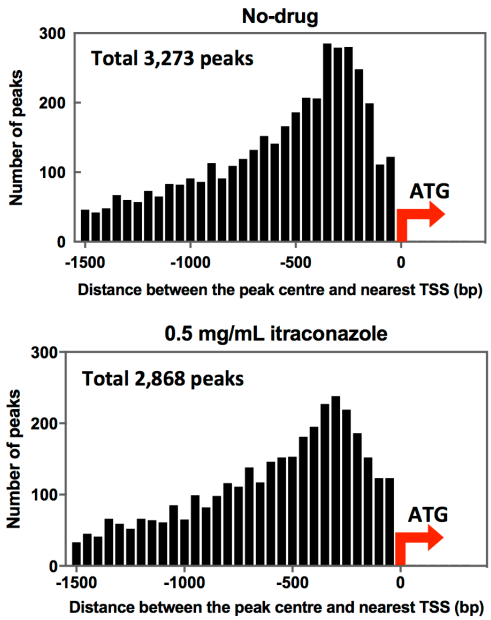

c.

No-drug

Consensus motif	Logo	*E- value*	Frequency
TATAWAW		4.0e-012	115/1,069
CCAATSA		4.1e-009	110/1,064
CGGARTA		1.7e-005	61/1,064
CACGTGAY		2.5e-004	40/1,064
AGMCWA		1.9e-004	263/1,064
GMGTCA		3.1e-003	125/1,064
CCACY		1.7e-002	479/1,064

0.5 mg/mL itraconazole

Consensus motif	Logo	*E- value*	Frequency
ATATAWA		1.4e-010	68/869
GCCAAK		2.1e-008	202/869
ACGTGAYW		2.8e-005	30/869
CTCYGTA		1.8e-004	50/869
RCGCTA		8.6e-003	94/869
TATWTA		4.1e-002	78/869

Figure 2.8: Genome-wide binding profile of NctA. (a) Venn diagram showing the overlap of NctA binding peaks obtained from no-drug and the 0.5 mg/mL itraconazole-treated conditions. **(b)** Distribution of the ChIP-seq peak location with respect to annotated genes. The frequency distribution of the distance between the merged peak summit and the translation start site (ATG) of the nearest annotated gene is plotted. **(c)** Conserved nucleotide motifs identified in the NctA ChIP-seq peak regions. A summary of the *de novo* motif discovery analysis is shown with the identified consensus motifs and it's sequence logos, the calculated *e*-values, and the frequency of the appearance of the motifs within the ChIP-seq peak set are analyzed.

We investigated the correlation between NctA occupancy and mRNA levels by comparing the ChIP-seq and the RNA-seq datasets. We expected that regulation of genes in close proximity to the NctA binding sites would be altered upon loss of *nctA*. However, for the total 3,292 genes having at least one NctA binding peak within 1.5 kbp of upstream region, only 732 genes (22%) showed differential mRNA levels and the remaining 2,560 genes exhibited no significant change (Figure 2.9a and b). Among the 732 differentially expressed genes, 351 genes were upregulated and 381 genes were downregulated in the *nctA* null mutant in no-drug conditions. Similar results were obtained for the itraconazole treated (0.5 mg/mL) sample (Figure 2.9c and d). These results suggest that binding of the NCT complex alone is not sufficient for it to elicit its regulatory function.

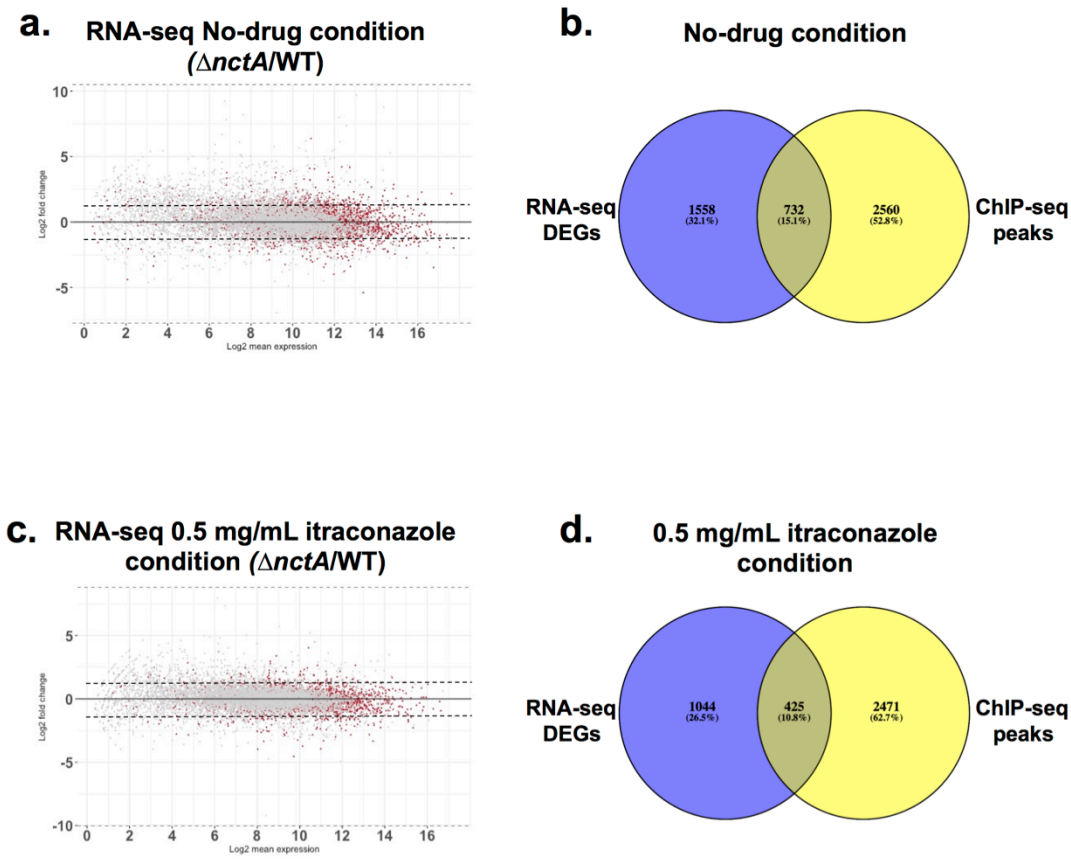

Figure 2.9: Correlation between NctA occupancy and gene expression changes. (a,c) MA-plot showing correlation between NctA occupancy and gene expression changes in the the *nctA* null mutant in **(a)** no-drug and **(c)** 0.5 mg/ml itraconazole conditions. Genes with a significant NctA binding peak (*p*-value<0.01, fold enrichment >1.5) are indicated with red dots. **(b,d)** Venn diagram showing overlap of genes that are differentially expressed in the *nctA* null mutant, and genes with significant NctA ChIP-seq peaks in **(b)** no-drug and **(d)** 0.5 mg/ml itraconazole conditions.

In order to obtain further insight into the molecular mechanisms driving the itraconazole-resistance in the *nctA* and the *nctB* null mutants, we analyzed binding of NctA on the promoter region of the genes related to ergosterol biosynthesis and their known transcriptional regulators (Figure 2.10a). Of the 16 genes, which showed differential expression in the RNA-seq analysis in the absence of itraconazole, nine genes (*erg10A, erg13B, erg11A, erg24A, erg25A, erg27, erg6, smt1, and erg5A*) were found to have at least one NctA binding peak within 1.5 kb of the upstream region. Similarly, among the 14 differentially expressed genes in the presence of itraconazole, 11 genes were shown to have the peak regions within the defined upstream region (*erg10A, erg13A, erg13B, erg11A, erg11B, erg24A, erg24B, erg25B, erg6, smt1, and erg3*). Interestingly, the genes encoding the regulatory proteins HapC, SrbA and AtrR were also confirmed to have an NctA binding peak in their upstream region (Figure 2.10b).

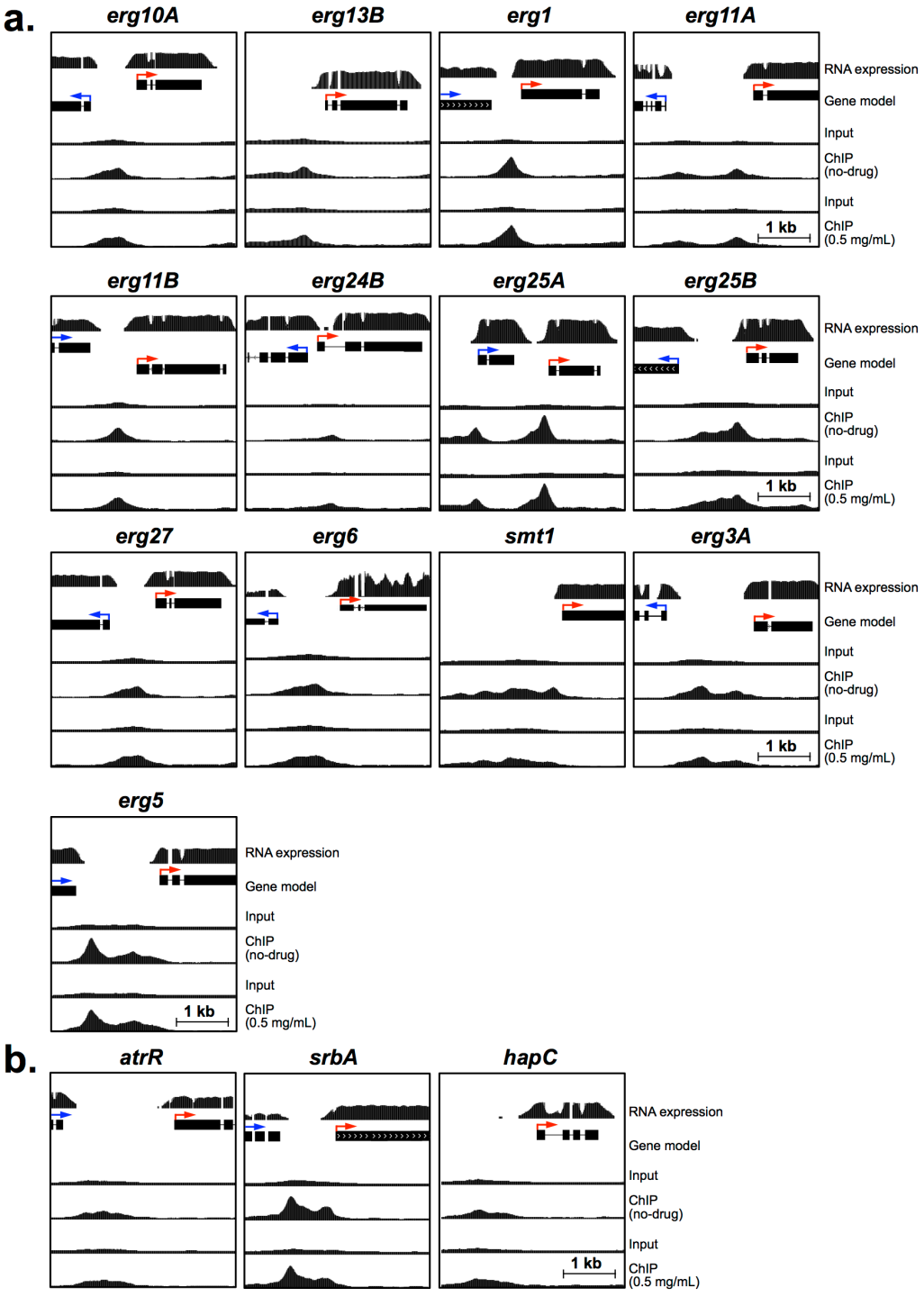

Figure 2.10: Binding of NctA on the 5'-upstream region of the genes involved in ergosterol biosynthesis and their known transcriptional regulators. *In vivo* binding of NctA on the 5'-upstream region of **(a)** ergosterol biosynthetic genes, and **(b)** their known transcriptional regulators. Tracks for the NctA ChIP-seq (ChIP) and their input DNA control (Input) are visualized in the UCSC genome browser together with annotated gene models and their transcript, which are expressed in the no-drug conditions. Direction of the target gene and the 5'-proximal gene are shown in red arrows and blue arrows, respectively.

2.3.8 Ergosterol levels are elevated in NCT complex mutants

To analyse the effect of the loss of the NCT complex on ergosterol biosynthesis, sterol levels were quantified using GC-MS. Consistent with our hypothesis we observed a 60% increase in ergosterol content (w/w) in both mutant strains when compared to the isogenic control ($p<0.04$; Figure 2.11). Ergosterol levels in the reconstituted strain were indistinguishable from the wild type ($p>0.85$) and lower than observed in the knockout ($p=0.0138$). Taken together our data suggest that NctA and NctB are negative regulators of ergosterol biosynthesis via their interaction at the promoters of *cyp51A* and other genes that encode components of the ergosterol biosynthetic pathway.

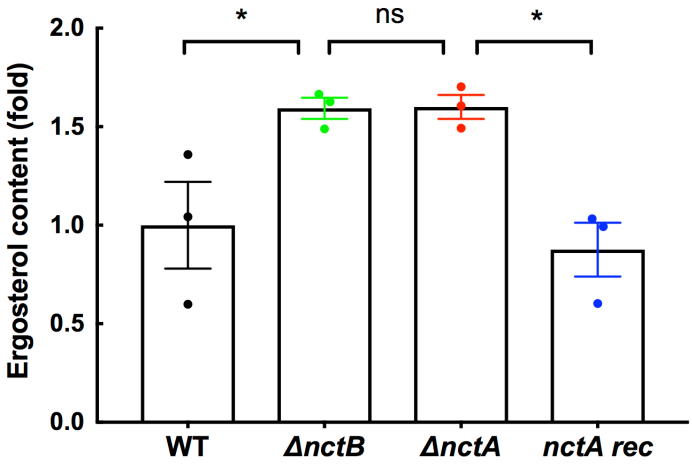

Figure 2.11: Loss of *nctA* and *nctB* increases the cellular ergosterol content. Ergosterol levels of the wild-type (WT), the *nctA* null mutant (Δ*nctA*), the *nctB* null mutant (Δ*nctB*), and the *nctA* reconstituted isolate (*nctA rec*) in RPMI-1640 incubated for 24 h were determined by GC-MS. Ergosterol content of each mutant was normalized to that of the wild-type and shown as a relative fold change. Samples were assessed in biological triplicates. *p*-values were calculated using one-way ANOVA: *, $P<0.05$; ns, $P>0.05$.

2.3.9 Levels of the azole transporter CDR1B are elevated in NCT mutants

The relatively modest increase in expression of *cyp51A* (ca. 2-fold) and cellular ergosterol content (ca. 1.6-fold) in the *nctA* mutant did not appear consistent with the relatively large increase in azole resistance (>32-fold) suggesting that factors independent of ergosterol biosynthesis may be influencing azole resistance in the NCT complex deficient strains.

Recently an association between azole resistance and increase in mRNA levels of the ABC transporter CDR1B has been described [21] and the transcriptional regulator AtrR has been shown to co-regulate both *cdr1B* and *cyp51A* expression [11]. We therefore examined our RNAseq data to see if *cdr1B* was dysregulated in the *nctA* and *nctB* null mutants. mRNA levels of *cdr1B* were increased by 3.1 (FDR=$2.5x10^{2}$) and 2.1 (FDR=0.15)-fold respectively in the *nctA* and the *nctB* null (Figure 2.12a). Furthermore, evaluation of our ChIPseq data suggested that this regulation was related to a direct interaction between the NCT complex and the *cdr1B* promoter (Figure 2.12b). To assess if this increase in transcript levels led to a concomitant increase in translated protein levels, we quantified levels of the transporter using an anti-CDR1B antibody [33]. In keeping with our transcriptomic results, CDR1B levels were increased in the *nctA* null mutant by >2.4 (Figure 2.12c and d).

a.

	no-drug		0.5mg/mL itraconazole	
	RNA-seq fold change	FDR	RNA-seq fold change	FDR
Δ*nctA*/WT	3.06	2.51E-02	2.37	6.58E-11
Δ*nctB*/WT	2.13	1.45E-01	1.98	1.67E-09

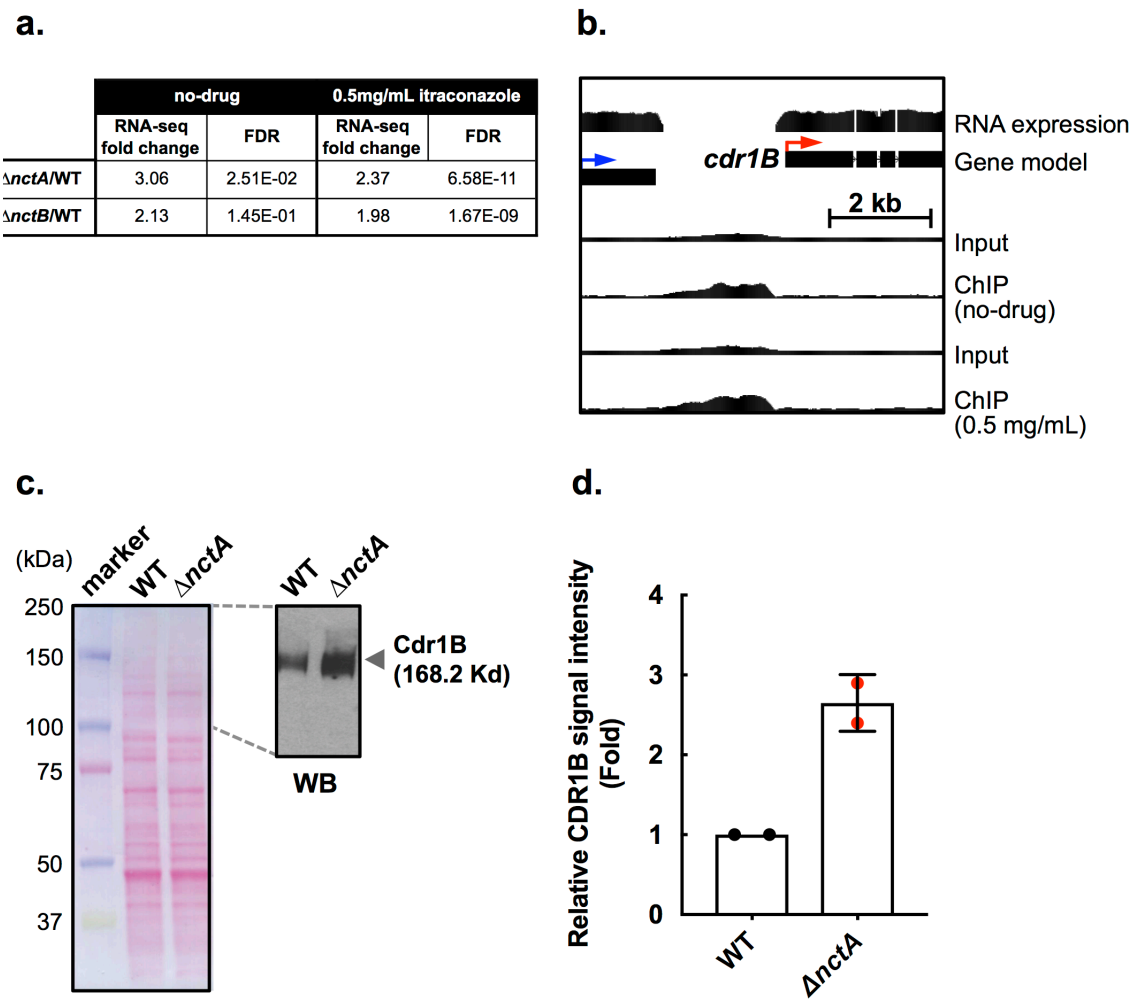

Figure 2.12: Defects in the NCT complex leads to transcriptional derepression of *cdr1B* and over-production of CDR1B protein. (a) Expression levels of *cdr1B* transcripts in the *nctA* null and the *nctB* null mutant in RNA-seq analysis. **(b)** *In vivo* binding of NctA on the 5'-upstream region of *cdr1B*. Tracks for the NctA ChIP-seq (ChIP) and their input DNA control (Input) are visualized in the UCSC genome browser together with annotated gene models and their transcript, which are expressed in the no-drug conditions. The direction of the target gene and the 5'-proximal gene are shown in red arrows and blue arrows, respectively. **(c)** Representative Western blot (WB) showing the increase in CDR1B protein levels in the Δ*nctA* mutant. Cell-free extracts were resolved via SDS-PAGE, and probed for CDR1B using a CDR1B specific antibody. Ponceau S staining was performed as an overall loading control. **(d)** Relative protein levels of CDR1B. The relative intensity of the CDR1B signal was quantified by densitometric scanning. The data represent the mean results of two biological replicates, and the error bars signify the standard deviations.

2.3.10 The immunogenic properties of A. fumigatus enhanced in the nctA null mutant.

Given the requirement of the NCT complex in the resistance to two leading classes of therapeutic agents used to treat aspergillosis, it was important to assess if NCT complex mediated regulation is important for pathogenicity of *A. fumigatus*. As our evidence to date suggest that the roles of NctA and NctB are non-redundant with respect to each other, we investigated pathogenic properties of the *nctA* mutants using both *in vitro* and *in vivo* infection models.

To assess contact mediated cytotoxicity, the *nctA* null mutant was co-cultured with human A549 alveolar epithelial cells and the murine macrophage RAW 264.7 cell line (Figure 2.13a and b). Our results indicate that loss of the NCT complex results in a significant reduction in cell damage when compared to either isogenic control or the reconstituted isolate. This result is consistent with the growth reduction seen for this strain in the media used for this experiment (Figure 2.13b). We next examined immunogenic properties of the *nctA* null mutants to mammalian immune cells. Murine macrophages challenged with live spores from the *nctA* mutant showed an increase in production of TNF-α, IL-6 and IL12p40 (Figure 2.13c-e) whereas human epithelial cells challenged with the *nctA* mutant showed an increase in production of IL-8 (Figure 2.13f). The *nctA* null mutant also resulted in more activation of dendritic cells compared to the wild-type (Figure 2.13g and h). These findings suggest that the *nctA* null mutant could potentially cause an aberrant immunogenic response during infection. The increased immunogenic properties observed for the *nctA* null mutant could be associated with an alteration in the cell wall structure or spore surface as the null mutant was hypersensitive to the cell wall synthesis inhibitory drugs and the perturbing agents Congo Red and Calcofluor White (Figure 2.3c). However, examination by TEM revealed that the thickness of the cell wall was unchanged in the *nctA* null mutant (Figure 2.14).

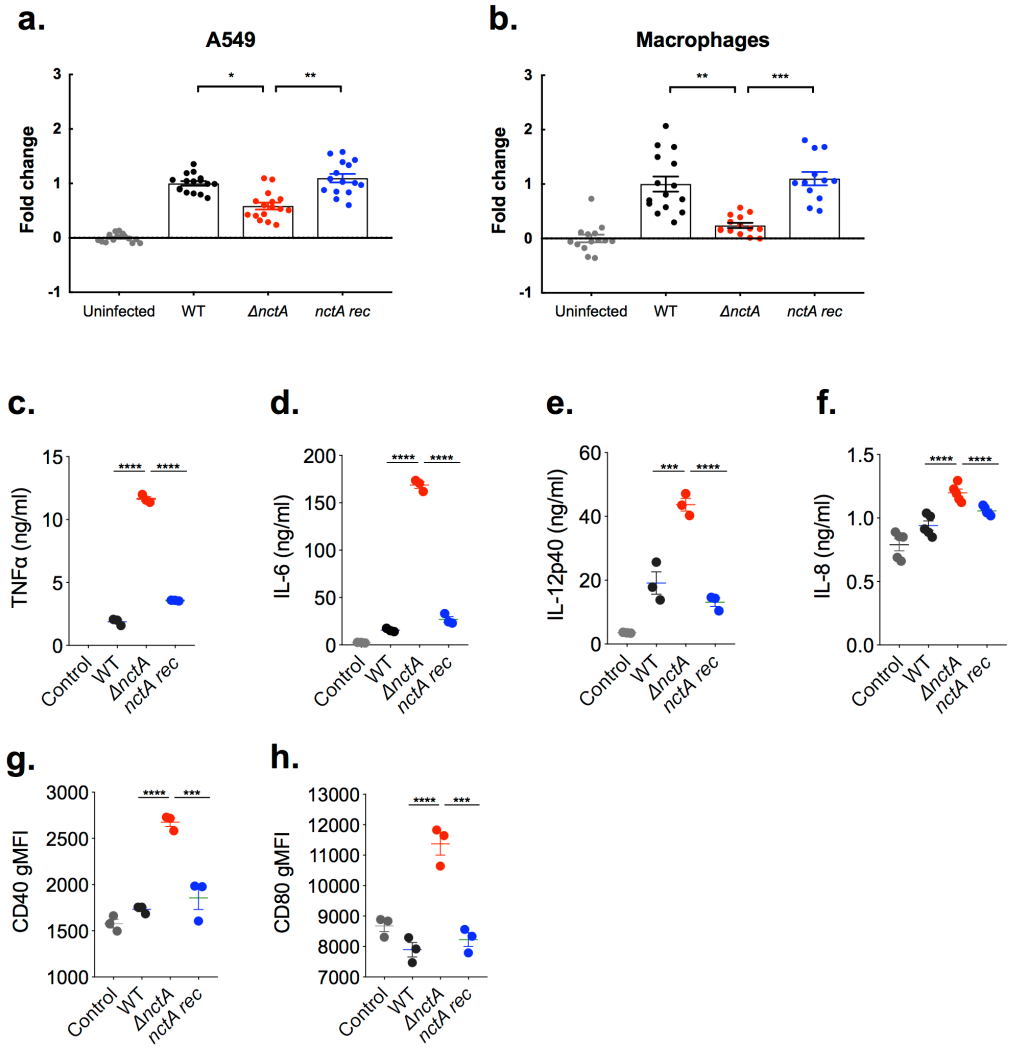

Figure 2.13: Cytotoxicity and immunogenic properties of the *nctA* null mutant. (a-b) A549 epithelial cells or macrophages were infected with the wild-type (WT), the *nctA* null mutant (Δ*nctA*), or the *nctA* reconstituted isolate (*nctA rec*) for 24 hours. Cytotoxicity of each mutant was evaluated by measuring the release of lactate dehydrogenase (LDH) activity into the culture medium. The data represents 5 different infection challenges with triplicate LDH activity measurements. Data are shown in fold change of LDH activity relative to the wild-type infected cells. The error bars mean the standard error of the mean (SEM), and *p*-values were calculated by Kruskal-Wallis test with Dunn's correction: *, P <0.0180; **, P <0.0056 (for **(a)** A549 cells). **, P <0.0032; ***, P <0.0007 (for **(b)** macrophages). **(c-f)** Granulocyte Macrophage colony-stimulating Factor induced bone marrow-derived dendritic cells (gm-csf BMDCs) were infected with the *A. fumigatus* strains with the multiplicity of infection (MOI) = 5:1. Proinflammatory cytokines were quantified by ELISA. Data represents 3 biological replicates **(c-e)** or 5 biological replicates **(f)** with ±SEM. p-values were calculated by ANOVA with Tukey's correction: ***, P <0.002; ****, P <0.0001. **(g-h)** Activation of dendritic cells measured by CD40 and CD80 markers by flow cytometry. Data represents 3 biological replicates with ± SEM. *p*-values were calculated by ANOVA: ***, P <0.0002; ****, P <0.0001 (for (g)). ***, P <0.0004; ****, P <0.0001 (for (h)).

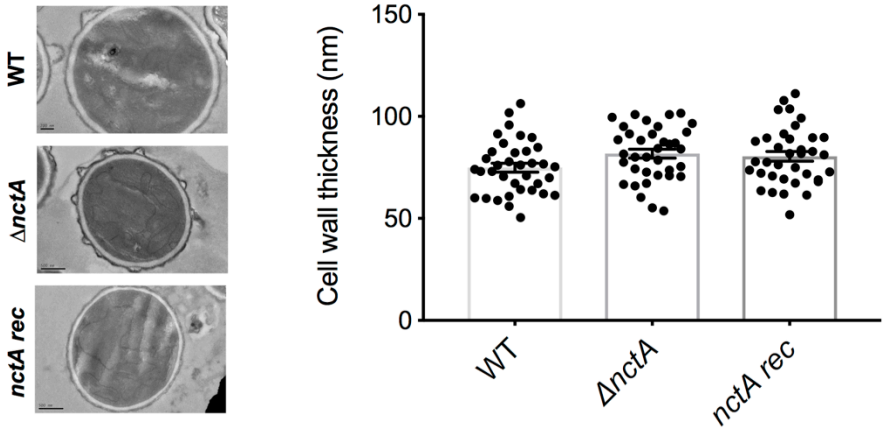

Figure 2.14: Loss of NCT function dose not affect cell wall thickness, and abnormal conidial surface structure. Width of the cell wall layer of the conidia determined by TEM image analysis are shown. The data represents the mean of 36 conidia of each strain.

2.3.11 A NCT mutant is virulent in a leukopenic and corticosteroid model of invasive aspergillosis.

To assess the impact of the loss of the NCT complex in pathogenicity, we compared the virulence of the *nctA* null mutant with that of the isogenic isolate MFIG001 in a leukopenic model of invasive aspergillosis. All mice challenged with the MFIG001 strain succumbed to infection (100% mortality) within 7 days post infection. Despite the significant growth defect (Figure 2.5b) and the reduced cytotoxicity (Figure 2.12a and b) observed in NCT mutants, the virulence of the *nctA* null mutant was statistically indistinguishable from the isogenic isolate (Figure 2.15a).

In the leukopenic aspergillosis model, the host cellular innate response is quantitatively attenuated particularly during the initiation of infection allowing the microbe to proliferate and cause host damage. Thus, we investigated the role of the NCT complex in virulence in a murine model that uses cortisone acetate as an immunosuppressive agent resulting in qualitative defects in innate immunity. This model has been shown to better reflect the host's immune response in relation to detection of fungal specific PAMPs. In this model overall murine mortality with the isogenic strain was 45 % at day 10 post-infection. Similarly, the *nctA* null mutant also showed 50 % mortality at the end of the infection time-course. Although the

nctA rec strain showed a slightly increased mortality compared to the other strains, no significant differences were observed in virulence between the all tested strains (Figure 2.15b).

One potential hypothesis that could explain the retention of virulence of the *nctA* null mutant is the aberrant immunogenic properties observed in the mutant *in vitro*. However, no significant differences were observed in the expression levels of cytokine encoding genes (TNF-α, IL12, and IL-6) between the strains at 36 hours post inoculation (p.i.) (Figure 2.15c). Furthermore, no obvious difference in the inflammatory response was observed between the strains in histopathology (Figure 2.15d). Contrary to our expectation from the *in vitro* studies, the *nctA* null mutant showed an indistinguishable level of fungal burden with the isogenic control at 36 hours p.i (Figure 2.15d). These results suggest that pathogenicity is maintained in this strain as its growth is not significantly altered *in vivo* and our results add to the growing body of evidence that poor *in vitro* growth is not an absolute indicator of virulence defects.

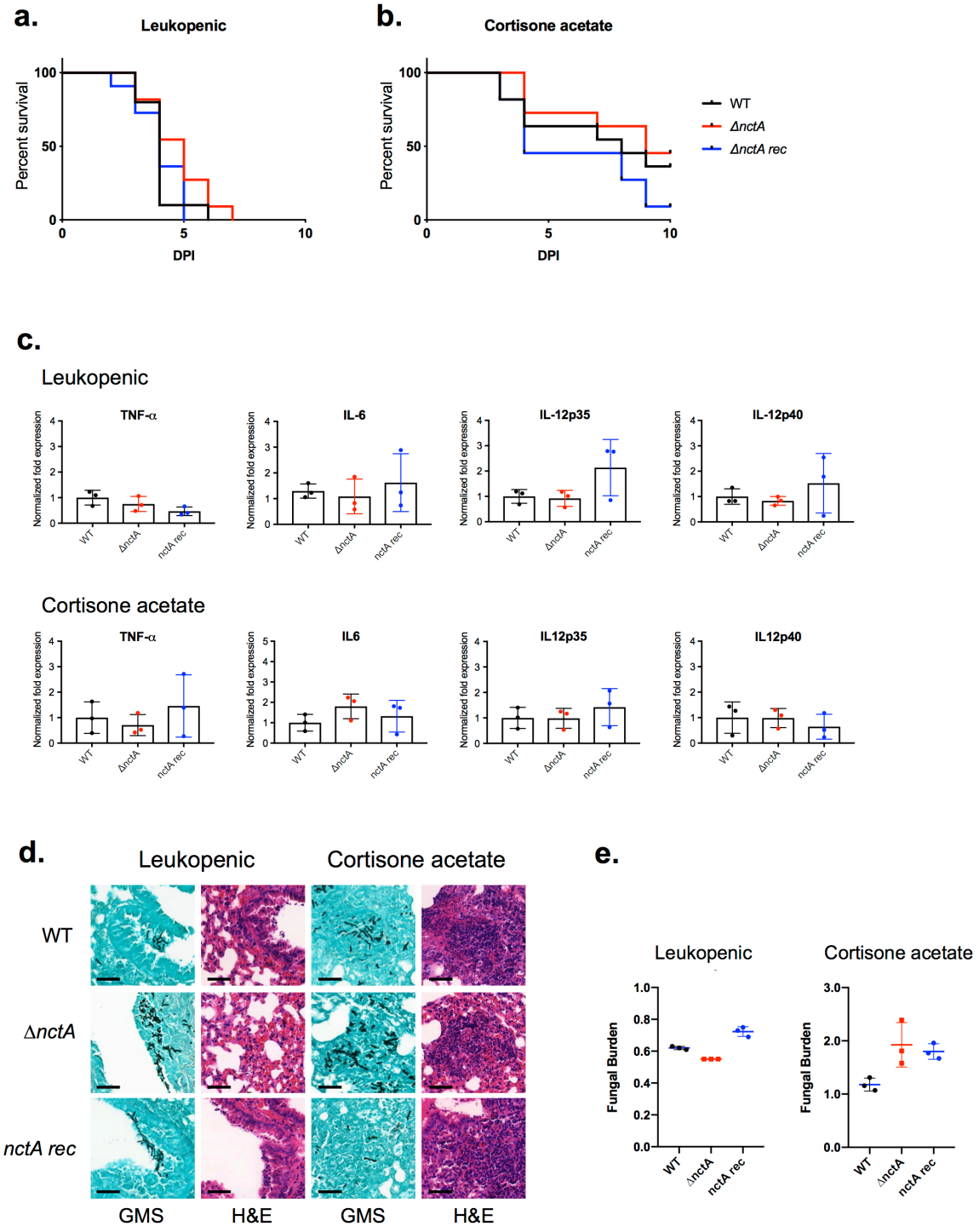

Figure 2.15: Assessing the effect of loss of *nctA* on the virulence of *A. fumigatus* in murine infection models. Mice were infected with the wild-type (WT), the *nctA* null mutant (Δ*nctA*), or the reconstituted isolate (*nctA rec*). **(a and b)** Kaplan-Meier curve for murine survival for mice treated via **(a)** intranasal infection with 5.0 x 10^5 conidia after mice were rendered neutropenic by treatment with cyclophosphamide, and **(b)** intranasal infection with 7.0 x 10^6 conidia after cortisone acetate treatment. A log rank analysis was used to compare results between the strains. **(c)** Relative expression levels of proinflammatory cytokines in the infected lung tissues. Data represents the mean of biological triplicates and error bars

illustrate the standard deviation. Statistical significance was calculated by Student's t test. **(d)** Histopathology of representative sections of lungs after 36 h post-infection with WT, Δ*nctA*, or *nctA rec*. Lung sections were stained with haematoxylin-eosin (HE) for visualization of the host cells, and Grocott's Methenamine Silver (GMS) for visualization of the fungal elements. Scale bar: 50 μm. (**f**) Quantification of the fungal burden in the infected lungs. Total genomic DNA was extracted from the same lung lobe samples used for the cytokine expression analysis, and fungal DNA concentration was determined by qPCR. Data represent the means of biological replicates. The statistical significance of variances between fungal burdens was calculated by using a non-parametric Mann-Whitney t test.

2.4 Discussion

In this study we have constructed a 484 member transcription factor null mutant library with the aim of providing a systematic evaluation of regulators that contribute to azole resistance in *A. fumigatus*. This library now provides an opportunity for the fungal community to further explore regulatory mechanisms and factors in the pathobiology of this important human fungal pathogen. To date much of our understanding of azole tolerance has been driven by hypotheses derived from model organisms that have significantly superior functional genomic resources. Functional screens of transcription factor null mutant libraries have been performed in the model yeasts *S. cerevisiae* [57] and *Schizosaccharomyces pombe* [58], the model filamentous fungus *Neurospora crassa* [59], and the pathogenic yeasts *Cryptococcus neoformans* and *Candida albicans* [60, 61]. Although these studies have proven to be effective in uncovering a number key regulators of drug resistance, the roles of transcription factors can vary significantly from species to species and large scale transcriptional rewiring is frequently observed (for a review see [62]). For example, in loss of the *A. fumigatus* pH-responsive transcriptional regulator PacC, results in a >20-fold increase in flucytosine sensitivity in *A. fumigatus* [63]. However, loss of the orthologue in *C. neoformans* (RIM101) leads to an increase in flucytosine resistance [60, 61]. Our screen of azole resistance in *A. fumigatus* highlights significant differences in the transcriptional regulation of azole tolerance in filamentous fungi compared to *S. cerevisiae*. Of the 12 transcription factors identified in our screen as having altered susceptibility to itraconazole, only half (HapB, SreA (SrbA) [61]), AdaB [45, 64], GisB [65] CreA and HapX [66] may have been predicted from previous screening efforts. Of the remaining regulators, orthologues of three (NctA, NctB and RscE) are essential for viability, and three (ZipD, AreA and AtrR) are absent in yeast.

We have explored, in detail, the role of the two CBF/NF-Y family transcription regulators, AFUB_029870 (NctA) and AFUB_045980 (NctB) in azole resistance. The orthologues of these regulators in *S. cerevisiae*, known respectively as Bur6 and Ncb2, are subunits of a heterotrimeric transcriptional regulator called Negative Cofactor 2 (NC2). The NC2 complex, originally identified as a TBP (TATA-Box binding protein) associated factor, acts as a negative regulator of RNA polymerase II transcription by inhibiting formation of the pre-initiation complex (PIC) [67, 68].

Assembly of the heteromeric PIC is required for transcription from RNA pol II-dependent promoters and its assembly is contingent upon recruitment of the TBP and the general transcription factors TFIIA and TFIIB. NC2 inhibits PIC formation by preventing the interaction of TBP with TFIIA and TFIIB [[69] and references therein]. In keeping with this function as a general transcriptional cofactor, genome wide binding studies in S. *cerevisiae, C. albicans* and *H. sapiens* have revealed interaction with in excess of 20% of all RNA pol II gene promoters [69-72]. These finding are consistent with our observation that NctA binds the promoters of over 30 % of protein encoding genes of *A. fumigatus*. However, given this general role, what appears remarkable is that *nctA* and *nctB* are not essential for viability of this fungus as they are in yeasts [53] and loss of function mutants have clear and very specific phenotypic traits.

The most striking phenotypes that we have observed for the *nctA* and the *nctB* null mutants aside from the resistance to the azole class of antifungals, is their resistance to the salvage therapeutic Amphotericin B and terbinafine which can be used in the management of patients with chronic or allergic disease [20]. Cross resistance to the azoles and terbinafine is understandable as both act on the ergosterol biosynthetic pathway (Terbinafine, inhibits the action of squalene epoxidase, an enzyme that catalyses the conversion of squalene to squalene 2,3-epoxide in the ergosterol biosynthesis pathway [73]). Cross-resistance between these agents and Amphotericin B is much harder to explain. Amphotericin B acts by selectively binding ergosterol in the fungal membrane and creating pores resulting in leakage of intracellular contents [74]. Theoretically therefore, resistance to the azoles caused by upregulation of ergosterol in the cell membrane should lead to increased sensitivity to Amphotericin B as this would enhance the interaction between the drug and its binding target. Indeed, this inverse correlation in resistance profiles has been observed in several mutants from *C. neoformans* [61]. Cross-resistance to the azoles and amphotericin B has previously been reported in artificially constructed yeast mutants. In *C. albicans*, laboratory generated strains lacking both copies of ERG11 (Cyp51A orthologue) or ERG3 (sterol 5,6, desaturase), are viable and resistant to fluconazole. As ergosterol is replaced in their cell membrane by alternative sterols, these isolates are also resistant to amphotericin B [75, 76]. However, depletion of ergosterol levels is clearly not the key cause of amphotericin B resistance in the NC2

mutants as they exhibit an increase in ergosterol content in line with the observed increased expression of *cyp51A* and other genes of the ergosterol biosynthetic pathway. There is limited information on the mechanisms of Amphotericin B resistance in *A. fumigatus*. However, it has been suggested that an increase in the production of oxidative stress reducing enzymes such as catalases that confers resistance to the oxidising abilities of Amphotericin B may contribute to resistance [76]. It is also possible that changes in the structure of the cell wall architecture in the *nctA/nctB* null strains is contributing to Amphotericin B resistance in these strains by limiting access to the ergosterol in the cell membrane. Clearly, additional studies are needed to further define the mechanism of Amphotericin resistance in these strains. Additionally, given the pleiotropic nature of the NC2 complex we cannot exclude that other factors, beyond the increase in ergosterol biosynthesis and upregulation of *cdr1B*, maybe contributing to the high levels of azole resistance evident in the *nctA* and *nctB* null mutants (Figure 2.16).

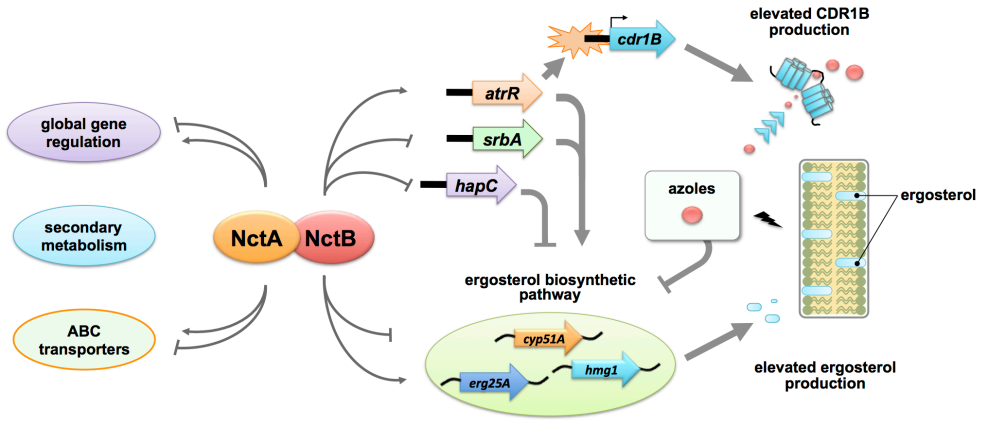

Figure 2.16: Proposed model highlighting the mechanistic basis of the azole resistance in the NCT complex. The NCT complex is a global regulator, which acts as both a negative and a positive regulator of a wide range of gene regulation that includes secondary metabolism, cellular transport, and sterol biosynthesis as important targets for virulence and azole resistance in *A. fumigatus*. The NCT complex fine-tunes expression of several genes in the ergosterol biosynthesis pathway and the azole efflux pump encoding *cdr1* by directly interacting with their core promoter region. The NCT complex also acts as a master regulator of azole resistance by modulating the expression levels of the transcription factors associated with ergosterol biosynthesis and azole resistance; transcriptional repression of the activator encoding *srbA* and *atrR,* and activation of the negative regulator encoding *hapC*. Therefore, the loss of the NCT complex causes an increased level of cellular ergosterol content and an elevated production of Cdr1B that leads to a multi-drug

resistance phenotype to the azoles as well as the salvage therapeutics amphotericin B and terbinafine.

Our results gain greater significance as we have observed that, despite significant growth defects *in vitro*, the *nctA* mutant retained similar levels of virulence and growth in murine models of infection. This suggests that resistance observed in the *nctA/B* null mutants might be clinically relevant. Clinical guidelines currently suggest that Amphotericin B may be used as salvage therapeutic when initial therapy with voriconazole fails [19]. This would clearly be contraindicated in an infection with a strain with NctA/NctB mediated azole resistance, so rapid detection of such isolates would support appropriate alternative therapeutic treatment such as an echinocandin to which these mutants are extremely sensitive (Figure 2.3c).

The relevance of our findings for clinical drug resistance in yeasts is unclear. Downregulation of Bur6 and Ncb2, in *C. albicans* does lead to a modest increase in azole resistance, which has been attributed to a slight (ca. 2-fold) increase in *cdr1* expression [53]. To our knowledge however there have been no reports of Amphotericin B resistance in these strains and resistant clinical isolates carrying mutations in Bur6 and Ncb2 have not been reported. Critically, as both Ncb2 and Bur6 are essential for viability in *C. albicans*, null mutants are unlikely to persist in a host setting [53].

In summary we have generated a library of transcription factor null mutants in the fungal pathogen *A. fumigatus*. This library is publically available and can be exploited by the research community to provide comprehensive insights into transcriptional networks governing critical factors associated with the cell biology, pathogenicity and allergenicity in this under-studied etiological agent. Using this resource we have identified the network of regulators governing azole resistance and identified a novel mechanism that, through a single genetic mutation, is able to drive both high level pan-azole resistance and cross-resistance to the salvage therapeutic amphotericin B and terbinafine without significantly impacting virulence.

2.5 References

1. http://www.gaffi.org/why/burden-of-disease-maps/ Accessed January 5th.
2. Brown, G.D., et al., *Hidden killers: human fungal infections.* Sci Transl Med, 2012. **4**(165): p. 165rv13.
3. Steinmann, J., et al., *Emergence of azole-resistant invasive aspergillosis in HSCT recipients in Germany.* J Antimicrob Chemother, 2015. **70**(5): p. 1522-6.
4. Chowdhary, A., et al., *Prevalence and mechanism of triazole resistance in Aspergillus fumigatus in a referral chest hospital in Delhi, India and an update of the situation in Asia.* Front Microbiol, 2015. **6**: p. 428.
5. Parameswaran, K., M. Joshi, and P. Ravindran, *Unusual radiological presentation and rapid fatal progression of invasive pulmonary aspergillosis in an immunocompetent young patient.* Respirology, 1999. **4**(3): p. 287-90.
6. Odds, F.C., A.J. Brown, and N.A. Gow, *Antifungal agents: mechanisms of action.* Trends Microbiol, 2003. **11**(6): p. 272-9.
7. van der Linden, J.W., et al., *Prospective multicenter international surveillance of azole resistance in Aspergillus fumigatus.* Emerg Infect Dis, 2015. **21**(6): p. 1041-4.
8. Mavridou, E., et al., *Composite survival index to compare virulence changes in azole-resistant Aspergillus fumigatus clinical isolates.* PLoS One, 2013. **8**(8): p. e72280.
9. Schillaci, D., et al., *Pharmaceutical Approaches to Target Antibiotic Resistance Mechanisms.* J Med Chem, 2017. **60**(20): p. 8268-8297.
10. Chung, D., et al., *ChIP-seq and in vivo transcriptome analyses of the Aspergillus fumigatus SREBP SrbA reveals a new regulator of the fungal hypoxia response and virulence.* PLoS Pathog, 2014. **10**(11): p. e1004487.
11. Hagiwara, D., et al., *A Novel Zn2-Cys6 Transcription Factor AtrR Plays a Key Role in an Azole Resistance Mechanism of Aspergillus fumigatus by Co-regulating cyp51A and cdr1B Expressions.* PLoS Pathog, 2017. **13**(1): p. e1006096.
12. Gsaller, F., et al., *Sterol Biosynthesis and Azole Tolerance Is Governed by the Opposing Actions of SrbA and the CCAAT Binding Complex.* PLoS Pathog, 2016. **12**(7): p. e1005775.

13. Willger, S.D., et al., *A sterol-regulatory element binding protein is required for cell polarity, hypoxia adaptation, azole drug resistance, and virulence in Aspergillus fumigatus.* PLoS Pathog, 2008. **4**(11): p. e1000200.
14. Blosser, S.J. and R.A. Cramer, *SREBP-dependent triazole susceptibility in Aspergillus fumigatus is mediated through direct transcriptional regulation of erg11A (cyp51A).* Antimicrob Agents Chemother, 2012. **56**(1): p. 248-57.
15. Paul, S., et al., *AtrR Is an Essential Determinant of Azole Resistance in Aspergillus fumigatus.* MBio, 2019. **10**(2).
16. Camps, S.M., et al., *Discovery of a HapE mutation that causes azole resistance in Aspergillus fumigatus through whole genome sequencing and sexual crossing.* PLoS One, 2012. **7**(11): p. e50034.
17. Schrettl, M., et al., *HapX-mediated adaption to iron starvation is crucial for virulence of Aspergillus fumigatus.* PLoS Pathog, 2010. **6**(9): p. e1001124.
18. Lee, T.I. and R.A. Young, *Regulation of gene expression by TBP-associated proteins.* Genes Dev, 1998. **12**(10): p. 1398-408.
19. Patterson, T.F., et al., *Executive Summary: Practice Guidelines for the Diagnosis and Management of Aspergillosis: 2016 Update by the Infectious Diseases Society of America.* Clin Infect Dis, 2016. **63**(4): p. 433-42.
20. Rodriguez-Goncer, I., R. Niven, and D.W. Denning, *Successful long-term terbinafine therapy in an asthmatic patient with Aspergillus sensitization and bronchiectasis.* Med Mycol Case Rep, 2017. **16**: p. 31-33.
21. Fraczek, M.G., et al., *The cdr1B efflux transporter is associated with non-cyp51a-mediated itraconazole resistance in Aspergillus fumigatus* Journal of Antimicrobial Chemotherapy, 2013. **68**(7): p. 1486-1496.
22. Szewczyk, E., et al., *Fusion PCR and gene targeting in Aspergillus nidulans.* Nat. Protocols, 2007. **1**(6): p. 3111-3120.
23. Fraczek, M.G., et al., *The cdr1B efflux transporter is associated with non-cyp51a-mediated itraconazole resistance in Aspergillus fumigatus.* J Antimicrob Chemother, 2013. **68**(7): p. 1486-96.
24. Arendrup, M.C., et al., *EUCAST technical note on Aspergillus and amphotericin B, itraconazole, and posaconazole.* Clin Microbiol Infect, 2012. **18**(7): p. E248-50.

25. Liu, H.L., et al., *The three fungal transmembrane nuclear pore complex proteins of Aspergillus nidulans are dispensable in the presence of an intact An-Nup84-120 complex.* Mol Biol Cell, 2009. **20**(2): p. 616-30.
26. Gsaller, F., et al., *Sterol Biosynthesis and Azole Tolerance Is Governed by the Opposing Actions of SrbA and the CCAAT Binding Complex.* PLOS Pathogens, 2016. **12**(7): p. e1005775.
27. Zhang, Y., et al., *Model-based analysis of ChIP-Seq (MACS).* Genome Biol, 2008. **9**(9): p. R137.
28. Bailey, T.L., et al., *MEME Suite: tools for motif discovery and searching.* Nucleic Acids Research, 2009. **37**(suppl_2): p. W202-W208.
29. Quinlan, A.R. and I.M. Hall, *BEDTools: a flexible suite of utilities for comparing genomic features.* Bioinformatics, 2010. **26**(6): p. 841-842.
30. Anders, S. and W. Huber, *Differential expression analysis for sequence count data.* Genome Biol, 2010. **11**(10): p. R106.
31. Priebe, S., et al., *FungiFun2: a comprehensive online resource for systematic analysis of gene lists from fungal species.* Bioinformatics, 2015. **31**(3): p. 445-446.
32. Parker, J.E., et al., *Prothioconazole and prothioconazole-desthio activities against Candida albicans sterol 14-alpha-demethylase.* Appl Environ Microbiol, 2013. **79**(5): p. 1639-45.
33. Paul, S., D. Diekema, and W.S. Moye-Rowley, *Contributions of Aspergillus fumigatus ATP-binding cassette transporter proteins to drug resistance and virulence.* Eukaryot Cell, 2013. **12**(12): p. 1619-28.
34. O'Hanlon, K.A., et al., *Targeted disruption of nonribosomal peptide synthetase pes3 augments the virulence of Aspergillus fumigatus.* Infect Immun, 2011. **79**(10): p. 3978-92.
35. MacDonald, A.S., et al., *CD8- dendritic cell activation status plays an integral role in influencing Th2 response development.* J Immunol, 2001. **167**(4): p. 1982-8.
36. Kummerfeld, S.K. and S.A. Teichmann, *DBD: a transcription factor prediction database.* Nucleic Acids Res, 2006. **34**(Database issue): p. D74-81.
37. Todd, R.B., et al., *Prevalence of transcription factors in ascomycete and basidiomycete fungi.* BMC Genomics, 2014. **15**: p. 214.

38. Mizutani, O., et al., *A defect of LigD (human Lig4 homolog) for nonhomologous end joining significantly improves efficiency of gene-targeting in Aspergillus oryzae.* Fungal Genet Biol, 2008. **45**(6): p. 878-89.
39. Krappmann, S., C. Sasse, and G.H. Braus, *Gene targeting in Aspergillus fumigatus by homologous recombination is facilitated in a nonhomologous end- joining-deficient genetic background.* Eukaryot Cell, 2006. **5**(1): p. 212-5.
40. da Silva Ferreira, M.E., et al., *The akuB(KU80) mutant deficient for nonhomologous end joining is a powerful tool for analyzing pathogenicity in Aspergillus fumigatus.* Eukaryot Cell, 2006. **5**(1): p. 207-11.
41. Ninomiya, Y., et al., *Highly efficient gene replacements in Neurospora strains deficient for nonhomologous end-joining.* Proc Natl Acad Sci U S A, 2004. **101**(33): p. 12248-53.
42. Yu, H. and M. Gerstein, *Genomic analysis of the hierarchical structure of regulatory networks.* Proc Natl Acad Sci U S A, 2006. **103**(40): p. 14724-31.
43. Beattie, S.R., et al., *Filamentous fungal carbon catabolite repression supports metabolic plasticity and stress responses essential for disease progression.* PLoS Pathog, 2017. **13**(4): p. e1006340.
44. Ries, L.N.A., et al., *The Aspergillus fumigatus CrzA Transcription Factor Activates Chitin Synthase Gene Expression during the Caspofungin Paradoxical Effect.* MBio, 2017. **8**(3).
45. Ramirez-Zavala, B., et al., *SAGA/ADA complex subunit Ada2 is required for Cap1- but not Mrr1-mediated upregulation of the Candida albicans multidrug efflux pump MDR1.* Antimicrob Agents Chemother, 2014. **58**(9): p. 5102-10.
46. Balciunas, D. and H. Ronne, *Yeast genes GIS1-4: multicopy suppressors of the Gal- phenotype of snf1 mig1 srb8/10/11 cells.* Mol Gen Genet, 1999. **262**(4-5): p. 589-99.
47. Hortschansky, P., et al., *The CCAAT-binding complex (CBC) in Aspergillus species.* Biochim Biophys Acta, 2017. **1860**(5): p. 560-570.
48. Goppelt, A. and M. Meisterernst, *Characterization of the basal inhibitor of class II transcription NC2 from Saccharomyces cerevisiae.* Nucleic Acids Res, 1996. **24**(22): p. 4450-5.

49. Cang, Y. and G. Prelich, *Direct stimulation of transcription by negative cofactor 2 (NC2) through TATA-binding protein (TBP).* Proc Natl Acad Sci U S A, 2002. **99**(20): p. 12727-32.
50. Tuckwell, D., D.W. Denning, and P. Bowyer, *A public resource for metabolic pathway mapping of Aspergillus fumigatus Af293.* Med Mycol, 2011. **49 Suppl 1**: p. S114-9.
51. Kimura, M., et al., *Protostadienol synthase from Aspergillus fumigatus: functional conversion into lanosterol synthase.* Biochem Biophys Res Commun, 2010. **391**(1): p. 899-902.
52. Machanick, P. and T.L. Bailey, *MEME-ChIP: motif analysis of large DNA datasets.* Bioinformatics, 2011. **27**(12): p. 1696-1697.
53. Shukla, S., et al., *Ncb2 is involved in activated transcription of CDR1 in azole-resistant clinical isolates of Candida albicans.* Eukaryot Cell, 2011. **10**(10): p. 1357-66.
54. Kamada, K., et al., *Crystal Structure of Negative Cofactor 2 Recognizing the TBP-DNA Transcription Complex.* Cell, 2001. **106**(1): p. 71-81.
55. Mermelstein, F., et al., *Requirement of a corepressor for Dr1-mediated repression of transcription.* Genes Dev, 1996. **10**(8): p. 1033-48.
56. Goppelt, A., et al., *A mechanism for repression of class II gene transcription through specific binding of NC2 to TBP-promoter complexes via heterodimeric histone fold domains.* Embo j, 1996. **15**(12): p. 3105-16.
57. Giaever, G., et al., *Functional profiling of the Saccharomyces cerevisiae genome.* Nature, 2002. **418**(6896): p. 387-91.
58. Vachon, L., et al., *Functional characterization of fission yeast transcription factors by overexpression analysis.* Genetics, 2013. **194**(4): p. 873-84.
59. Colot, H.V., et al., *A high-throughput gene knockout procedure for Neurospora reveals functions for multiple transcription factors.* Proc Natl Acad Sci U S A, 2006. **103**(27): p. 10352-10357.
60. Homann, O.R., et al., *A phenotypic profile of the Candida albicans regulatory network.* PLoS Genet, 2009. **5**(12): p. e1000783.
61. Jung, K.W., et al., *Systematic functional profiling of transcription factor networks in Cryptococcus neoformans.* Nat Commun, 2015. **6**: p. 6757.
62. Li, H. and A.D. Johnson, *Evolution of transcription networks--lessons from yeasts.* Curr Biol, 2010. **20**(17): p. R746-53.

63. Gsaller, F., et al., *Mechanistic Basis of pH-Dependent 5-Flucytosine Resistance in Aspergillus fumigatus.* Antimicrob Agents Chemother, 2018. **62**(6).
64. Yu, S.J., Y.L. Chang, and Y.L. Chen, *Deletion of ADA2 Increases Antifungal Drug Susceptibility and Virulence in Candida glabrata.* Antimicrob Agents Chemother, 2018. **62**(3).
65. Kapitzky, L., et al., *Cross-species chemogenomic profiling reveals evolutionarily conserved drug mode of action.* Mol Syst Biol, 2010. **6**: p. 451.
66. Caza, M., et al., *The Zinc Finger Protein Mig1 Regulates Mitochondrial Function and Azole Drug Susceptibility in the Pathogenic Fungus Cryptococcus neoformans.* mSphere, 2016. **1**(1).
67. Inostroza, J.A., et al., *Dr1, a TATA-binding protein-associated phosphoprotein and inhibitor of class II gene transcription.* Cell, 1992. **70**(3): p. 477-89.
68. Meisterernst, M. and R.G. Roeder, *Family of proteins that interact with TFIID and regulate promoter activity.* Cell, 1991. **67**(3): p. 557-67.
69. Albert, T.K., et al., *Global distribution of negative cofactor 2 subunit-alpha on human promoters.* Proc Natl Acad Sci U S A, 2007. **104**(24): p. 10000-5.
70. Gomez-Navarro, N., et al., *Defects in the NC2 repressor affect both canonical and non-coding RNA polymerase II transcription initiation in yeast.* BMC Genomics, 2016. **17**: p. 183.
71. Shariq, M., et al., *The global regulator Ncb2 escapes from the core promoter and impacts transcription in response to drug stress in Candida albicans.* Sci Rep, 2017. **7**: p. 46084.
72. van Werven, F.J., et al., *Cooperative action of NC2 and Mot1p to regulate TATA-binding protein function across the genome.* Genes Dev, 2008. **22**(17): p. 2359-69.
73. Ryder, N.S., *Terbinafine: mode of action and properties of the squalene epoxidase inhibition.* Br J Dermatol, 1992. **126 Suppl 39**: p. 2-7.
74. Gray, K.C., et al., *Amphotericin primarily kills yeast by simply binding ergosterol.* Proc Natl Acad Sci U S A, 2012. **109**(7): p. 2234-9.
75. Sanglard, D., et al., *Candida albicans mutations in the ergosterol biosynthetic pathway and resistance to several antifungal agents.* Antimicrob Agents Chemother, 2003. **47**(8): p. 2404-12.

76. Chamilos, G. and D.P. Kontoyiannis, *Update on antifungal drug resistance mechanisms of Aspergillus fumigatus.* Drug Resist Updat, 2005. **8**(6): p. 344-58.

2.6 Supplementary data

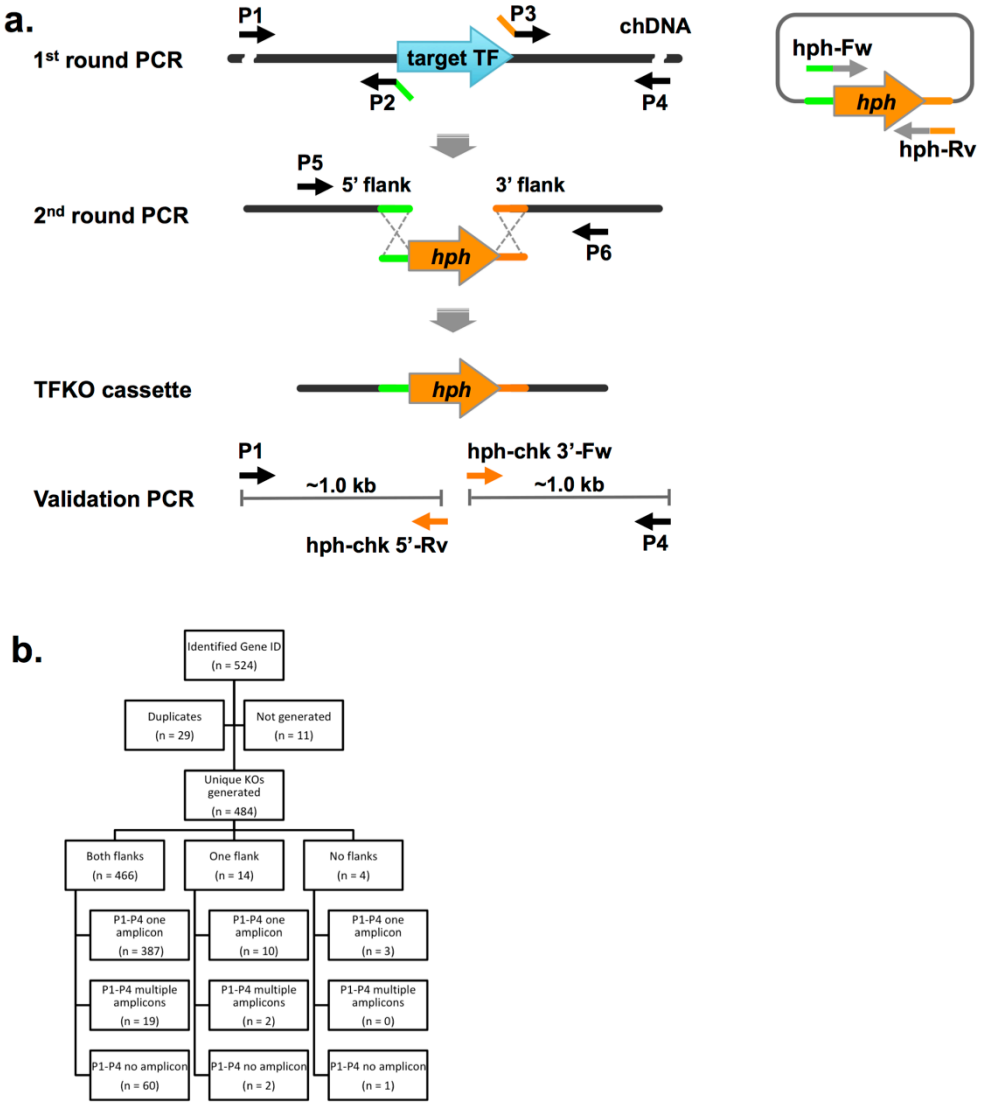

Figure S2.1: Generation of *A. fumigatus* transcription factor knockout mutants. (a) Schematic diagram of the construction of a transcription factor knockout (TFKO) cassette by fusion PCR. The flanking regions of the target gene are amplified independently from the chromosomal DNA using the primer pairs P1/P2 and P3/P4, respectively. Primers P2 and P3 are designed to include a 20-bp of 5'-tail (shown in green and orange) homologous to the ends of the hygromycin resistance (*hph*) marker cassette. Each pre-amplified fragment is fused together by fusion PCR using nested primers P5 and P6 to give a TFKO cassette. Homologous integration of the TFKO cassette was verified by PCR using the primer pairs P1/hph-chk-57-Rv (for 5'-junction), hph-chk 3'-Fw/P4 (for 3'-junction), and P1/P4 (for entire TFKO cassette). **(b)** Flowchart describing the construction of the *A. fumigatus* TFKO library and its quality control process.

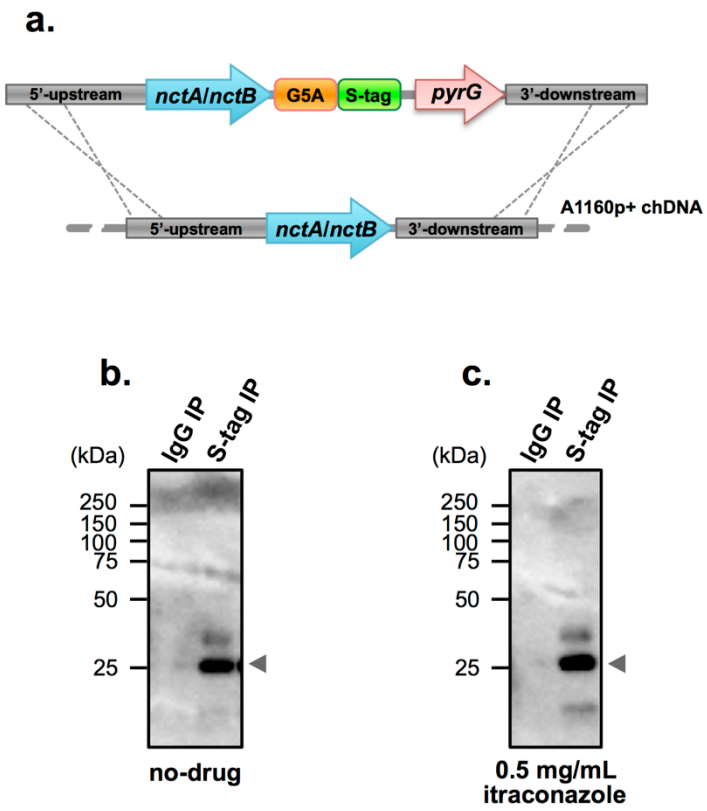

Figure S2.2: Validation of chromatin immunoprecipitation (ChIP) conditions for the C-terminally S-tagged derivative of NctA (NctA-S-tag). (a) Schematic representation of the construction of the S-tagged NctA and NctB expressing strains. **(b-c)** Immunoprecipitation followed by Western blotting (IP-WB) analysis of the NctA-S-tag expressing strain. Cell-free extract of the NctA-S-tag expressing mutant prepared from **(a)** no-drug and **(b)** 0.5 mg/mL itraconazole conditions were immunoprecipitated with a S-tag specific polyclonal antibody (S-tag IP) or a control rabbit IgG (IgG IP), and then subjected to WB. Specific signals derived from NctA-S-tag protein is indicated by triangles. The estimated molecular weight of NctA-S-tag is 30.2 kDa.

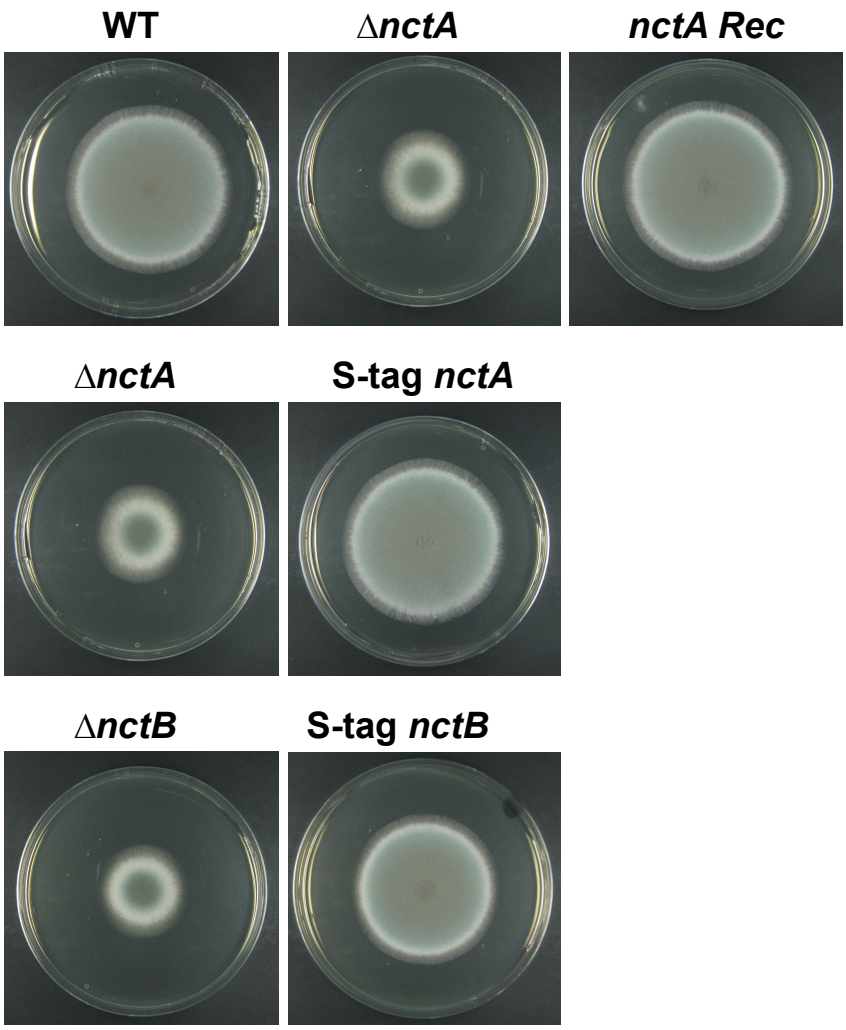

Figure S2.3: Phenotypes of NctA and NctB mutants and constructed tagged strains. Spot tests on Aspergillus Complete Medium grown for 72 hour. Reconstitution of NctA resulted in rescue of the growth phenotype observed for the null mutant. Introduction of an S-tagged NctA or NctB in their respective null background strain rescued the growth phenotype.

Chapter

3

Genetically distinct transcriptional circuits drive stress-adaptation and host cytotoxicity in a mould pathogen of the human lung.

Norman van Rhijn, Takanori Furukawa, Sayema Rahman, Panos Papastamoulis, Frans Rodenburg, Rachael Fortune-Grant, Magnus Rattray, Michael J Bromley, Elaine Bignell

3. Genetically distinct transcriptional circuits drive stress-adaptation and host cytotoxicity in a mould pathogen of the human lung

Authors: Norman van Rhijn†[1,2], Takanori Furukawa†[1,2], Sayema Rahman[1,2], Panos Papastamoulis[1], Frans Rodenburg, Rachael Fortune-Grant[1,2], Magnus Rattray[1,2], Michael J Bromley[1,2], Elaine Bignell[1,2]

[1] Manchester Fungal Infection Group, Division of Infection, Immunity and Respiratory Medicine, Faculty of Biology, Medicine and Health, University of Manchester, CTF Building, 46 Grafton Street, Manchester, M13 9NT, UK.

[2] Lydia Becker Institute of Immunology and Inflammation, Manchester Collaborative Centre for Inflammation Research, Division of Infection, Immunity and Respiratory Medicine, Faculty of Biology, Medicine and Health, University of Manchester, Manchester Academic Health Science Centre, Manchester, UK.

†The authors wish it to be known that, in their opinion, the first two authors should be regarded as joint First Authors.

Target Journal: Nature Microbiology

Abstract:

Aspergillus fumigatus is a saphrophytic environmental mould, which can cause life threatening lung diseases in humans. Inhaled spores are able to reach deep into the alveoli due to their small size and airborne buoyancy. Here, the fungus is able to resist the exogenous stress imposed by the lung environment and grow, when not cleared by the immune system. Regulation of adaptation within the lung is tightly regulated by transcription factors. Here, we explore transcription factors that are required for fitness, adaptation to environmental stress and epithelial invasion by high-throughput phenotyping of a genome wide transcription factor null library. This resulted in identification of two distinct regulatory networks required for adaptation and invasion, pointing towards the environmental nature of this fungus and lays the basis for exploring the coincidental evolution of pathogenicity theory.

3.1 Introduction

Inhaled spores of the saprophytic environmental mould *Aspergillus fumigatus* are a major cause of life threatening lung diseases in man, which are collectively referred to as pulmonary aspergilloses. The pathology of aspergillus-related disease is governed by host immune status, ranging from rapidly fatal invasive pulmonary aspergillosis (IPA) in severely immunocompromised cancer sufferers or organ transplantees, to semi-invasive chronic pulmonary aspergillosis (CPA) or allergic bronchopulmonary aspergillosis, respectively in the settings of chronic underlying lung disease or asthma [1]**.** The estimated all cause burden of aspergilloses per annum, in Europe alone, approaches 2 million [2].

A. fumigatus is a prolific producer of minute (2-5 μM) haploid spores (conidia) that are abundant in the airborne microflora [3]. Immune dysfunction leads to persistence of inhaled *A. fumigatus* spores in the respiratory tract where spore germination, followed by the production of elongated cells called hyphae, leads to fungal invasion of the respiratory epithelium. Amongst more than 200 species comprising the genus *Aspergillus*, *A. fumigatus* predominates as the major cause of human lung disease. The evolutionary origin of pathogenicity amongst Aspergillus species has therefore been widely debated. Whilst spore-associated factors such as small size and airborne buoyancy are likely contribute to the prevalence of *A. fumigatus* as a pathogen of the mammalian lung, so too are high spore germination rates and resistance to the exogenous stress imposed by *in vivo* niches [4]. Comparative analyses of the sequenced *Aspergillus* genomes negates the occurrence of large-scale genomic rearrangements or the presence of accessory chromosomes as being causal of the pathogenic lifestyle [5]. In contrast, mutational analyses of *A. fumigatus* transcription factors have repeatedly identified environmental adaptation as a critical driver of infectious growth (Table 3.1).

In the natural environment *A. fumigatus* is commonly associated with compost, where a by-product of microbial breakdown of organic material leads to sustained elevations in temperature to >40°C. The microenvironments encountered in the mammalian lung impose nutritional limitation, and altered pH, temperature and

oxygen availability, transcriptional adaptation to which is a prominent component of the host-adapting *A. fumigatus* transcriptome [6]. Evolutionary adaptation to thermal stress coupled with ubiquity of airborne *A. fumigatus* spores which become accidental colonisers of the human lung are highly suggestive of a coincidental evolutionary basis for *A. fumigatus* pathogenicity. However, the tools with which to test this theory have thus far been lacking [7].

Recent expansion of the methodological toolkit with which to engineer filamentous fungal genomes has recently facilitated the construction of a genome-scale library of *A. fumigatus* transcription factor null mutants (TFKOs) which has allowed us, for the first time, to perform a genome-scale census of TFs driving adaptation to host-imposed stress. In this study we have constructed and mined a high-density compendium of *A. fumigatus* transcriptomes seeking highly conserved transcriptional adaptations to host imposed stresses. Via high throughput, highly quantitative phenotypic analysis we identified a highly interconnected network of transcription factors, which drive adaptation to these stresses, involving 20 known and 21 novel TFs amongst the latter of which we show seven are novel regulators of murine pathogenicity. We show that the stress-adapting network of transcription factors has a functional identity, which is entirely distinct from that which governs epithelial cytotoxicity supporting the co-incidental evolution model of *A. fumigatus* pathogenicity. Our study delivers a first-in-field genome-wide phenotypic analysis of transcription factors in *A. fumigatus,* which provides a robust footing for onward analysis of pathogenicity with much-needed focus upon transcription factors driving virulence.

Table 3.1 Previously characterised transcription factors in *A. fumigatus*

	TF	AF293 Locus ID	Function	Reference(s)	Required for pathogenicity
Conidiation and development	Ace2	Afu3g11250	Conidial formation, cell wall architecture	Ejzykowicz et al. (2009)	+ (CA), -
	BrlA	Afu1g16590	Condiation, hyphael maturation	Twumasi-Boaten et al (2009)	NP
	MtfA	Afu6g02690	Conidiation, protease and gliotoxin production	Smith and Calvo (2014)	✓
	AbaA	Afu1g04830	Conidiation	Tao and Yu (2011)	NP
	StuA	Afu2g07900	Asexual reproduction, secondary metabolite pathways	Sheppard et al. (2005) Twumasi-Boateng et al. (2009)	-
	MybA	Afu3g07070	Conidiation, maturation	Valsecchi et al. (2017)	✓
	FlbB	Afu1g03210	Morphological development, gliotoxin production	Xiao et al. (2010)	NP
	FlbC	Afu2g13770	Asexual development	Xiao et al. (2010)	NP
	FlbD	Afu1g0210	Asexual development	Xiao et al. (2010)	NP
	NsdC	Afu3g13870	Asexual development/sexual development	Gross et al. (2008)	NP
	Ads4	Afu1g16460	Antifungal azole stress	Szewczyk et al. (2010)	NP
	NosA	Afu4g09710	Sexual development	Soukup et al. (2012)	+ (hyper)
Adhesion	MedA	Afu2g13260	Biofilm formation, adherence	Gravelat et al. (2010) Al Abdallah et al. (2012)	✓
	SomA	Afu7g02260	Conidiation, adhesion	Lin et al. (2015)	✓ (Tet mutant)
Nutrient acquisition	SrbA	Afu2g01260	Hypoxia response, ergosterol biosynthesis, siderophore biosynthesis	Blatzer et al. (2011) Chung et al. (2014) Willger et al. (2008)	✓
	SrbB	Afu4g03460	Hypoxia response, carbohydrate metabolism, heme biosynthesis	Chung et al. (2014)	✓
	AtrR	Afu2g02690	Hypoxia response, ergosterol biosynthesis	Hagiwara et al. (2017), Paul et al. (2019)	✓
	Afmac1	Afu1g13190	Copper starvation	Kusuya et al. (2017), Wiemann et al. (2017)	Conflicted reports
	AceA	Afu6g07780	Copper toxicity	Wiemann et al. (2017)	✓/-
	CufA	Afu2g01190	Copper binding TF	Wiemann et al. (2017)	-
	HapX	Afu5g03920	Iron homeostasis (deplete conditions)	Brandon et al. (2015) Schrettl et al. (2010)	✓
	SreA	Afu5g11260	Iron homeostasis (replete conditions)	Brandon et al. (2015) Schrettl et al. (2008)	-
	AcuK	Afu2g05830	Gluconeogenesis, iron acquisition	Pongpom et al. (2015)	✓/-
	AcuM	Afu2g12330	Gluconeogenesis, iron acquisition	Liu et al. (2010) Pongpom et al. (2015)	✓
	CrzA	Afu1g06900	Calcium homeostasis	De Castro et al. (2014) Soriani et al. (2008) Cramer et al. (2008)	✓
	MetR	Afu4g06530	Acquisition of inorganic sulfur	Amich et al. (2013)	✓
	LeuB	Afu2g03460	Leucine biosynthesis/ iron acquisition	Long et al. (2018)	✓
	ZafA	Afu1g10080	Zinc homeostasis	Amich et al. (2010) Amich et al. (2014) Moreno et al. (2007) Amich and Calera (2014) Vicentefranqueira et al. (2015)	✓
	AreA	Afu6g01970	Nitrogen utilization	Hensel et al. (1998) Krappmann et al. (2005)	✓
Environmental stress adaptation	PacC	Afu3g11970	Alkaline pH response	Bertuzzi et al. (2014) Amich et al. (2010) Tilburn et al. (1995)	✓
	SebA	Afu4g09080	Heat shock, nutrient and oxidative stress	Dinamarco et al. (2012)	✓
	HacA	Afu3g04070	Unfolded protein response	Richie et al. (2009) Richie et al. (2011)	✓
	CpcA	Afu4g12470	Cross-pathway control system	Krappmann et al. (2004)	✓
	Yap1	Afu6g09930	Oxidative stress response	Lessing et al. (2007) Qiao et al. (2008)	-
	AtfA	Afu3g11330	Conidia stress response	Hagiwara et al. (2014), Takahashi et al. (2017)	✓
	ZipD	Afu2g03280	Calcium/calcineurin-dependent response	Ries et al. (2017)	NP
	CreA	Afu2g11780	Hypoxic adaptation, carbon catabolite repression	Beattie et al. (2017)	✓/-
Host-pathogen interaction	DvrA	Afu3g09820	Host cell damage	Ejzykowicz et al. (2010)	+ (Gall), +(CA), - (CA,CP)
	RlmA	Afu3g08520	Cell wall integrity	Rocha et al. (2016) Valiante et al. (2016)	✓
Secondary metabolism	GliZ	Afu6g09630	Gliotoxin production	Bok et al. (2006)	-
	RsmA	Afu2g02540	Gliotoxin production	Sekonyela et al. (2013)	- (OE)
	HasA	Afu3g12890	hexadehydro-astechrome production	Yin et al. (2013)	+ (OE)
	FumR	Afu8g00420	Fumagillin production	Dhingra et al. (2013)	NP
	GipA	Afu6g01910	Gliotoxin production	Shorbele et al. (2014)	NP
	PrtT	Afu4g10120	Extracellular proteolytic activities	Bergmann et al. (2009)	-
	XprG	Afu8g04050	Protease prodution	Shemesh et al. (2018)	-
	LaeA	Afu1g14660	Secondary metabolite production	Bok and Keller (2004), Sugui et al (2007)	✓

3.2 Material & Methods

3.2.1 Fungal strains and media

The library of *A. fumigatus* transcription factor knock out (TFKO) mutants was generated previously by Furukawa et al 2019 (in press). *A. fumigatus* strains were cultured at 37 °C in Sabouraud agar or *Aspergillus* Complete Media (ACM). For preparation of *A. fumigatus* glycerol stocks, spores were harvested in phosphate buffered saline (PBS) + 0.01% Tween-20 (Sigma) and normalised to 4 x 10^7 spores/mL in PBS + 0.01% Tween-20 + 20% glycerol. These were stored at -80 C until use. Spore stocks were diluted to 4 x 10^5 spores/mL in PBS + 0.01% Tween-20. The composition of fungal RPMI, Aspergillus complete media, Aspergillus minimal media, RPMI-1640 and DMEM can be found in Table S3.3.

3.2.2 96-well growth assay

Multiple rounds of optimisation were performed to establish a microculture platform for phenotyping. To facilitate rapid enumeration of fungal spores and standardise fungal inocula, a spectrophotometric method was developed which performed comparably to manual enumeration (Figure S3.1) whereby spore concentrations were normalised via an OD based method and microscopy. Multiple blank wells were included for every 96 well plate analysed to monitor occurrence rates of cross-contamination contamination. Contamination was assessed based on fungal growth within these blank wells as well as overgrowth in wells containing mutants with a slow-growth phenotype (Figure S3.1). Lastly, having observed a consistent, but artefactual increase in optical density in the outer wells of 96 well plates, CytoOne 96 well plates (Starlab) clear plates specifically designed to combat this phenomenon was found to resolve this 'edge effect'.

For optimisation of culture medium, and subsequent phenotypic analyses, 2000 spores of each TFKO mutant were inoculated per well followed by overlay with either fRPMI, RPMI1640 or Dulbecco's Modified Eagle Medium (DMEM, Sigma), ACM or *Aspergillus* Minimal Media, to a total volume of 200 µL. For growth curve analysis OD_{600} was measured every 10 minutes on a BioTek Powerwave X-1 plate reader. Endpoint assays were performed as single time point OD_{600} measurements on

a BioTek Synergy-2**.** All experiments were performed in biological triplicate. High-throughput growth curves were generated using the BEAST package with default settings in R (version 3.6.1) [8].

3.2.3 Microscopy germination and hyphal extension.

$5x10^4$ spores were inoculated into a 24 well glass bottom plate (Greiner Bio-one). Spores were allowed to settle for 45-60 min. Growth was imaged at 37 °C using a confocal microscope (Leica X, SP8). Bright field images were taken using an argon laser set at 100% for 514 nm wavelength. The format and speed of capture was set to 1024x1024 pixels, 400 ms. Images were taken using an automatic 'mark and find' option of the confocal microscope at 10x magnification in each well of the plate at every hour up to 48 hours after set-up. To analyse germination of *A. fumigatus*, a field of view to include approx. 100 spores was selected from each well. Random regions within the well were selected as technical replicates for each strain. Total number of spores and the number of germinated spores were counted every time point using FIJI. Lengths of individual hyphae were measured at each time-point starting from germination, by using the segmented tool of FIJI. Optimum clusters for germination and hyphal extention rate were found using the package factoextra in R (version 3.6.1).

3.2.4 Leukopenic mouse model of aspergillosis

The murine infection experiments were performed under UK Home office Project Licence PDF8402B7 and approved by the University of Manchester Ethics Committee. *A. fumigatus* was cultured on ACM containing 5 mM ammonium tartrate for 6 days at 37 ˚C and conidia were harvested in sterile saline.

CD1 male mice (Charles River UK, Ltd.) were housed in groups of 3-4 in IVC cages with access to food and water *ab libitum*. All mice were given 2 g/L neomycin sulphate in drinking water throughout the course of the study. Mice were rendered leukopenic by administration of cyclophosphamide (150 mg/kg of body weight; intraperitoneal) on days -3, -1, +2, and every subsequent third day, and a single subcutaneous dose of cortisone acetate (250 mg/kg) was administrated on day -1. Mice were anaesthetized by exposure to 2-3 % inhalational isoflurane and infected intranasally with a spore suspension containing 1.25 x 10^7 conidia/ml in 40 µl of

saline solution. Mice were weighed every 24 h from day -3, relative to day of infection, and visual inspections were made twice daily. In the majority of cases, the endpoint for experimentation was a 20% reduction in body weight measured from day of infection, at which point mice were sacrificed. Kaplan-Meier survival analysis was used to create a population survival curve and to estimate survival over time, and p-values were calculated through a log rank analysis.

3.2.5 High throughput phenotyping

Four different phases of *A. fumigatus* growth in fungal RPMI were identified by change-point analysis. Phase 4 does not correspond to submerged growth of fungal cells. Therefore, the transition points between phase 3 and 4 was used as the time-point for fitness measurements. To this end, *A. fumigatus* A1160pyrG+ (MFIG001) was cultivated under culture conditions used for phenotyping. Each condition was individually optimised to ensure sufficient growth to measure phenotypic differences. The transition time-points were determined as 36 h for iron depleting conditions, 38 h for thermotolerance at 48 ˚C, 48 h for thermotolerance at 30 ˚C, 48 h for alkaline pH, 38 h for acidic pH, 72 h for hypoxia, 34 h for CO_2, 48 h for zinc, 48 h for serum phenotype screenings. 2000 spores of each TFKO mutant were inoculated per well of CytoOne 96 well plates (Starlab) and OD_{600} was measured at previously determined time-points. Fitness was calculated as OD_{600} normalised to MFIG001 OD_{600} under the same condition. Clustering of the data was performed using mclust.

Optical density readings for multifactorial stress were corrected using a set of offsets in each linear model. These offsets were estimated by fitting a linear mixed effects model on the optical density of the blank and wildtype replicates on all 96-well assay plates:

$$\mathcal{Y}_{ijk} = \mathbf{X}\beta_{ij} + c_i + s_{ij} + \epsilon_{ijk}c_i \sim \mathcal{N}(0, \sigma_c), \quad s_{ij} \sim \mathcal{N}(0, \sigma_s)$$

Where **X** are the fixed effects, nested in 96-well plate *j*, nested in the original growth plate i. $\mathcal{Y}$ is the multifactorial stress effect, calculated by a linear mixed model of growth under multifactorial stressed condition β, given growth under single stress conditions *c* and *s*. Estimates were obtained through restricted maximum likelihood with the lme4 package [9]. Using these offsets, multifactorial stress effects were estimated in a linear model as first-order interactions. Additional corrections for spatial autocorrelation within plates were considered, but deemed unnecessary upon

inspection of the model residuals, via the Moran's I test from the R package 'ape' [10]. Plots were produced using the Bioconductor package 'EnhancedVolcano'.

3.2.6 High throughput analysis of A. fumigatus cytotoxity

The commercially available carcinomic human alveolar basal epithelial cell line-A549 cell line was used in this study (American type culture collection, CCL-185). The A549 cells were grown from frozen stock or passaged in T75 flasks (Sarstedt, UK) with RPMI-1640 medium with L-glutamine, (Sigma-Aldrich) supplemented with 10% fetal bovine serum (FBS) (Gibco, UK) and 1% penicillin- streptomycin (Sigma-Aldrich) with 5% CO_2 at 37 °C. At 90% confluent, the cells were rinsed gently with PBS (Sigma) to remove traces of FBS and detached using 5 ml of Trypsin/EDTA for 5-10 min incubation at 37 °C. Detached cells were collected in a 50 ml falcon tube (Corning, UK) and pelleted at 1200 RPM for 4 min in a centrifuge (MSE Mistal 2000). The cell pellet was re-suspended in 15 ml of supplemented RPMI-1640 medium and counted. Cells were seeded at $0.5x10^5$ cells/ml for a 24 well plate (Greiner Bio-one) and at $0.75x10^5$ cells/ml for a 96 well plate (Greiner Bio- one) and incubated for 48 hours at 37 °C with 5% CO_2. Media from each well was replaced with fungal RPMI. $5x10^5$ *A. fumigatus* spores were used to challenge the A549 monolayer. Following co-incubation with *A. fumigatus* spores for 24 hours, cell culture supernatants were collected to measure cell lysis via LDH assay. WT, well characterised non-invasive TF mutant Δ*pacC* (Δ*afub_037210*) and an un-infected control were included.

The LDH released in the culture supernatants was measured according to the Cytox 96 Non-radioactive cytotoxicity assay kit (Promega). Each replicate was duplicated in a 96 or a 384 well plate in a 1:5 dilution with PBS. Recombinant porcine LDH enzyme (Sigma-Aldrich) was used in 2-fold serial dilution with concentrations ranging from between 15 to 960 µmol/ml as a standard curve. OD_{490} was measured with a Synergy 2 microplate reader (Biotek, UK). LDH concentrations were quantified via extrapolation from the LDH concentrations of the standard curve. Viability was assessed by plating 100 spores onto solid ACM media in duplicate. Plates were incubated for 24-48 hours at 37 °C and the single viable colonies were counted.

3.2.7 Detachment assay

A549 epithelial cells were grown in a glass bottomed 96 well plate (Greiner Bio-one, UK) to 100% confluency. Media from the wells was replaced with fungal RPMI. $2x10^5$ *A. fumigatus* spores were used to challenge the A549 monolayer. The assay was performed in 5 technical replicates. Infections were incubated for 16 hours at 37 °C with 5% CO_2, the A549 monolayers were washed once with pre-warmed PBS (Thermo-Fisher Scientific) to remove detached or non-adherent A549 cells. Adherent A549 cells were fixed with 4% formaldehyde in PBS for 10 min (Alfa Aesar, UK) and permeabilised with 0.2% Triton-X100 (VWR) for 2 min. Nuclei of the adherent A549 cells were stained with DAPI (Alfa Aesar) at 300 nM/ml concentration for 5 min at room temperature, protected from direct light. Following two washes with PBS, the plates were stored in PBS at -4 °C to be imaged.

DAPI fluorescence in adherent A549 cells was excited with a diode laser and imaged in high-throughput automation using a confocal microscope (Leica X, SP8) to collect emission between 405-600nm. Automated MATRIX software was used to image A549 cells in 9 fields of view in the centre of each well at 40x magnification (HC PL APOCS 40x/0.85 DRY objective). The number of A549 cells in each image was quantified using an in-house image analysis for FIJI.

Summarised data were analysed using GraphPad Prism 8 and the results expressed as mean ± SEM. The difference between means was determined using one-way ANOVA. Data was plotted using the EnhancedVolcano package in R (version 3.6.1).

3.2.8 Transcriptome compendium: culture conditions, RNA extraction and transcriptional analyses

For analyses of *in vitro* stress adaptation in fRPMI, $1x10^6$ spores/ml *A. fumigatus* MFIG001 was grown in 50 mL of fungal RPMI, at either 37 or 42 °C on a rotary shaker (180 rpm), with or without serum to produce germlings (8-10 hour) or hyphae (18 hour). Fungal biomass was harvested through filtration and snapfrozen in liquid N_2. Total RNA was extracted using TRI Reagent® (Sigma-Aldrich) according to the manufacturer's instructions. The extracted RNA samples were treated with RQ1 RNase-Free DNase (Promega) and further purified using the RNeasy Mini Kit (Qiagen). For analyses of in-host gene expression time-series analyses of fungal

colonization in the murine lung were performed as previously described [11, 12]. Fungal RNA was doubly amplified prior to array hybridization and a 70-mer oligotide glass slide DNA microarray platform was used (Pathogen Functional Genomic Resource Centre, JCVI, Rockville).

3.2.9 Transcriptome compendium: Data treatments and construction of data matrix

For in vivo transcripomes derived from microarray experimentation, a single-channel approach was applied using quantile normalization to extract, from dual channel co-hybridisation data as previously described [12]. Following normalization, spot intensity values were averaged between technical replicates at each time point, producing a single measurement of transcript abundance per gene per condition and time point. Quantile-normalized transcript abundance, calculated as a function of all expressed genes in the analysis, was used as a proxy measure of standing in overall ranking of transcript abundance and to standardise the data distributions of all datasets of diverse origins included in the data matrix. A data matrix comprised of >300 individual *A. fumigatus* transcriptomes drawn from 5 genetically distinct strains and >50 conditions and timepoints was generated (to be included as supplementary data and curated at FungiDB).

3.2.10 Aspergillus species environmental stress

Aspergillus species (Table S3.1) cultures were obtained (3-5 individual isolates per species) and grown on Sabouraud agar for 7 days at 37 °C, followed by harvesting in PBS+0.01% Tween. 2000 spores were inoculated in a CytoOne (Starlab) 96 well plate. An overlay with fungal RPMI (pH 7.0, pH 4.0, pH 8.0, lacking $FeSO_4$ + 100 μM BPS, addition of FBS) was performed and incubated at 37 °C or 48 °C for 48 hours. OD_{600} measurements were taken every 10 minutes in Powerwave X-2 spectrometer. Data was plotted using ggplot2 in R (version 3.6.1).

3.3 Results

3.3.1 A high density compendium of A. fumigatus transcriptomes identifies a conserved pathogenic regulon which is dominated by adaptation to abiotic stresses

In order to identify transcriptional signatures driving niche adaptation we constructed a compendium of >300 individual *A. fumigatus* transcriptional signatures and sought cohorts of genes whose expression is explicitly governed by the mammalian host environment, which is shown in yellow (Figure 3.1). A data matrix of >3 million data points comprising 55 distinct conditions and drawn from 5 diverse *A. fumigatus* genomes was constructed using all data to date deposited into public databases and a repertoire of more than 200 new transcriptomes generated for this study. An exemplar output is presented in Figure 3.1.

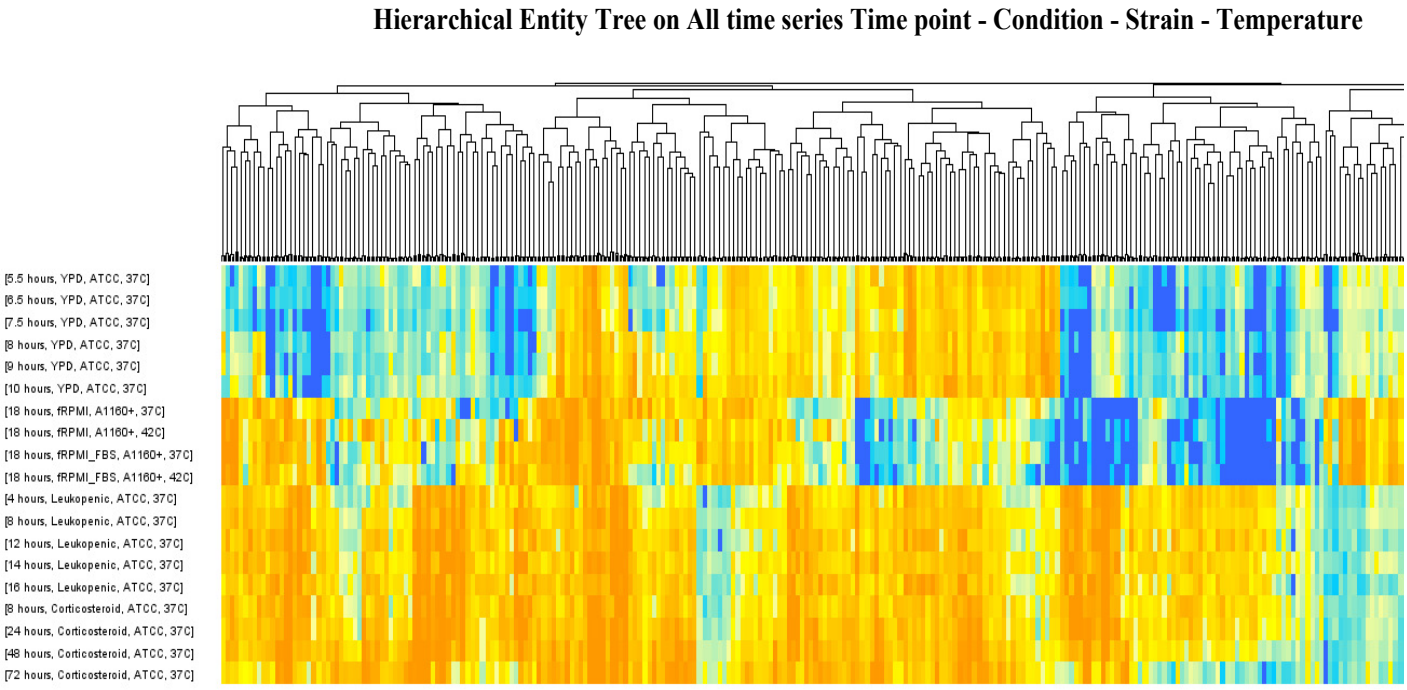

Figure 3.1 Signature heatmap of summarised transcriptome. Heatmap showing transcript abundance (yellow high – blue low) under lab conditions compared to the *in vivo* transcriptome dataset. Signatures of fRPMI mimic *in vivo* conditions as shown in overlap of highly expressed genes in the Leukopenic/Corticosteroid and fRPMI transcriptomes.

3.3.2 High throughput quantitation of A. fumigatus morphogenesis identifies and classifies fitness defects with a high degree of accuracy

Airborne *A. fumigatus* spores are over-wintering propagules, which promote mobility of otherwise sessile fungal colonies. Upon reaching a moist and carbon-rich environment the spore will undergo a genetically programmed morphogenesis involving swelling, germination, and rapid hyphal growth and branching. Concomitant with the metabolic exertion required to generate new biomass, the fungus must also adapt in real time to dynamic environmental cues and stressors it faces in the new niche. In order to design an assay which closely mimics the growth programme and sequential stresses encountered in the mammalian host, we sought a high throughput liquid culture format which could a) amply support the viability and proliferation of both host and pathogen cells and b) deliver highly quantitative information about fungal growth characteristics under the ambient conditions expected in the lung (Figure S3.1).

To support a standardised and comparative high throughput analysis of TFKO phenotypes under biotic and abiotic stressors we combined the use of this approach with culture under varying types of host-imposed stress. We first sought a synthetic host and pathogen co-culture medium, which could serve as a baseline comparator to sequentially-applied stresses. By assessing host and pathogen fitness in standard fungal (ACM or MM) or tissue culture DMEM or RPMI-1640 media (Figure 3.2) we found that culture of human cells in standard fungal culture media exerted a significantly cytotoxic effect (Figure 3.2) while fungal biomass was undetectable in DMEM culture after 48 hours (data not shown). However, RPMI-1640 was found to support comparable fungal growth to that of standard fungal MM. Moreover fRPMI (adapted RPMI-1640 including Cove's trace elements) a 2-fold increase in fungal biomass was achieved. fRPMI did not effect concomitant cytotoxicity to mammalian epithelial cells. The optimised RPMI medium was designated fungal RPMI (fRPMI), and utilised for all subsequent analyses described in this study.

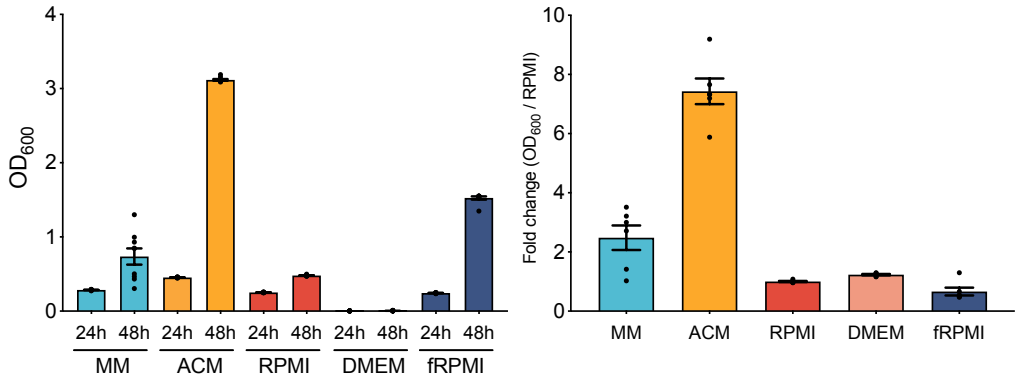

Figure 3.2 Comparison of fungal growth in medium generally used for culturing *A. fumigatus.* a) Growth in MM, ACM, RPMI-1640, DMEM and fungal RPMI is measured after 48 hours as optical density in a 96-well assay using CytoOne 96-well plates. **b)** Cell toxicity to A549 cells measured by LDH analysis of culture medium generally used for *A. fumigatus* growth and infection assays. Data are normalised to cell toxicity measured in RPMI-1640.

Adopting the change-point methodology recently described by Papastamoulis et al [8] we analysed a 48 hour time course of type strain culture, acquiring OD_{600} at 10 minute intervals for the *A. fumigatus* isolate A1160 (Figure 3.3A). Three distinct phases of fungal growth, captured as change-points in growth gradients, were reproducibly identified which corresponded to isotropic growth and germination of the fungal spore (phase1), generation of primary (phase 2) and branching (phase 3) hyphae. An analytical algorithm integrating the number of, and durations between, change points was developed and used for clustering mutant growth behaviours. Under basal liquid culture conditions in fRPMI we first assessed the growth kinetics of the 484 TFKO strains in fRPMI following culture at 37 °C for 48 hours (Figure 3.3b).

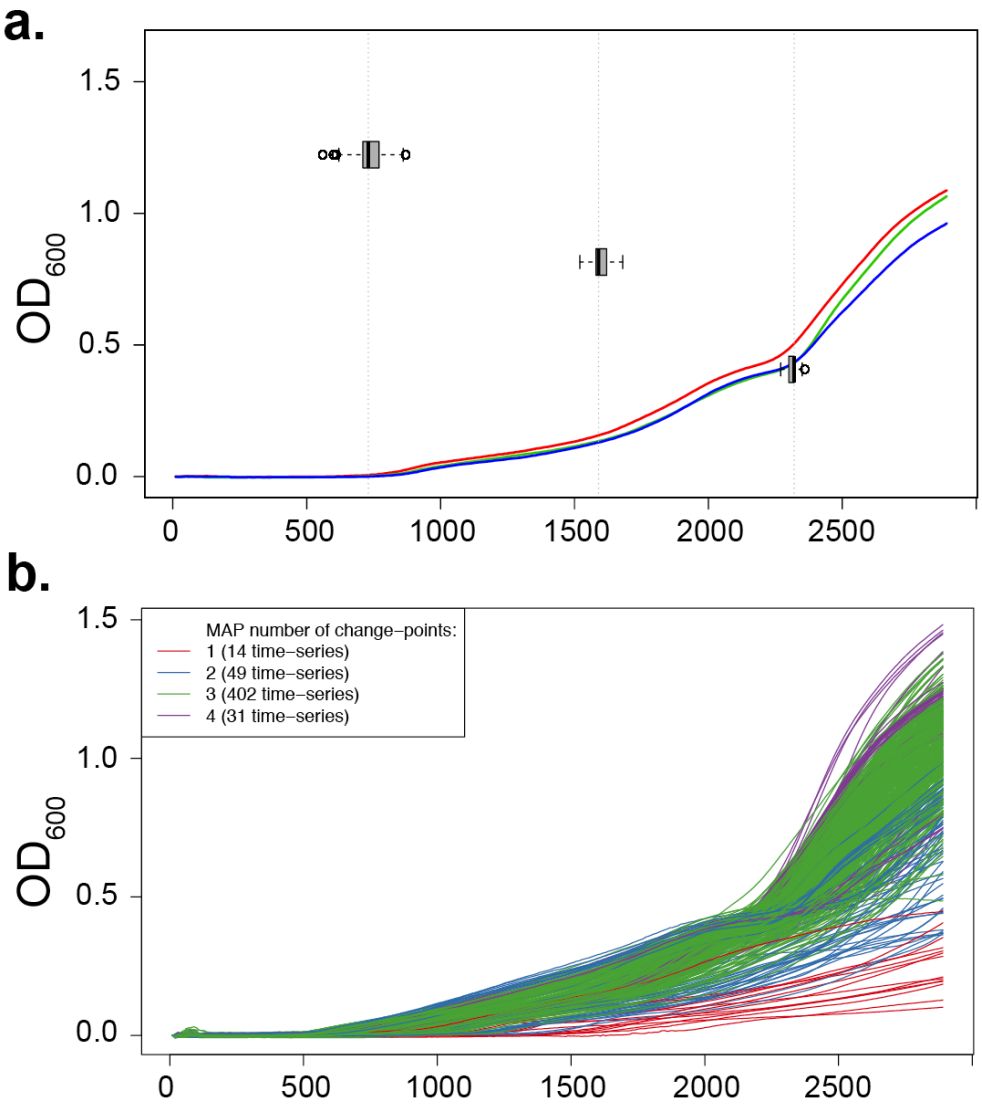

Figure 3.3 Growth curve analysis of 484 TFKO mutants a) Change point analysis of A1160 (type strain) morphogenesis in *in vitro* liquid culture in fRPMI. Time is in minutes and growth is measured as optical density in a 96-well plate assay every 10 minutes for 48 hours. Data from three replicates is shown. Change-points were calculated by running 10,000 simulations resulting in phase1: 780±39, phase 2: 1670±24, phase 3: 2180±15 **b)** Change point analysis of 484 TFKO mutants in fRPMI pH 7.0. Each TFKO mutant growth curve was performed in triplicate.

Using this approach, we identified forty-nine TFKOs (Table S3.2). having an intermediate phenotype defined by two change-points (C2 mutants) and fourteen TFKOs exhibiting a severe slow growth phenotype defined by only one change-point (C1 mutants) (Table 3.2). Low throughput analysis of the fourteen C1 mutants confirmed the findings of the highly quantitative phenotyping algorithm, identifying

n=8 null mutants having previously characterised growth aberrancies and n=6 previously uncharacterised isolates. Amongst those already characterised, mutants lacking the pH-responsive PacC transcription factor, known to be critical for normal cell wall biosynthesis and hyphal branching, or the sterol-regulatory element binding protein SrbA, required for hypoxia adaptation, cell morphogenesis and sterol biosynthesis [11, 13].

Table 3.2 C1 mutants, all with one change-point throughout the growth curve

Generic name	TFKO ID	Gene ID	Function	Reference(s)	Infection model	Required for pathogenicity	Strain background
Afmac1	AFUB_012670	1C6	Copper acquisition	Kusuya et al. (2017), Park et al. (2017)	Cyclo/cortisone acetate, cyclo (IN)	Conflicting reports	A1160
	AFUB_014000	1C11					
SrbA	AFUB_018340	1F1	Hypoxia response, ergosterol biosynthesis, siderophore biosynthesis	Blatzer et al. (2011) Chung et al. (2014) Willger et al. (2008)	Cyclo/Triamcinolone acetonide (IN) B6.129S6-Cyb^{btm1Din}	✓	CEA17
AtrR	AFUB_019790	1F3	Hypoxia response, ergosterol biosynthesis	Hagiwara et al. (2017)	Cyclo/cortisone acetate mice for AfS35 (IT), Cortisone acetate for AF293 (IT)	✓	AF293, AfS35
LeuB	AFUB_020530	1F6	Leucine biosynthesis, iron acquisition	Long et al. (2018)	Galleria	✓	A1160
HapB	AFUB_030360	1H5	CBC component	Gsaller et al. (2010)		NP	
PacC	AFUB_037210	2B5	Alkaline pH response	Bertuzzi et al. (2014) Amich et al. (2010) Tilburn et al. (1995)	Cyclo/cortisone acetate (IN)	✓	ATCC, CEA10
MetR	AFUB_063610	3B1	Acquisition of inorganic sulfur	Amich et al. (2013)	Cyclo/cortisone acetate mice (IN, IV)	✓	ATCC
SebA	AFUB_066180	3B2	Heat shock, nutrient and oxidative stress	Dinamarco et al. (2012)	Cyclo/cortisone acetate (IN)	✓	CEA17
NsdC	AFUB_089440	5H5	Asexual/sexual development	Gross et al. (2008)		NP	D141
	AFUB_012020	1C4					
RfeC	AFUB_026340	1G9					
	AFUB_050260	6B1					
AdaB	AFUB_026420	7B7					

Pathogenic growth of *A. fumigatus* in the immunocompromised mammalian lung involves hyphal branching and tissue invasion. It was therefore expected that mutants exhibiting significant growth defects would also be less virulent. Of the fourteen slow-growing mutants identified using the high throughput phenotyping algorithm, we identified n=7 having previously demonstrated virulence deficits: MacA, SrbA, AtrR, LeuB, PacC, MetR and SebA (Table 3.1) and n=7 strains which had not been characterised (AFUB_014000 (1C11), AFUB_030360 (HapB), AFUB_089440 (NsdC), AFUB_012020 (1C4), AFUB_050260 (6B1), AFUB_026420 (AdaB)). In filamentous fungi aberrant growth phenotypes can result from abnormal germination efficiency, hyphal extension rates or hyphal branching

frequencies, or combinations thereof. In order to precisely define the nature of growth deficits underlying slow growth phenotypes and altered pathogenicity we undertook a detailed phenotypic analysis of the slow-growing mutants by quantifying spore germination efficiencies and dynamics, hyphal extension rates and cytotoxicity to cultured human pulmonary epithelial cells. Clustering analysis identified four distinct behaviours amongst the fourteen isolates analysed (Figure 3.4, Figure S3.2 and Figure S3.3). However, no correlation between a defect in germination or hyphal extension rate with cytotoxicity and defects in pathogenicity was found.

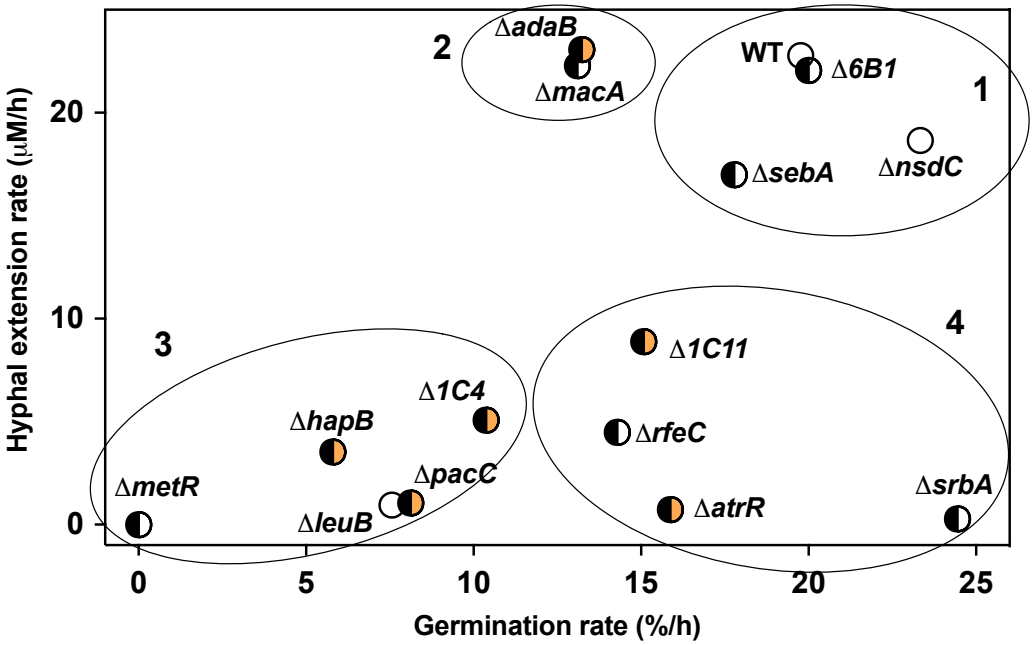

Figure 3.4 Phenotyping of C1 mutants. Hyphal extension rate and germination rate for each of the C1 mutants. Clustering analysis revealed an optimum of four clusters, which are circled. Orange within the icon shows a significant decrease in cell toxicity and black indicates an *in vivo* pathogenicity defect**.**

3.3.3 A core set of transcription factors required for environmental adaptation.

Amongst a predicted genomic repertoire of >484 transcription factors, the functions of only 45 have been characterised, amongst these 20 have been found to be critical for virulence in whole animals. Despite the small sample size, the available data support the view that *A. fumigatus* stress responses are often required for virulence. However, most of these studies have arisen from a priori hypotheses on what might be important, the mutants have been constructed in 9 different genetic

backgrounds and tested for pathogenicity in a raft of unstandardized models. And moreover, whilst the host imposes multiple different stresses, in combination and often occurring in specific sequences – all of the TF studies to date in *A. fumigatus* have looked at individual stressors.

During progression of infection, *A. fumigatus* is exposed to various host imposed stresses including nutrient limitation, pH changes, temperature changes etc. Adaptation to these stresses is tightly regulated at the transcriptional level. In order to identify transcription factor null mutants with altered growth fitness to these infection-related stresses, large-scale phenotyping was carried out in ten different conditions being; pH4, pH8, pH7, -Fe, -Zn, -S, hypoxia (1% oxygen), 30 °C, 48 °C, addition of fetal bovine serum. Mutants that matched an outlier cluster and were significantly different compared to wildtype were considered as mutants with a differential growth profile Figure S3.4, Table 3.3). All other TFKO considered hits from the end-point screening were validated in time course growth curve experiments.

Table 3.3 TFKOs with significantly decreased fitness under environmental stress

-Fe hits

Generic name	TFKO ID	Gene ID	Function	Reference(s)	Required for pathogenicity	Strain background
HapX	AFUB_052420	2G3	Iron homeostasis (deplete conditions)	Brandon et al. (2015) Schrettl et al. (2010)	✓	ATCC

pH 8 hits

Generic name	TFKO ID	Gene ID	Function	Reference(s)	Required for pathogenicity	Strain background
PacC	AFUB_037210	2B5	Alkaline pH response	Bertuzzi et al. (2014) Amich et al. (2010) Tilburn et al. (1995)	✓	ATCC, CEA10
MetR	AFUB_063610	3B1	Acquisition of inorganic sulfur	Amich et al. (2013)	✓	ATCC
MtfA	AFUB_095620	5H9	Conidiation, protease and gliotoxin production	Smith and Calvo (2014)	✓	Galleria
NsdD	AFUB_089440	5H5	Asexual/sexual development	Gross et al. (2008)	NP	D141
	AFUB_037150	2B3				
HapX	AFUB_052420	2G3	Iron homeostasis (deplete conditions)		✓	ATCC
AtfA	AFUB_037850	2B7	Conidia stress response	Hagiwara et al. (2014)	NP	
CreA	AFUB_027530	1G11	Hypoxic adaptation, carbon catabolite repression	Beattie et al. (2017)	✓	

48 Celsius hits

Generic name	TFKO ID	Gene ID	Function	Reference(s)	Required for pathogenicity	Strain background
HapB	AFUB_030360	1H5	CBC component	Gsaller et al. (2010)	NP	
PacC	AFUB_037210	2B5	Alkaline pH response	Bertuzzi et al. (2014) Amich et al. (2010) Tilburn et al. (1995)	✓	ATCC, CEA10
MetR	AFUB_063610	3B1	Acquisition of inorganic sulfur	Amich et al. (2013)	✓	ATCC
	AFUB_058240	2H7				
	AFUB_037150	2B3				
	AFUB_031840	5B10				
NctA	AFUB_029870	1H4				
	AFUB_034630	2A5				
	AFUB_024050	5B5				
	AFUB_091020	4A1				

pH 4 hits

Generic name	TFKO ID	Gene ID	Function	Reference(s)	Required for pathogenicity	Infection model
NsdD	AFUB_089440	5H5	Asexual/sexual development	Gross et al. (2008)	NP	
AdaB	AFUB_026420	7B7				
AreA	AFUB_096370	7G8	Nitrogen utilization	Hensel et al. (1998) Krappmann et al. (2005)	✓	Cyclo/cortisone acetate mice (IN)
ZafA	AFUB_009490	7H4	Zinc homeostasis	Amich et al. (2010) Amich et al. (2014) Moreno et al. (2007) Amich and Calera (2014) Vicentefranqueira et al. (2015)	✓	Cortisone acetate (IN)
ZipD	AFUB_020350	1F4	Calcium/calcineurin-dependent response	Ries et al. (2017)	NP (Goldmann performed not published)	
	AFUB_037150	2B3				
	AFUB_096010	7G6				

Screening the transcription factor null library under infection-related stresses revealed 20 previously uncharacterised transcription factors. Furthermore, new phenotypes were discovered for 16 previously identified transcription factors (Figure 3.5). High interconnected transcription factors were required for pathogenicity as the majority have been previously tested in a murine model of virulence (Figure 3.5). The highly interconnected transcription factor 2B3 (AFUB_037150) is required for hypoxia, alkaline, acidic stress, addition of serum and thermotolerance. In a murine model of virulence this transcription factor null mutant was found to be attenuated compared to the parental isolate and the reconstituted strain, highlighting the importance of adaptation to environmental stress (Figure 3.6).

Multiplicities of environmental stress potentially exhibit a synergistic effect upon *A. fumigatus*. Therefore, the transcription factor library was screened under multifactorial stress combining pH, iron availability and temperature. The interaction effect between two individual stresses was calculated by fitting linear regressions including first-order interactions between pH, temperature and iron availability. The largest effect upon the data was observed under alkaline and iron restrictive conditions, which resulted in the identification of three transcription factors that are significantly affected by the interaction of these environmental stresses, namely the SrbA transcription factor, 5A4 (AFUB_002050), 5C6 (AFUB_048890) and 5E9 (AFUB_009690) (Figure 3.7).

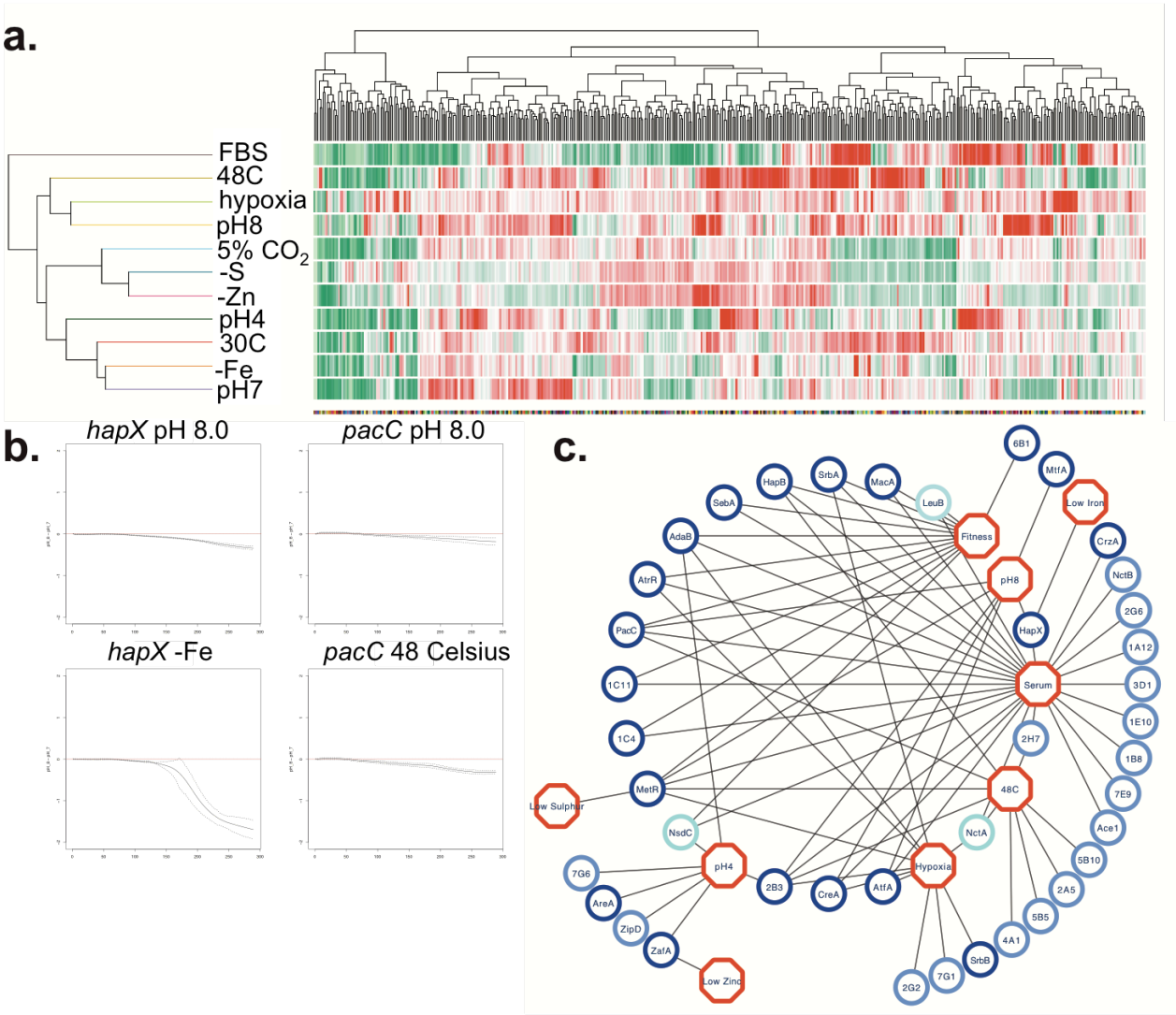

Figure 3.5 Environmental stress phenotyping of 484 TFKOs a) Heatmap of high-throughput phenotyping under 11 conditions (. Clustering was performed on conditions and mutants. Green and red represents higher fitness and lower fitness, respectively, compared to the parental isolate **b)** Representative plots of fitness in time for TF null mutants considered significantly different from the parental isolate as identified by high-throughput phenotyping. Dotted lines show the 95% confidence interval calculated using limma. A significant different fitness is shown when the zero is outside the outer limits **c)** Network of validated TFKO hits required for adaptation to environmental stress. Transcription factors assessed for pathogenicity are coloured dark blue (attenuated for pathogenicity) or light blue (not attenuated for pathogenicity).

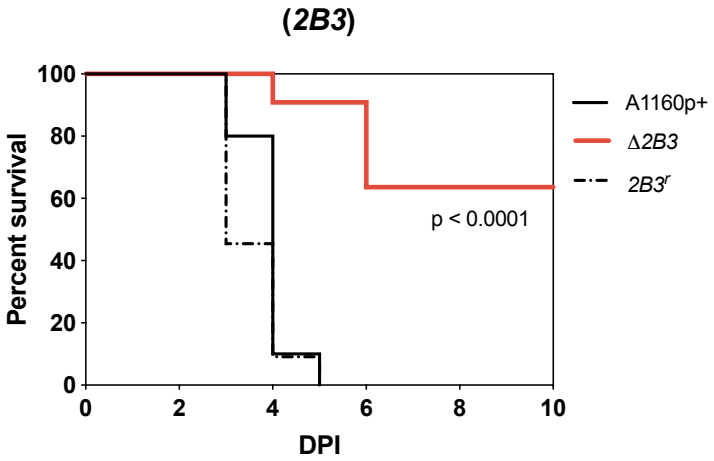

Figure 3.6 Survival in murine model of aspergillosis for transcription factor "2B3" (AFUB_037150) required for adaptation to several environmental stressed conditions. Survival curve in a leukopenic murine model of aspergillosis (n = 11) for Δ2B3 (Δ*afub_037150*). Significance was assessed by Mantel-Cox test.

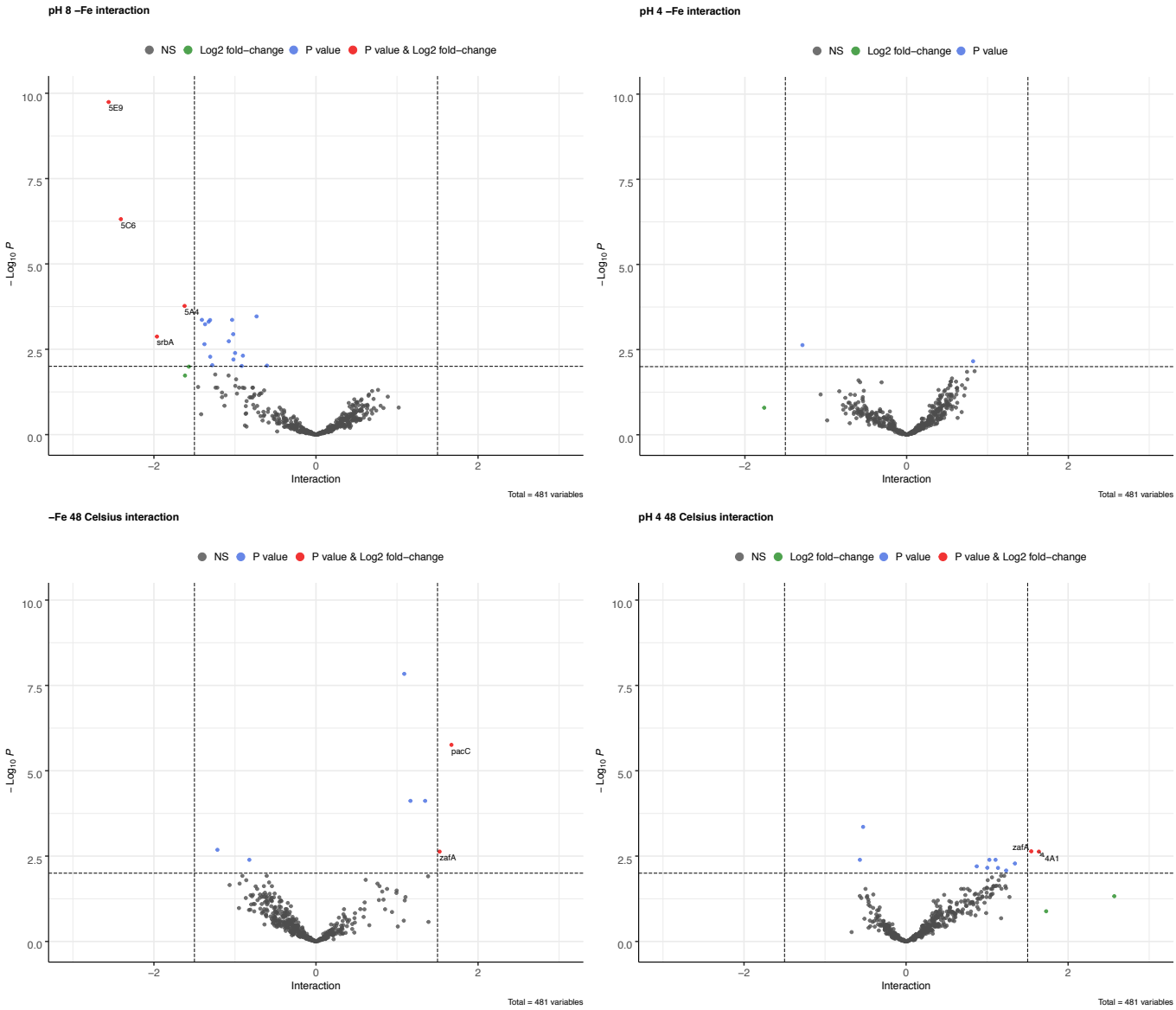

Figure 3.7 Combinatorial stress interactions. The interaction between stresses was calculated from linear models. The strength of the interaction (x-axis) and statistical significance of the interaction (y-axis) are plotted for each multifactorial stresses condition.

3.3.4 Regulatory basis of tissue invasion

Adaptation to environmental stress is key for growth within the host environment. The next step during infection once growth is established is tissue damage and invasion. The ability of the fungus to damage and detach epithelial cells from the alveoli is essential for infection as mutants deficient in damage capabilities are

attenuated in mouse models of infection. Two modes of breaking epithelial layers have been proposed. One being direct cell damage and lysis of epithelial cells and one via detachment from the epithelial layer. Here we assess the regulators required for both methods of epithelial invasion in high-throughput screening assays.

Detachment was determined as the ability of the fungus to detach a monolayer of epithelial cells from the surface. This was quantified by counting the number of attached epithelial cells after 16 hours of coincubation with *A. fumigatus* spores. A double criterion consisting of biological difference to wildtype and statistical difference was used to screen the transcription factor null mutant library. This resulted in 28 transcription factor null mutants with a decreased capability to detach epithelial cells (Figure 3.8a). Cell toxicity was assessed by measuring release of LDH by epithelial cells after coincubation with *A. fumigatus* for 24 hours. A double criterion was used to assess the transcription factor null mutant library. Firstly, statistical significance was assessed using t-distributions, comparing inferred wildtype distributions to the null mutant data distribution (Figure S3.5). Secondly, biological effect size compared to the parental isolate was taken into consideration. This resulted in the identification of 24 transcription factor mutant with decreased ability to cause epithelial cell toxicity (Figure 3.8b).

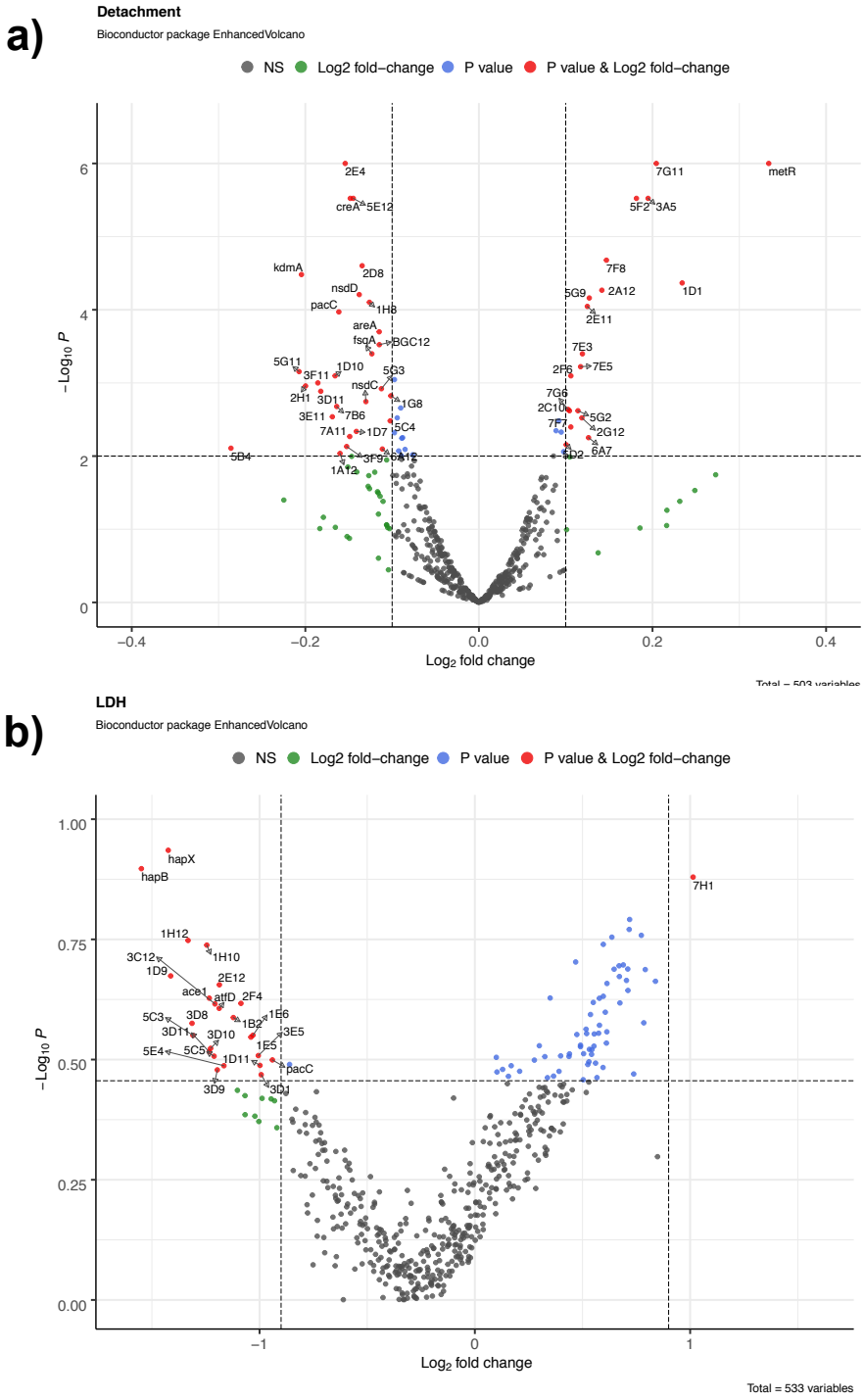

Figure 3.8 LDH and Detachment. Fold change towards the wildtype is plotted on the x-axis and the statistical difference from the wildtype is plotted on the Y-axis. Cut-offs have been determined by assessing the minimum effect and statistical difference observed for the *pacC* null mutant control. Null mutants considered a hit are highlighted in red. **a)** Detachment screening of the TFKO library **b)** Cytotoxicity screening of the TFKO library.

Several transcription factors associated with detachment have been linked to secondary metabolism and regulation of biosynthetic gene clusters, such as FsqA and the regulator of the biosynthetic gene cluster 12 (BGC12). Little overlap between regulators required for detachment or cell toxicity was identified as the only transcription factor null mutant causing less detachment and cell toxicity was the Δ*pacC*, highlighting that these processes have unique regulatory networks. Generally, transcription factors required for environmental stress adaptation and fitness were not required for cell toxicity and detachment. Only the HapB, CreA, HapX, PacC, AreA, NsdC and Ace1 transcription factor played roles in fitness, stress adaptation and invasion. These regulators have growth defects in fRPMI containing serum potentially causing less invasion due to growth defects. However, other transcription factors required for fitness are not required for invasion. Transcription factors required for cell damage are a distinct set from transcription factors required for environmental adaptation (Figure 3.9).

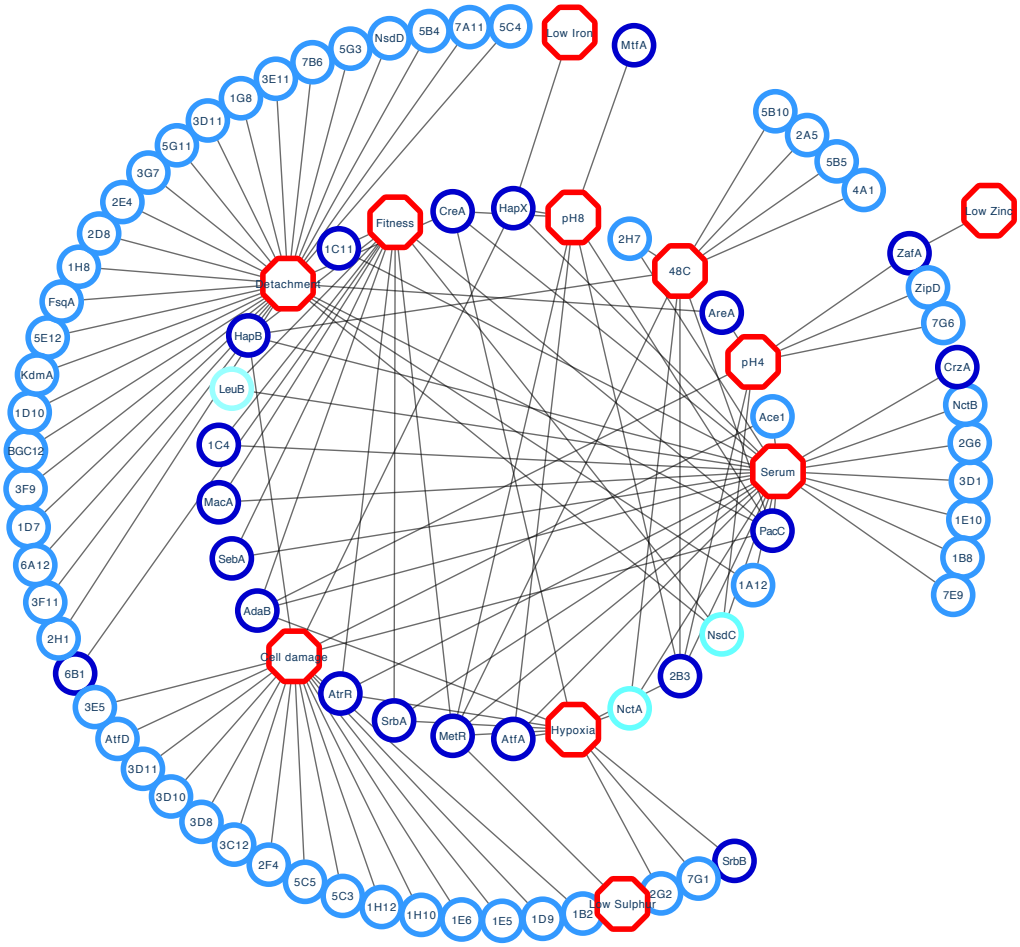

Figure 3.9 Phenotypic network of transcription factors required for adaptation to environmental stress, cell toxicity and pathogenicity. Cytoscape network of TFKOs required for fitness, environmental adaptation, cell toxicity and detachment. TFKOs with attenuated virulence are shown in dark blue and non-attenuated TFKOs in light blue.

3.3.5 Adaptation to stress underlies pathogenicity amongst species of the genus

In basal fungal RPMI without any additional stress condition *A. fumigatus* shows an increased fitness compared to other *Aspergillus species*. This fitness increase in maintained throughout stressed conditions, while several other *Aspergillus* species are unable to adapt to one or more conditions (Figure 3.10). Interestingly, under elevated temperatures *A. fumigatus* is the only species that is able to grow within 48

hours. This shows that *A. fumigatus* specifically is tailored to growth under several infection-related stressed conditions, unlike other *Aspergillus* species.

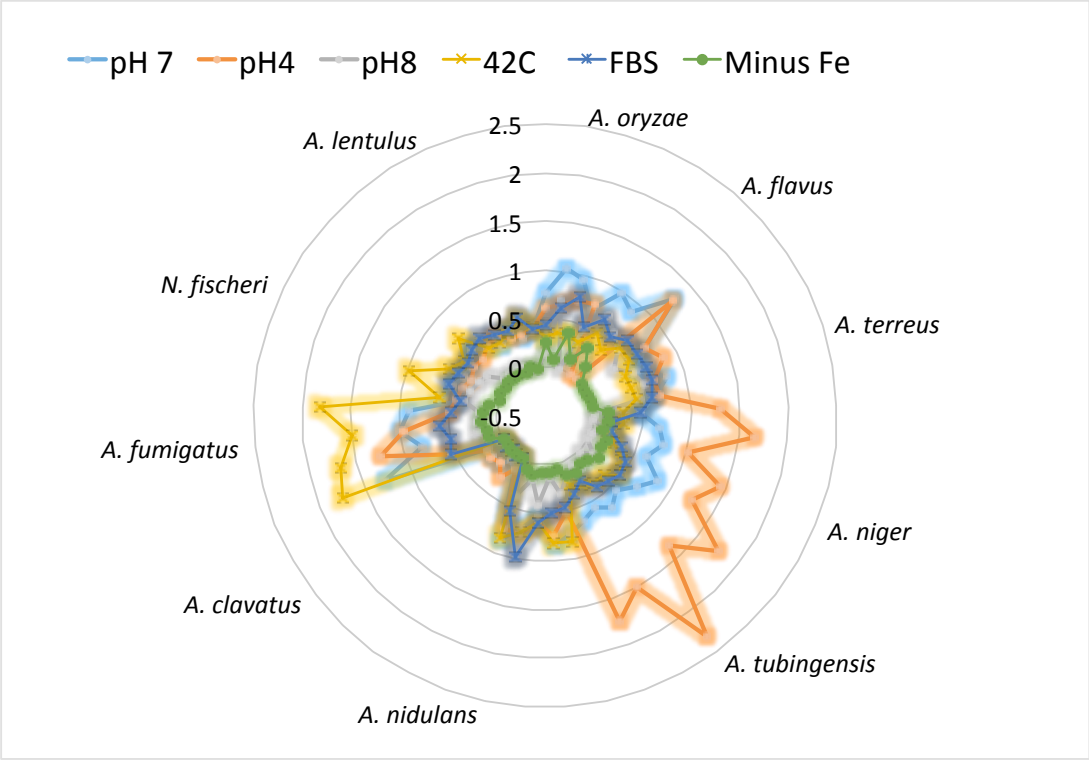

Figure 3.10 Aspergillus species adaptation to stress. Growth of ten different *Aspergillus* species under six stress conditions measured as optical density in a 96-well plate assay. *A. fumigatus* showed an increased growth compared to other species under elevated temperature. *A. tubingensis* and *A. niger* showed an increased growth under acidic conditions in line with literature. *A. oryzae* showed an increased growth under iron limitation conditions and *A. nidulans* when fetal bovine serum was added.

3.4 Discussion

Aspergillus fumigatus is the causative agent of over 8 million mycoses. However, the mechanistic basis of pathogenicity is not clearly understood. This study assesses a genome wide transcription factor null library for adaptation to infection-related stresses and invasion. Furthermore, high-throughput screening methodologies have been established. *A. fumigatus* is able to adapt to a range of environmental stresses, which require a highly interconnected network of transcription factors. These transcription factors are a distinct set from regulators required for epithelial cell detachment and toxicity. The regulatory networks underlying these transcription factors could provide new insight into the mechanistic basis of pathogenicity and the evolutionary explanation of pathogenicity.

The development of a new culture media, fRPMI, allowed us to optimise and perform high-throughput phenotyping as well as *in vitro* infection experiments with A549 epithelial cells. Furthermore, this allows us to modify the culture media to limit specific trace elements. Liquid culture based methodologies are the standard for drug development screenings and biotechnological applications [14]. Till date, solid culture medium based screening has been applied for phenotyping of filamentous fungus [15-17]. Our analytical pipeline can be expanded for usage in bioreactors as continuous culture in specific growth phases can be measured and utilised in high throughput and volume. Moreover, high throughput liquid cultures can be used for drug development screenings for new antifungals, allowing monitoring of growth inhibition in real time.

In other fungi the regulatory landscape of stress adaptation has become well defined. In 2002, 96% of all annotated ORFs in *Saccharomyes cerevisae* were deleted which allowed fitness profiling on a genome level [18]. Almost ten years later collections of null mutants were established for *Candida albicans* (n= 166) and *Candida glabrata* (n = 619) [19, 20]. For filamentous fungi, which exhibit much lower frequencies and fidelity of homologous recombination, the discovery and exploitation of non-homologous end rejoining factors spawned the first collection of null mutants for a filamentous fungus; *Neurospora crassa* in 2006, followed by

Magnaporthe oryzae in 2007 [16, 21]. Recently, the first *A. fumigatus* null mutant collection containing 484 isolates was constructed by Furukawa et al 2019 (in press). Here, we looked at a range of conditions involved in pathogenicity of *A. fumigatus*. It is clear that several previous identified transcription factors were not identified in our screenings. These transcription factors: *rlmA*, *medA*, *hacA* are involved in cell wall integrity, adhesion or interaction with leukocytes [22-24]. These transcription factors show an interaction with the host that we have yet to fully explore.

Stress phenotyping revealed an interconnected network of transcription factors. Interestingly, components between alkalinity, hypoxia and thermotolerance are strongly linked. Stress imposed by these factors might be highly similar as transcription factors identified to be essential for adaptation regulate similar processes. Hypoxia induced cell wall thickening and ergosterol production [25]. Similar changes have been observed under alkaline conditions in *A. fumigatus* and *S. cerevisiae* as ergosterol is required for membrane fluidity [11, 26]. While little is known about thermotolerance in *A. fumigatus*, a link between thermotolerance and ergosterol production has been found in *S. cerevisiae* [27]. However, adaptation to each condition contains dinstinct sets of transcription factors, pointing towards a regulatory hierarchy with more interconnected transcription factor being of higher order [28].

In *S. cerevisiae*, *C. albicans* and *S. pombe* a general stress response to a range of stresses, called the Enviromental Stress Response, has been described [29-31]. This response involves the transcriptional regulators *msn4/msn2* and *atf1*, in *S. cerevisiae* and *S. pombe* respectively. The orthologue of the *msn4* regulator in *A. fumigatus* is the *sebA* transcription factor [32]. In this study, the *sebA* transcription factor is required for general fitness in fRPMI, highlighting this medium is a stressful enviroment for the fungus. The orthologue of the *aft1* regulator is the *atfA* transcription factor in *A. fumigatus* [33]. In this study the *atfA* transcription factor is required for adaptation to environmental stresses, being alkaline pH, hypoxia and fetal bovine serum stress. *Aft1* mutants in other species only show sensitivity to a subset of stresses being in line with our study [34].

Evolutionary theorists have developed two major evolutionary models to explain the emergence of microbial pathogenicity [35]. Co-evolution of virulence factor expression and stress adaptation occurs where pathogens have become highly adapted to the host environment, a common regulatory paradigm which links stress adaptation to the expression of virulence factors. Examples include *Mycobacterium tuberculosis* where alternative sigma factors, which link stress responses to upregulation of entire cohorts of virulence-promoting genes. In fungi, which commensalise humans such as *C. albicans*, where the physiological response to environmental changes such as pH, temperature or nutrient shifts has become coupled to a morphological (yeast-to-hyphae) switch which drives immune evasion and is inextricably linked to host damage and expression of virulence factors and toxins such as candidalysin [36-38]. Conversely, coincidental evolution of pathogenicity occurs where a pathogen is exposed to a stress and in the process of adapting to that stress, concomitantly expresses factors, which also happen to facilitate survival in the pathogenic niche. In the case of normally saprophytic fungi the microenvironments encountered in the mammalian lung impose nutritional limitation, and altered pH, temperature and oxygen availability. Concordantly, transcription factors modulating adaption to such conditions have been repeatedly demonstrated to make major contributions towards *A. fumigatus* pathogenicity (Table 3.1).

These findings are consistent with an evolutionary model in which hierarchical governance of stress-adaptation has evolved in a species-specific manner and in accordance with the respective environmental niches of each species yielding, in *A. fumigatus*, a regulatory circuitry which has been further accessorised by alterations in associated secondary metabolite repertoires, cell surface-exposed antigens and secreted proteins. This observation differs from transcriptional networks found in *C. albicans* where fitness and adaptation to stress is tightly linked to the ability to infect [19, 39]. Similar functional correlations were found in *C. neoformans* [40]. Our findings support the theory of coincidental evolution of pathogenicity, where adaptation to the environment and host damage originate from evolution to several different niches and to environmental predators [41]. In *A. fumigatus* the 'amoeboid predator-fungal animal virulence' hypothesis may provide an explanation as amoeba and immune cells share common mechanisms suggesting a similarity in

environments [7]. However, this might not explain the difference in prevalence between aspergillosis caused by *A. fumigatus* compared to *A. fischeri.* Like in *C. albicans* circuit rewiring of identified transcriptional regulators compared to *S. cerevisiae* might provide this explanation [19]. However, genomic and transcriptomic dataset are scarce in *A. fischeri*. These findings identify transcription factors that are pathogenicity determinants and could provide new insight into evolutionary mechanisms through rewiring of transcriptional networks and can provide new antifungal targets in the future.

3.5 Supplemental Figure and Tables

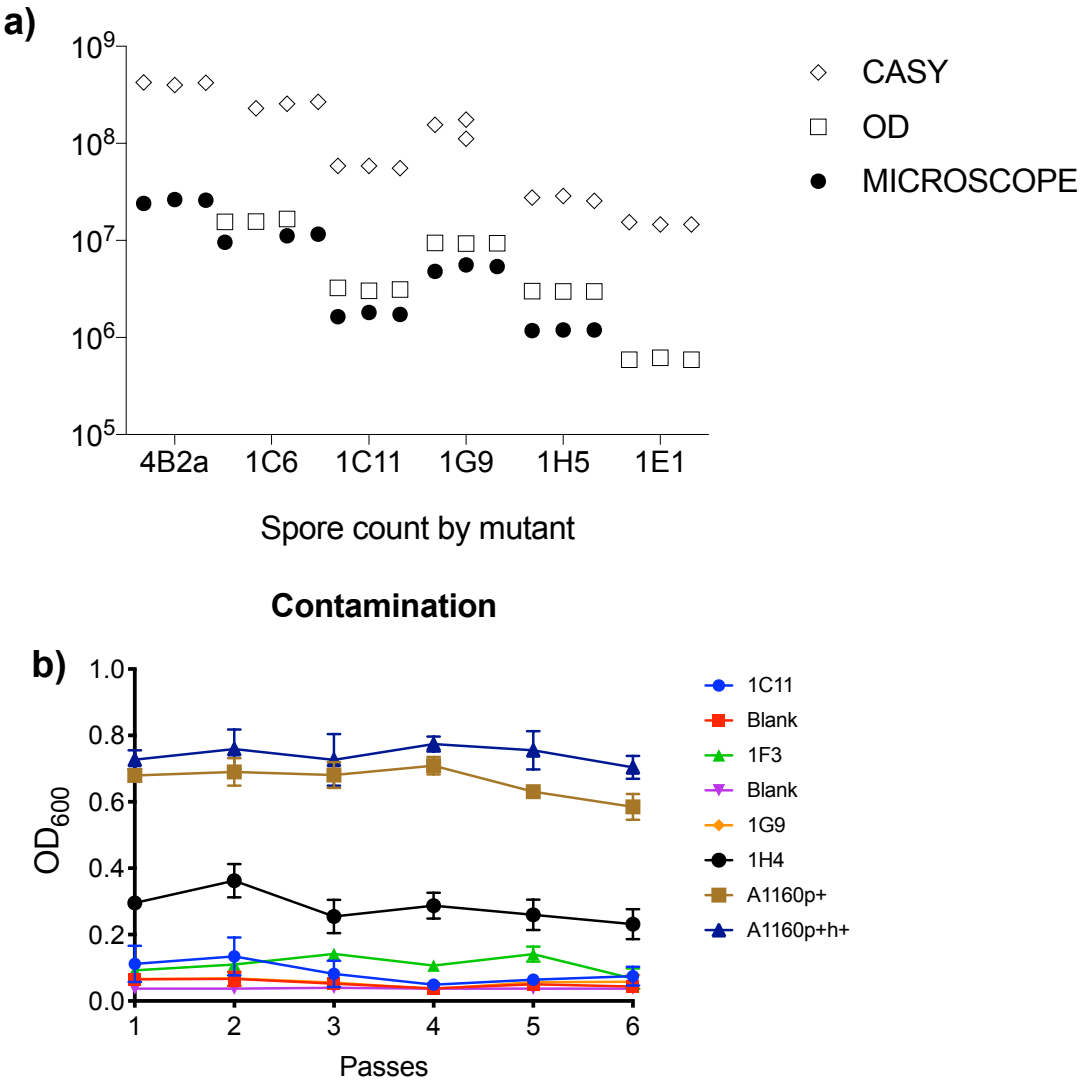

Figure S3.1 Optimisation of 96-well assay a) Enumeration of *A. fumigatus* spores by spectrophotometric methods. An automated CaSY cell counter was compared to optical density (counting via a standard curve generated from 4B2a spores, hence lacking OD data) and counting via haemocytometer. **b)** 6 passes of spores for a selection of TFKO strains were performed to assess for differences in growth and contamination of blank wells.

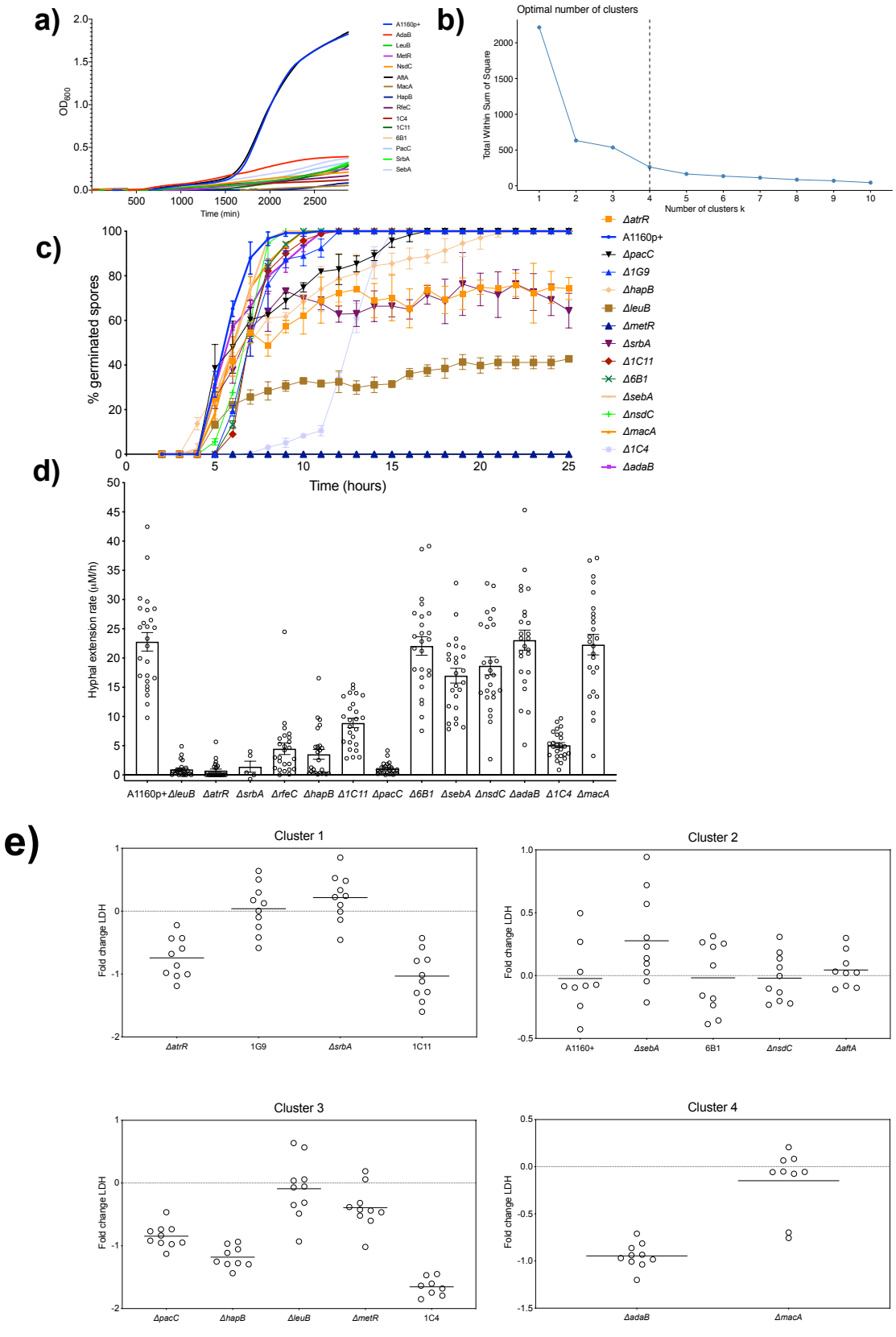

Figure S3.2 In depth phenotyping of C1 mutants a) Validation of C1 mutants in a 48 hour timed growth curve. Optical density was measured every ten minutes for 48 hours **b)** Optimal number of clusters of germination rate vs hyphal extension of

C1 mutants. The dotted line reveals the optimal number of clusters based on predetermined cut-offs of the total within sum of squares. **c)** Percent germination of a field of view containing ~100 spores for all C1 mutants in fungal RPMI + FBS, images were taken every hour for 25 hours. **d)** hyphal extension rate measured from 14-17 hours by automated microscopy. Fungal length was measured by FIJI and rates were calculated by hyphal elongation per hour **e)** LDH analysis for slow growing TFKOs, measured by 3 biological replicates with each 3 technical replicates (n = 9). Significance was assessed via one-way ANOVA. Strains were grouped according to clusters determined by germination and hyphal extension rate.

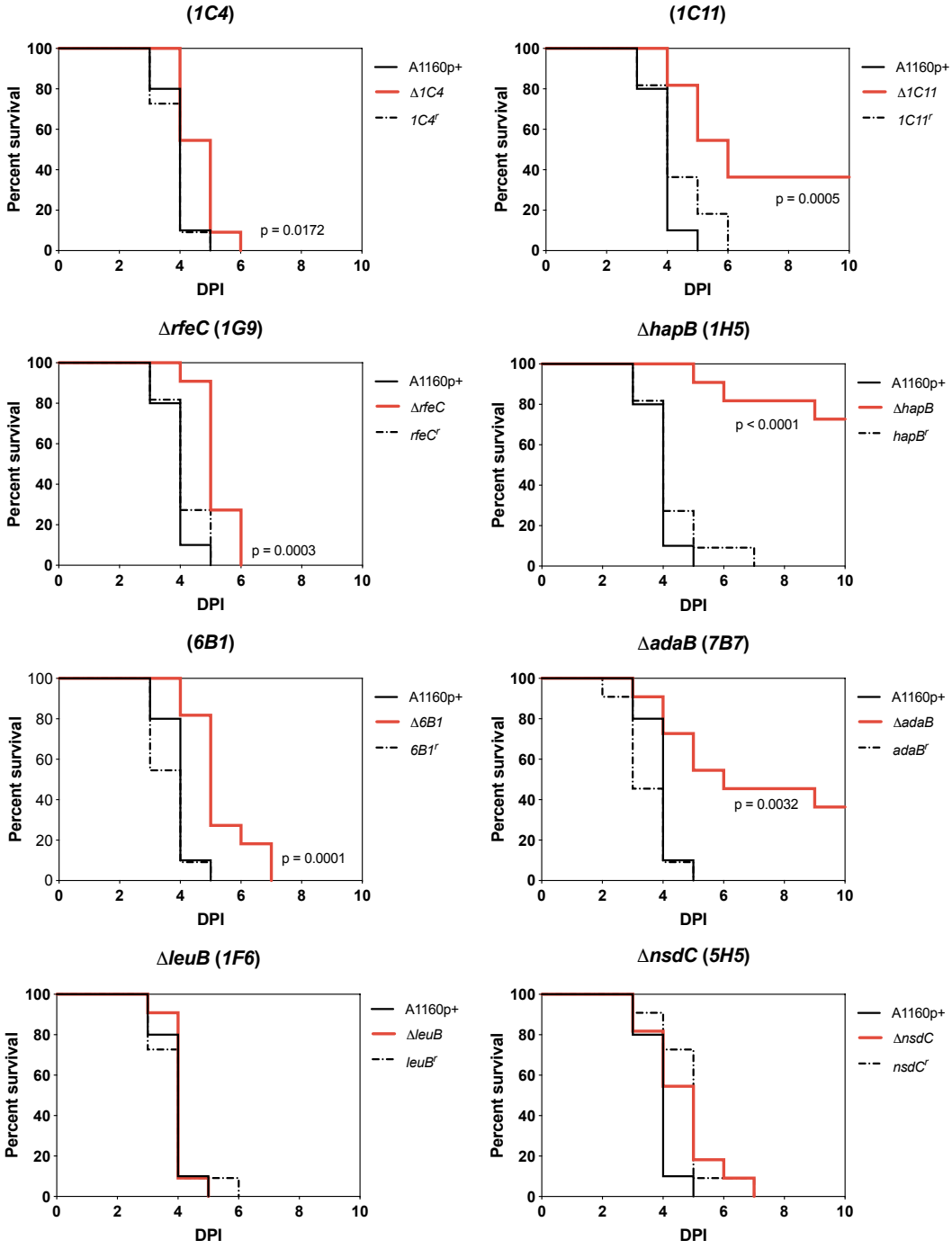

Figure S3.3 Survival in murine model for C1 mutants. Survival curves of C1 mutants in a leukopenic murine model of aspergillosis (n = 11). Significance was assessed by Mantel-Cox log rank test.

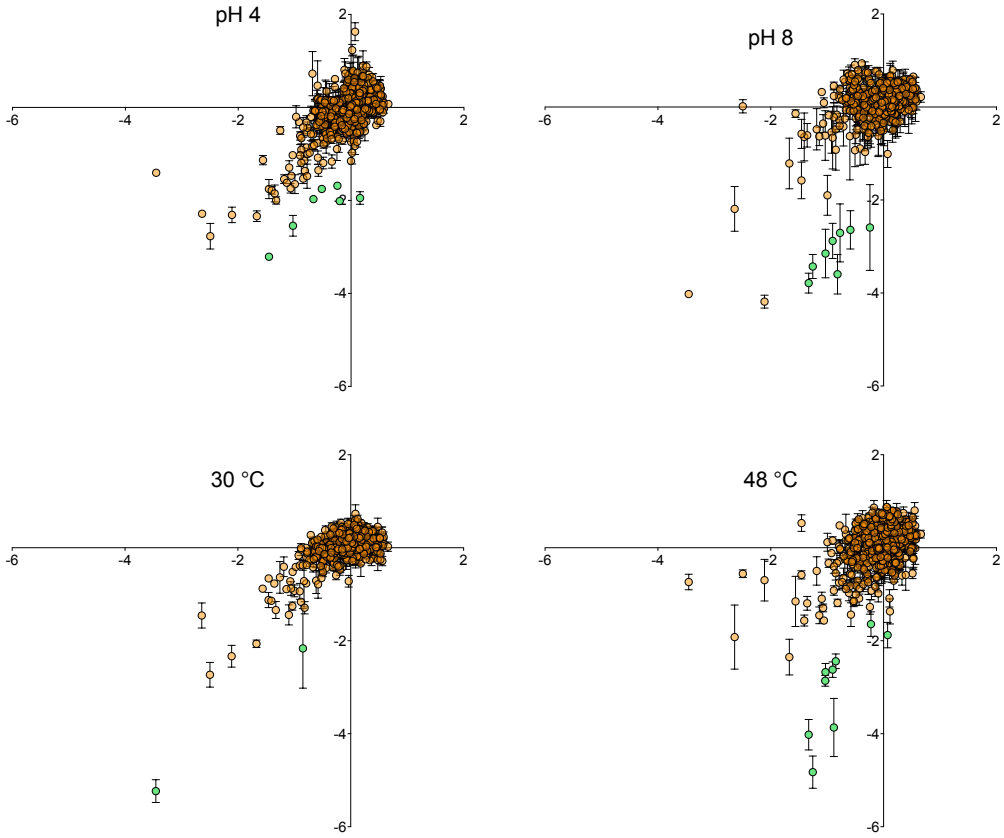
pH 4
pH 8
30 °C
48 °C
-6
-4
-2
2

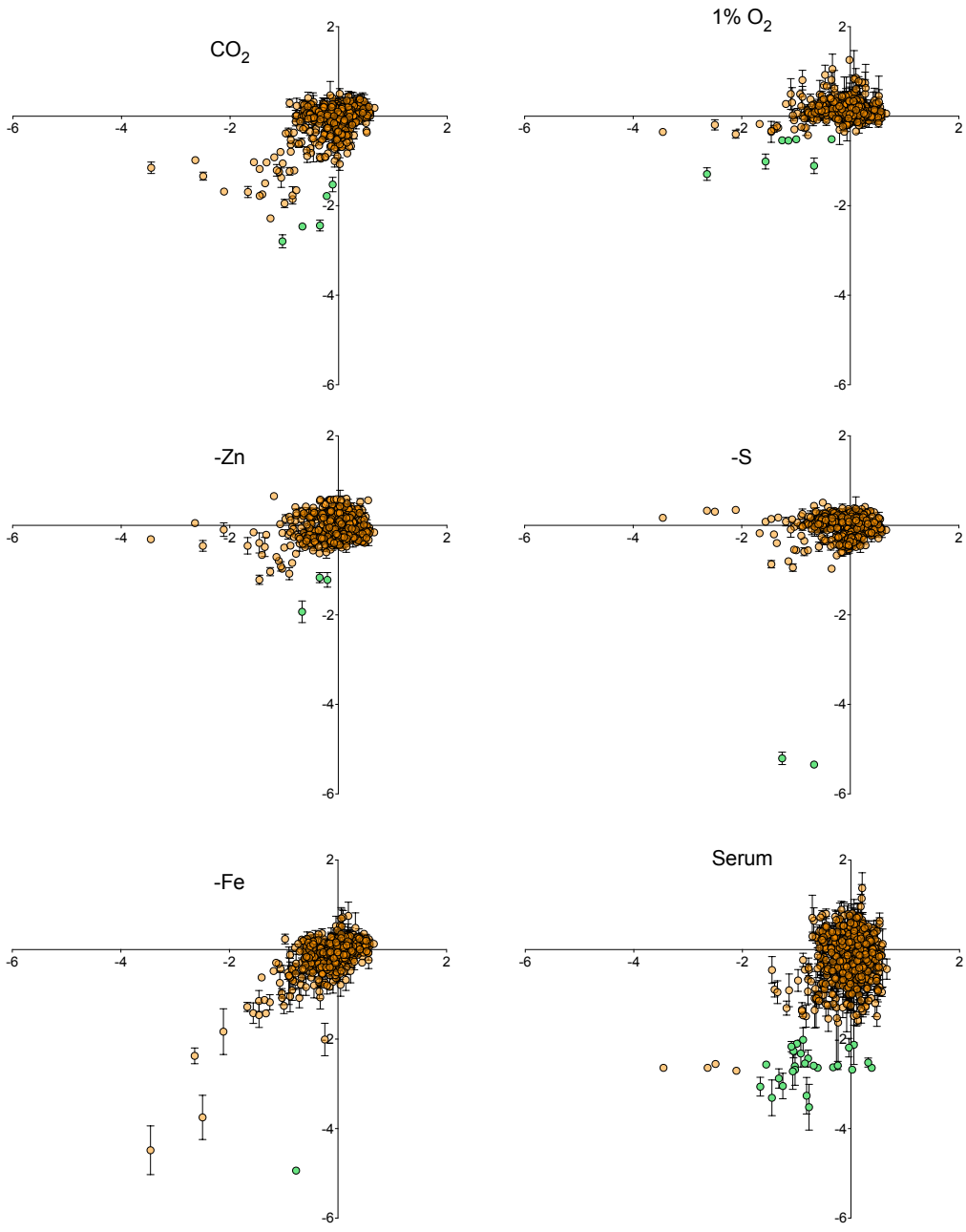

Figure S.3.4 High-throughput phenotyping of 484 TFKOs. Summarised fitness plots highlighting TFKO mutants with a statically significant decrease in fitness under environmental stressed conditions (green). Fitness is calculated as optical density normalised to the parental strain. In each plot the X-axis is fitness under fRPMI (pH 7.0) 37 °C, and the Y-axis is fitness under stress.

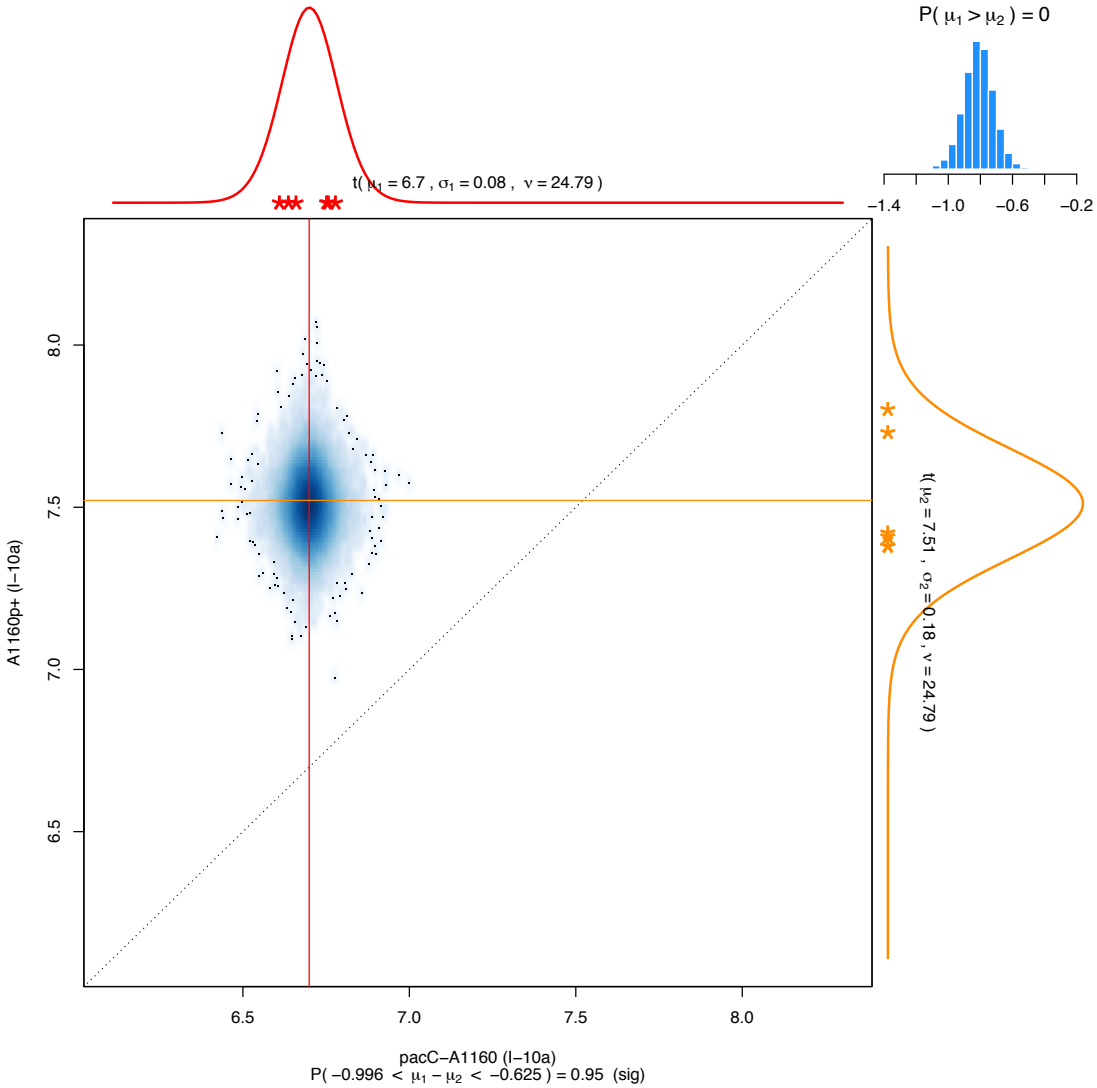

Figure S3.5 Statistical analysis of LDH. T-distributions for the LDH assay for 484 TFKOs measuring lactodehydrogenase release from epithelial cells, the Δ*pacC* (control) and A1160p+ (control) were made. Distributions were compared using a mcmc sampler. Shown is a representative example plot of a statistically significant difference, which can be seen as a deviation from the trendline.

Table S3.1 *Aspergillus* species and their origin, used in this study. Kindly gifted by Prof. Paul Dyer

Species and isolate number	Origin	Strain ID
A. niger 8-1		N402
A. niger 8-187	Czech Rep	
A. niger 8-186	Italy	
A. niger 8-172	Dublin	
A. niger 8-173	Brazil	
A. tubingensis 76-2	Dublin	
A. tubingensis 76-26	Norfolk, UK	
A. tubingensis 76-39	Thailand	
A. tubingensis 76-40	Brazil	
A. tubingensis 76-41	Turkey	
N. fischeri 53-1	Netherlands	CBS 544.65
N. fischeri 53-2	Dominican Rep	CBS 116.145
N. fischeri 53-13	Lima	
N. fischeri 53-14	Sri Lanka	
N. fischeri 53-15	Fiji Islands	
A. nidulans 2-137	Birmingham, UK	
A. nidulans 2-220	Zimbabwe	
A. nidulans 2-226	Hungary	
A. nidulans 2-227	California	
A. nidulans 2-231	Barbados	
A. terreus 49-10	Bristol, UK	
A. terreus 49-11	Madrid, Spain	
A. terreus 49-12	Netherlands	
A. terreus 49-2-	Connecticut, USA	

A. terreus 49-23	New Zealand	
A. oryzae 55-20		RIB40
A. oryzae 55-4		
A. oryzae 55-5		
A. oryzae 55-14		CBS 108.24
A. flavus 57-5	Virginia, USA	ATCC 204304
A. flavus 57-6	USA	CBS 128.202
A. flavus 57-7	coal UK	

Table S3.2 Table of frequencies of the most probably change-points. Strains with a blank field do not this particular number of change-points. A summary with the probability is given in column 2 (# Change Point (Probability)). The number of change-points any given growth curve contains is used a classification for further analysis (C1 mutants equal 1 change-point, C2 mutants 2 change-points, etc.). Time of change-points are given in measures of 10 minutes (ie. 86 is 860 minutes).

# Change-points	1	2	3	4
# Strains	14	49	402	31

Summary per time-series

Gene ID	# Change-point (probability)	Time of Change-point #1	Time of Change-point #2	Time of Change-point #3	Time of Change-point #4
AFUB_000110:	3 change-points=1	86	167	255	
AFUB_000400:	3 change-points=1	84	159	256	
AFUB_000600:	3 change-points=1	83	172	256	
AFUB_001060:	3 change-points=1	86	171	258	
AFUB_001990:	3 change-points=0.99	77	157	259	
AFUB_003240:	3 change-points=1	78	163	254	
AFUB_004210:	3 change-points=1	83	166	259	
AFUB_004470:	3 change-points=0.99	74	159	269	
AFUB_004520:	2 change-points=0.68	82	169		
AFUB_005350:	3 change-points=1	86	159	261	
AFUB_005510:	2 change-points=1	117	209		
AFUB_005770:	3 change-points=1	80	162	249	
AFUB_006120:	3 change-points=1	82	168	249	
AFUB_006920:	3 change-points=1	77	161	248	
AFUB_007280:	2 change-points=1	81	244		
AFUB_009120:	3 change-points=1	73	160	261	
AFUB_009490:	3 change-points=1	78	158	234	
AFUB_009640:	3 change-points=1	75	166	234	

9970:	AFUB_00	2 change-points=0.99	116	213	
0000:	AFUB_01	2 change-points=0.78	81	170	
0180:	AFUB_01	2 change-points=1	82	172	
0420:	AFUB_01	3 change-points=1	74	155	266
0950:	AFUB_01	3 change-points=1	80	157	266
1060:	AFUB_01	3 change-points=1	76	155	249
1240:	AFUB_01	3 change-points=1	72	154	250
1800:	AFUB_01	2 change-points=1	91	197	
2020:	AFUB_01	1 change-points=0.68	120		
2530:	AFUB_01	3 change-points=1	73	161	241
2670:	AFUB_01	1 change-points=1	98		
2800:	AFUB_01	3 change-points=0.99	73	161	244
3000:	AFUB_01	3 change-points=1	73	157	243
3240:	AFUB_01	3 change-points=1	81	171	260
3910:	AFUB_01	3 change-points=1	69	154	252
4000:	AFUB_01	1 change-points=1	169		
4300:	AFUB_01	3 change-points=1	74	159	265
4400:	AFUB_01	3 change-points=1	76	157	260
4490:	AFUB_01	3 change-points=1	71	162	266
4780:	AFUB_01	3 change-points=0.97	77	158	266
4910:	AFUB_01	3 change-points=1	73	158	239
5020:	AFUB_01	3 change-points=1	73	156	243
5090:	AFUB_01	3 change-points=0.99	80	164	248
5380:	AFUB_01	3 change-points=1	79	157	245
5440:	AFUB_01	3 change-points=1	76	156	239
5560:	AFUB_01	3 change-points=0.99	71	153	250

5750:	AFUB_01	3 change-points=1	84	170	265
5800:	AFUB_01	3 change-points=1	79	150	239
5960:	AFUB_01	3 change-points=1	89	162	265
5990:	AFUB_01	3 change-points=1	75	156	247
6220:	AFUB_01	3 change-points=1	73	149	249
6540:	AFUB_01	3 change-points=1	72	155	246
6630:	AFUB_01	3 change-points=1	72	153	237
6720:	AFUB_01	3 change-points=1	75	157	237
6730:	AFUB_01	3 change-points=0.62	72	158	224
6820:	AFUB_01	3 change-points=1	76	157	237
7020:	AFUB_01	3 change-points=1	71	147	240
7180:	AFUB_01	3 change-points=1	80	155	246
7410:	AFUB_01	3 change-points=0.99	76	147	255
7530:	AFUB_01	3 change-points=1	85	151	254
8340:	AFUB_01	1 change-points=0.99	73		
9640:	AFUB_01	3 change-points=1	81	161	252
9790:	AFUB_01	1 change-points=1	213		
0350:	AFUB_02	2 change-points=1	75	201	
0500:	AFUB_02	3 change-points=1	73	153	242
0530:	AFUB_02	1 change-points=1	160		
1220:	AFUB_02	3 change-points=1	76	160	240
1320:	AFUB_02	3 change-points=1	74	160	231
1650:	AFUB_02	3 change-points=1	73	152	243
2280:	AFUB_02	3 change-points=1	75	155	257
2340:	AFUB_02	3 change-points=1	82	153	257
2390:	AFUB_02	3 change-points=1	83	154	258

2410:	AFUB_02	2 change-points=0.58	78	152	
3210:	AFUB_02	3 change-points=1	84	159	261
4170:	AFUB_02	3 change-points=1	83	176	267
4220:	AFUB_02	3 change-points=0.99	77	157	251
5230:	AFUB_02	3 change-points=1	77	159	245
6210:	AFUB_02	3 change-points=1	78	158	255
6340:	AFUB_02	1 change-points=1	84		
6550:	AFUB_02	3 change-points=1	93	164	267
7530:	AFUB_02	3 change-points=1	111	183	243
7770:	AFUB_02	3 change-points=1	95	157	258
7970:	AFUB_02	2 change-points=1	83	157	
7990:	AFUB_02	2 change-points=1	94	171	
9020:	AFUB_02	2 change-points=1	85	177	
9870:	AFUB_02	2 change-points=1	101	195	
0360:	AFUB_03	1 change-points=1	150		
0440:	AFUB_03	3 change-points=1	115	195	272
0930:	AFUB_03	3 change-points=1	88	158	240
1000:	AFUB_03	3 change-points=1	86	156	251
1270:	AFUB_03	3 change-points=1	94	159	256
1980:	AFUB_03	3 change-points=1	86	150	243
2870:	AFUB_03	3 change-points=1	89	154	258
3470:	AFUB_03	3 change-points=1	87	150	255
3540:	AFUB_03	3 change-points=1	73	160	239
3580:	AFUB_03	3 change-points=1	76	161	244
3930:	AFUB_03	3 change-points=0.99	71	160	242
4470:	AFUB_03	3 change-points=1	72	151	239

AFUB_03 4630:	3 change-points=1	73	156	236		
AFUB_03 5280:	3 change-points=0.99	74	155	242		
AFUB_03 5330:	2 change-points=1	70	209			
AFUB_03 5590:	3 change-points=1	70	150	242		
AFUB_03 6250:	3 change-points=1	73	152	240		
AFUB_03 6300:	3 change-points=1	74	155	236		
AFUB_03 6390:	3 change-points=1	80	150	235		
AFUB_03 6440:	3 change-points=1	94	176	249		
AFUB_03 7000:	3 change-points=1	72	162	237		
AFUB_03 7020:	4 change-points=0.6	76	149	209	261	
AFUB_03 7150:	2 change-points=1	84	230			
AFUB_03 7190:	3 change-points=1	63	150	235		
AFUB_03 7210:	1 change-points=1	95				
AFUB_03 7220:	3 change-points=1	72	161	248		
AFUB_03 7920:	3 change-points=1	100	180	251		
AFUB_03 8200:	2 change-points=0.99	73	180			
AFUB_03 8290:	3 change-points=1	69	155	233		
AFUB_03 9010:	3 change-points=1	73	152	248		
AFUB_03 9350:	4 change-points=0.51	76	182	239	262	
AFUB_03 9500:	3 change-points=1	72	159	243		
AFUB_04 0000:	4 change-points=1	73	167	235	266	
AFUB_04 0580:	4 change-points=0.74	67	168	237	267	
AFUB_04 1060:	3 change-points=1	73	167	248		
AFUB_04 1100:	2 change-points=1	74	202			
AFUB_04 2310:	4 change-points=1	70	161	221	259	
AFUB_04 2770:	3 change-points=0.99	72	157	233		

3000:	AFUB_04	3 change-points=1	68	154	236	
3270:	AFUB_04	3 change-points=1	69	158	231	
3860:	AFUB_04	3 change-points=1	74	160	235	
4040:	AFUB_04	3 change-points=1	64	154	236	
4060:	AFUB_04	3 change-points=1	65	158	234	
4290:	AFUB_04	3 change-points=0.95	64	154	228	
4300:	AFUB_04	3 change-points=0.99	78	164	234	
4670:	AFUB_04	4 change-points=0.81	70	161	230	264
4930:	AFUB_04	4 change-points=1	68	156	226	254
5020:	AFUB_04	3 change-points=0.95	68	156	227	
5330:	AFUB_04	3 change-points=1	65	152	230	
5540:	AFUB_04	3 change-points=1	70	156	236	
5580:	AFUB_04	3 change-points=0.99	75	149	241	
5780:	AFUB_04	3 change-points=0.99	71	159	235	
5820:	AFUB_04	3 change-points=1	70	157	235	
5980:	AFUB_04	2 change-points=1	107	205		
6160:	AFUB_04	3 change-points=1	67	154	237	
6210:	AFUB_04	3 change-points=1	68	159	236	
6330:	AFUB_04	3 change-points=1	70	160	230	
6410:	AFUB_04	3 change-points=1	69	169	241	
6540:	AFUB_04	3 change-points=0.56	64	156	227	
6890:	AFUB_04	3 change-points=0.84	68	158	228	
7470:	AFUB_04	3 change-points=1	71	157	234	
7730:	AFUB_04	3 change-points=1	71	151	229	
8380:	AFUB_04	3 change-points=1	84	154	239	
8740:	AFUB_04	3 change-points=1	71	156	236	

AFUB_048990:	3 change-points=1	72	154	236		
AFUB_049390:	3 change-points=1	73	161	236		
AFUB_049550:	3 change-points=1	71	162	238		
AFUB_050090:	3 change-points=1	91	185	259		
AFUB_050190:	3 change-points=0.98	71	156	229		
AFUB_050230:	3 change-points=1	64	150	236		
AFUB_050800:	3 change-points=0.8	68	155	227		
AFUB_051340:	3 change-points=0.99	67	165	235		
AFUB_051400:	3 change-points=1	80	155	236		
AFUB_051540:	3 change-points=0.95	72	152	236		
AFUB_051950:	2 change-points=0.99	87	194			
AFUB_052420:	3 change-points=1	75	163	248		
AFUB_052710:	3 change-points=1	72	161	242		
AFUB_052860:	3 change-points=0.99	77	157	238		
AFUB_053150:	3 change-points=1	90	209	244		
AFUB_053740:	3 change-points=1	73	150	239		
AFUB_053880:	3 change-points=1	73	154	232		
AFUB_053950:	4 change-points=1	68	156	226	260	
AFUB_054360:	3 change-points=1	77	158	239		
AFUB_055060:	3 change-points=1	74	148	228		
AFUB_056530:	3 change-points=1	82	155	237		
AFUB_056620:	2 change-points=1	108	188			
AFUB_056790:	3 change-points=1	70	154	240		
AFUB_057290:	3 change-points=1	70	148	236		
AFUB_057630:	3 change-points=1	71	150	239		
AFUB_057730:	3 change-points=1	73	150	246		

7890:	AFUB_05	3 change-points=0.99	76	151	240
8240:	AFUB_05	3 change-points=0.88	90	187	226
8640:	AFUB_05	3 change-points=1	70	148	238
8830:	AFUB_05	2 change-points=0.67	85	214	
8960:	AFUB_05	3 change-points=1	80	160	236
9600:	AFUB_05	3 change-points=1	79	147	230
9650:	AFUB_05	3 change-points=1	73	155	219
0620:	AFUB_06	3 change-points=1	78	158	230
0680:	AFUB_06	3 change-points=1	74	155	226
1020:	AFUB_06	3 change-points=1	79	160	227
1530:	AFUB_06	3 change-points=0.97	74	158	220
1940:	AFUB_06	3 change-points=1	80	162	230
2000:	AFUB_06	3 change-points=1	74	154	228
2090:	AFUB_06	3 change-points=0.99	72	156	227
2110:	AFUB_06	3 change-points=0.99	78	162	230
2210:	AFUB_06	3 change-points=1	75	154	226
3310:	AFUB_06	3 change-points=1	78	155	246
3540:	AFUB_06	3 change-points=1	82	152	233
3610:	AFUB_06	1 change-points=1	156		
6180:	AFUB_06	1 change-points=1	75		
6820:	AFUB_06	3 change-points=1	75	157	222
6970:	AFUB_06	3 change-points=0.99	75	159	222
7230:	AFUB_06	3 change-points=1	92	167	239
7280:	AFUB_06	3 change-points=0.97	73	158	220
7320:	AFUB_06	3 change-points=0.99	78	163	225
7340:	AFUB_06	2 change-points=0.64	106	222	

8700:	AFUB_06	3 change-points=0.99	83	170	237	
9160:	AFUB_06	3 change-points=1	79	165	233	
9420:	AFUB_06	3 change-points=1	81	163	239	
9500:	AFUB_06	3 change-points=0.99	77	157	230	
9610:	AFUB_06	3 change-points=1	78	160	219	
9670:	AFUB_06	3 change-points=1	77	162	223	
9960:	AFUB_06	3 change-points=0.98	76	162	219	
1780:	AFUB_07	3 change-points=1	83	168	225	
1830:	AFUB_07	3 change-points=1	90	177	236	
1920:	AFUB_07	3 change-points=1	80	165	224	
2930:	AFUB_07	3 change-points=1	75	158	219	
3070:	AFUB_07	3 change-points=1	78	162	229	
3490:	AFUB_07	3 change-points=1	69	159	224	
3520:	AFUB_07	3 change-points=1	75	163	220	
3940:	AFUB_07	3 change-points=1	88	176	236	
4510:	AFUB_07	3 change-points=0.98	78	157	223	
4560:	AFUB_07	3 change-points=0.99	91	169	224	
4750:	AFUB_07	3 change-points=1	74	162	225	
5930:	AFUB_07	3 change-points=0.85	74	163	221	
5990:	AFUB_07	3 change-points=0.99	72	158	226	
6060:	AFUB_07	4 change-points=0.4 7	74	165	223	263
6110:	AFUB_07	3 change-points=0.98	73	160	222	
6200:	AFUB_07	3 change-points=1	71	157	220	
7130:	AFUB_07	3 change-points=0.58	73	166	219	
7250:	AFUB_07	3 change-points=1	69	159	224	
7460:	AFUB_07	3 change-points=1	83	166	238	

7530:	AFUB_07	3 change-points=1	82	160	241
7740:	AFUB_07	3 change-points=0.97	74	163	215
8120:	AFUB_07	3 change-points=0.98	79	168	220
8150:	AFUB_07	3 change-points=0.99	79	168	221
8160:	AFUB_07	3 change-points=0.95	75	166	217
8520:	AFUB_07	3 change-points=1	79	158	240
9150:	AFUB_07	3 change-points=0.97	80	162	221
9450:	AFUB_07	3 change-points=0.99	76	162	228
9560:	AFUB_07	3 change-points=1	74	160	224
9700:	AFUB_07	3 change-points=1	72	160	228
9810:	AFUB_07	3 change-points=1	71	158	228
9860:	AFUB_07	3 change-points=1	70	157	232
9880:	AFUB_07	3 change-points=0.99	77	148	251
0380:	AFUB_08	3 change-points=1	77	163	228
0460:	AFUB_08	3 change-points=1	72	165	219
0600:	AFUB_08	3 change-points=0.99	73	163	221
0790:	AFUB_08	3 change-points=1	83	169	234
1310:	AFUB_08	3 change-points=1	83	170	229
1500:	AFUB_08	3 change-points=0.99	70	160	223
1700:	AFUB_08	3 change-points=0.99	79	162	223
2080:	AFUB_08	2 change-points=1	79	164	
2260:	AFUB_08	3 change-points=1	80	169	238
2950:	AFUB_08	3 change-points=1	71	158	230
3430:	AFUB_08	3 change-points=1	80	159	241
3880:	AFUB_08	3 change-points=1	77	160	228
3950:	AFUB_08	3 change-points=1	88	173	233

AFUB_08 4330:	3 change-points=1	73	159	229	
AFUB_08 4620:	3 change-points=1	75	159	227	
AFUB_08 5380:	3 change-points=1	85	166	231	
AFUB_08 5450:	3 change-points=1	81	163	233	
AFUB_08 5460:	3 change-points=1	73	159	228	
AFUB_08 5820:	2 change-points=1	116	205		
AFUB_08 6990:	3 change-points=1	85	169	238	
AFUB_08 6680:	3 change-points=1	95	180	238	
AFUB_08 6770:	3 change-points=1	95	170	235	
AFUB_08 7340:	3 change-points=1	81	157	225	
AFUB_08 7890:	3 change-points=0.99	76	156	227	
AFUB_08 8210:	3 change-points=1	87	166	227	
AFUB_08 8380:	3 change-points=1	90	178	241	
AFUB_08 8390:	3 change-points=1	74	156	220	
AFUB_08 8460:	3 change-points=1	84	161	226	
AFUB_08 9710:	3 change-points=1	97	180	233	
AFUB_08 9880:	3 change-points=0.99	89	164	232	
AFUB_09 0440:	3 change-points=1	85	153	229	
AFUB_00 0190:	3 change-points=1	72	150	240	
AFUB_00 0960:	3 change-points=1	68	151	234	
AFUB_00 1960:	3 change-points=1	76	158	235	
AFUB_00 2050:	3 change-points=1	72	156	239	
AFUB_00 2240:	3 change-points=0.98	74	151	245	
AFUB_00 4190:	3 change-points=1	74	158	232	
AFUB_00 4490:	3 change-points=0.99	81	166	233	
AFUB_00 8120:	3 change-points=1	71	155	234	

AFUB_00 8610:	3 change-points=0.99	69	158	229		
AFUB_01 0090:	3 change-points=0.97	73	158	240		
AFUB_01 0720:	3 change-points=0.99	77	165	229		
AFUB_01 3830:	3 change-points=1	87	163	239		
AFUB_01 5210:	3 change-points=0.99	80	162	233		
AFUB_02 0250:	3 change-points=1	66	156	232		
AFUB_02 2860:	2 change-points=0.85	72	152			
AFUB_02 3530:	3 change-points=0.99	74	158	237		
AFUB_02 4050:	3 change-points=1	78	199	237		
AFUB_02 5190:	3 change-points=0.63	71	159	215		
AFUB_02 6630:	3 change-points=0.97	68	163	227		
AFUB_02 7200:	3 change-points=1	69	161	228		
AFUB_02 9740:	3 change-points=1	69	158	231		
AFUB_03 1840:	2 change-points=0.95	90	233			
AFUB_03 3560:	3 change-points=1	70	160	230		
AFUB_03 6510:	3 change-points=0.99	70	151	231		
AFUB_03 8600:	3 change-points=1	69	155	233		
AFUB_04 6750:	4 change-points=0.88	67	160	225	259	
AFUB_04 7970:	3 change-points=0.71	67	160	223		
AFUB_04 8230:	3 change-points=0.86	74	165	221		
AFUB_04 8890:	4 change-points=0.99	73	164	223	260	
AFUB_05 0000:	3 change-points=1	72	165	226		
AFUB_05 4000:	2 change-points=0.91	96	211			
AFUB_05 7470:	3 change-points=0.98	68	161	221		
AFUB_06 0650:	3 change-points=0.73	67	164	221		
AFUB_06 7240:	3 change-points=1	83	169	241		

7440:	AFUB_06 3 change-points=1	69	152	234		
8850:	AFUB_06 3 change-points=0.99	78	176	231		
1380:	AFUB_07 3 change-points=0.99	71	163	227		
4500:	AFUB_07 4 change-points=0.92	73	165	223	261	
5680:	AFUB_07 4 change-points=0.56	75	165	224	264	
0530:	AFUB_08 4 change-points=0.71	71	164	224	264	
1800:	AFUB_08 4 change-points=0.87	74	163	223	261	
3600:	AFUB_08 3 change-points=0.93	64	177	219		
4440:	AFUB_08 3 change-points=0.95	68	161	222		
4670:	AFUB_08 3 change-points=1	74	161	222		
5170:	AFUB_08 3 change-points=0.99	71	161	259		
2740:	AFUB_09 3 change-points=0.99	75	151	230		
4860:	AFUB_09 4 change-points=0.99	78	169	222	261	
5440:	AFUB_09 4 change-points=0.53	78	168	225	264	
6380:	AFUB_09 4 change-points=0.95	77	170	224	259	
9770:	AFUB_09 3 change-points=0.51	75	166	225		
1950:	AFUB_10 4 change-points=0.85	78	168	225	264	
1820:	AFUB_00 3 change-points=0.97	73	165	226		
2390:	AFUB_00 3 change-points=1	85	178	242		
4120:	AFUB_00 3 change-points=1	78	162	231		
9690:	AFUB_00 2 change-points=1	80	181			
9160:	AFUB_01 3 change-points=1	72	160	233		
9830:	AFUB_01 3 change-points=0.99	70	153	246		
1470:	AFUB_02 3 change-points=0.99	81	168	225		
9400:	AFUB_02 4 change-points=0.99	75	175	214	263	
0770:	AFUB_03 4 change-points=0.75	74	167	224	266	

1910:	AFUB_03	3 change-points=1	77	166	252	
2220:	AFUB_03	4 change-points=0.95	79	169	224	265
2890:	AFUB_03	4 change-points=0.98	78	166	223	263
5140:	AFUB_03	3 change-points=1	107	189	247	
2120:	AFUB_04	3 change-points=0.94	74	164	222	
6000:	AFUB_04	3 change-points=1	93	188	255	
7310:	AFUB_04	3 change-points=0.99	79	151	239	
5490:	AFUB_05	2 change-points=1	115	198		
6710:	AFUB_05	3 change-points=1	74	168	229	
4180:	AFUB_06	3 change-points=1	79	191	234	
7480:	AFUB_06	3 change-points=1	82	181	237	
8500:	AFUB_06	4 change-points=0.82	72	168	226	261
0520:	AFUB_07	3 change-points=0.99	74	163	226	
0960:	AFUB_07	3 change-points=0.98	78	168	225	
1460:	AFUB_07	3 change-points=0.97	76	164	229	
1660:	AFUB_07	3 change-points=0.99	72	161	229	
7190:	AFUB_07	3 change-points=1	88	186	244	
7270:	AFUB_07	2 change-points=1	114	190		
8010:	AFUB_07	3 change-points=0.99	80	158	239	
2490:	AFUB_08	3 change-points=0.95	80	165	225	
3250:	AFUB_08	3 change-points=1	87	167	230	
3260:	AFUB_08	3 change-points=1	80	162	226	
3370:	AFUB_08	3 change-points=0.98	83	161	225	
9440:	AFUB_08	1 change-points=1	152			
1540:	AFUB_09	3 change-points=0.99	79	158	230	
2820:	AFUB_09	3 change-points=0.99	82	170	232	

AFUB_095290:	3 change-points=0.99	74	165	231	
AFUB_095620:	2 change-points=1	82	206		
AFUB_096430:	2 change-points=1	91	161		
AFUB_096690:	3 change-points=1	84	162	238	
AFUB_097590:	3 change-points=1	78	150	238	
AFUB_091870:	3 change-points=0.99	82	160	236	
AFUB_091930:	3 change-points=1	82	166	247	
AFUB_092060:	3 change-points=1	79	161	236	
AFUB_092130:	3 change-points=1	86	165	237	
AFUB_092490:	3 change-points=1	77	158	233	
AFUB_093120:	3 change-points=0.98	82	161	226	
AFUB_093280:	3 change-points=0.99	84	160	218	
AFUB_095180:	3 change-points=0.82	86	162	218	
AFUB_096500:	3 change-points=1	74	160	229	
AFUB_097300:	3 change-points=1	76	161	231	
AFUB_097320:	3 change-points=0.99	78	161	228	
AFUB_097380:	3 change-points=0.99	72	160	229	
AFUB_098690:	3 change-points=0.9	78	166	221	
AFUB_099050:	3 change-points=1	73	162	244	
AFUB_099350:	3 change-points=1	73	161	228	
AFUB_099630:	3 change-points=0.99	78	164	224	
AFUB_101260:	3 change-points=1	77	157	235	
AFUB_101510:	3 change-points=1	82	161	234	
WT_A1160:	3 change-points=0.99	73	159	232	
WT_A1160:	3 change-points=0.99	74	157	226	
AFUB_100050:	3 change-points=0.99	82	171	222	

6450:	AFUB_01	3 change-points=0.93	70	163	218	
5550:	AFUB_05	3 change-points=0.99	100	188	250	
9590:	AFUB_09	3 change-points=0.86	71	180	263	
7880:	AFUB_00	3 change-points=0.99	74	163	223	
9440:	AFUB_01	2 change-points=1	131	235		
0050:	AFUB_02	3 change-points=1	75	163	225	
0080:	AFUB_02	4 change-points=0.68	78	168	219	248
1980:	AFUB_04	2 change-points=0.53	132	229		
2180:	AFUB_04	3 change-points=0.98	83	166	227	
0260:	AFUB_05	1 change-points=0.99	156			
9050:	AFUB_05	3 change-points=0.82	118	206	251	
4650:	AFUB_06	4 change-points=0.99	85	174	223	259
7880:	AFUB_00	3 change-points=1	82	173	222	
8270:	AFUB_01	4 change-points=0.98	76	169	224	263
9440:	AFUB_01	3 change-points=1	87	182	234	
0050:	AFUB_02	3 change-points=0.99	85	169	227	
0080:	AFUB_02	3 change-points=0.99	81	167	251	
2490:	AFUB_03	3 change-points=0.99	76	165	224	
1980:	AFUB_04	3 change-points=0.97	76	168	228	
2180:	AFUB_04	3 change-points=1	84	172	231	
3720:	AFUB_04	3 change-points=0.99	89	179	226	
0260:	AFUB_05	2 change-points=0.96	87	238		
0:	WT_A116	3 change-points=0.92	78	167	218	
0:	WT_A116	4 change-points=0.55	76	166	220	267
0:	WT_A116	3 change-points=0.95	77	164	220	
0:	WT_CEA1	3 change-points=1	93	195	252	

WT_CEA10:	3 change-points=1	92	191	250		
WT_CEA10:	3 change-points=1	89	191	249		
AFUB_029870:	2 change-points=1	110	193			
AFUB_000040:	3 change-points=0.52	58	126	227		
AFUB_002740:	3 change-points=0.99	51	132	232		
AFUB_003620:	2 change-points=0.53	61	228			
AFUB_003630:	3 change-points=0.99	54	132	230		
AFUB_005170:	3 change-points=0.99	59	141	229		
AFUB_007960:	3 change-points=0.98	51	126	236		
AFUB_011060:	3 change-points=1	52	133	231		
AFUB_013550:	3 change-points=0.99	74	144	232		
AFUB_014200:	3 change-points=0.99	52	104	200		
WT_A1160:	2 change-points=0.96	72	247			
AFUB_017960:	2 change-points=0.85	78	233			
AFUB_020110:	3 change-points=1	65	147	228		
AFUB_020420:	3 change-points=1	47	125	225		
AFUB_021540:	3 change-points=0.99	49	126	226		
AFUB_022560:	3 change-points=0.98	46	129	232		
AFUB_023920:	3 change-points=1	78	154	198		
AFUB_023950:	3 change-points=1	49	138	221		
AFUB_025730:	3 change-points=0.99	49	131	229		
AFUB_026420:	3 change-points=1	55	131	234		
AFUB_028890:	3 change-points=1	62	154	215		
AFUB_029970:	2 change-points=0.99	62	231			
AFUB_033200:	3 change-points=1	52	120	231		
AFUB_037970:	4 change-points=0.99	54	115	205	238	

	AftA:	1 change-points=0.96	100			
9150:	AFUB_03	3 change-points=0.99	62	158	220	
0460:	AFUB_04	3 change-points=0.95	46	134	244	
1990:	AFUB_04	3 change-points=1	55	145	204	
2300:	AFUB_04	3 change-points=1	49	142	216	
	A1160:	3 change-points=1	44	124	219	
3680:	AFUB_04	3 change-points=1	51	161	239	
3860:	AFUB_04	2 change-points=0.83	66	242		
4120:	AFUB_04	2 change-points=0.99	59	230		
4350:	AFUB_04	2 change-points=1	61	232		
5600:	AFUB_04	3 change-points=1	52	147	221	
6430:	AFUB_04	3 change-points=1	49	132	224	
7250:	AFUB_04	3 change-points=1	52	136	225	
8830:	AFUB_04	3 change-points=1	46	136	216	
8940:	AFUB_04	3 change-points=0.88	44	132	214	
9780:	AFUB_04	3 change-points=1	42	125	225	
0200:	AFUB_05	3 change-points=1	44	132	221	
0430:	AFUB_05	3 change-points=1	53	146	230	
1220:	AFUB_05	3 change-points=0.93	56	124	230	
5080:	AFUB_05	3 change-points=1	66	165	248	
7600:	AFUB_05	4 change-points=1	66	161	200	234
0430:	AFUB_06	3 change-points=0.99	67	145	205	
0620:	AFUB_06	3 change-points=1	52	144	214	
1420:	AFUB_06	3 change-points=1	57	141	226	
7520:	AFUB_06	3 change-points=0.99	55	151	220	
1090:	AFUB_07	3 change-points=1	48	142	219	

1570:	AFUB_07	3 change-points=0.99	53	142	226
3170:	AFUB_07	3 change-points=0.99	59	145	225
3740:	AFUB_07	3 change-points=1	60	162	231
3760:	AFUB_07	3 change-points=1	85	169	228
5630:	AFUB_07	3 change-points=0.99	62	147	224
7920:	AFUB_07	3 change-points=0.72	66	136	231
0070:	AFUB_08	2 change-points=1	68	228	
0850:	AFUB_08	3 change-points=1	55	152	220
1750:	AFUB_08	3 change-points=1	48	137	223
3510:	AFUB_08	3 change-points=0.99	66	166	229
4770:	AFUB_08	3 change-points=1	52	138	230
5630:	AFUB_08	3 change-points=0.99	52	149	220
6150:	AFUB_08	3 change-points=1	48	133	224
7240:	AFUB_08	3 change-points=1	47	126	227
8740:	AFUB_08	3 change-points=0.99	57	141	218
8810:	AFUB_08	3 change-points=1	59	154	200
0360:	AFUB_09	3 change-points=1	55	142	244
0370:	AFUB_09	2 change-points=1	60	233	
0650:	AFUB_09	2 change-points=1	73	233	
1090:	AFUB_09	3 change-points=1	59	169	237
2100:	AFUB_09	3 change-points=0.99	53	138	220
2720:	AFUB_09	3 change-points=0.99	54	133	216
2760:	AFUB_09	3 change-points=0.99	47	134	222
3890:	AFUB_09	3 change-points=1	49	144	226
6010:	AFUB_09	3 change-points=1	46	191	232
6230:	AFUB_09	3 change-points=0.9	63	149	213

AFUB_09 6370:	2 change-points=1	64	140			
AFUB_09 7690:	2 change-points=0.98	61	230			
AFUB_09 7790:	3 change-points=1	71	140	225		
AFUB_09 8510:	4 change-points=1	68	146	206	240	
AFUB_10 1600:	2 change-points=1	70	235			
AFUB_10 1810:	3 change-points=1	51	140	223		
AFUB_10 1870:	3 change-points=1	57	134	226		
AFUB_10 1990:	3 change-points=0.93	48	125	234		
AFUB_00 9490:	3 change-points=1	49	125	234		
AftA:	3 change-points=0.99	51	131	235		

Table S3.3 Media comparison

DEME Dalbecco's Modified Eagle Medium)			
Components	**Molecular Weight**	**Concentration (mg/L)**	**mM**
Amino Acids			
Glycine	75.0	30.0	0.400
L-Arginine hydrochloride	211.0	84.0	0.398
L-Cystine 2HCl	313.0	63.0	0.201
L-Glutamine	146.0	584.0	4.000
L-Histidine hydrochloride-H2O	210.0	42.0	0.200
L-Isoleucine	131.0	105.0	0.802
L-Leucine	131.0	105.0	0.802
L-Lysine hydrochloride	183.0	146.0	0.798
L-Methionine	149.0	30.0	0.201
L-Phenylalanine	165.0	66.0	0.400
L-Serine	105.0	42.0	0.400
L-Threonine	119.0	95.0	0.798
L-Tryptophan	204.0	16.0	0.078
L-Tyrosine disodium salt dihydrate	261.0	104.0	0.398
L-Valine	117.0	94.0	0.803
Vitamins			
Choline chloride	140.0	4.00	0.0286
D-Calcium pantothenate	477.0	4.00	0.0084
Folic Acid	441.0	4.00	0.0091
Niacinamide	122.0	4.00	0.0328
Pyridoxine hydrochloride	206.0	4.00	0.0194
Riboflavin	376.0	0.40	0.0011
Thiamine hydrochloride	337.0	4.00	0.0119
i-Inositol	180.0	7.20	0.0400
Inorganic Salts			
Calcium Chloride (CaCl2) (anhyd.)	111.0	200.0	1.802
Ferric Nitrate (Fe(NO3)3"9H2O)	404.0	0.1	0.000
Magnesium Sulfate (MgSO4) (anhyd.)	120.0	97.7	0.814
Potassium Chloride (KCl)	75.0	400.0	5.333
Sodium Bicarbonate (NaHCO3)	84.0	3700.0	44.048
Sodium Chloride (NaCl)	58.0	6400.0	110.345
Sodium Phosphate monobasic (NaH2PO4-H2O)	138.0	125.0	0.906
Other Components			
D-Glucose (Dextrose)	180.0	4500	25.00
Phenol Red	376.4	15	0.04

RPMI-1640			
Components	**Molecular Weight**	**Concentration (mg/L)**	**mM**
Amino Acids			
Glycine	75.0	10.0	0.133
L-Arginine	174.0	200.0	1.149
L-Asparagine	132.0	50.0	0.379
L-Aspartic acid	133.0	20.0	0.150
L-Cystine 2HCl	313.0	65.0	0.208
L-Glutamic Acid	147.0	20.0	0.136
L-Glutamine	146.0	300.0	2.055
L-Histidine	155.0	15.0	0.097
L-Hydroxyproline	131.0	20.0	0.153
L-Isoleucine	131.0	50.0	0.382
L-Leucine	131.0	50.0	0.382
L-Lysine hydrochloride	183.0	40.0	0.219
L-Methionine	149.0	15.0	0.101
L-Phenylalanine	165.0	15.0	0.091
L-Proline	115.0	20.0	0.174
L-Serine	105.0	30.0	0.286
L-Threonine	119.0	20.0	0.168
L-Tryptophan	204.0	5.0	0.025
L-Tyrosine disodium salt dihydrate	261.0	29.0	0.111
L-Valine	117.0	20.0	0.171
Vitamins			
Biotin	244.0	0.20	0.0008
Choline chloride	140.0	3.00	0.0214
D-Calcium pantothenate	477.0	0.25	0.0005
Folic Acid	441.0	1.00	0.0023
Niacinamide	122.0	1.00	0.0082
Para-Aminobenzoic Acid	137.0	1.00	0.0073
Pyridoxine hydrochloride	206.0	1.00	0.0049
Riboflavin	376.0	0.20	0.0005
Thiamine hydrochloride	337.0	1.00	0.0030
Vitamin B12	1355.0	0.01	0.0000
i-Inositol	180.0	35.00	0.1944
Inorganic Salts			
Calcium nitrate (Ca(NO3)2 4H2O)	236	100	0.42
Magnesium Sulfate (MgSO4) (anhyd.)	120	48.84	0.41
Potassium Chloride (KCl)	75	400	5.33
Sodium Bicarbonate (NaHCO3)	84	2000	23.81
Sodium Chloride (NaCl)	58	6000	103.45
Sodium Phosphate dibasic (Na2HPO4) anhydrous	142	800	5.63
Other Components			
D-Glucose (Dextrose)*1	180	2000	11.1111
Glutathione (reduced)	307	1	0.0033
Phenol Red	376.4	5	0.0133

Aspergillus minumal medium (AMM) + vitamin solution			
Components	**Molecular Weight**	**Concentration (mg/L)**	**mM**
carbon source			
D-glucose	180	10000	55.00
Nitrogen source			
Ammonium tartrate	184.148	10000	5.00
Inorganic salts			
Potassium Chloride (KCl)	75	520	6.93
Magnesium Sulfate (MgSO4) (anhyd.)	120	520	4.33
Pottasium Phosphate monobasic (KH2PO4)	136.086	1520	11.2
trace elements			
Na2B4O7.10H2O	381	0.04	1.05E-03
CuSO4. 5H2O	250	0.40	1.60E-03
FePO4. 2H2O	187	0.80	4.28E-03
MnSO4. 2H2O	187	0.80	4.28E-03
Na2MoO4. 2H2O	430	0.80	1.86E-03
ZnSO4. 7H2O	288	8.00	2.78E-02
Vitamins			
Para-Aminobenzoic Acid	137	4	2.9E-02
Thiamine hydrochloride (aneurin)	337	0.5	1.5E-03
Biotin	244	0.01	4.1E-05
i-Inositol	180	240	1.3E+00
Nicotinic acid	123.1094	1	8.12E-03
Pyridoxine hydrochloride	206	2.5	1.2E-02
Riboflavin	376	1	2.7E-03
Choline chloride	140	14	1.0E-01
Panto (DL-phantothenic acid)	219.24	2	9.12E-03

Fungal RPMI			
Components	**Molecular Weight**	**Concentration (mg/L)**	**mM**
Amino Acids			
Glycine	75.0	10.0	0.133
L-Arginine	174.0	200.0	1.149
L-Asparagine	132.0	50.0	0.379
L-Aspartic acid	133.0	20.0	0.150
L-Cystine 2HCl	313.0	65.0	0.208
L-Glutamic Acid	147.0	20.0	0.136
L-Glutamine	146.0	300.0	2.055
L-Histidine	155.0	15.0	0.097
L-Hydroxyproline	131.0	20.0	0.153
L-Isoleucine	131.0	50.0	0.382
L-Leucine	131.0	50.0	0.382
L-Lysine hydrochloride	183.0	40.0	0.219
L-Methionine	149.0	15.0	0.101
L-Phenylalanine	165.0	15.0	0.091
L-Proline	115.0	20.0	0.174
L-Serine	105.0	30.0	0.286
L-Threonine	119.0	20.0	0.168
L-Tryptophan	204.0	5.0	0.025
L-Tyrosine disodium salt dihydrate	261.0	29.0	0.111
L-Valine	117.0	20.0	0.171
Vitamins			
Biotin	244.0	0.20	0.0008
Choline chloride	140.0	3.00	0.0214
D-Calcium pantothenate	477.0	0.25	0.0005
Folic Acid	441.0	1.00	0.0023
Niacinamide	122.0	1.00	0.0082
Para-Aminobenzoic Acid	137.0	1.00	0.0073
Pyridoxine hydrochloride	206.0	1.00	0.0049
Riboflavin	376.0	0.20	0.0005
Thiamine hydrochloride	337.0	1.00	0.0030
Vitamin B12	1355.0	0.01	0.0000
i-Inositol	180.0	35.00	0.1944
Inorganic Salts			
Ammonium tartrate			5.00
Magnesium Sulfate (MgSO4) (anhyd.)	120	48.84	0.41
Potassium Chloride (KCl)	75	400	5.33
Sodium Bicarbonate (NaHCO3)	84	2000	23.81
Sodium Chloride (NaCl)	58	6000	103.45
Sodium Phosphate dibasic	142	800	5.63
Other Components			
D-Glucose (Dextrose)	180	20000	111.1000
Glutathione (reduced)	307	1	0.0033
MOPS	209.26	34,530	165.0000
Calcium chloride (CaCl2)	110.98	46.6	0.42
Trace elements			
Components	**Molecular Weight**	**Concentration (mg/L)**	**mM**
Na2B4O7.10H2O	381	0.04	1.05E-03
CuSO4. 5H2O	250	0.40	1.60E-03
FePO4. 2H2O	187	0.80	4.28E-03
MnSO4. 2H2O	187	0.80	4.28E-03
Na2MoO4. 2H2O	430	0.80	1.86E-03
ZnSO4. 7H2O	288	8.00	2.78E-02

3.6 References

1. Brown, G.D., et al., *Hidden killers: human fungal infections.* Sci Transl Med, 2012. **4**(165): p. 165rv13.
2. European Centre for Disease Prevention and Control (ECDC), *European Centre for Disease Prevention and Control. Risk assessment on the impact of environmental usage of triazoles on the development and spread of resistance to medical triazoles in Aspergillus species.* 2013.
3. Cohen, J., et al., *Particle size matters: diagnostics and treatment of small airways involvement in asthma.* Eur Respir J, 2011. **37**(3): p. 532-40.
4. Araujo, R. and A.G. Rodrigues, *Variability of germinative potential among pathogenic species of Aspergillus.* J Clin Microbiol, 2004. **42**(9): p. 4335-7.
5. de Vries, R.P., et al., *Comparative genomics reveals high biological diversity and specific adaptations in the industrially and medically important fungal genus Aspergillus.* Genome Biol, 2017. **18**(1): p. 28.
6. McDonagh, A., et al., *Sub-telomere directed gene expression during initiation of invasive aspergillosis.* PLoS Pathog, 2008. **4**(9): p. e1000154.
7. Casadevall, A., et al., *The 'Amoeboid Predator-Fungal Animal Virulence' Hypothesis.* J Fungi (Basel), 2019. **5**(1).
8. Papastamoulis, P., et al., *Bayesian Detection of Piecewise Linear Trends in Replicated Time-Series with Application to Growth Data Modelling.* Int J Biostat, 2019.
9. Bates, D., et al. *Fitting Linear Mixed-Effects Models using lme4*. arXiv e-prints, 2014.
10. Paradis, E. and K. Schliep, *ape 5.0: an environment for modern phylogenetics and evolutionary analyses in R.* Bioinformatics, 2019. **35**(3): p. 526-528.
11. Bertuzzi, M., et al., *The pH-responsive PacC transcription factor of Aspergillus fumigatus governs epithelial entry and tissue invasion during pulmonary aspergillosis.* PLoS Pathog, 2014. **10**(10): p. e1004413.
12. Bignell, E., et al., *Secondary metabolite arsenal of an opportunistic pathogenic fungus.* Philos Trans R Soc Lond B Biol Sci, 2016. **371**(1709).

13. Willger, S.D., et al., *A sterol-regulatory element binding protein is required for cell polarity, hypoxia adaptation, azole drug resistance, and virulence in Aspergillus fumigatus.* PLoS Pathog, 2008. **4**(11): p. e1000200.
14. Arendrup, M.C., et al., *EUCAST technical note on Aspergillus and amphotericin B, itraconazole, and posaconazole.* Clin Microbiol Infect, 2012. **18**(7): p. E248-50.
15. Carrillo, A.J., et al., *Functional Profiling of Transcription Factor Genes in Neurospora crassa.* G3 (Bethesda), 2017. **7**(9): p. 2945-2956.
16. Colot, H.V., et al., *A high-throughput gene knockout procedure for Neurospora reveals functions for multiple transcription factors.* Proc Natl Acad Sci U S A, 2006. **103**(27): p. 10352-10357.
17. Son, H., et al., *A phenome-based functional analysis of transcription factors in the cereal head blight fungus, Fusarium graminearum.* PLoS Pathog, 2011. **7**(10): p. e1002310.
18. Giaever, G., et al., *Functional profiling of the Saccharomyces cerevisiae genome.* Nature, 2002. **418**(6896): p. 387-91.
19. Homann, O.R., et al., *A phenotypic profile of the Candida albicans regulatory network.* PLoS Genet, 2009. **5**(12): p. e1000783.
20. Schwarzmuller, T., et al., *Systematic phenotyping of a large-scale Candida glabrata deletion collection reveals novel antifungal tolerance genes.* PLoS Pathog, 2014. **10**(6): p. e1004211.
21. Betts, M.F., et al., *Development of a high throughput transformation system for insertional mutagenesis in Magnaporthe oryzae.* Fungal Genet Biol, 2007. **44**(10): p. 1035-49.
22. Gravelat, F.N., et al., *Aspergillus fumigatus MedA governs adherence, host cell interactions and virulence.* Cell Microbiol, 2010. **12**(4): p. 473-88.
23. Richie, D.L., et al., *A role for the unfolded protein response (UPR) in virulence and antifungal susceptibility in Aspergillus fumigatus.* PLoS Pathog, 2009. **5**(1): p. e1000258.
24. Rocha, M.C., et al., *Aspergillus fumigatus MADS-Box Transcription Factor rlmA Is Required for Regulation of the Cell Wall Integrity and Virulence.* G3 (Bethesda), 2016. **6**(9): p. 2983-3002.

25. Shepardson, K.M., et al., *Hypoxia enhances innate immune activation to Aspergillus fumigatus through cell wall modulation.* Microbes Infect, 2013. **15**(4): p. 259-69.
26. Zhang, Y.Q., et al., *Requirement for ergosterol in V-ATPase function underlies antifungal activity of azole drugs.* PLoS Pathog, 2010. **6**(6): p. e1000939.
27. Liu, G., et al., *Elimination of the last reactions in ergosterol biosynthesis alters the resistance of Saccharomyces cerevisiae to multiple stresses.* FEMS Yeast Res, 2017. **17**(6).
28. Song, L., et al., *A transcription factor hierarchy defines an environmental stress response network.* Science, 2016. **354**(6312).
29. Chen, D., et al., *Global transcriptional responses of fission yeast to environmental stress.* Mol Biol Cell, 2003. **14**(1): p. 214-29.
30. Gasch, A.P., *Comparative genomics of the environmental stress response in ascomycete fungi.* Yeast, 2007. **24**(11): p. 961-76.
31. Gasch, A.P., et al., *Genomic expression programs in the response of yeast cells to environmental changes.* Mol Biol Cell, 2000. **11**(12): p. 4241-57.
32. Dinamarco, T.M., et al., *Molecular characterization of the putative transcription factor SebA involved in virulence in Aspergillus fumigatus.* Eukaryot Cell, 2012. **11**(4): p. 518-31.
33. Hagiwara, D., et al., *The role of AtfA and HOG MAPK pathway in stress tolerance in conidia of Aspergillus fumigatus.* Fungal Genet Biol, 2014. **73**: p. 138-49.
34. Taymaz-Nikerel, H., A. Cankorur-Cetinkaya, and B. Kirdar, *Genome-Wide Transcriptional Response of Saccharomyces cerevisiae to Stress-Induced Perturbations.* Front Bioeng Biotechnol, 2016. **4**: p. 17.
35. Diard, M. and W.D. Hardt, *Evolution of bacterial virulence.* FEMS Microbiol Rev, 2017. **41**(5): p. 679-697.
36. Azadmanesh, J., et al., *Filamentation Involves Two Overlapping, but Distinct, Programs of Filamentation in the Pathogenic Fungus Candida albicans.* G3 (Bethesda), 2017. **7**(11): p. 3797-3808.
37. Chauhan, R., et al., *Reconstruction and topological characterization of the sigma factor regulatory network of Mycobacterium tuberculosis.* Nat Commun, 2016. **7**: p. 11062.

38. Moyes, D.L., et al., *Candidalysin is a fungal peptide toxin critical for mucosal infection.* Nature, 2016. **532**(7597): p. 64-8.
39. Nobile, C.J., et al., *A recently evolved transcriptional network controls biofilm development in Candida albicans.* Cell, 2012. **148**(1-2): p. 126-38.
40. Jung, K.W., et al., *Systematic functional profiling of transcription factor networks in Cryptococcus neoformans.* Nat Commun, 2015. **6**: p. 6757.
41. Hillmann, F., et al., *Virulence determinants of the human pathogenic fungus Aspergillus fumigatus protect against soil amoeba predation.* Environ Microbiol, 2015. **17**(8): p. 2858-69.

Chapter

4

Development of marker-free gene tagging and gene mutation system using a CRISPR-Cas9 mediated transformation in the pathogenic mold *Aspergillus fumigatus*

Norman van Rhijn, Takanori Furukawa, Can Zhao, Beth McCann, Elaine Bignell, Michael Bromley

4. Development of marker-free gene tagging and gene mutation system using a CRISPR-Cas9 mediated transformation in the pathogenic mold Aspergillus fumigatus

Authors: Norman van Rhijn[1,2], Takanori Furukawa[1,2], Can Zhao[1,2,] Beth McCann[1,2], Elaine Bignell[1,2] Michael J Bromley[1,2]

[1] Manchester Fungal Infection Group, Division of Infection, Immunity and Respiratory Medicine, Faculty of Biology, Medicine and Health, University of Manchester, CTF Building, 46 Grafton Street, Manchester, M13 9NT, UK.

[2] Lydia Becker Institute of Immunology and Inflammation, Manchester Collaborative Centre for Inflammation Research, Division of Infection, Immunity and Respiratory Medicine, Faculty of Biology, Medicine and Health, University of Manchester, Manchester Academic Health Science Centre, Manchester, UK.

Target Journal: Fungal Biology & Genetics

Abstract:

Aspergillus fumigatus is a saphrophytic fungal pathogen, which is the cause of more than 300,000 life threatening infections annually. Our understanding of pathogenesis and factors contributing to disease progression are limited. Development of rapid and versatile gene editing methodologies for *A. fumigatus* is essential. CRISPR-Cas9 mediated transformation has been widely used as a novel genome editing tool. In *A. fumigatus*, this technique has been recently developed and used for a variety of editing techniques, such as protein tagging and gene deletions. However, successful transformation relies on extensive cloning paired with the use of selection markers. We have used an *in vitro* CRISPR-Cas9 assembly methodology to perform selection free transformations. The repair template used during this transformation can be obtained with a single PCR reaction, decreasing time required for difficult genome editing techniques such as protein tagging and gene deletion.

4.1 Introduction

A. fumigatus is a saphrophytic fungus and the primary aetiological agent of invasive aspergillosis. This disease affects immunocompromised individuals and causes over 200,000 life-threatening infections annually. *A. fumigatus* may also cause chronic and allergic diseases in immunocompetent individuals which affects around 3 million and 20 million people, respectively [1]. Our understanding of the pathogen and host factors that contribute to these diseases is limited. Unlike the model yeast *Saccharomyces cerevisiae*, targeted allele replacement in *A. fumigatus* is complicated by low rates of homologous recombination and the fact that replacement cassettes require long homology arms (LHA), typically 1,000 bp [2]. The low homologous recombination efficiency was partly solved by employing strains deficient in the non-homologous end-joining (NHEJ) pathway (Δ*ku80*, Δ*ku70, and* Δ*lig4* strains). However, LHAs are still required to facilitate homologous recombination in these strains [3]. Construction of gene replacement cassettes with LHAs can be achieved rapidly using PCR based fragment fusion approaches [4]. However, generation of gene tagging or promoter replacement cassettes where there is limited flexibility for the integration site, or point mutations cassettes, where four or more DNA fragments need to be combined becomes laborious. To accelerate functional genomics research in *A. fumigatus* and other filamentous fungi, the development of rapid and versatile gene tagging and mutagenesis methodologies is necessary.

Genome editing technologies that employ clustered regularly interspaced short palindromic repeats (CRISPR) and CRISPR-associated nucleases (CAS), have been applied to filamentous fungi [5-9]. The most straightforward of these mutagenesis approaches takes advantage of the type II CRISPR system derived from *Streptococcus pyogenes*. In this system, site directed DNA cleavage is carried out by the RNA-guided endonuclease, Cas9 which is directed to its target by a guide RNA (gRNA) consisting of crRNA and tracrRNA [10]. The crRNA is a short sequence that is complementary to the target sequence. The tracrRNA anneals to the crRNA as a scaffold between the Cas9 protein and the RNA complex. The gRNA binds to Cas9, which results in formation of a RNP (ribonucleoprotein) complex to catalyse a double-strand break in the target DNA. Repair of the damaged DNA is managed through use of available complementary DNA. In 2015, CRISPR-Cas9 was

successfully utilised in several *Aspergillus* species using a system that relied on in vivo expression of Cas9 and gRNA from the *tef1* and *gdpA* promoters, respectively [8]. In *A. fumigatus,* the first introduction of the CRISPR-Cas9 technology was based upon a three-component system and was exemplified by causing a point-mutation within the polyketide synthase gene *pksP* that is required for the biosynthesis of DHN-melanin which gives *A. fumigatus* spores their green colour. This system incorporated the *cas9* gene and the *pskP*-gRNA, each constitutively expressed *in vivo* [5]. Following this study, the first micro-homology mediated end joining CRISPR-Cas9 system was developed based on transformation with two plasmids; one containing the Cas9 gene and the other the *pksP*-sgRN, resulting in insertion of a repair template within the *pskP* gene [11]. Furthermore, this methodology was used to insert a GFP tag towards the N-terminus of CnaA [11] and it has been used for promoter replacements using a *hph-hspA* repair template [12].

These studies relied on *in vivo* expression of Cas9 and the gRNA. Recently, an *in vitro* assembled CRISPR-Cas9 transformation system combined with microhomology repair templates was developed [13]. This methodology is highly efficient, rapid and, as it does not require *in vivo* expression of the Cas9 nuclease and gRNA, limits the possibility of off-target effects and is highly flexible [14]. Here we present further exemplification of this *in vitro* CRISPR-Cas9 transformation methodology and show that can be widely applied for various genetic manipulations. Specifically we demonstrate that gene replacement and protein fusions are generated with such high efficiency that the technique can be carried out without the need of a selection marker, therefore bypassing the need to generate complex constructs.

4.2 Materials and Methods

4.2.1 Strains, plasmids, gRNA and repair template generation

A. fumigatus MFIG001 (Δ*ku80*::*AnpyrG,* Δ*pyrG*::*AfpyrG*) was used as the parental isolate for transformations (Furukawa et al. in press). The hygromycin resistance cassette was amplified from the pAN7.1 plasmid. GFP and 3xFLAG were amplified from PUpacC-GFP and PUpacC-3xFLAG, respectively. EuPaGDT is a program that can be used for designing a target specific guide RNA as well as oligos to prepare a repair template providing us a versatile gRNA-designing platform. Since the genome sequence of our model strain *A. fumigatus* MFIG001 (derived from the clinical strain CEA10) is not available on the webserver, we manually uploaded the genome of the strain, which was downloaded from CADRE genomic database [15], and run the program with default setting to design gRNAs to the *aft4, pacC* and *srbA* loci. As a result, several candidate gRNAs were obtained, and one of the closest gRNAs to the target integration sites with the highest QC scores was manually selected for the transformation experiments (Table 4.1). To prepare DNA fragments for homology directed repair (HDR) mediated transformation, 50-bp of homology arms are included during the primer design. Generally, point mutations were introduced into the PAM sequence within the repair template to prevent any degradation of the template during and after transformation by receiving an attack from the target gRNA-assembled Cas9. However, since the *in vitro* assembled Cas9-mediated transformation only allows a transient existence of gRNA-Cas9 complex in the fungus, we didn't introduce mutations into the PAM sequence of our repair template.

RNP complexes were assembled *in vitro* using purified Cas9 protein, tracrRNA and locus specific crRNA (Integrated DNA Technologies). TracrRNA and crRNA were resuspended in nuclease-free duplex buffer (Integrated DNA Technologies) and hybridized by mixing equal amounts in duplex buffer. This was heated to 98 °C and cooled to room temperature gradually in a thermal cycler for 10 minutes. To generate RNPs hybridised crRNA and tracrRNA was mixed with Cas9 protein in Cas9 working buffer and incubated at room temperature for 5 minutes. Repair templates were generated by PCR using primers listed in Table 4.1 with Phusion Flash Master Mix (Thermo Fisher Scientific). PCR products were validated and purified by gel

electrophoresis followed by gel extraction following the Nucleospin protocol (Macherey-Nagel).

Table 4.1 Primers and guide RNA used in this study

Guide RNA_ID	5'-3'	Use
atfA_crRNA_273	TCTCCTTCATAAGCGACCAG	Guide RNA for *atf4*
pacC_crRNA_174	AAGGGACAAGAAATCAGTCT	Guide RNA for *pacC*
srbA_crRNA_3066	TCATCATCACTACGACTCAT	Guide RNA for C-terminal tagging
srbA_crRNA_82	TGAAACACGATGTCCACCCC	Guide RNA for N-terminal tagging
Primers	**5'-3'**	**Use**
aft4-hph-HDR_Fw	TCTTCCAGTTCTGGATATAGCATATAGATCTTCTCCTTCATAAGCGACCACCGGCTCGGTAACAGAACTA	amplification of the HDR template
aft4-hph-HDR_Rv	TTATGATTTGGCCTCCATACTCCCCTGATCTCAATCCAGTTGAGAACCTCGTTGGAGCATATCGTTCAGAGC	amplification of the HDR template
pacC-HDR-Fw	GACTTTACAGCTTGTTTTGCG	primer for PCR amplification and sequencing
pacC-HDR_Rv	CAAGCAGGAAAGTTGTTCATC	primer for PCR amplification and sequencing
pacC-174-HDR_Fw1	ATATCCTCCCTTCATTCTCCGCTGCTCCCAAGAAAAGGGACAAGAAATCAGTCTTGGCACAATGGACTACAAGGACCACGACG	amplification of the HDR template
pacC-174-HDR_Fw2_PAM	ATATCCTCCCTTCATTCTCCGCTGCTCCCAAGAAAAGGGACAAGAAATCAGTCTTCGCACAATGGACTACAAGGACCACGACG	amplification of the HDR template
pacC-174-HDR_Rv1	GAAGGCGAAGCAGTTGTGTTGTTGTTGGTTGCGGTATCTTGGTGTTCAGACTTATCGTCATCGTCCTTGTAATC	amplification of the HDR template
pacC-174-HDR_Rv2	GAAGGCGAAGCAGTTGTGTTGTTGTTGGTTGCGGTATCTTGGTGTTCAGACTTATCGTCATCGTCCTTG	amplification of the HDR template
srbA_NGF_Fw	GACTATTCTCAGTACATCTGATGGTCCAAGACCAGCAGTGAAACACGATGGTGAGCAAGGGCGAGGAGCTGTTC	amplification of N-terminal GFP
srbA_NGF_Rv	GACTCGAGAGGTGAGAACAACTGGAAATCCCCACCAATGCCGGGGGTGGACCATGTTTCGCGCGGCCGC	amplification of N-terminal GFP
srbA_NFL_Fw	GACTATTCTCAGTACATCTGATGGTCCAAGACCAGCAGTGAAACACGATGGACTACAAGGACCACGACGGCGAC	amplification of N-terminal 3xFLAG
srbA_NFL_Rv	GACTCGAGAGGTGAGAACAACTGGAAATCCCCACCAATGCCGGGGGTGGACTTATCGTCATCGTCCTTGTAATC	amplification of N-terminal 3xFLAG
srbA_CGF_Fw	CTGGCGGCAATGAAGAAGCCTCTGACAATCTACTGCTCTCCGATGAGTCGGTGAGCAAGGGCGAGGAGCTGTTC	amplification of C-terminal GFP
srbA_CGF_Rv	TACTCTGCTCGCCAGCTTTCAAGCTTCTGGCAGTAGCGTCATCATCACTACCATGTTTCGCGCGGCCGC	amplification of C-terminal GFP
srbA_CFL_Fw	CTGGCGGCAATGAAGAAGCCTCTGACAATCTACTGCTCTCCGATGAGTCGGACTACAAGGACCACGACGGCGAC	amplification of C-terminal 3xFLAG
srbA_CFL_Rv	TACTCTGCTCGCCAGCTTTCAAGCTTCTGGCAGTAGCGTCATCATCACTACTTATCGTCATCGTCCTTGTAATC	amplification of C-terminal 3xFLAG
srbA_N-term_Seq_Fw	TCTCCTGATTAGCGTGCTCG	PCR amplification and sequencing of N terminal tagged SrbA
srbA_N-term_Seq_Rv	CGAAGCATTTGCAGTTTCTGG	PCR amplification and sequencing of N terminal tagged SrbA
srbA_C-term_Seq_Fw	CGGCTTCACGTCAAACCTTG	PCR amplification and sequencing of C terminal tagged SrbA
srbA_C-term_Seq_Rv	ACCGAGAGAGAAACGCCTTG	PCR amplification and sequencing of C terminal tagged SrbA

4.2.2 Transformation and validation of transformants

Our CRISPR-Cas9 transformation protocol is based upon methodology from Al Abdallah [13]. Briefly, conidia were inoculated in liquid *Aspergillus* Complete Medium (ACM) at a concentration of 1 x 10^6 conidia/mL and cultured for 16 h at 37 °C with shaking at 120rpm. Mycelia were harvested through filtration with Myracloth and resuspended in ACM with protoplasting buffer (Vinotaste®Pro (Lamoth-Abiet) in KCl+Citric Acid). This was incubated for 4 h at 37 °C with shaking at 120rpm. Protoplasts were harvested through filtration and centrifuging for 10 minutes at 3,500rpm. Protoplasts were washed 3 times in KCl and resuspended in KCl+$CaCl_2$. This was mixed with repair template, RNP complexes (see above) and PEG-$CaCl_2$ buffer and incubated on ice for 50 minutes. 1 mL of PEG-$CaCl_2$ was added and incubated at room temperature for 25 minutes. Transformation mixture was plated on YPS plates containing either hygromycin (120 µg/mL) or no selection and incubated at room temperature for 24 h. Subsequently, plates were incubated at 37 °C for 3 days. Transformants were purified by streaking on ACM twice and harvested for downstream analysis. DNA of transformants was extracted via Cetyl Trimethyl Ammonium Bromide (CTAB) extraction [16]. Validation PCR was

performed using Phusion Flash Master Mix (Thermo Fisher Scientific) and respective primer pairs (Supplemental Table 4.1). PCR products were assessed by gel electrophoresis. Sanger sequencing was performed by Source Bioscience.

4.2.3 Fluorescent microscopy

2000 spores of *A. fumigatus* SrbA-GFP and PacC-GFP were grown for 16 h at 37 °C in 200 µL Watch Minimal Media (WMM) in an 8 well chamber (Ibidi). SrbA-GFP and PacC-GFP were shifted for 3 h to WMM + 0.25 mg/L itraconazole (Sigma) or WMM (pH 8.0), respectively. Fluorescent and bright field live-cell imaging were performed using a Leica TCS SP8 confocal laser scanning microscope equipped with hybrid GaAsP (HyD) detectors and a 63× water immersion objective. Argon laser 488nm was used for fluorescence excitation. Confocal microscopy images were analysed and processed with Imaris 8.0 developed by Bitplane (Zurich, Switzerland).

4.2.4 Western Blotting

Western blotting was performed as previously described [17]. As primary antibody a GFP-polyclonal antibody A11122 (ThermoFischer Scientific) and Anti-FLAG polyclonal antibody FLAG7425 (Sigma) were used. Goat anti-rabbit IgG H&L Ab6721 (Abcam) was used as a secondary antibody.

4.3 Results

4.3.1 High efficiency transformation using an in vitro CRISPR-Cas9 system reveals the potential for marker-less genome editing of Aspergillus fumigatus.

In previous studies, two different gRNAs were used to introduce a gene replacement cassette using the *in vivo* assembled CRISPR-Cas9 transformation system [5, 13]. However, single gRNA mediated insertion of a homology directed repair (HDR) template was not investigated. We adopted an experimental pipeline (Figure 4.1) by combining a web-based gRNA designing software EuPaGDT (http://grna.ctegd.uga.edu/) and the *in vitro*-assembled CRISPR-Cas9 mediated transformation system [13, 18] to assess the efficiency of single gRNA mediated insertion of a 2.7-kb of a hygromycin resistance marker (*hph*) with 50bp homology arms into the *A. fumigatus* genome. To this end, a guide RNA was designed to target *aft4*, a locus that appears to encode a non-functional transposable element due to a non-sense mutation within the putative transposase-encoding gene [19]. Detailed molecular characterization of this locus will be described elsewhere (Furukawa et al. in preparation).

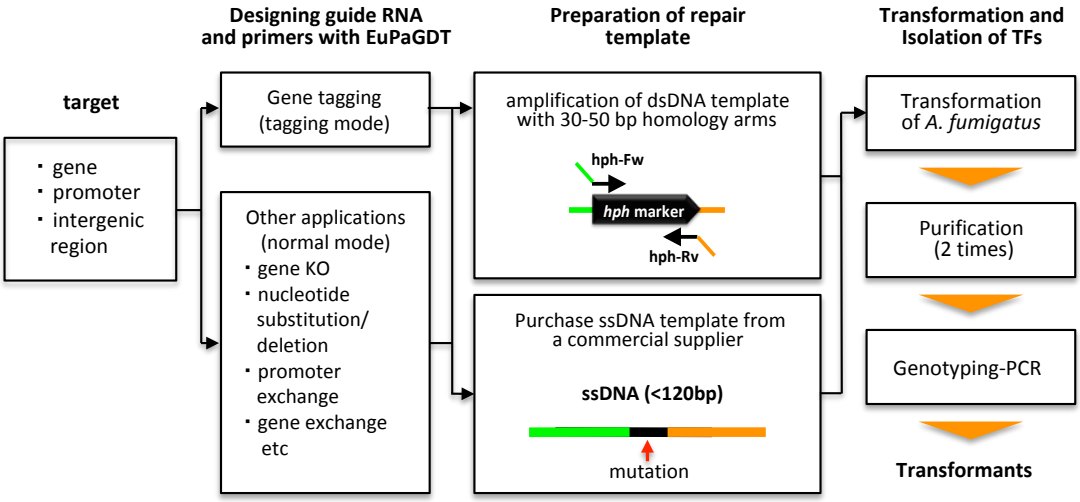

Figure 4.1 Workflow of CRISPR-Cas9 mediated transformation in *A. fumigatus*. The target sequence was used as input for EuPaGDT to design the gRNA. This tool includes tagging mode for epitope tagging and normal mode for other applications. gRNA includes design of the homology arms. The repair template can either be designed to be amplified or purchased as an oligo.

In our preliminary experiments gRNA^{aft4}-Cas9 complex mediated transformation of the *hph* cassette into MFIG001 protoplasts yielded 272 hygromycin resistant colonies from c.300 protoplasts, indicating that the *hph* cassette had been incorporated into the nuclei of around 91% of protoplasts (Supplemental Figure 1). 95 candidate transformants were single colony purified two times under hygromycin selection and integration of the *hph* cassette at the *aft4* locus was analysed by PCR (Figure S4.1). This revealed a remarkably high efficiency (93 %) of gene integration in the single gRNA mediated DNA integration (Figure 4.2).

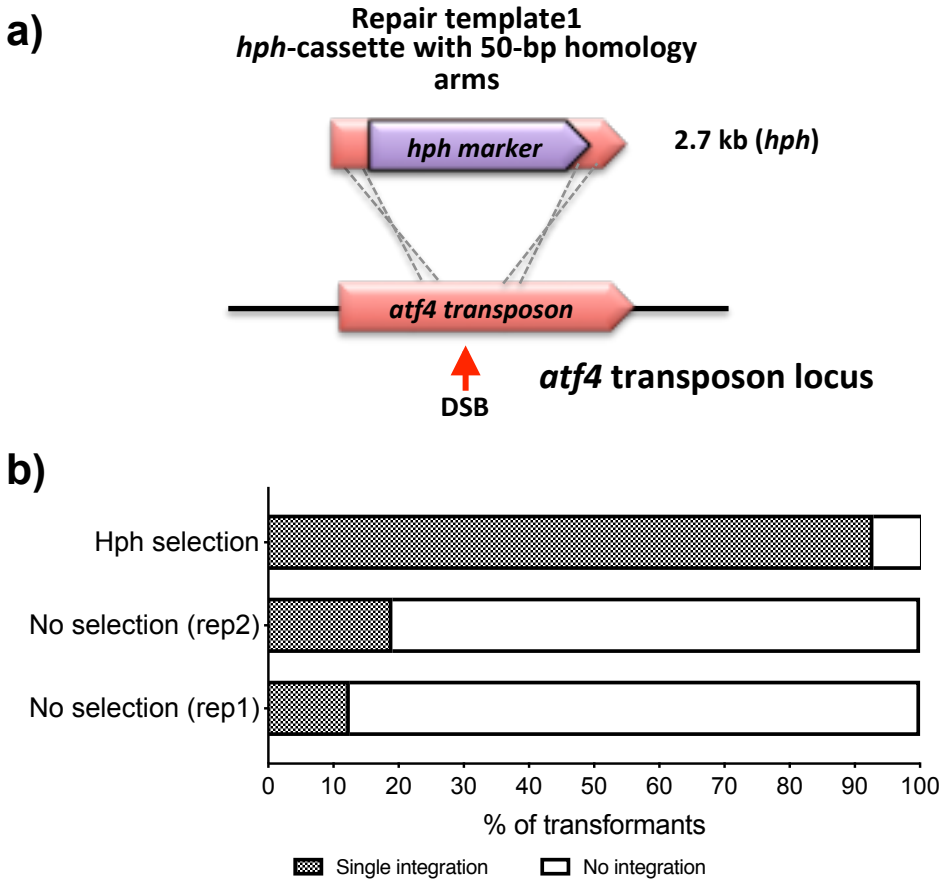

Figure 4.2 CRISPR-Cas9 transformation using a selective and non-selective conditions a) Schematic representation of CRISPR-Cas9 mediated gene replacement of *aft4*. b) Efficiency of integration of DNA into the *A. fumigatus* MFIG001 genome either with or without hygromycin selection after transformation. Under selective conditions efficiency is up to 90% of all transformants, while under non-selective conditions, efficiency is 10-20%.

As the frequency of transformation in our pilot experiment was so high, we investigated the possibility of non-selection marker mediated transformation of *A. fumigatus*. Again we performed a gRNA^{aft4}-Cas9 complex mediated transformation of MFIG001 protoplasts using the same mutagenesis cassette. However on this occasion, the transformation mix was plated on media lacking hygromycin. Growing colonies were colony-purified twice under non-selective conditions. Of the candidate transformants assessed by PCR from 2 independent experiments (n = 95 from each), 19% and 12.5% of transformants resulted in a positive signal for integration of the *hph* cassette-containing repair template (Figure 4.2).

4.3.2 Development of a marker-free epitope-tagging method using the CRISPR-Cas9 system.

Our ability to perform directed gene replacement without the need for selection prompted us to assess if we would be able to introduce epitope-tags to genes without selection. Chimeric proteins are often used to facilitate our understanding of a number of aspects of protein function such as protein localisation and identification of interacting partners. The generation of protein fusion cassettes can however be a time consuming process, requiring integration of multiple components. The well characterized pH-responsive transcription factor PacC was selected as a target for our study. An eGFP-encoding HDR template was amplified by PCR using primers that incorporated 50-bp homology arms to target the PAM site proximate to the *pacC* start codon and was introduced into MFIG001 using gRNA mediated CRISPR-Cas9 transformation to the N-terminal region of the *pacC*-encoding gene. Since we found that integration of the *hph* cassette at the *aft4* locus occurred with 10-20% efficiency, we selected 95 candidate strains that were recovered on, and subsequently purified on a non-selective medium (Sabouraud agar). Integration of the eGFP tag was assessed by PCR (Figure S4.2). Consistent with the results of the insertion of the *hph* marker, we successfully obtained transformants, which showed integration of *egfp*-tag at the desired locus for 13/95 (14%) of strains. Precise integration of eGFP at the start codon of the *pacC* gene and absence of any other mutations at this site was confirmed by Sanger sequencing (Figure 4.3).

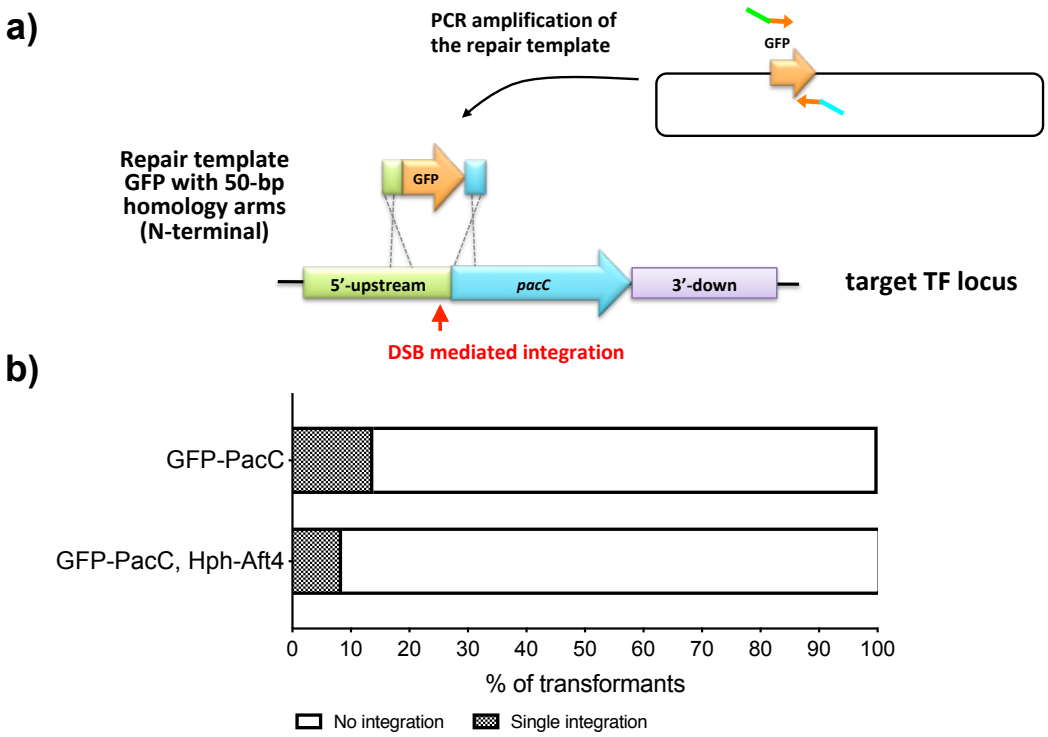

Figure 4.3 Epitope tagging using non-selective CRISPR-Cas9 transformation and co-transformation with a selectable marker a) Schematic of epitope tagging for *pacC* eGFP and cotransformation with the hygromycin marker. **b)** Efficiency of C-terminal GFP integration to the *pacC* locus with and without cotransformation of the hygromycin selection marker towards the *aft4* locus

In an attempt to improve the efficiency of integration of the egfp-tag, we investigated a co-transformation approach, in which the *pacC*-targeted *e*GFP-tag was introduced together with the *atf4* targeted *hph* marker. The transformants were selected on media containing hygromycin and analyzed by PCR as described above (Figure S4.3). No improvements were observed, as 8.5% of the *hph* positive transformants showed co-insertion of the *egfp*-tag at the *pacC* locus (Figure 4.3). To further exemplify our gene tagging strategy, we tested integration of a short tag sequence (3XFLAG tag, 63 bp) together with the *egfp*-tag (0.7 kbp) in a different genetic locus. We selected *srbA*, which encodes a sterol regulatory element binding protein that mediates ergosterol biosynthesis in *A. fumigatus,* as a target because integration of an epitope tag has already been reported at this locus at both N- and C-terminal region of the protein [20].

A PCR amplified eGFP- or 3XFLAG-encoding HDR template with 50-bp homology arms to either the N- or C-terminus of the coding sequence was

introduced with a gRNA mediated CRISPR-Cas9 transformation. We isolated and purified 10 different candidates on a non-selective medium (Sabouraud agar), and examined integration of each tag using PCR. In agreement with the other non-selection mediated transformation attempts, we obtained two GFP C-terminal SrbA mutants, two N-terminal 3xFLAG tagged SrbA mutants and one C-terminal 3xFLAG tagged SrbA mutant. By Sanger sequencing of the PCR products we were able to confirm precise integration of the epitope-tag cassette without introducing any other mutation at the target site (Figure 4.4a-c). Furthermore, we confirmed expression of the epitope-tagged SrbA protein in all PCR-positive mutants by Western blotting using a corresponding epitope-tag specific antibody (Figure 4.4d). Localisation of the PacC and SrbA-GFP proteins were assessed using confocal microscopy. The PacC transcription factor is required under alkaline conditions and the SrbA transcription factor is activated during azole mediated depletion in ergosterol biosynthesis [21, 22]. Localisation to the nucleus for PacC-GFP and SrbA-GFP after alkaline shift or itraconazole treatment respectively was confirmed by fluorescent microscopy, (Figure 4.4e, Figure 4.5).

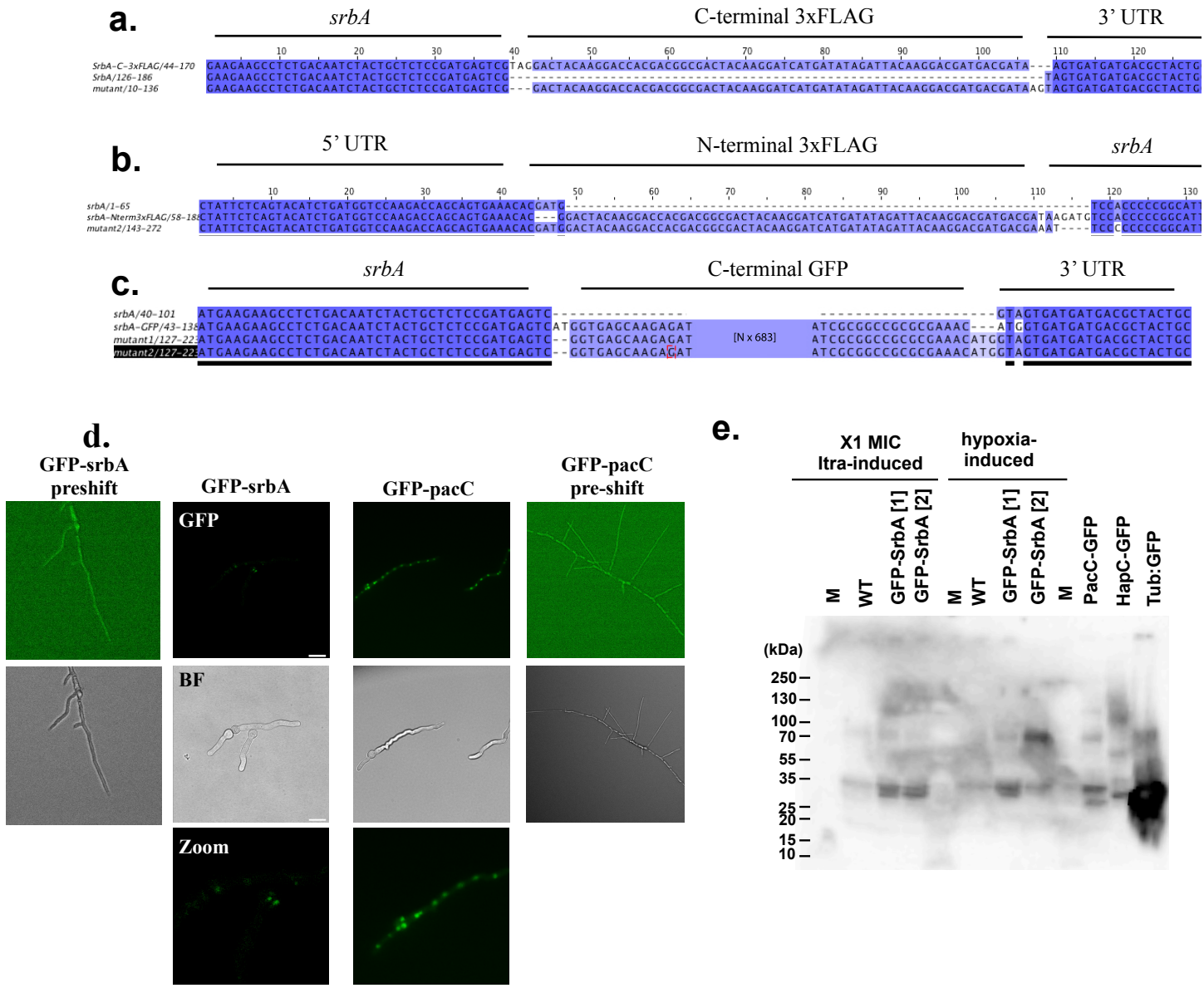

Figure 4.4: Integration of epitope tags into the *pacC* and *srbA* locus via CRISPR-Cas9 transformation. a-c) Multiple alignments of C-terminal 3xFLAG tagged, N-terminal 3xFLAG and C-terminal GFP tagged *srbA* locus, respectively. Wildtype sequence and predicted sequence are included as controls, **d)** Fluorescence microscopy of the GFP-SrbA and GFP-PacC after itraconazole or pH shift, respectively. Showing Brightfield (BF) and a digitally zoomed view towards single nuclei (scalebar equals 50 µm) **e)** Whole-cell protein extract of GFP tagged SrbA strains, isogenic wildtype, PacC-GFP (control), HapC-GFP (control) and Tubulin-GFP (control) analyzed by Western blotting using an anti-GFP polyclonal antibody.

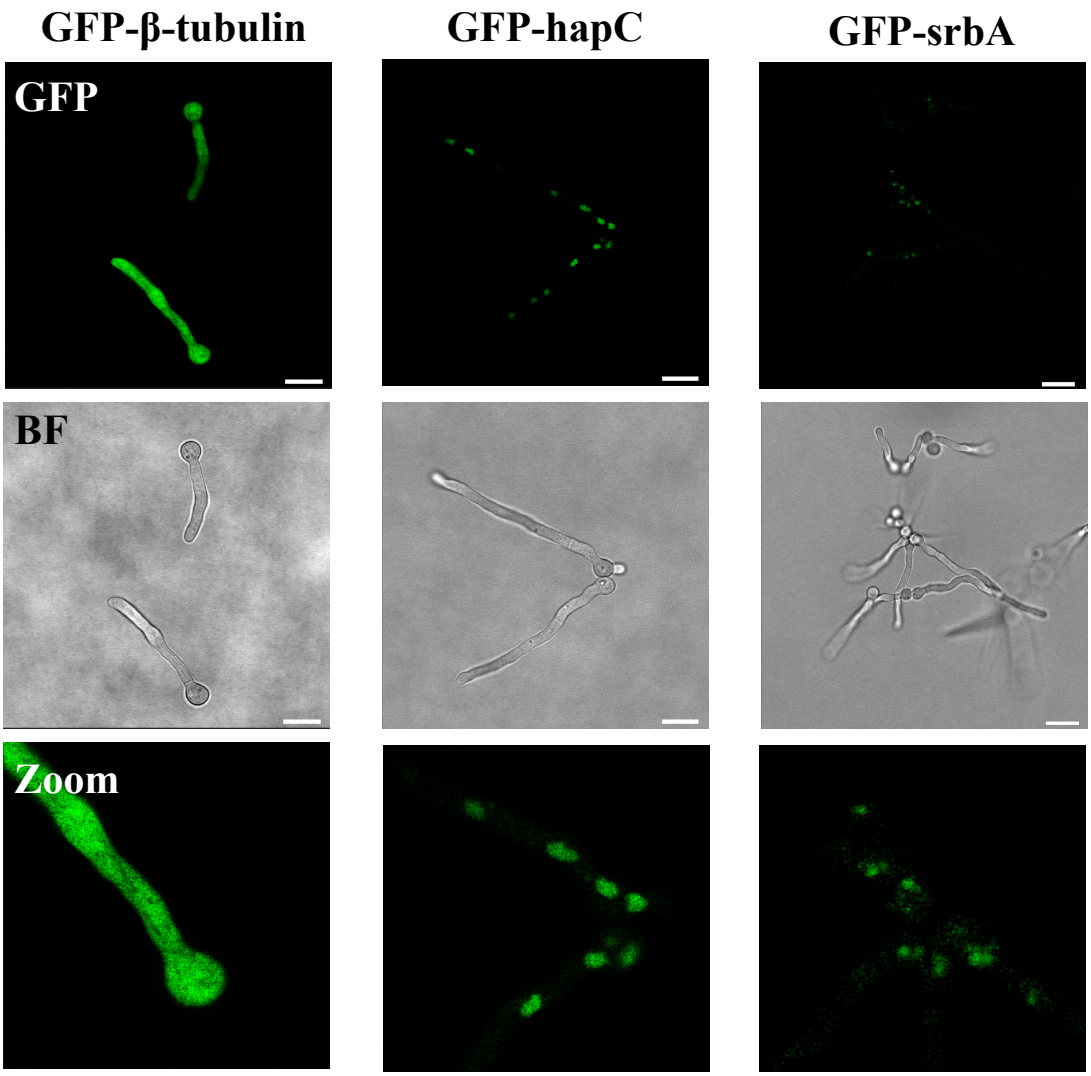

Figure 4.5. Confocal microscopy of CRISPR transformed GFP-SrbA. Controls including beta-tubulin GFP and GFP-hapC to assess signal strength were included. HapC is a highly expressed component of the CBC complex, which is localised within the nucleus. GFP-srbA localisation was assessed 2 hours after an itraconazole shift.

4.3 Discussion

In this study we have developed and optimised a useful range of selection-free CRISPR based genome-editing techniques. These methodologies allow targeted genetic manipulations overcoming the need for time consuming and complex cassette construction, and the use of dominant selection markers that incorporate promoters that drive high levels of expression and have the potential to interfere with the outcome of experiments. To date, constructing protein fusion constructs and generating strains with targeted point mutations have been labour intensive due to the need for large constructs including dominant markers such as the hygromycin, pyrithimine or bleomycin resistance cassettes. Initial CRISPR/Cas9 systems for manipulation of filamentous fungi used *in vivo* expressed Cas9 endonuclease. Expression of Cas9 is generally under the expression of constitutive or highly expressed inducible promoters resulting in the production of high levels of Cas9 protein. However, evidence from *S. cerevisiae* and *Magnaporthe oryzae* suggests overexpression of Cas9 is toxic to the cells resulting in reduction of viability, in line with observations in human cell lines [23-25]. A recent iteration of this system used *in vitro* assembly of RNP complexes resulting in a highly efficient transformation of *A. fumigatus* protoplasts while reducing toxicity [13]. Furthermore, *in vitro* assembly and transformation does not result in increased off target mutations [14]. It was evident that this efficiency could lend itself to a selection free CRISPR/Cas9 transformation methodology.

Epitope tagging of proteins via CRISPR mediated transformation was first developed in mammalian cells to generate fluorescent isolates (CRISPR-TAG) [26, 27]. In *Magnaporthe oryzae* and *Fusarium oxysporum* GFP fusion proteins via CRISPR/Cas9 mediated transformation have been constructed. However, construct generation via these methods is time consuming and requires several transformations [28, 29]. Using microhomology arms of 30bp and a single plasmid based CRISPR system Zhang et al were able to construct a functional C-terminal CnaA GFP protein fusion in *A. fumigatus* [11]. However, a non-targeted hygromycin selection marker was used that randomly integrated into the genome, potentially resulting in off-target effects. With our transformation methodology both C-terminal and N-terminal fusion protein strains could be obtained with a similar rate of integration (10-20%) without introduction of a selection marker. Furthermore, marker-free transformation keeps

the flanking regions of the target gene unedited. Insertion of a selectable marker driven by a strong promoter can have effect on expression of the target gene. The untranscribed region has a function in regulation of translation and mRNA stability. For example, in *A. nidulans* the 3' UTR of the *areA* mRNA is involved in transcript degradation [30], as is the *niaD* transcript that is affected by deadenylation of the 3' UTR [31].

Using selection-mediated transformation, over 90% transformation efficiency was observed. However, this dropped to 10% under non-selective conditions. Transformants are generated from multi-nucleate protoplasts, potentially causing the loss of transformants upon non-selective purification (Figure S4.4). Producing uninucleate protoplasts, potentially from spores, needs to be explored to overcome loss of transformants upon purity. In this study we have used a Δ*ku80* strain, which lacks a functional NHEJ-pathway. This background is generally used as a lab strain due to higher transformation efficiency. Cas9 DSBs can be repaired through either NHEJ or homologous recombination pathways, but are generally generated through the NHEJ pathway [32]. However, efficiency of CRISPR/Cas9 transformation through homologous recombination in NHEJ competent backgrounds has not been assessed. This may indicate that the marker-free system detailed in this study would be significantly less effective in strains that are NHEJ competent and reduce the utility of this method for the evaluation of environmental and clinical isolates. To overcome this, inhibition of NHEJ via chemical inhibitors can significantly increase HDR efficiency [33-35]. Inhibition of NHEJ has been studied in *C. neoformans* where addition of several chemical inhibitors significantly increases integration via homologous recombination [36]. Expression of recombinant proteins can increase the efficiency of homologous recombination. A Rad52-Cas9 fusion increased transformation efficiency up to 3-fold in human cells [37]. Additionally, a Cas9-DN1S fusion increased homologous recombination up to 86% in human cells. The HR pathway is only active during the S/G2 phase of the cell cycle. Therefore, synchronising cell populations via chemical inhibition proved to significantly increase transformation efficiency in *Yarrowia lipolytica* [38]. However, these methods have not been optimised for filamentous fungi yet.

In summary we have generated and optimised a CRISPR-Cas9 transformation methodology without the need of dominant selection markers. This transformation methodology can be used for the generation of deletion mutants and protein fusions. Here, we have generated several reconstituted strains with an efficiency of ~20%. Similar efficiency has been observed for the generation of fusion protein strains, either N-terminal or C-terminal. This efficiency is independent of the targeted locus or epitope used. Overall, this methodology may facilitate more efficient genome editing and reduce off target effects caused by introduction of large constructs in *A. fumigatus* and other fungi.

4.4 References

1. Bongomin, F., et al., *Global and Multi-National Prevalence of Fungal Diseases-Estimate Precision.* J Fungi (Basel), 2017. **3**(4).
2. Stafa, A., et al., *In Saccharomyces cerevisiae gene targeting fidelity depends on a transformation method and proportion of the overall length of the transforming and targeted DNA.* FEMS Yeast Res, 2017. **17**(4).
3. da Silva Ferreira, M.E., et al., *The akuB(KU80) mutant deficient for nonhomologous end joining is a powerful tool for analyzing pathogenicity in Aspergillus fumigatus.* Eukaryot Cell, 2006. **5**(1): p. 207-11.
4. Zhao, C., et al., *High-Throughput Gene Replacement in Aspergillus fumigatus.* Current Protocols in Microbiology, 2019. **54**(1): p. e88.
5. Fuller, K.K., et al., *Development of the CRISPR/Cas9 System for Targeted Gene Disruption in Aspergillus fumigatus.* Eukaryot Cell, 2015. **14**(11): p. 1073-80.
6. Liu, R., et al., *Efficient genome editing in filamentous fungus Trichoderma reesei using the CRISPR/Cas9 system.* Cell Discov, 2015. **1**: p. 15007.
7. Matsu-Ura, T., et al., *Efficient gene editing in Neurospora crassa with CRISPR technology.* Fungal Biol Biotechnol, 2015. **2**: p. 4.
8. Nodvig, C.S., et al., *A CRISPR-Cas9 System for Genetic Engineering of Filamentous Fungi.* PLoS One, 2015. **10**(7): p. e0133085.
9. Barrangou, R., et al., *CRISPR provides acquired resistance against viruses in prokaryotes.* Science, 2007. **315**(5819): p. 1709-12.
10. Nozawa, T., et al., *CRISPR inhibition of prophage acquisition in Streptococcus pyogenes.* PLoS One, 2011. **6**(5): p. e19543.
11. Zhang, C., et al., *Highly efficient CRISPR mutagenesis by microhomology-mediated end joining in Aspergillus fumigatus.* Fungal Genet Biol, 2016. **86**: p. 47-57.
12. Rybak, J.M., et al., *Mutations in hmg1, Challenging the Paradigm of Clinical Triazole Resistance in Aspergillus fumigatus.* MBio, 2019. **10**(2).
13. Al Abdallah, Q., W. Ge, and J.R. Fortwendel, *A Simple and Universal System for Gene Manipulation in Aspergillus fumigatus: In Vitro-Assembled Cas9-Guide RNA Ribonucleoproteins Coupled with Microhomology Repair Templates.* mSphere, 2017. **2**(6).

14. Al Abdallah, Q., et al., *Whole-genome sequencing reveals highly specific gene targeting by in vitro assembled Cas9-ribonucleoprotein complexes in Aspergillus fumigatus.* Fungal Biol Biotechnol, 2018. **5**: p. 11.
15. Mabey Gilsenan, J., J. Cooley, and P. Bowyer, *CADRE: the Central Aspergillus Data REpository 2012.* Nucleic Acids Res, 2012. **40**(Database issue): p. D660-6.
16. Fraczek, M.G., et al., *The cdr1B efflux transporter is associated with non-cyp51a-mediated itraconazole resistance in Aspergillus fumigatus.* J Antimicrob Chemother, 2013. **68**(7): p. 1486-96.
17. Paul, S., D. Diekema, and W.S. Moye-Rowley, *Contributions of Aspergillus fumigatus ATP-binding cassette transporter proteins to drug resistance and virulence.* Eukaryot Cell, 2013. **12**(12): p. 1619-28.
18. Peng, D. and R. Tarleton, *EuPaGDT: a web tool tailored to design CRISPR guide RNAs for eukaryotic pathogens.* Microb Genom, 2015. **1**(4): p. e000033.
19. Hey, P.M., *Characterisation of mariner type transposons in the human opportunistic pathogen Aspergillus fumigatus and development of tagged transposon mutagenesis tools*, in *School of Biological Sciences*. 2007, University of Manchester. p. 251.
20. Willger, S.D., et al., *Dsc orthologs are required for hypoxia adaptation, triazole drug responses, and fungal virulence in Aspergillus fumigatus.* Eukaryot Cell, 2012. **11**(12): p. 1557-67.
21. Vaknin, Y., et al., *Identification and Characterization of a Novel Aspergillus fumigatus Rhomboid Family Putative Protease, RbdA, Involved in Hypoxia Sensing and Virulence.* Infect Immun, 2016. **84**(6): p. 1866-1878.
22. Bertuzzi, M., et al., *The pH-responsive PacC transcription factor of Aspergillus fumigatus governs epithelial entry and tissue invasion during pulmonary aspergillosis.* PLoS Pathog, 2014. **10**(10): p. e1004413.
23. DiCarlo, J.E., et al., *Genome engineering in Saccharomyces cerevisiae using CRISPR-Cas systems.* Nucleic Acids Res, 2013. **41**(7): p. 4336-43.
24. Foster, A.J., et al., *CRISPR-Cas9 ribonucleoprotein-mediated co-editing and counterselection in the rice blast fungus.* Sci Rep, 2018. **8**(1): p. 14355.
25. Morgens, D.W., et al., *Genome-scale measurement of off-target activity using Cas9 toxicity in high-throughput screens.* Nat Commun, 2017. **8**: p. 15178.

26. Chen, B., et al., *Efficient labeling and imaging of protein-coding genes in living cells using CRISPR-Tag.* Nat Commun, 2018. **9**(1): p. 5065.
27. Lackner, D.H., et al., *A generic strategy for CRISPR-Cas9-mediated gene tagging.* Nat Commun, 2015. **6**: p. 10237.
28. Yamato, T., et al., *Single crossover-mediated targeted nucleotide substitution and knock-in strategies with CRISPR/Cas9 system in the rice blast fungus.* Sci Rep, 2019. **9**(1): p. 7427.
29. Wang, Q. and J.J. Coleman, *CRISPR/Cas9-mediated endogenous gene tagging in Fusarium oxysporum.* Fungal Genet Biol, 2019. **126**: p. 17-24.
30. Morozov, I.Y., et al., *A defined sequence within the 3′ UTR of the areA transcript is sufficient to mediate nitrogen metabolite signalling via accelerated deadenylation.* Mol Microbiol, 2000. **37**(5): p. 1248-57.
31. Caddick, M.X., et al., *Opposing signals differentially regulate transcript stability in Aspergillus nidulans.* Mol Microbiol, 2006. **62**(2): p. 509-19.
32. Frit, P., et al., *Alternative end-joining pathway(s): bricolage at DNA breaks.* DNA Repair (Amst), 2014. **17**: p. 81-97.
33. Chu, V.T., et al., *Increasing the efficiency of homology-directed repair for CRISPR-Cas9-induced precise gene editing in mammalian cells.* Nat Biotechnol, 2015. **33**(5): p. 543-8.
34. Maruyama, T., et al., *Increasing the efficiency of precise genome editing with CRISPR-Cas9 by inhibition of nonhomologous end joining.* Nat Biotechnol, 2015. **33**(5): p. 538-42.
35. Yu, C., et al., *Small molecules enhance CRISPR genome editing in pluripotent stem cells.* Cell Stem Cell, 2015. **16**(2): p. 142-7.
36. Arras, S.D. and J.A. Fraser, *Chemical Inhibitors of Non-Homologous End Joining Increase Targeted Construct Integration in Cryptococcus neoformans.* PLoS One, 2016. **11**(9): p. e0163049.
37. Shao, S., et al., *Enhancing CRISPR/Cas9-mediated homology-directed repair in mammalian cells by expressing Saccharomyces cerevisiae Rad52.* Int J Biochem Cell Biol, 2017. **92**: p. 43-52.
38. Jang, I.S., et al., *Improving the efficiency of homologous recombination by chemical and biological approaches in Yarrowia lipolytica.* PLoS One, 2018. **13**(3): p. e0194954.

4.5 Supplementary Data

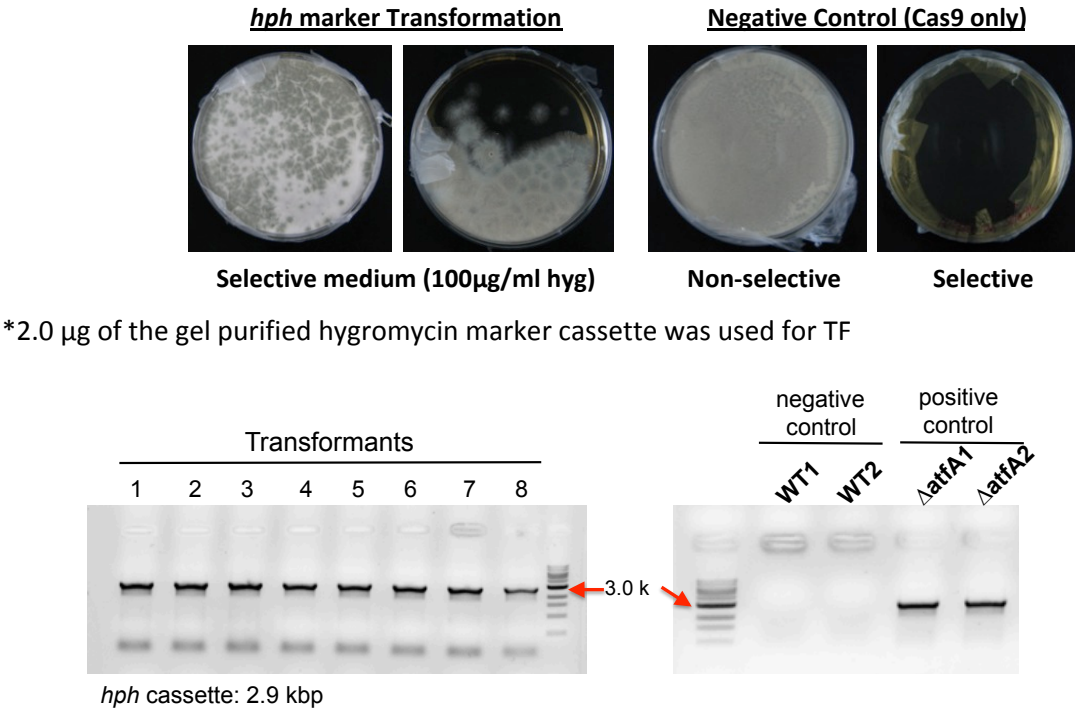

Figure S4.1 Design of *hph* marker integration. gRNA was designed to cause a double stranded break (DSB) in the *atf4* transposon locus, which is a defective transposon. The *hph* marker was amplified with 50bp homology arms towards the flanking region of the DSB, to guide integration towards this site. After CRISPR transformation this resulted in several 100 transformants on an YPS+hyg petridish, while the negative control under selective media was clear.

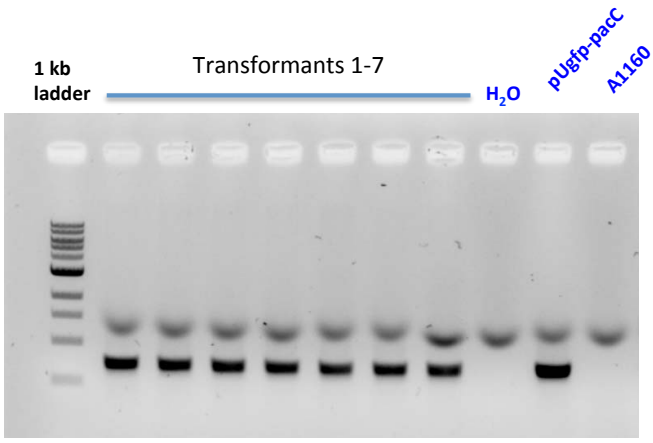

Figure S4.2. Gel electrophoresis of PCR amplified (n = 7). GFP products from screened *pacC-GFP* transformants (n = 90). A product of 750bp was expected. Negative controls containing A1160 genomic DNA and H_2O and positive controls containing the pUgfp-pacC plasmid as template DNA were included.

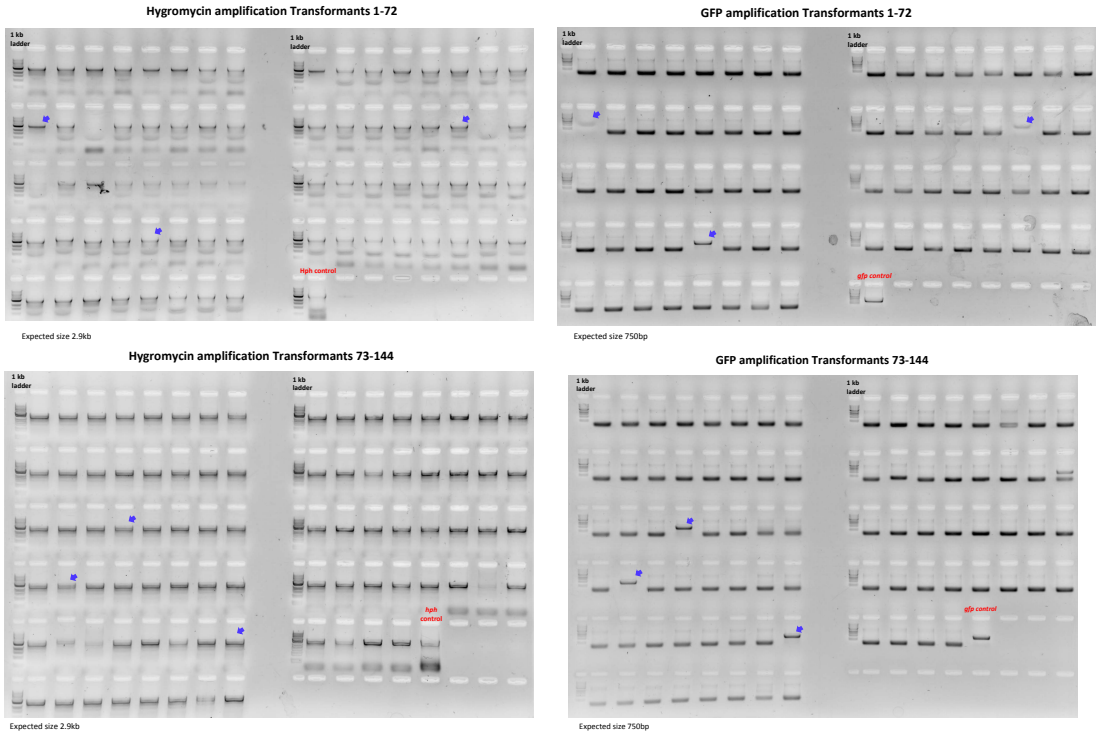

Figure S4.3. Co-transformation by CRISPR-Cas9 of GFP and a hygromycin selection marker. Gel electrophoresis (1% agarose) of PCR amplified GFP from CRISPR transformed *pacC-GFP* co-transformed with *aft4-hph*. Blue arrows represents positive signal detecting GFP and hygromycin (*hph*) amplicons.

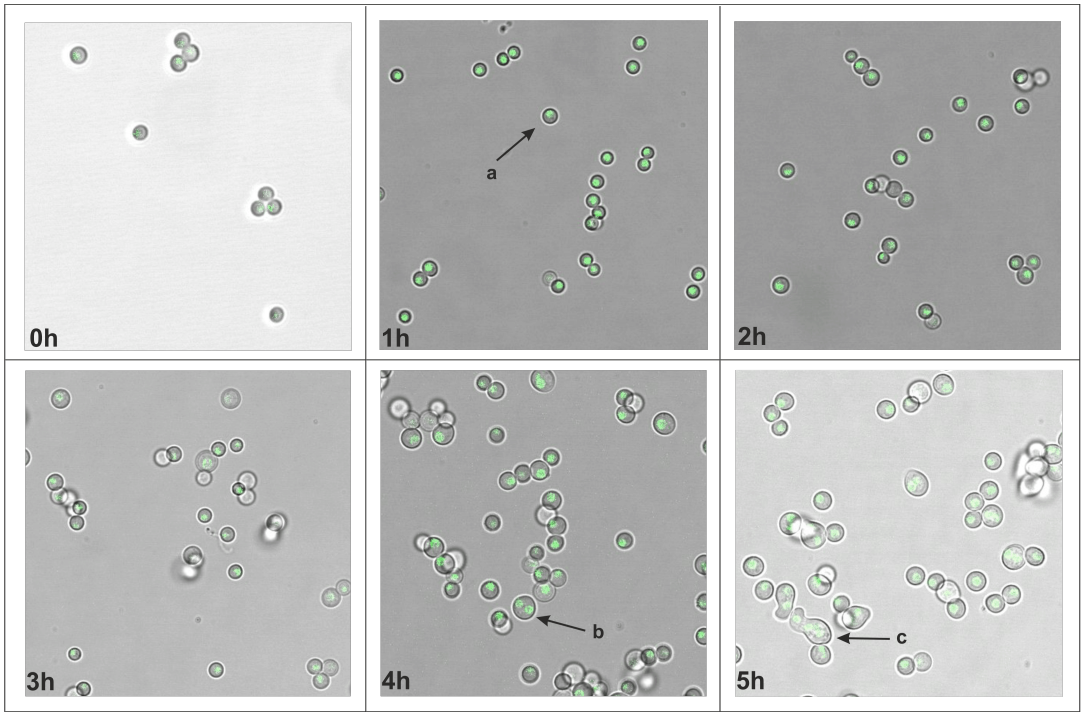

Figure S4.4. Confocal microscopy images of H1 GFP spores. Images were taken at 1 hour intervals (0 -5 hours), incubated as a static culture. A) Example of uni-nucleate condia b) example of multi-nucleate conidia beginning to form after 4 hour incubation c) Example of multi-nucleate conidia after 5 hours.

5. Discussion

The search for new antifungals requires an understanding of fungal pathogenesis and molecular mechanisms of infection. A review estimated that 2% of the global population suffers from a fungal disease [1]. There are no vaccines available for fungal diseases and a limited range of antifungals paired with an increase in antifungal resistance [2-4]. Between 1997 and 2010 only 2% of the total budget was spent on fungal disease of the £2.6 billion spent on infectious disease [5]. This did not represent low funding success rates, but a small number of applications put forward [6]. It highlights the need for more research into fungal diseases and understanding pathogenesis.

The second chapter of this thesis introduces the transcription factor knockout library, consisting of 484 transcription factor null mutants, which represents the complete predicted genomic cohort of transcription factors. Here, we developed a liquid microculture 96-well methodology with a new fungal medium, fungal RPMI, which can be used for growth assays and infection experiments with A549 epithelial cells. The development of this methodological pipeline is key to identify previously uncharacterised regulators, not only in *A. fumigatus* but can also be adapted for filamentous fungi in general. So far, high-throughput phenotyping of filamentous fungi has relied on screening on solid media due the lack of quantification of growth in microculture [7-9]. The itraconazole phenotype screening identified previously uncharacterised regulators, NctA and NctB. Furthermore, several regulators previously unlinked to azole susceptibility were identified: CreA, RfeC, AdaB and GisB for azole sensitivity and AreA and RscE for azole resistance. In the future, the mode of action of these regulators should be determined to fully understand mechanism of azole resistance and potentially identifying the mechanistic basis for non-*cyp51a* resistance in clinical isolates [10]. Furthermore, these regulators and the genes they regulate could be new interesting targets for antifungal therapeutics as these are likely to be involved in mechanism that are essential for infection related cellular processes.

The third chapter of this thesis focuses on the molecular mechanisms of pathogenicity, with a focus on three key *in vivo* events. Firstly, the ability of *A. fumigatus* to be fit *in vitro* and *in vivo*. Secondly, adaptation to environmental stress

and lastly, the ability to invade epithelial barriers and cause damage to the host. Results show that regulators required for fitness and environmental adaptation do not play a role in invasion and damage of the host epithelium. Proving independent regulation of these processes by distinct transcription factors is the first step towards an understanding of the evolutionary models available to explain *A. fumigatus* pathogenicity. In *C. albicans,* co-evolution with the host has been shown to integrate adaptation to environmental stress and host damage within one regulatory network [11]. To reveil the regulatory network essential during *A. fumigatus* infection it is important to characterise the genes regulated. Further studies need to show what processes drive infection. Other research highlights environmental adaptation as the major driver of infection [12]. In the future, target genes of these regulators and the overlap of the regulon under these conditions may provide further support for the "accidental pathogen" hypothesis [13].

The last chapter of this thesis shows the addition of a versatile CRISPR-Cas9 transformation system to the *A. fumigatus* genetic toolbox. This tool can be used for protein tagging and gene deletion. Epitope tagging of proteins are labour and time intensive experiments. However, with this CRISPR-Cas9 transformation technique transformants can be obtained within two weeks compared to several months. In the future, this technique can be expanded to generation of targeted point mutations or promoter replacements. Delivering targeted genome edits can lead to a reduction in off-target effects. Generally selection markers are introduced flanking the target gene. However, untranslated regions have effects on expression and subcellular location [14, 15]. In future experiments, CRISPR-Cas9 mediated protein tagging could be used to regulators identified in chapter 3 in ChIP-seq experiments to assess promoters bound by these regulators. While more than 30 regulators have been identified, the CRISPR-Cas9 methodology can easily be upscaled to facilitate this workload, in attempt to identify the cohort of genes involved in pathogenicity.

This thesis has shown the development of a high-throughput microculture methodology, which can be used for filamentous fungi. A pilot study identifying regulators involved in itraconazole resistance highlighted the role of the NC2 complex in *A. fumigatus.* We have uncovered transcription factor required for a range of environmental stresses and epithelial cell toxicity (see Figure 5.1). While

we have performed extensive *in vitro* analysis of transcription factors, *in vivo* studies will further prove which transcription factors are essential for pathogenicity. In *C. albicans* a pooled infection model has been established with barcoded strains and similar strategies could be applied to *A. fumigatus.* To be able to further characterise the genes regulated by these transcription factors we have developed a CRISPR-Cas9 mediated transformation technique which allows for epitope tagging of proteins for ChIP-seq analysis and fluorescent microscopy.

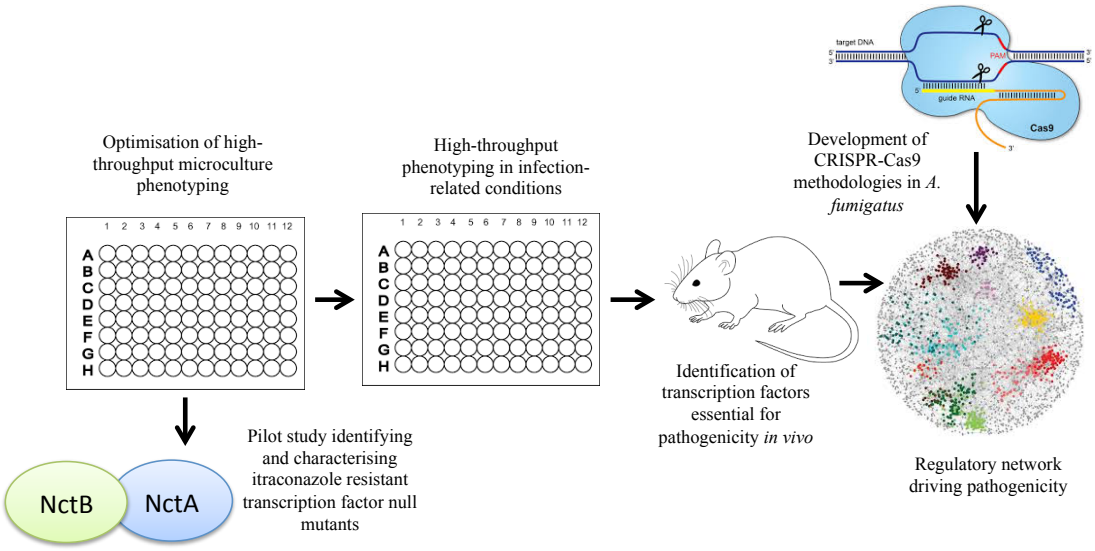

Figure 5.1 Overview of work in this thesis and future work. Schematic overview of work presented in this thesis and the potential for future work. The optimisation of high-throughput microculture phenotyping of *A. fumigatus* and the pilot study performed to characterise transcription factors involved in azole resistance, described in Chapters 2 and 3 respectively. This can lead to identifying transcription factors essential in a murine model of aspergillosis. Using CRISPR-Cas9 mediated transformation, described in Chapter 4, strains can be generated to perform ChIP-seq to unveil the regulatory network driving pathogenicity of *A. fumigatus.*

Future studies on regulators required for pathogenicity will involve performing ChIP-seq and RNA-seq to uncover the mode of action and the genes being regulated by these factors. Parallel transcriptome analysis together with ChIP-seq would allow inferring a regulatory network. A similar study has been performed in *C. albicans* for biofilm formation, assessing 6 transcription factors essential for biofilm formation and the genes regulated by these [16]. Furthermore, in *C. albicans* a transcriptional regulatory network governing gut colonisation and systemic infection have been characterised resulting in a network of over 800 genes genes [11]. In *A. fumigatus*

this thesis has optimised several methodologies taken a step towards performing these type of studies.

5.1 References

1. Denning, D.W., *Calling upon all public health mycologists : To accompany the country burden papers from 14 countries.* Eur J Clin Microbiol Infect Dis, 2017. **36**(6): p. 923-924.
2. Buied, A., et al., *High-level expression of cyp51B in azole-resistant clinical Aspergillus fumigatus isolates.* J Antimicrob Chemother, 2013. **68**(3): p. 512-4.
3. Bowyer, P. and D.W. Denning, *Environmental fungicides and triazole resistance in Aspergillus.* Pest Manag Sci, 2014. **70**(2): p. 173-8.
4. Denning, D.W. and M.J. Bromley, *Infectious Disease. How to bolster the antifungal pipeline.* Science, 2015. **347**(6229): p. 1414-6.
5. Head, M.G., et al., *UK investments in global infectious disease research 1997-2010: a case study.* Lancet Infect Dis, 2013. **13**(1): p. 55-64.
6. Gow, N.A.R., et al., *Strategic Research Funding: A Success Story for Medical Mycology.* Trends Microbiol, 2018. **26**(10): p. 811-813.
7. Son, H., et al., *A phenome-based functional analysis of transcription factors in the cereal head blight fungus, Fusarium graminearum.* PLoS Pathog, 2011. **7**(10): p. e1002310.
8. Saitoh, H., et al., *Large-scale gene disruption in Magnaporthe oryzae identifies MC69, a secreted protein required for infection by monocot and dicot fungal pathogens.* PLoS Pathog, 2012. **8**(5): p. e1002711.
9. Park, G., et al., *High-throughput production of gene replacement mutants in Neurospora crassa.* Methods Mol Biol, 2011. **722**: p. 179-89.
10. Sharma, C., et al., *Genomic perspective of triazole resistance in clinical and environmental Aspergillus fumigatus isolates without cyp51A mutations.* Fungal Genet Biol, 2019. **132**: p. 103265.
11. Perez, J.C., C.A. Kumamoto, and A.D. Johnson, *Candida albicans commensalism and pathogenicity are intertwined traits directed by a tightly knit transcriptional regulatory circuit.* PLoS Biol, 2013. **11**(3): p. e1001510.
12. Watkins, T.N., et al., *Comparative transcriptomics of Aspergillus fumigatus strains upon exposure to human airway epithelial cells.* Microb Genom, 2018. **4**(2).

13. Casadevall, A., et al., *The 'Amoeboid Predator-Fungal Animal Virulence' Hypothesis.* J Fungi (Basel), 2019. **5**(1).
14. Dvir, S., et al., *Deciphering the rules by which 5'-UTR sequences affect protein expression in yeast.* Proc Natl Acad Sci U S A, 2013. **110**(30): p. E2792-801.
15. Macdonald, P.M., et al., *RNA regulatory element BLE1 directs the early steps of bicoid mRNA localization.* Development, 1993. **118**(4): p. 1233-43.
16. Nobile, C.J. and A.P. Mitchell, *Regulation of cell-surface genes and biofilm formation by the C. albicans transcription factor Bcr1p.* Curr Biol, 2005. **15**(12): p. 1150-5.

Appendix I

AFUB gene ID	CADRE gene ID	Generic name	Gene description	Summary of verification PCR		
				5'-junction	3'-junction	TFKO cassette
AFUB_000110	CADAFUBG00000011		PrnA-like fungal specific transcription factor, putative; encoded by transcript AFUB_000110A similar to GB:CAA11374.1: PrnA protein [Emericella nidulans] PMID: 9622360	Y	Y	Y
AFUB_000400	CADAFUBG00000040		C6 transcription factor, putative; encoded by transcript AFUB_000400A	Y	Y	Y
AFUB_000600	CADAFUBG00000060		C6 transcription factor, putative; encoded by transcript AFUB_000600A	Y	Y	NA
AFUB_001060	CADAFUBG00000106		APSES transcription factor Xbp1, putative; encoded by transcript AFUB_001060A	Y	Y	Y
AFUB_001990	CADAFUBG00000199		C6 transcription factor, putative; encoded by transcript AFUB_001990A	Y	Y	Y
AFUB_003240	CADAFUBG00000324		C2H2 transcription factor, putative; encoded by transcript AFUB_003240A	Y	Y	Y
AFUB_004210	CADAFUBG00000422		C6 transcription factor, putative; encoded by transcript AFUB_004210A	Y	Y	Y
AFUB_004470	CADAFUBG00000448		C2H2 transcription factor, putative; encoded by transcript AFUB_004470A	Y	Y	Y
AFUB_004520	CADAFUBG00000454		fungal specific transcription factor, putative; encoded by transcript AFUB_004520A	Y	Y	N
AFUB_005170	CADAFUBG00000519	*abaA*	transcription factor AbaA; encoded by transcript AFUB_005170A similar to GB:AAA33286.1: abaA protein [Emericella nidulans]	Y	Y	NA
AFUB_005350	CADAFUBG00000537		RNA polymerase III transcription factor TFIIIC subunit (Tfc4), putative; encoded by transcript AFUB_005350A			
AFUB_005510	CADAFUBG00000553		C2H2 transcription factor (TFIIIA), putative; encoded by transcript AFUB_005510A	Y	Y	Y
AFUB_005770	CADAFUBG00000579		transcription factor SipA3, putative; encoded by transcript AFUB_005770A	Y	Y	Y
AFUB_006120	CADAFUBG00000615		C6 transcription factor, putative; encoded by transcript AFUB_006120A	Y	Y	Y
AFUB_006920	CADAFUBG00000695		C6 transcription factor, putative; encoded by transcript AFUB_006920A	Y	Y	Y
AFUB_007280	CADAFUBG00000731	*crzA*	C2H2 transcription factor Crz1, putative; encoded by transcript AFUB_007280A	Y	Y	Y
AFUB_009120	CADAFUBG00000916		HLH transcription factor (GlcD gamma), putative; encoded by transcript AFUB_009120A	Y	Y	Y
AFUB_009490	CADAFUBG00000954	*zafA*	C2H2 transcription factor, putative; encoded by transcript AFUB_009490A	Y	Y	NA
AFUB_009640	CADAFUBG00000969		C2H2 transcription factor (Egr2), putative; encoded by transcript AFUB_009640A	Y	Y	NA
AFUB_009970	CADAFUBG00001002		CBF/NF-Y family transcription factor, putative; encoded by transcript AFUB_009970A	Y	Y	Y
AFUB_010000	CADAFUBG00001005		homeobox transcription factor, putative; encoded by transcript AFUB_010000A	Y	Y	Y
AFUB_010180	CADAFUBG00001023		CCAAT-box-binding transcription factor; encoded by transcript AFUB_010180A	Y	Y	Y
AFUB_010420	CADAFUBG00001047		C6 transcription factor, putative; encoded by transcript AFUB_010420A	Y	Y	Y
AFUB_010950	CADAFUBG00001100		fungal specific transcription factor, putative; encoded by transcript AFUB_010950A	Y	Y	Y
AFUB_011060	CADAFUBG00001111		C6 transcription factor QutA, putative; encoded by transcript AFUB_011060A			
AFUB_011240	CADAFUBG00001129		HLH transcription factor, putative; encoded by transcript AFUB_011240A	Y	Y	Y
AFUB_011800	CADAFUBG00001185		jumonji family transcription factor, putative; encoded by transcript AFUB_011800A	Y	Y	NA
AFUB_012020	CADAFUBG00001207		membrane-tethered transcription factor (SPT23), putative; encoded by transcript AFUB_012020A	Y	Y	Y
AFUB_012530	CADAFUBG00001258		C2H2 transcription factor, putative; encoded by transcript AFUB_012530A	Y	N	N
AFUB_012670	CADAFUBG00001272		copper-activated transcription factor GRISEA, putative; encoded by transcript AFUB_012670A	Y	Y	Y

AFUB_012800	CADAFUBG00001285		bZIP transcription factor, putative; encoded by transcript AFUB_012800A	Y	Y	Y
AFUB_013000	CADAFUBG00001305		C6 transcription factor FacB; encoded by transcript AFUB_013000A	Y	Y	NA
AFUB_013240	CADAFUBG00001329		C2H2 transcription factor (Rpn4), putative; encoded by transcript AFUB_013240A	Y	Y	NA
AFUB_013910	CADAFUBG00001396		C6 transcription factor, putative; encoded by transcript AFUB_013910A	Y	Y	Y
AFUB_014000	CADAFUBG00001405		fungal specific transcription factor, putative; encoded by transcript AFUB_014000A	N	Y	Y
AFUB_014290	CADAFUBG00001434		transcription factor TFIIA complex subunit Toa1, putative; encoded by transcript AFUB_014290A			
AFUB_014300	CADAFUBG00001435		C2H2 transcription factor (Sfp1), putative; encoded by transcript AFUB_014300A	Y	N	NA
AFUB_014400	CADAFUBG00001445		bZIP transcription factor, putative; encoded by transcript AFUB_014400A	Y	Y	Y
AFUB_014490	CADAFUBG00001454		C6 transcription factor, putative; encoded by transcript AFUB_014490A	Y	Y	NA
AFUB_014780	CADAFUBG00001483		C6 transcription factor, putative; encoded by transcript AFUB_014780A	Y	Y	Y
AFUB_014910	CADAFUBG00001496		C6 transcription factor, putative; encoded by transcript AFUB_014910A	N	Y	Y
AFUB_015020	CADAFUBG00001507		C6 transcription factor (UaY), putative; encoded by transcript AFUB_015020A	Y	Y	Y
AFUB_015090	CADAFUBG00001514		homeobox and C2H2 transcription factor, putative; encoded by transcript AFUB_015090A	Y	Y	Y
AFUB_015380	CADAFUBG00001543		C6 transcription factor, putative; encoded by transcript AFUB_015380A	Y	Y	Y
AFUB_015440	CADAFUBG00001549		C6 transcription factor RosA-like, putative; encoded by transcript AFUB_015440A	Y	Y	Y
AFUB_015560	CADAFUBG00001561		C6 transcription factor, putative; encoded by transcript AFUB_015560A	Y	Y	N
AFUB_015750	CADAFUBG00001580		C6 transcription factor, putative; encoded by transcript AFUB_015750A	Y	N	Y
AFUB_015800	CADAFUBG00001585	*ads4*	bZIP transcription factor (LziP), putative; encoded by transcript AFUB_015800A	Y	Y	Y
AFUB_015960	CADAFUBG00001601	*brlA*	C2H2 type conidiation transcription factor BrlA; encoded by transcript AFUB_015960A			
AFUB_015990	CADAFUBG00001604		C6 transcription factor, putative; encoded by transcript AFUB_015990A	Y	Y	Y
AFUB_016220	CADAFUBG00001627		C6 transcription factor, putative; encoded by transcript AFUB_016220A	Y	Y	Y
AFUB_016540	CADAFUBG00001659		C6 transcription factor, putative; encoded by transcript AFUB_016540A	Y	Y	Y
AFUB_016630	CADAFUBG00001668		C6 transcription factor, putative; encoded by transcript AFUB_016630A	N	N	Y
AFUB_016720	CADAFUBG00001677		CP2 transcription factor, putative; encoded by transcript AFUB_016720A	N	N	Y
AFUB_016730	CADAFUBG00001678		bZIP transcription factor (BACH2), putative; encoded by transcript AFUB_016730A	Y	Y	Y
AFUB_016820	CADAFUBG00001687		C6 transcription factor, putative; encoded by transcript AFUB_016820A	Y	Y	Y
AFUB_017020	CADAFUBG00001706		C6 transcription factor RegA; encoded by transcript AFUB_017020A	N	Y	Y
AFUB_017180	CADAFUBG00001713		C6 transcription factor Aro80, putative; encoded by transcript AFUB_017180A	Y	Y	Y
AFUB_017410	CADAFUBG00001736		homeobox and C2H2 transcription factor, putative; encoded by transcript AFUB_017410A	Y	Y	Y
AFUB_017530	CADAFUBG00001748		C6 transcription factor, putative; encoded by transcript AFUB_017530A	Y	Y	Y
AFUB_018340	CADAFUBG00001828	*srbA*	HLH transcription factor, putative; encoded by transcript AFUB_018340A	Y	Y	Y
AFUB_019640	CADAFUBG00001958		bZIP transcription factor (Fcr3), putative; encoded by transcript AFUB_019640A	Y	Y	Y
AFUB_019790	CADAFUBG00001973		fungal specific transcription factor, putative; encoded by transcript AFUB_019790A	Y	Y	Y
AFUB_020350	CADAFUBG00002029		bZIP transcription factor, putative; encoded by transcript AFUB_020350A	Y	Y	Y

AFUB_020500	CADAFUBG00002044		C6 transcription factor, putative; encoded by transcript AFUB_020500A	Y	Y	Y
AFUB_020530	CADAFUBG00002047		C6 transcription factor (Leu3), putative; encoded by transcript AFUB_020530A	Y	Y	Y
AFUB_021220	CADAFUBG00002116		C6 transcription factor, putative; encoded by transcript AFUB_021220A	Y	Y	Y
AFUB_021320	CADAFUBG00002126		C6 transcription factor, putative; encoded by transcript AFUB_021320A	Y	Y	Y
AFUB_021650	CADAFUBG00002159		C6 transcription factor, putative; encoded by transcript AFUB_021650A	Y	Y	Y
AFUB_022280	CADAFUBG00002222		transcription factor RfeD, putative; encoded by transcript AFUB_022280A	Y	Y	Y
AFUB_022340	CADAFUBG00002228		C6 transcription factor, putative; encoded by transcript AFUB_022340A	Y	Y	Y
AFUB_022390	CADAFUBG00002233		C6 transcription factor, putative; encoded by transcript AFUB_022390A	Y	Y	Y
AFUB_022410	CADAFUBG00002235		C6 transcription factor, putative; encoded by transcript AFUB_022410A	Y	Y	Y
AFUB_023210	CADAFUBG00002315		fungal specific transcription factor, putative; encoded by transcript AFUB_023210A	Y	Y	Y
AFUB_023920	CADAFUBG00002386	*stuA*	APSES transcription factor StuA; encoded by transcript AFUB_023920A			
AFUB_024170	CADAFUBG00002411		RNA polymerase II transcription factor SIII (Elongin) subunit A,putative; encoded by transcript AFUB_024170A	Y	Y	Y
AFUB_024220	CADAFUBG00002416		C6 transcription factor, putative; encoded by transcript AFUB_024220A	Y	Y	Y
AFUB_024400	CADAFUBG00002434		transcription factor TFIIE complex alpha subunit, putative; encoded by transcript AFUB_024400A			
AFUB_025230	CADAFUBG00002517		C6 transcription factor, putative; encoded by transcript AFUB_025230A	Y	Y	Y
AFUB_026210	CADAFUBG00002615		C6 transcription factor, putative; encoded by transcript AFUB_026210A	Y	Y	Y
AFUB_026340	CADAFUBG00002628		C2H2 transcription factor (RfeC), putative; encoded by transcript AFUB_026340A	Y	Y	Y
AFUB_026550	CADAFUBG00002649		C2H2 transcription factor (Con7), putative; encoded by transcript AFUB_026550A	Y	Y	Y
AFUB_027530	CADAFUBG00002746	*creA*	C2H2 transcription factor (Crea), putative; encoded by transcript AFUB_027530A	Y	Y	Y
AFUB_027770	CADAFUBG00002771		C6 transcription factor, putative; encoded by transcript AFUB_027770A	Y	Y	Y
AFUB_027970	CADAFUBG00002791		HLH transcription factor, putative; encoded by transcript AFUB_027970A	Y	Y	N
AFUB_027990	CADAFUBG00002793	*acuM*	Zn cluster transcription factor Rds2, putative; encoded by transcript AFUB_027990A	Y	Y	Y
AFUB_029020	CADAFUBG00002897		GATA transcription factor (AreB), putative; encoded by transcript AFUB_029020A	Y	Y	Y
AFUB_029870	CADAFUBG00002982		CBF/NF-Y family transcription factor, putative; encoded by transcript AFUB_029870A	Y	Y	Y
AFUB_030360	CADAFUBG00003031	*hapB*	CCAAT-binding transcription factor subunit HAPB; encoded by transcript AFUB_030360A	Y	Y	Y
AFUB_030440	CADAFUBG00003039		HLH transcription factor (Hpa3), putative; encoded by transcript AFUB_030440A	Y	Y	Y
AFUB_030930	CADAFUBG00003088		C6 transcription factor (Leu3), putative; encoded by transcript AFUB_030930A	Y	Y	Y
AFUB_031000	CADAFUBG00003095		AflR-like C6 transcription factor, putative; encoded by transcript AFUB_031000A	Y	Y	Y
AFUB_031270	CADAFUBG00003122		C6 transcription factor, putative; encoded by transcript AFUB_031270A	Y	Y	Y
AFUB_031980	CADAFUBG00003193		fungal specific transcription factor, putative; encoded by transcript AFUB_031980A	Y	Y	Y
AFUB_032870	CADAFUBG00003282		C2H2 transcription factor (AmdX), putative; encoded by transcript AFUB_032870A	Y	Y	Y
AFUB_033470	CADAFUBG00003342		C6 transcription factor, putative; encoded by transcript AFUB_033470A	Y	Y	Y
AFUB_033540	CADAFUBG00003349		C6 transcription factor, putative; encoded by transcript AFUB_033540A	Y	Y	NA
AFUB_033580	CADAFUBG00003353		C6 transcription factor, putative; encoded by transcript AFUB_033580A	Y	Y	Y

AFUB_033930	CADAFUBG00003379		C6 transcription factor, putative; encoded by transcript AFUB_033930A	Y	Y	Y
AFUB_034470	CADAFUBG00003433		fungal specific transcription factor, putative; encoded by transcript AFUB_034470A	Y	Y	Y
AFUB_034630	CADAFUBG00003449		fungal specific transcription factor, putative; encoded by transcript AFUB_034630A	Y	Y	Y
AFUB_035280	CADAFUBG00003515		APSES transcription factor, putative; encoded by transcript AFUB_035280A	N	N	Y
AFUB_035330	CADAFUBG00003520	*nsdD*	sexual development transcription factor NsdD; encoded by transcript AFUB_035330A	Y	Y	Y
AFUB_035590	CADAFUBG00003546		C6 transcription factor, putative; encoded by transcript AFUB_035590A	Y	Y	Y
AFUB_036250	CADAFUBG00003612		C6 transcription factor, putative; encoded by transcript AFUB_036250A predicted by EVM similar to transcriptional activator involved in regulation ofproteins of the lysine biosynthesis pathway; requires 2-aminoadipate semialdehyde as co-inducer; Lys14p (GI:6320237) [Saccharomyces cerevisiae]	Y	Y	Y
AFUB_036300	CADAFUBG00003617		C6 transcription factor GliZ-like, putative; encoded by transcript AFUB_036300A	Y	Y	Y
AFUB_036390	CADAFUBG00003626		C6 transcription factor, putative; encoded by transcript AFUB_036390A	Y	Y	Y
AFUB_036440	CADAFUBG00003631		transcription factor TFIIIB complex subunit Brf1, putative; encoded by transcript AFUB_036440A	Y	Y	NA
AFUB_037000	CADAFUBG00003687		C6 transcription factor, putative; encoded by transcript AFUB_037000A	Y	Y	NA
AFUB_037020	CADAFUBG00003689		homeobox transcription factor, putative; encoded by transcript AFUB_037020A	Y	Y	Y
AFUB_037150	CADAFUBG00003702		PHD transcription factor, putative; encoded by transcript AFUB_037150A	Y	Y	Y
AFUB_037190	CADAFUBG00003706		C6 transcription factor (Mut3), putative; encoded by transcript AFUB_037190A	Y	Y	Y
AFUB_037210	CADAFUBG00003708	*pacC*	C2H2 transcription factor PacC, putative; encoded by transcript AFUB_037210A	Y	Y	Y
AFUB_037220	CADAFUBG00003709		forkhead transcription factor Fkh1/2, putative; encoded by transcript AFUB_037220A	Y	Y	Y
AFUB_037850	CADAFUBG00003772		bZIP transcription factor (AtfA), putative; encoded by transcript AFUB_037850A	Y	Y	Y
AFUB_037920	CADAFUBG00003779	*ace2*	C2H2 transcription factor (Swi5), putative; encoded by transcript AFUB_037920A	Y	Y	Y
AFUB_038200	CADAFUBG00003807		bZIP transcription factor (MeaB), putative; encoded by transcript AFUB_038200A	Y	Y	Y
AFUB_038290	CADAFUBG00003816		zinc knuckle transcription factor/splicing factor MSL5/ZFM1, putative; encoded by transcript AFUB_038290A			
AFUB_038770	CADAFUBG00003864		transcription factor TFIIIC complex subunit Tfc6, putative; encoded by transcript AFUB_038770A			
AFUB_039010	CADAFUBG00003888		C6 transcription factor, putative; encoded by transcript AFUB_039010A	Y	Y	NA
AFUB_039050	CADAFUBG00003892		RNA polymerase I and III transcription factor complex component Tbp, putative; encoded by transcript AFUB_039050A			
AFUB_039350	CADAFUBG00003922	*dvrA*	C2H2 transcription factor, putative; encoded by transcript AFUB_039350A	Y	Y	Y
AFUB_039500	CADAFUBG00003937		C6 transcription factor, putative; encoded by transcript AFUB_039500A	Y	Y	NA
AFUB_040000	CADAFUBG00003987		C6 transcription factor, putative; encoded by transcript AFUB_040000A	Y	Y	Y
AFUB_040580	CADAFUBG00004045	*rlmA*	SRF-type transcription factor RlmA; encoded by transcript AFUB_040580A	Y	Y	Y
AFUB_041060	CADAFUBG00004093		C6 transcription factor (OTam), putative; encoded by transcript AFUB_041060A	Y	Y	Y
AFUB_041100	CADAFUBG00004097		C2H2 transcription factor (Ace1), putative; encoded by transcript AFUB_041100A	Y	Y	Y
AFUB_042310	CADAFUBG00004220		C6 transcription factor (Gal4), putative; encoded by transcript AFUB_042310A	Y	Y	Y
AFUB_042770	CADAFUBG00004266		C6 transcription factor, putative; encoded by transcript AFUB_042770A	Y	Y	Y
AFUB_043000	CADAFUBG00004290		fungal specific transcription factor, putative; encoded by transcript AFUB_043000A	Y	Y	Y

AFUB_043110	CADAFUBG00004301		transcription factor Rba50, putative; encoded by transcript AFUB_043110A			
AFUB_043250	CADAFUBG00004315		GATA transcription factor LreA; encoded by transcript AFUB_043250A			
AFUB_043270	CADAFUBG00004317		C6 transcription factor (Fcr1), putative; encoded by transcript AFUB_043270A	Y	Y	Y
AFUB_043860	CADAFUBG00004376		bZIP transcription factor (HacA), putative; encoded by transcript AFUB_043860A			
AFUB_044040	CADAFUBG00004394		C6 transcription factor, putative; encoded by transcript AFUB_044040A	Y	Y	Y
AFUB_044060	CADAFUBG00004396		C6 transcription factor, putative; encoded by transcript AFUB_044060A	Y	Y	Y
AFUB_044290	CADAFUBG00004419		bZIP transcription factor; encoded by transcript AFUB_044290A	Y	Y	Y
AFUB_044300	CADAFUBG00004420		CP2 transcription factor, putative; encoded by transcript AFUB_044300A similar to GB:AAH69638.1: transcription factor CP2-like 3 {Homo sapiens;}	Y	Y	Y
AFUB_044670	CADAFUBG00004457		fungal specific transcription factor, putative; encoded by transcript AFUB_044670A	Y	Y	Y
AFUB_044930	CADAFUBG00004483		C6 transcription factor, putative; encoded by transcript AFUB_044930A	Y	Y	Y
AFUB_045020	CADAFUBG00004492		bZIP transcription factor, putative; encoded by transcript AFUB_045020A	Y	Y	Y
AFUB_045330	CADAFUBG00004523		C6 transcription factor, putative; encoded by transcript AFUB_045330A	Y	Y	Y
AFUB_045540	CADAFUBG00004544		C6 transcription factor, putative; encoded by transcript AFUB_045540A	Y	Y	Y
AFUB_045580	CADAFUBG00004548		C6 transcription factor, putative; encoded by transcript AFUB_045580A	Y	Y	NA
AFUB_045780	CADAFUBG00004569		PUT3-like fungal specific transcription factor, putative; encoded by transcript AFUB_045780A similar to SP:P25502: Proline utilization trans-activator. {Saccharomyces cerevisiae;}	Y	Y	Y
AFUB_045820	CADAFUBG00004573		C6 transcription factor, putative; encoded by transcript AFUB_045820A	Y	Y	Y
AFUB_045980	CADAFUBG00004589		CBF/NF-Y family transcription factor, putative; encoded by transcript AFUB_045980A	Y	Y	Y
AFUB_046160	CADAFUBG00004607		C6 transcription factor, putative; encoded by transcript AFUB_046160A	Y	Y	Y
AFUB_046210	CADAFUBG00004612		C6 transcription factor, putative; encoded by transcript AFUB_046210A	Y	Y	Y
AFUB_046330	CADAFUBG00004624		C2H2 transcription factor, putative; encoded by transcript AFUB_046330A	Y	Y	Y
AFUB_046410	CADAFUBG00004631		C6 transcription factor Ctf1B-like, putative; encoded by transcript AFUB_046410A	Y	Y	Y
AFUB_046540	CADAFUBG00004644		fungal specific transcription factor, putative; encoded by transcript AFUB_046540A	Y	Y	Y
AFUB_046890	CADAFUBG00004679		C6 transcription factor, putative; encoded by transcript AFUB_046890A	Y	Y	Y
AFUB_047470	CADAFUBG00004737		C6 transcription factor, putative; encoded by transcript AFUB_047470A	Y	Y	Y
AFUB_047730	CADAFUBG00004763		C6 transcription factor, putative; encoded by transcript AFUB_047730A	Y	Y	Y
AFUB_048380	CADAFUBG00004828		C6 transcription factor, putative; encoded by transcript AFUB_048380A similar to SP:P05085: Arginine metabolism regulation protein II. {Saccharomyces cerevisiae;}	Y	Y	Y
AFUB_048740	CADAFUBG00004854		C6 transcription factor, putative; encoded by transcript AFUB_048740A	Y	Y	Y
AFUB_048990	CADAFUBG00004879		C6 transcription factor, putative; encoded by transcript AFUB_048990A	Y	Y	Y
AFUB_049390	CADAFUBG00004919		C6 transcription factor, putative; encoded by transcript AFUB_049390A	Y	Y	Y
AFUB_049550	CADAFUBG00004935		C6 transcription factor, putative; encoded by transcript AFUB_049550A	Y	Y	Y
AFUB_050090	CADAFUBG00004989		C6 transcription factor, putative; encoded by transcript AFUB_050090A	N	Y	Y
AFUB_050190	CADAFUBG00004999		bZIP transcription factor JlbA/IDI-4; encoded by transcript AFUB_050190A	Y	Y	Y
AFUB_050230	CADAFUBG00005003		C6 transcription factor, putative; encoded by transcript AFUB_050230A	Y	Y	Y

AFUB_050430	CADAFUBG00005023		heat shock transcription factor Hsf1, putative; encoded by transcript AFUB_050430A			
AFUB_050800	CADAFUBG00005060		C6 transcription factor, putative; encoded by transcript AFUB_050800A	N	Y	NA
AFUB_051080	CADAFUBG00005088		RNA polymerase III transcription factor subunit, putative; encoded by transcript AFUB_051080A			
AFUB_051340	CADAFUBG00005114		C6 transcription factor, putative; encoded by transcript AFUB_051340A	Y	Y	Y
AFUB_051400	CADAFUBG00005120		C6 transcription factor, putative; encoded by transcript AFUB_051400A	Y	Y	Y
AFUB_051540	CADAFUBG00005134		C6 transcription factor, putative; encoded by transcript AFUB_051540A	Y	Y	NA
AFUB_051950	CADAFUBG00005175		PHD transcription factor (Rum1), putative; encoded by transcript AFUB_051950A	Y	Y	Y
AFUB_052420	CADAFUBG00005222	*hapX*	bZIP transcription factor (HapX), putative; encoded by transcript AFUB_052420A	Y	Y	Y
AFUB_052710	CADAFUBG00005251		HLH transcription factor (PalcA), putative; encoded by transcript AFUB_052710A	Y	Y	Y
AFUB_052860	CADAFUBG00005266		transcription factor and DNA repair complex, core TFIIH, putative; encoded by transcript AFUB_052860A similar to gi|6323033|ref|NP_013105.1| Component of RNA polymerase transcription factor TFIIH,SSL1 [Saccharomyces cerevisiae]	Y	Y	Y
AFUB_053150	CADAFUBG00005295		forkhead transcription factor (Sep1), putative; encoded by transcript AFUB_053150A	Y	Y	Y
AFUB_053740	CADAFUBG00005354	*steA*	sexual development transcription factor SteA; encoded by transcript AFUB_053740A	Y	Y	NA
AFUB_053880	CADAFUBG00005368		DNA repair and transcription factor Ada, putative; encoded by transcript AFUB_053880A	Y	Y	Y
AFUB_053950	CADAFUBG00005375		C2H2 transcription factor (AmdA), putative; encoded by transcript AFUB_053950A	Y	Y	Y
AFUB_054360	CADAFUBG00005416		C6 transcription factor, putative; encoded by transcript AFUB_054360A	Y	Y	Y
AFUB_055060	CADAFUBG00005486		C6 transcription factor AlcR; encoded by transcript AFUB_055060A	Y	Y	Y
AFUB_056530	CADAFUBG00005632		transcription factor RfeG, putative; encoded by transcript AFUB_056530A	Y	Y	Y
AFUB_056620	CADAFUBG00005641		transcription factor (SPT8), putative; encoded by transcript AFUB_056620A	Y	Y	Y
AFUB_056790	CADAFUBG00005658		transcription factor (Snd1/p100), putative; encoded by transcript AFUB_056790A	Y	Y	Y
AFUB_057290	CADAFUBG00005708		C6 transcription factor, putative; encoded by transcript AFUB_057290A	Y	Y	Y
AFUB_057630	CADAFUBG00005742		C6 transcription factor, putative; encoded by transcript AFUB_057630A	Y	Y	Y
AFUB_057730	CADAFUBG00005752		bZIP transcription factor, putative; encoded by transcript AFUB_057730A	Y	Y	Y
AFUB_057890	CADAFUBG00005768		AflR-like C6 zinc cluster transcription factor, putative; encoded by transcript AFUB_057890A	Y	Y	Y
AFUB_058240	CADAFUBG00005803		CBF/NF-Y family transcription factor, putative; encoded by transcript AFUB_058240A	Y	Y	Y
AFUB_058640	CADAFUBG00005843		C6 transcription factor (ArcA), putative; encoded by transcript AFUB_058640A	Y	Y	Y
AFUB_058830	CADAFUBG00005862	*sreA*	siderophore transcription factor SreA; encoded by transcript AFUB_058830A	Y	Y	Y
AFUB_058960	CADAFUBG00005876		APSES transcription factor, putative; encoded by transcript AFUB_058960A	Y	Y	Y
AFUB_059150	CADAFUBG00005895		transcription factor TFIIH subunit Tfb4, putative; encoded by transcript AFUB_059150A			
AFUB_059600	CADAFUBG00005940		C6 transcription factor (NirA), putative; encoded by transcript AFUB_059600A	Y	Y	Y
AFUB_059650	CADAFUBG00005945	*hof*	C2H2 transcription factor, putative; encoded by transcript AFUB_059650A	Y	Y	Y
AFUB_060620	CADAFUBG00006042		GATA transcription factor (Ams2), putative; encoded by transcript AFUB_060620A			
AFUB_060680	CADAFUBG00006048		bZIP transcription factor (Atf21), putative; encoded by transcript AFUB_060680A	Y	Y	Y
AFUB_061020	CADAFUBG00006082		C6 transcription factor, putative; encoded by transcript AFUB_061020A	Y	Y	Y
AFUB_061530	CADAFUBG00006132		C6 transcription factor (Acr-2), putative; encoded by transcript AFUB_061530A	Y	Y	Y

AFUB_061940	CADAFUBG00006172		C6 transcription factor, putative; encoded by transcript AFUB_061940A	Y	Y	Y
AFUB_062000	CADAFUBG00006178		C6 transcription factor, putative; encoded by transcript AFUB_062000A	Y	Y	Y
AFUB_062090	CADAFUBG00006187		C6 transcription factor, putative; encoded by transcript AFUB_062090A	Y	Y	Y
AFUB_062110	CADAFUBG00006189		C6 transcription factor, putative; encoded by transcript AFUB_062110A	Y	Y	Y
AFUB_062210	CADAFUBG00006198		C6 transcription factor, putative; encoded by transcript AFUB_062210A	Y	Y	Y
AFUB_063310	CADAFUBG00006279		fungal specific transcription factor, putative; encoded by transcript AFUB_063310A	Y	Y	Y
AFUB_063540	CADAFUBG00006302		fungal specific transcription factor, putative; encoded by transcript AFUB_063540A	Y	Y	Y
AFUB_063610	CADAFUBG00006310		bZIP transcription factor (MetR), putative; encoded by transcript AFUB_063610A	Y	Y	N
AFUB_066180	CADAFUBG00006568	*sebA*	C2H2 transcription factor (Seb1), putative; encoded by transcript AFUB_066180A	Y	Y	Y
AFUB_066820	CADAFUBG00006630	*rosA/nosA*	C6 sexual development transcription factor, putative; encoded by transcript AFUB_066820A	Y	Y	Y
AFUB_066970	CADAFUBG00006644		C6 transcription factor, putative; encoded by transcript AFUB_066970A	Y	Y	Y
AFUB_067230	CADAFUBG00006670		homeobox transcription factor, putative; encoded by transcript AFUB_067230A	Y	Y	Y
AFUB_067280	CADAFUBG00006675		C6 transcription factor (AmyR), putative; encoded by transcript AFUB_067280A	Y	Y	Y
AFUB_067320	CADAFUBG00006679		transcription factor RfeF, putative; encoded by transcript AFUB_067320A	Y	Y	Y
AFUB_067340	CADAFUBG00006681		homeobox transcription factor (RfeB), putative; encoded by transcript AFUB_067340A	Y	Y	NA
AFUB_068700	CADAFUBG00006818		RNA polymerase II transcription factor related protein; encoded by transcript AFUB_068700A	Y	Y	NA
AFUB_069160	CADAFUBG00006864		C6 transcription factor Prf, putative; encoded by transcript AFUB_069160A	Y	Y	NA
AFUB_069420	CADAFUBG00006890	*cpcA*	bZIP transcription factor CpcA; encoded by transcript AFUB_069420A identical to cross-pathway control protein CpcA (GI:33340527) [Aspergillus fumigatus] similar to transcriptional activator CpcA (GI:15824382) [Emericella nidulans] similar to transcriptional activator of amino acid biosynthetic genes in response to amino acid starvation; expression is tightly regulated at both the transcriptional and translational levels; Gcn4p (GI:6320828) [Saccharomyces cerevisiae]	Y	Y	Y
AFUB_069500	CADAFUBG00006898		C6 transcription factor, putative; encoded by transcript AFUB_069500A	Y	Y	Y
AFUB_069610	CADAFUBG00006909		GATA transcription factor LreB; encoded by transcript AFUB_069610A	Y	Y	Y
AFUB_069670	CADAFUBG00006915		transcription factor, putative; encoded by transcript AFUB_069670A			
AFUB_069960	CADAFUBG00006944		zinc knuckle transcription factor (CnjB), putative; encoded by transcript AFUB_069960A	Y	Y	Y
AFUB_071780	CADAFUBG00007127		C6 transcription factor (AflR), putative; encoded by transcript AFUB_071780A	Y	Y	Y
AFUB_071830	CADAFUBG00007132		C6 transcription factor, putative; encoded by transcript AFUB_071830A	Y	Y	N
AFUB_071920	CADAFUBG00007141		C6 transcription factor, putative; encoded by transcript AFUB_071920A	Y	Y	Y
AFUB_072930	CADAFUBG00007233		C6 transcription factor RosA; encoded by transcript AFUB_072930A similar to transcriptional regulatory protein Pro1 (Swiss-Prot:Q9P326) [Neurospora crassa] PMID: 12081464 similar to repressor of sexual development RosA (GI:27526404) [Emericella nidulans] PMID: 15520269	Y	Y	Y
AFUB_073070	CADAFUBG00007247		C6 transcription factor, putative; encoded by transcript AFUB_073070A	Y	Y	Y
AFUB_073490	CADAFUBG00007289		bZIP transcription factor, putative; encoded by transcript AFUB_073490A	Y	Y	Y
AFUB_073520	CADAFUBG00007292		transcription factor Rap1, putative; encoded by transcript AFUB_073520A	Y	Y	N
AFUB_073940	CADAFUBG00007334		fungal specific transcription factor, putative; encoded by transcript AFUB_073940A	Y	Y	Y

AFUB_074510	CADAFUBG00007391		C6 transcription factor, putative; encoded by transcript AFUB_074510A	Y	Y	Y
AFUB_074560	CADAFUBG00007396		transcription factor TFIID complex 145 kDa subunit, putative; encoded by transcript AFUB_074560A	Y	Y	Y
AFUB_074750	CADAFUBG00007415		C6 transcription factor (PrnA), putative; encoded by transcript AFUB_074750A	Y	Y	Y
AFUB_075870	CADAFUBG00007527		transcription factor AATF/Che-1, putative; encoded by transcript AFUB_075870A			
AFUB_075930	CADAFUBG00007533		C6 transcription factor, putative; encoded by transcript AFUB_075930A	Y	Y	N
AFUB_075990	CADAFUBG00007539	*yap1*	bZIP transcription factor (AP-1), putative; encoded by transcript AFUB_075990A	Y	Y	Y
AFUB_076060	CADAFUBG00007546		C6 transcription factor, putative; encoded by transcript AFUB_076060A	Y	Y	Y
AFUB_076110	CADAFUBG00007551		C6 transcription factor (PRO1), putative; encoded by transcript AFUB_076110A	Y	Y	Y
AFUB_076200	CADAFUBG00007560		C6 transcription factor, putative; encoded by transcript AFUB_076200A	Y	Y	Y
AFUB_077130	CADAFUBG00007653		C6 transcription factor, putative; encoded by transcript AFUB_077130A	Y	Y	Y
AFUB_077250	CADAFUBG00007665		C6 transcription factor, putative; encoded by transcript AFUB_077250A	Y	Y	Y
AFUB_077460	CADAFUBG00007686		C6 transcription factor, putative; encoded by transcript AFUB_077460A	Y	Y	Y
AFUB_077530	CADAFUBG00007693		C6 transcription factor, putative; encoded by transcript AFUB_077530A	Y	Y	Y
AFUB_077740	CADAFUBG00007714		C6 transcription factor, putative; encoded by transcript AFUB_077740A	Y	Y	Y
AFUB_078120	CADAFUBG00007750		C6 transcription factor, putative; encoded by transcript AFUB_078120A	Y	Y	Y
AFUB_078150	CADAFUBG00007753		bZIP transcription factor (Atf7), putative; encoded by transcript AFUB_078150A	Y	Y	Y
AFUB_078160	CADAFUBG00007754		C6 transcription factor, putative; encoded by transcript AFUB_078160A	Y	Y	Y
AFUB_078520	CADAFUBG00007790		stress response regulator/HFS transcription factor, putative; encoded by transcript AFUB_078520A similar to GB:AAN75016.1: stress response regulator SrrA [Emericella nidulans]	Y	Y	Y
AFUB_079150	CADAFUBG00007853		C6 transcription factor, putative; encoded by transcript AFUB_079150A	Y	Y	Y
AFUB_079450	CADAFUBG00007883		C6 transcription factor, putative; encoded by transcript AFUB_079450A	Y	Y	Y
AFUB_079560	CADAFUBG00007893		C6 transcription factor, putative; encoded by transcript AFUB_079560A	Y	Y	Y
AFUB_079700	CADAFUBG00007907		fungal specific transcription factor, putative; encoded by transcript AFUB_079700A	Y	Y	Y
AFUB_079810	CADAFUBG00007918		fungal specific transcription factor, putative; encoded by transcript AFUB_079810A similar to SP:P52959: Cutinase transcription factor 1 beta. {Nectria haematococca mpVI;}	Y	Y	Y
AFUB_079860	CADAFUBG00007923		fungal specific transcription factor, putative; encoded by transcript AFUB_079860A	Y	Y	Y
AFUB_079880	CADAFUBG00007925		C6 transcription factor, putative; encoded by transcript AFUB_079880A	Y	Y	Y
AFUB_080380	CADAFUBG00007966		C6 transcription factor, putative; encoded by transcript AFUB_080380A	Y	Y	Y
AFUB_080460	CADAFUBG00007974		C6 transcription factor, putative; encoded by transcript AFUB_080460A	Y	Y	N
AFUB_080600	CADAFUBG00007987		C6 transcription factor, putative; encoded by transcript AFUB_080600A	Y	Y	Y
AFUB_080790	CADAFUBG00008006		C6 transcription factor, putative; encoded by transcript AFUB_080790A	Y	Y	Y
AFUB_081310	CADAFUBG00008059		C6 transcription factor, putative; encoded by transcript AFUB_081310A	Y	Y	Y
AFUB_081500	CADAFUBG00008078		C6 transcription factor, putative; encoded by transcript AFUB_081500A	Y	Y	Y
AFUB_081700	CADAFUBG00008098		fungal specific transcription factor, putative; encoded by transcript AFUB_081700A	Y	Y	Y
AFUB_081990	CADAFUBG00008127		transcription factor (Sin3), putative; encoded by transcript AFUB_081990A			

AFUB_082080	CADAFUBG00008137		bZIP transcription factor, putative; encoded by transcript AFUB_082080A	Y	Y	Y
AFUB_082260	CADAFUBG00008155		C6 transcription factor, putative; encoded by transcript AFUB_082260A	Y	Y	Y
AFUB_082950	CADAFUBG00008224		C6 transcription factor, putative; encoded by transcript AFUB_082950A	Y	Y	Y
AFUB_083430	CADAFUBG00008272		C6 transcription factor (Ctf1B), putative; encoded by transcript AFUB_083430A	Y	Y	Y
AFUB_083880	CADAFUBG00008317		C6 transcription factor, putative; encoded by transcript AFUB_083880A	Y	N	Y
AFUB_083950	CADAFUBG00008324		C6 transcription factor, putative; encoded by transcript AFUB_083950A	Y	Y	Y
AFUB_084330	CADAFUBG00008362		C6 transcription factor, putative; encoded by transcript AFUB_084330A	Y	Y	Y
AFUB_084620	CADAFUBG00008391		C6 transcription factor, putative; encoded by transcript AFUB_084620A	Y	Y	Y
AFUB_085380	CADAFUBG00008468		C6 transcription factor, putative; encoded by transcript AFUB_085380A	Y	Y	Y
AFUB_085450	CADAFUBG00008476		C6 transcription factor, putative; encoded by transcript AFUB_085450A	Y	Y	Y
AFUB_085460	CADAFUBG00008477		C6 transcription factor, putative; encoded by transcript AFUB_085460A	Y	Y	Y
AFUB_085820	CADAFUBG00008513		C2H2 transcription factor, putative; encoded by transcript AFUB_085820A	Y	Y	Y
AFUB_086150	CADAFUBG00008547		C6 finger transcription factor, putative; encoded by transcript AFUB_086150A			
AFUB_086680	CADAFUBG00008580		C6 transcription factor, putative; encoded by transcript AFUB_086680A	Y	Y	NA
AFUB_086770	CADAFUBG00008589		C6 transcription factor, putative; encoded by transcript AFUB_086770A	Y	Y	Y
AFUB_086990	CADAFUBG00008611		C6 transcription factor, putative; encoded by transcript AFUB_086990A	Y	Y	Y
AFUB_087340	CADAFUBG00008646		C6 transcription factor, putative; encoded by transcript AFUB_087340A	Y	Y	Y
AFUB_087890	CADAFUBG00008703		C6 transcription factor, putative; encoded by transcript AFUB_087890A	Y	Y	Y
AFUB_088210	CADAFUBG00008735		C6 transcription factor, putative; encoded by transcript AFUB_088210A	Y	Y	Y
AFUB_088380	CADAFUBG00008752		C6 transcription factor, putative; encoded by transcript AFUB_088380A	Y	Y	Y
AFUB_088390	CADAFUBG00008753		C6 transcription factor, putative; encoded by transcript AFUB_088390A	Y	Y	Y
AFUB_088460	CADAFUBG00008760		C6 transcription factor, putative; encoded by transcript AFUB_088460A	Y	Y	Y
AFUB_089710	CADAFUBG00008885		C6 transcription factor, putative; encoded by transcript AFUB_089710A	Y	Y	Y
AFUB_089880	CADAFUBG00008902		C6 transcription factor, putative; encoded by transcript AFUB_089880A	Y	Y	Y
AFUB_090250	CADAFUBG00008939		NF-X1 finger transcription factor, putative; encoded by transcript AFUB_090250A			
AFUB_090370	CADAFUBG00008951		C6 transcription factor, putative; encoded by transcript AFUB_090370A			
AFUB_090440	CADAFUBG00008958		C6 transcription factor, putative; encoded by transcript AFUB_090440A	Y	Y	Y
AFUB_090650	CADAFUBG00008979		C6 transcription factor, putative; encoded by transcript AFUB_090650A			
AFUB_000190	CADAFUBG00000019		C6 finger domain protein, putative; encoded by transcript AFUB_000190A	Y	Y	Y
AFUB_000960	CADAFUBG00000096		C6 finger domain protein, putative; encoded by transcript AFUB_000960A	Y	Y	Y
AFUB_001960	CADAFUBG00000196		C6 finger domain protein, putative; encoded by transcript AFUB_001960A	Y	Y	Y
AFUB_002050	CADAFUBG00000205		C6 finger domain protein, putative; encoded by transcript AFUB_002050A	Y	Y	Y
AFUB_002240	CADAFUBG00000224		C6 finger domain protein, putative; encoded by transcript AFUB_002240A	Y	Y	Y
AFUB_004190	CADAFUBG00000420		C6 finger domain protein, putative; encoded by transcript AFUB_004190A	Y	Y	Y

AFUB_004490	CADAFUBG00000451		C6 finger domain protein, putative; encoded by transcript AFUB_004490A	Y	Y	N
AFUB_008120	CADAFUBG00000816		C6 finger domain protein, putative; encoded by transcript AFUB_008120A	Y	Y	Y
AFUB_008610	CADAFUBG00000865		C6 finger domain protein, putative; encoded by transcript AFUB_008610A	Y	Y	Y
AFUB_010090	CADAFUBG00001014		C6 finger domain protein, putative; encoded by transcript AFUB_010090A	Y	Y	NA
AFUB_010720	CADAFUBG00001077		C6 finger domain protein, putative; encoded by transcript AFUB_010720A	Y	Y	Y
AFUB_013830	CADAFUBG00001388		C6 finger domain protein, putative; encoded by transcript AFUB_013830A	Y	Y	Y
AFUB_015210	CADAFUBG00001526		C6 finger domain protein, putative; encoded by transcript AFUB_015210A	Y	Y	Y
AFUB_020250	CADAFUBG00002019		C6 finger domain protein, putative; encoded by transcript AFUB_020250A	Y	Y	NA
AFUB_022860	CADAFUBG00002280	*acuK*	C6 finger domain protein, putative; encoded by transcript AFUB_022860A	Y	Y	Y
AFUB_023530	CADAFUBG00002347		C6 finger domain protein, putative; encoded by transcript AFUB_023530A	Y	Y	Y
AFUB_024050	CADAFUBG00002399		C6 finger domain protein, putative; encoded by transcript AFUB_024050A	Y	Y	Y
AFUB_025190	CADAFUBG00002513		C6 finger domain protein, putative; encoded by transcript AFUB_025190A	Y	Y	Y
AFUB_026630	CADAFUBG00002657		C6 finger domain protein, putative; encoded by transcript AFUB_026630A	Y	Y	Y
AFUB_027200	CADAFUBG00002713		C6 finger domain protein, putative; encoded by transcript AFUB_027200A	Y	Y	Y
AFUB_029740	CADAFUBG00002969		C6 finger domain protein, putative; encoded by transcript AFUB_029740A	Y	Y	NA
AFUB_031840	CADAFUBG00003179		C6 finger domain protein, putative; encoded by transcript AFUB_031840A	Y	Y	NA
AFUB_033560	CADAFUBG00003351		C6 finger domain protein, putative; encoded by transcript AFUB_033560A	Y	Y	Y
AFUB_036510	CADAFUBG00003638		C6 finger domain protein Acr-2, putative; encoded by transcript AFUB_036510A	Y	Y	N
AFUB_038600	CADAFUBG00003847		C6 finger domain protein, putative; encoded by transcript AFUB_038600A	Y	Y	Y
AFUB_045600	CADAFUBG00004551		C6 finger domain protein, putative; encoded by transcript AFUB_045600A			
AFUB_046750	CADAFUBG00004665		C6 finger domain protein, putative; encoded by transcript AFUB_046750A	Y	Y	Y
AFUB_047970	CADAFUBG00004787		C6 finger domain protein, putative; encoded by transcript AFUB_047970A	Y	Y	Y
AFUB_048230	CADAFUBG00004813		C6 finger domain protein, putative; encoded by transcript AFUB_048230A	Y	Y	NA
AFUB_048890	CADAFUBG00004869		C6 finger domain protein, putative; encoded by transcript AFUB_048890A	Y	Y	N
AFUB_050000	CADAFUBG00004980		C6 finger domain protein, putative; encoded by transcript AFUB_050000A	Y	Y	Y
AFUB_054000	CADAFUBG00005380		C6 finger domain protein, putative; encoded by transcript AFUB_054000A	Y	Y	N
AFUB_057470	CADAFUBG00005726		C6 finger domain protein, putative; encoded by transcript AFUB_057470A	Y	Y	Y
AFUB_060650	CADAFUBG00006045		C6 finger domain protein, putative; encoded by transcript AFUB_060650A	Y	Y	NA
AFUB_067240	CADAFUBG00006671	*prtT*	C6 finger domain protein, putative; encoded by transcript AFUB_067240A	Y	Y	Y
AFUB_067440	CADAFUBG00006691		C6 finger domain protein, putative; encoded by transcript AFUB_067440A	N	Y	NA
AFUB_068850	CADAFUBG00006833		C6 finger domain protein, putative; encoded by transcript AFUB_068850A	Y	N	Y
AFUB_071380	CADAFUBG00007086		C6 finger domain protein, putative; encoded by transcript AFUB_071380A	Y	Y	Y
AFUB_073760	CADAFUBG00007316		C6 finger domain protein, putative; encoded by transcript AFUB_073760A			
AFUB_074500	CADAFUBG00007390		C6 finger domain protein, putative; encoded by transcript AFUB_074500A similar to GB:AAS92247.1: SndA [Emericella nidulans]	Y	Y	NA

AFUB_075680	CADAFUBG00007508	*gliZ*	C6 finger domain protein GliZ; encoded by transcript AFUB_075680A	Y	Y	Y
AFUB_080530	CADAFUBG00007980		C6 finger domain protein, putative; encoded by transcript AFUB_080530A	Y	Y	NA
AFUB_081800	CADAFUBG00008108		C6 finger domain protein, putative; encoded by transcript AFUB_081800A	Y	Y	Y
AFUB_083600	CADAFUBG00008289		C6 finger domain protein, putative; encoded by transcript AFUB_083600A	Y	Y	Y
AFUB_084440	CADAFUBG00008373		C6 finger domain protein, putative; encoded by transcript AFUB_084440A	Y	Y	Y
AFUB_084670	CADAFUBG00008396		C6 finger domain protein, putative; encoded by transcript AFUB_084670A	Y	Y	Y
AFUB_085170	CADAFUBG00008447		C6 finger domain protein, putative; encoded by transcript AFUB_085170A	Y	N	Y
AFUB_092740	CADAFUBG00009186		C6 finger domain protein, putative; encoded by transcript AFUB_092740A	Y	Y	NA
AFUB_094860	CADAFUBG00009389		C6 finger domain protein, putative; encoded by transcript AFUB_094860A	Y	Y	Y
AFUB_095440	CADAFUBG00009446		C6 finger domain protein, putative; encoded by transcript AFUB_095440A	Y	Y	Y
AFUB_096380	CADAFUBG00009540		C6 finger domain protein, putative; encoded by transcript AFUB_096380A	Y	Y	Y
AFUB_099770	CADAFUBG00009873		C6 finger domain protein, putative; encoded by transcript AFUB_099770A	Y	Y	Y
AFUB_101950	CADAFUBG00010082		C6 finger domain protein, putative; encoded by transcript AFUB_101950A	Y	Y	N
AFUB_001820	CADAFUBG00000182		C2H2 finger domain protein, putative; encoded by transcript AFUB_001820A	Y	Y	Y
AFUB_002390	CADAFUBG00000239		C2H2 finger domain protein, putative; encoded by transcript AFUB_002390A	Y	Y	Y
AFUB_004120	CADAFUBG00000413		C2H2 finger domain protein, putative; encoded by transcript AFUB_004120A	Y	Y	N
AFUB_009690	CADAFUBG00000974		C2H2 finger domain protein (Gli3), putative; encoded by transcript AFUB_009690A	Y	Y	Y
AFUB_013550	CADAFUBG00001360		C2H2 finger domain protein, putative; encoded by transcript AFUB_013550A			
AFUB_019160	CADAFUBG00001910		C2H2 finger domain protein, putative; encoded by transcript AFUB_019160A	Y	Y	Y
AFUB_019830	CADAFUBG00001977		C2H2 finger domain protein, putative; encoded by transcript AFUB_019830A	Y	Y	Y
AFUB_021470	CADAFUBG00002141		C2H2 finger domain protein, putative; encoded by transcript AFUB_021470A	Y	N	Y
AFUB_029400	CADAFUBG00002935		C2H2 finger domain protein FlbC; encoded by transcript AFUB_029400A	Y	Y	N
AFUB_030770	CADAFUBG00003072		C2H2 finger domain protein, putative; encoded by transcript AFUB_030770A	Y	Y	Y
AFUB_031910	CADAFUBG00003186		C2H2 finger domain protein, putative; encoded by transcript AFUB_031910A	Y	Y	Y
AFUB_032220	CADAFUBG00003217		C2H2 finger domain protein, putative; encoded by transcript AFUB_032220A	Y	Y	Y
AFUB_032890	CADAFUBG00003284		C2H2 finger domain protein, putative; encoded by transcript AFUB_032890A	Y	Y	N
AFUB_035140	CADAFUBG00003500		C2H2 finger domain protein, putative; encoded by transcript AFUB_035140A	Y	Y	Y
AFUB_042120	CADAFUBG00004201		C2H2 zinc finger domain protein, putative; encoded by transcript AFUB_042120A	Y	Y	Y
AFUB_043680	CADAFUBG00004358		C2H2 finger domain protein, putative; encoded by transcript AFUB_043680A			
AFUB_044110	CADAFUBG00004401		C2H2 type zinc finger domain protein; encoded by transcript AFUB_044110A			
AFUB_046000	CADAFUBG00004591		C2H2 finger domain protein (Kin17), putative; encoded by transcript AFUB_046000A	Y	Y	NA
AFUB_047310	CADAFUBG00004721		C2H2 finger domain protein, putative; encoded by transcript AFUB_047310A	Y	Y	Y
AFUB_055490	CADAFUBG00005528		C2H2 finger and ankyrin domain protein, putative; encoded by transcript AFUB_055490A	Y	Y	Y
AFUB_056710	CADAFUBG00005650		C2H2 finger domain protein, putative; encoded by transcript AFUB_056710A	Y	Y	Y

AFUB_064180	CADAFUBG00006367		C2H2 finger domain protein, putative; encoded by transcript AFUB_064180A	Y	Y	Y
AFUB_067480	CADAFUBG00006695		C2H2 finger domain protein, putative; encoded by transcript AFUB_067480A	Y	Y	NA
AFUB_068500	CADAFUBG00006798		C2H2 finger domain protein, putative; encoded by transcript AFUB_068500A	Y	Y	Y
AFUB_070520	CADAFUBG00007000		C2H2 finger domain protein, putative; encoded by transcript AFUB_070520A	Y	Y	Y
AFUB_070960	CADAFUBG00007044		C2H2 finger domain protein, putative; encoded by transcript AFUB_070960A	Y	Y	Y
AFUB_071460	CADAFUBG00007094		C2H2 finger domain protein; encoded by transcript AFUB_071460A	Y	Y	Y
AFUB_071660	CADAFUBG00007115		C2H2 finger domain protein, putative; encoded by transcript AFUB_071660A	Y	Y	Y
AFUB_077190	CADAFUBG00007659		C2H2 finger domain protein (Ezf), putative; encoded by transcript AFUB_077190A	Y	Y	Y
AFUB_077270	CADAFUBG00007667		C2H2 finger domain protein, putative; encoded by transcript AFUB_077270A	Y	Y	NA
AFUB_078010	CADAFUBG00007740		C2H2 finger domain protein, putative; encoded by transcript AFUB_078010A	Y	Y	Y
AFUB_082490	CADAFUBG00008178	*zfpA*	C2H2 finger domain protein, putative; encoded by transcript AFUB_082490A	Y	Y	Y
AFUB_083250	CADAFUBG00008254		C2H2 finger domain protein, putative; encoded by transcript AFUB_083250A	Y	Y	Y
AFUB_083260	CADAFUBG00008255		C2H2 finger domain protein, putative; encoded by transcript AFUB_083260A	Y	Y	Y
AFUB_083370	CADAFUBG00008266		C2H2 zinc finger protein; encoded by transcript AFUB_083370A	Y	Y	NA
AFUB_089440	CADAFUBG00008858		C2H2 zinc finger protein; encoded by transcript AFUB_089440A	Y	Y	Y
AFUB_091540	CADAFUBG00009067		C2H2 finger domain protein, putative; encoded by transcript AFUB_091540A	Y	Y	Y
AFUB_092820	CADAFUBG00009194		C2H2 finger domain protein, putative; encoded by transcript AFUB_092820A	Y	Y	Y
AFUB_095290	CADAFUBG00009431		C2H2 finger domain protein (Zms1), putative; encoded by transcript AFUB_095290A	Y	Y	Y
AFUB_095620	CADAFUBG00009464	*mtfA*	C2H2 finger domain protein, putative; encoded by transcript AFUB_095620A	Y	Y	Y
AFUB_096430	CADAFUBG00009545	*gipA*	C2H2 finger domain protein, putative; encoded by transcript AFUB_096430A	Y	Y	NA
AFUB_096690	CADAFUBG00009571		C2H2 finger domain protein; encoded by transcript AFUB_096690A	Y	Y	Y
AFUB_097590	CADAFUBG00009664		C2H2 finger domain protein; encoded by transcript AFUB_097590A	Y	Y	Y
AFUB_091020	CADAFUBG00009015		transcription factor Tos4, putative; encoded by transcript AFUB_091020A	Y	Y	Y
AFUB_091200	CADAFUBG00009033		APSES transcription factor (MbpA), putative; encoded by transcript AFUB_091200A			
AFUB_091870	CADAFUBG00009100		C6 transcription factor, putative; encoded by transcript AFUB_091870A	Y	Y	Y
AFUB_091930	CADAFUBG00009106		C6 transcription factor, putative; encoded by transcript AFUB_091930A	Y	Y	Y
AFUB_092060	CADAFUBG00009119		fungal specific transcription factor, putative; encoded by transcript AFUB_092060A	Y	Y	Y
AFUB_092130	CADAFUBG00009126		fungal specific transcription factor, putative; encoded by transcript AFUB_092130A	Y	Y	NA
AFUB_092490	CADAFUBG00009162		fungal specific transcription factor, putative; encoded by transcript AFUB_092490A	Y	Y	Y
AFUB_092760	CADAFUBG00009188		SRF-type transcription factor family protein; encoded by transcript AFUB_092760A			
AFUB_093120	CADAFUBG00009215	*azf1*	C2H2 transcription factor (Azf1), putative; encoded by transcript AFUB_093120A	Y	Y	Y
AFUB_093280	CADAFUBG00009231		C6 transcription factor, putative; encoded by transcript AFUB_093280A	Y	Y	Y
AFUB_093890	CADAFUBG00009292		transcription factor TFIIIB component, putative; encoded by transcript AFUB_093890A			
AFUB_095180	CADAFUBG00009420		C6 transcription factor, putative; encoded by transcript AFUB_095180A	Y	Y	Y
AFUB_096230	CADAFUBG00009525		SRF-type transcription factor (Umc1), putative; encoded by transcript AFUB_096230A	Y	Y	N

AFUB_096500	CADAFUBG00009552		C6 transcription factor, putative; encoded by transcript AFUB_096500A	Y	Y	Y
AFUB_097300	CADAFUBG00009632		fungal specific transcription factor, putative; encoded by transcript AFUB_097300A	Y	Y	Y
AFUB_097320	CADAFUBG00009634		C6 transcription factor, putative; encoded by transcript AFUB_097320A	Y	N	Y
AFUB_097380	CADAFUBG00009643		C6 transcription factor, putative; encoded by transcript AFUB_097380A	Y	Y	Y
AFUB_098690	CADAFUBG00009765		homeobox transcription factor, putative; encoded by transcript AFUB_098690A	Y	Y	Y
AFUB_099050	CADAFUBG00009801	*farA*	C6 transcription factor Ctf1A, putative; encoded by transcript AFUB_099050A	Y	Y	NA
AFUB_099350	CADAFUBG00009831		C6 transcription factor, putative; encoded by transcript AFUB_099350A	Y	Y	Y
AFUB_099630	CADAFUBG00009859		C6 transcription factor, putative; encoded by transcript AFUB_099630A	Y	Y	Y
AFUB_100190	CADAFUBG00009915		bZIP transcription factor, putative; encoded by transcript AFUB_100190A	Y	Y	Y
AFUB_101260	CADAFUBG00010011		C6 transcription factor, putative; encoded by transcript AFUB_101260A	Y	Y	Y
AFUB_101510	CADAFUBG00010036		C6 transcription factor, putative; encoded by transcript AFUB_101510A	Y	Y	Y
AFUB_101990	CADAFUBG00010086		C6 transcription factor, putative; encoded by transcript AFUB_101990A			
AFUB_100050	CADAFUBG00009901		C2H2 finger domain protein, putative; encoded by transcript AFUB_100050A	Y	Y	Y
AFUB_016450	CADAFUBG00001650	*srbB*	HLH DNA binding domain protein, putative; encoded by transcript AFUB_016450A	Y	Y	Y
AFUB_055550	CADAFUBG00005534		HLH DNA binding protein (Penr2), putative; encoded by transcript AFUB_055550A	Y	Y	Y
AFUB_063950	CADAFUBG00006344		HLH DNA binding domain protein, putative; encoded by transcript AFUB_063950A	Y	Y	Y
AFUB_099590	CADAFUBG00009855	*srbB*	HLH DNA binding domain protein, putative; encoded by transcript AFUB_099590A	Y	Y	Y
AFUB_003630	CADAFUBG00000364	*flbD*	MYB family conidiophore development protein FlbD, putative; encoded by transcript AFUB_003630A			
AFUB_007880	CADAFUBG00000792		MYB DNA-binding domain protein; encoded by transcript AFUB_007880A	Y	Y	Y
AFUB_019440	CADAFUBG00001938		MYB DNA-binding domain protein; encoded by transcript AFUB_019440A	Y	Y	Y
AFUB_020050	CADAFUBG00001999		MYB DNA-binding domain protein; encoded by transcript AFUB_020050A	Y	Y	Y
AFUB_020080	CADAFUBG00002002		MYB DNA-binding domain protein; encoded by transcript AFUB_020080A	Y	Y	Y
AFUB_041980	CADAFUBG00004187		MYB DNA-binding domain protein; encoded by transcript AFUB_041980A	Y	Y	Y
AFUB_042180	CADAFUBG00004207		MYB DNA-binding domain protein; encoded by transcript AFUB_042180A	Y	Y	Y
AFUB_050260	CADAFUBG00005006		MYB DNA-binding domain protein; encoded by transcript AFUB_050260A	Y	Y	Y
AFUB_059050	CADAFUBG00005885		MYB DNA binding protein (Tbf1), putative; encoded by transcript AFUB_059050A	Y	Y	Y
AFUB_064650	CADAFUBG00006414		MYB and HSA domain protein; encoded by transcript AFUB_064650A	Y	Y	NA
AFUB_007880	CADAFUBG00000792		MYB DNA-binding domain protein; encoded by transcript AFUB_007880A	Y	Y	Y
AFUB_018270	CADAFUBG00001821		Cu-dependent DNA-binding protein, putative; encoded by transcript AFUB_018270A similar to GB:AAB70928.1: proline rich protein [Santalum album]	Y	Y	Y
AFUB_019440	CADAFUBG00001938		MYB DNA-binding domain protein; encoded by transcript AFUB_019440A	Y	Y	N
AFUB_020050	CADAFUBG00001999		MYB DNA-binding domain protein; encoded by transcript AFUB_020050A	Y	Y	Y
AFUB_020080	CADAFUBG00002002		MYB DNA-binding domain protein; encoded by transcript AFUB_020080A	Y	Y	Y
AFUB_023400	CADAFUBG00002334		replication protein A 70 kDa DNA-binding subunit; encoded by transcript AFUB_023400A			
AFUB_032490	CADAFUBG00003244		curved DNA-binding protein (42 kDa protein); encoded by transcript AFUB_032490A	Y	Y	Y

AFUB_041980	CADAFUBG00004187		MYB DNA-binding domain protein; encoded by transcript AFUB_041980A	N	N	NA
AFUB_042180	CADAFUBG00004207		MYB DNA-binding domain protein; encoded by transcript AFUB_042180A	Y	Y	Y
AFUB_043720	CADAFUBG00004362		DNA-binding protein HGH1, putative; encoded by transcript AFUB_043720A	Y	Y	N
AFUB_050260	CADAFUBG00005006		MYB DNA-binding domain protein; encoded by transcript AFUB_050260A	Y	N	N
AFUB_082330	CADAFUBG00008162		Myb-like DNA-binding domain protein; encoded by transcript AFUB_082330A			
AFUB_000040	CADAFUBG00000004		hypothetical protein; encoded by transcript AFUB_000040A	Y	Y	NA
AFUB_002740	CADAFUBG00000274		conserved hypothetical protein; encoded by transcript AFUB_002740A	Y	Y	Y
AFUB_003620	CADAFUBG00000362		hypothetical protein; encoded by transcript AFUB_003620A	Y	Y	Y
AFUB_003630	CADAFUBG00000364	*flbD*	MYB family conidiophore development protein FlbD, putative; encoded by transcript AFUB_003630A	Y	Y	Y
AFUB_005170	CADAFUBG00000519	*abaA*	transcription factor AbaA; encoded by transcript AFUB_005170A similar to GB:AAA33286.1: abaA protein [Emericella nidulans]	Y	Y	Y
AFUB_007960	CADAFUBG00000800		zinc knuckle domain protein (Byr3), putative; encoded by transcript AFUB_007960A	Y	Y	NA
AFUB_011060	CADAFUBG00001111		C6 transcription factor QutA, putative; encoded by transcript AFUB_011060A	Y	Y	Y
AFUB_013550	CADAFUBG00001360		C2H2 finger domain protein, putative; encoded by transcript AFUB_013550A	Y	Y	Y
AFUB_014200	CADAFUBG00001425	*laeA*	regulator of secondary metabolism LaeA; encoded by transcript AFUB_014200A	Y	Y	NA
AFUB_015960	CADAFUBG00001601		C2H2 type conidiation transcription factor BrlA; encoded by transcript AFUB_015960A			
AFUB_017960	CADAFUBG00001791		conserved hypothetical protein; encoded by transcript AFUB_017960A	Y	Y	Y
AFUB_020110	CADAFUBG00002005		forkhead domain protein; encoded by transcript AFUB_020110A	Y	Y	Y
AFUB_020420	CADAFUBG00002036		MIZ zinc finger domain protein; encoded by transcript AFUB_020420A	Y	Y	NA
AFUB_021540	CADAFUBG00002148		conserved hypothetical protein; encoded by transcript AFUB_021540A similar to GB:AAK11170.1: putative cysteine-binding protein FliY [Haloferax volcanii] PMID: 12579374	Y	Y	Y
AFUB_022560	CADAFUBG00002250		cell division control protein (Cdc5), putative; encoded by transcript AFUB_022560A	Y	Y	Y
AFUB_023920	CADAFUBG00002386	*stuA*	APSES transcription factor StuA; encoded by transcript AFUB_023920A	Y	Y	Y
AFUB_023950	CADAFUBG00002389		hypothetical protein; encoded by transcript AFUB_023950A	Y	Y	Y
AFUB_025730	CADAFUBG00002567		conserved hypothetical protein; encoded by transcript AFUB_025730A	Y	Y	Y
AFUB_038290	CADAFUBG00003816		zinc knuckle transcription factor/splicing factor MSL5/ZFM1, putative; encoded by transcript AFUB_038290A	N	Y	NA
AFUB_028890	CADAFUBG00002883	*medA*	transcriptional regulator Medusa; encoded by transcript AFUB_028890A	Y	Y	NA
AFUB_029970	CADAFUBG00002992		AT DNA binding protein, putative; encoded by transcript AFUB_029970A	Y	Y	Y
AFUB_033200	CADAFUBG00003315		conserved hypothetical protein; encoded by transcript AFUB_033200A	Y	Y	Y
AFUB_037970	CADAFUBG00003784		conserved hypothetical protein; encoded by transcript AFUB_037970A	Y	Y	Y
AFUB_026420	CADAFUBG00002636		SAGA complex subunit (Ada2), putative; encoded by transcript AFUB_026420A			
AFUB_038920	CADAFUBG00003879		Ccr4-Not transcription complex subunit (NOT1), putative; encoded by transcript AFUB_038920A			
AFUB_039150	CADAFUBG00003902		forkhead domain protein; encoded by transcript AFUB_039150A	Y	Y	NA
AFUB_040460	CADAFUBG00004033		coactivator bridging factor 1 (Mbf1), putative; encoded by transcript AFUB_040460A	Y	Y	Y
AFUB_041990	CADAFUBG00004188		hypothetical protein; encoded by transcript AFUB_041990A	Y	Y	Y
AFUB_042300	CADAFUBG00004219		hypothetical protein; encoded by transcript AFUB_042300A	Y	Y	Y
AFUB_042780	CADAFUBG00004267		hypothetical protein; encoded by transcript AFUB_042780A			

AFUB_043250	CADAFUBG00004315		GATA transcription factor LreA; encoded by transcript AFUB_043250A			
AFUB_043680	CADAFUBG00004358		C2H2 finger domain protein, putative; encoded by transcript AFUB_043680A	Y	Y	Y
AFUB_043860	CADAFUBG00004376	*hacA*	bZIP transcription factor (HacA), putative; encoded by transcript AFUB_043860A	Y	Y	Y
AFUB_044120	CADAFUBG00004402		conserved hypothetical protein; encoded by transcript AFUB_044120A	Y	Y	Y
AFUB_044350	CADAFUBG00004425		hypothetical protein; encoded by transcript AFUB_044350A	Y	Y	Y
AFUB_045460	CADAFUBG00004536		hypothetical protein; encoded by transcript AFUB_045460A			
AFUB_045600	CADAFUBG00004551		C6 finger domain protein, putative; encoded by transcript AFUB_045600A	Y	Y	NA
AFUB_046430	CADAFUBG00004633		chromatin structure remodeling complex protein RSC3, putative; encoded by transcript AFUB_046430A	Y	Y	Y
AFUB_047250	CADAFUBG00004715		conserved hypothetical protein; encoded by transcript AFUB_047250A	Y	Y	Y
AFUB_048830	CADAFUBG00004863		hypothetical protein; encoded by transcript AFUB_048830A	Y	Y	Y
AFUB_048940	CADAFUBG00004874		conserved hypothetical protein; encoded by transcript AFUB_048940A	Y	Y	Y
AFUB_049780	CADAFUBG00004958		hypothetical protein; encoded by transcript AFUB_049780A	Y	Y	Y
AFUB_050200	CADAFUBG00005000		conserved hypothetical protein; encoded by transcript AFUB_050200A	Y	Y	Y
AFUB_050430	CADAFUBG00005023	*hsf1*	heat shock transcription factor Hsf1, putative; encoded by transcript AFUB_050430A	Y	Y	Y
AFUB_051220	CADAFUBG00005102		hypothetical protein; encoded by transcript AFUB_051220A	Y	Y	Y
AFUB_053680	CADAFUBG00005348		DNA damage and replication checkpoint protein Rfx1, putative; encoded by transcript AFUB_053680A			
AFUB_055080	CADAFUBG00005488		conserved hypothetical protein; encoded by transcript AFUB_055080A	Y	Y	Y
AFUB_057600	CADAFUBG00005739		conserved hypothetical protein; encoded by transcript AFUB_057600A	Y	N	NA
AFUB_060430	CADAFUBG00006023		CCCH zinc finger DNA binding protein; encoded by transcript AFUB_060430A	Y	Y	NA
AFUB_060620	CADAFUBG00006042		GATA transcription factor (Ams2), putative; encoded by transcript AFUB_060620A	Y	Y	Y
AFUB_061420	CADAFUBG00006121		hypothetical protein; encoded by transcript AFUB_061420A	Y	Y	Y
AFUB_067520	CADAFUBG00006699		DNA binding protein SART-1, putative; encoded by transcript AFUB_067520A	Y	Y	Y
AFUB_071090	CADAFUBG00007057		hypothetical protein; encoded by transcript AFUB_071090A	Y	Y	Y
AFUB_071570	CADAFUBG00007106		hypothetical protein; encoded by transcript AFUB_071570A	Y	Y	Y
AFUB_073170	CADAFUBG00007257		hypothetical protein; encoded by transcript AFUB_073170A	Y	Y	Y
AFUB_073740	CADAFUBG00007314		Copper fist DNA binding domain protein; encoded by transcript AFUB_073740A	Y	Y	NA
AFUB_073760	CADAFUBG00007316		C6 finger domain protein, putative; encoded by transcript AFUB_073760A	Y	Y	NA
AFUB_075630	CADAFUBG00007503		conserved hypothetical protein; encoded by transcript AFUB_075630A	Y	Y	NA
AFUB_077920	CADAFUBG00007731		WSC domain protein, putative; encoded by transcript AFUB_077920A	Y	Y	Y
AFUB_080070	CADAFUBG00007935		hypothetical protein; encoded by transcript AFUB_080070A	Y	Y	Y
AFUB_080850	CADAFUBG00008012		hypothetical protein; encoded by transcript AFUB_080850A	Y	Y	NA
AFUB_081750	CADAFUBG00008103	*finA*	hypothetical protein; encoded by transcript AFUB_081750A	Y	Y	Y
AFUB_083510	CADAFUBG00008280	*xprG*	NDT80_PhoG domain protein PcaG; encoded by transcript AFUB_083510A	Y	Y	Y
AFUB_084770	CADAFUBG00008406		conserved hypothetical protein; encoded by transcript AFUB_084770A	Y	Y	NA
AFUB_085630	CADAFUBG00008494		conserved hypothetical protein; encoded by transcript AFUB_085630A	Y	Y	Y

AFUB_086150	CADAFUBG00008547	*fumR*	C6 finger transcription factor, putative; encoded by transcript AFUB_086150A	Y	Y	NA
AFUB_087240	CADAFUBG00008636		hypothetical protein; encoded by transcript AFUB_087240A	Y	Y	NA
AFUB_088740	CADAFUBG00008788		zinc knuckle nucleic acid binding protein, putative; encoded by transcript AFUB_088740A	Y	Y	Y
AFUB_088810	CADAFUBG00008795	*somA*	cAMP-dependent protein kinase pathway protein (Som1), putative; encoded by transcript AFUB_088810A	Y	Y	NA
AFUB_090360	CADAFUBG00008950		conserved hypothetical protein; encoded by transcript AFUB_090360A	Y	Y	Y
AFUB_090370	CADAFUBG00008951		C6 transcription factor, putative; encoded by transcript AFUB_090370A	Y	Y	Y
AFUB_090650	CADAFUBG00008979		C6 transcription factor, putative; encoded by transcript AFUB_090650A	Y	Y	Y
AFUB_091090	CADAFUBG00009022		RSC complex subunit (RSC8), putative; encoded by transcript AFUB_091090A	Y	Y	Y
AFUB_092100	CADAFUBG00009123		hypothetical protein; encoded by transcript AFUB_092100A	Y	Y	NA
AFUB_092720	CADAFUBG00009184		hypothetical protein; encoded by transcript AFUB_092720A	Y	Y	Y
AFUB_092760	CADAFUBG00009188		SRF-type transcription factor family protein; encoded by transcript AFUB_092760A	Y	Y	NA
AFUB_093890	CADAFUBG00009292		transcription factor TFIIIB component, putative; encoded by transcript AFUB_093890A	Y	Y	NA
AFUB_096010	CADAFUBG00009503		hypothetical protein; encoded by transcript AFUB_096010A	Y	Y	NA
AFUB_096230	CADAFUBG00009525	*mcmA*	SRF-type transcription factor (Umc1), putative; encoded by transcript AFUB_096230A	Y	Y	NA
AFUB_096370	CADAFUBG00009539	*areA*	GATA transcriptional activator AreA; encoded by transcript AFUB_096370A	Y	Y	Y
AFUB_097690	CADAFUBG00009674		hypothetical protein; encoded by transcript AFUB_097690A	Y	Y	Y
AFUB_097790	CADAFUBG00009684		hypothetical protein; encoded by transcript AFUB_097790A	Y	Y	NA
AFUB_098510	CADAFUBG00009747		hypothetical protein; encoded by transcript AFUB_098510A	Y	Y	Y
AFUB_101600	CADAFUBG00010046		hypothetical protein; encoded by transcript AFUB_101600A	Y	Y	Y
AFUB_101810	CADAFUBG00010068		conserved hypothetical protein; encoded by transcript AFUB_101810A	N	Y	Y
AFUB_101870	CADAFUBG00010074		hypothetical protein; encoded by transcript AFUB_101870A	Y	Y	Y
AFUB_101990	CADAFUBG00010086		C6 transcription factor, putative; encoded by transcript AFUB_101990A	Y	Y	NA